UNIVERSITY OF SOUTHAMPTON

Flavour predictions in the Standard Model and beyond

by

Maria Dimou

A thesis submitted in partial fulfillment for the
degree of Doctor of Philosophy

in the
Faculty of Physical Sciences and Engineering
Physics and Astronomy

February 2016

UNIVERSITY OF SOUTHAMPTON

ABSTRACT

FACULTY OF PHYSICAL SCIENCES AND ENGINEERING
PHYSICS AND ASTRONOMY

Doctor of Philosophy

by Maria Dimou

This thesis reports on two projects concerning flavour physics. In the first project it is shown how approximate Minimal Flavour Violation (MFV) can emerge from an $SU(5)$ Supersymmetric Grand Unified Theory (SUSY GUT) supplemented by an $S_4 \times U(1)$ family symmetry, which provides a good description of all quark and lepton (including neutrino) masses, mixings and CP violation. Assuming a SUSY breaking mechanism which respects the family symmetry, the low energy mass insertion parameters are calculated in full explicit detail in the super-CKM basis, including the effects of canonical normalisation and renormalisation group running. It is found that the very simple family symmetry $S_4 \times U(1)$ is sufficient to approximately reproduce the effects of low energy MFV where required but there is also a suggestion of testable new physics. Numerical estimates of the low energy mass insertion parameters are presented for well-defined ranges of SUSY parameters and the naive model expectations are compared to the numerical scans and the experimental bounds. The results are then used to estimate the predictions for Electric Dipole Moments (EDMs), Lepton Flavour Violation (LFV), B and K meson mixing as well as rare B decays. The largest observable deviations from MFV come from the LFV process $\mu \to e\gamma$ and the EDMs.

In the second project, matrix elements of the chromomagnetic operator, often denoted by $\mathcal{O}_8$, between B/D-states and light mesons plus an off-shell photon are calculated, by employing the method of light-cone sum rules (LCSR) at leading twist 2. These matrix elements are relevant for flavour changing transition processes, such as $B \to K^* l^+ l^-$ and they can be seen as the analogues of the well-known penguin form factors $T_{1,2,3}$ and f_T. A large CP-even phase is found, for which a long-distance (LD) interpretation is given. Results are compared to QCD factorisation (QCDF), for which the spectator photon emission is end-point divergent. The analytic structure of the correlation function used in the LCSR method, admits a complex anomalous threshold on the physical sheet, the meaning and handling of which is discussed.

Contents

Declaration of Authorship

I, Maria Dimou, declare that this thesis and the work presented in it are my own and has been generated by me as the result of my own original research.

Flavour predictions in the Standard Model and beyond

I confirm that:

- this work was done wholly or mainly while in candidature for a research degree at this University;
- where any part of this thesis has previously been submitted for a degree or any other qualification at this University or any other institution, this has been clearly stated;
- where I have consulted the published work of others, this is always clearly attributed;
- where I have quoted from the work of others, the source is always given. With the exception of such quotations, this thesis is entirely my own work;
- I have acknowledged all main sources of help;
- where the thesis is based on work done by myself jointly with others, I have made clear exactly what was done by others and what I have contributed myself;
- parts of this work have been published as: [see *List of Publications*];

Maria Dimou

February 2016

List of Tables

List of Figures

Acknowledgements

I would like to express my sincere gratitude to my supervisor Stephen F. King, for his expert guidance and endless patience. I have been blessed to have worked under the supervision of not only an outstanding scientist but also a great, inspiring teacher, who has always been available, kind and motivating, ungrudgingly offering his support.

I would also like to thank Roman Zwicky for productive collaboration; James Lyon for being a great collaborator and a good friend; Christoph Luhn for late night skyping over Christmas but mainly for invaluable collaboration; Claudia Hagedorn for her wisdom and many insightful conversations; Alex Stuart for his humour, advice and for making physics bearable.

To my good friends, Shane Drury, Marc Thomas, Jürgen Dietz, Daniele Barducci, Miguel Romão and Juri Fiaschi, thank you for the countless useful discussions and moments of laughter. You have made office 4005 such a pleasant and stimulating work environment. Jason Hammett, thank you for offering me your valuable computing expertise and for being a true friend. Maria Magou and Elena Mavrona, thank you for being there for me, always giving me reasons to cheer.

Finally, I would like to thank my beloved parents and brother, for I could not have made it without their encouragement, love and support. And to Graham Hesketh, thank you for sticking by my side through all this; thank you for believing in me when I found it difficult to believe in myself.

In loving memory of my grandparents and my best friend Liza...

Chapter 1

Introduction

"*This result is too beautiful to be false; it is more important to have beauty in one's equations than to have them fit experiment*" - Paul Dirac, 1963 [1].

A more conservative view, is that a beautiful theory is more likely to be true. The theories described as beautiful within the physics community, are usually the ones that are formulated by means of symmetries. In fact, the most ground breaking claims have been based upon symmetry arguments: from Plato's "theory of everything", based on the symmetrical properties of the "five platonic solids"; to Galois' mathematical description of symmetry through group theory; Poincaré's symmetry of spacetime; Einstein's symmetry geometrization; Noether's connection between symmetries and conserved quantities; Maxwell-Yang-Mills' description of the non-gravitational fundamental forces through the imposition of local gauge symmetries and the emergence of the corresponding vector gauge bosons; and Higgs'[1] association of broken symmetries with massive vector bosons.

It has been a long journey of pioneering developments that led to the construction of the Standard Model (SM) of particle physics in the second half of the 20th century [3]. The electroweak (EW) and strong nuclear interactions, three out of the four fundamental forces of nature, have been described with tremendous success and the observation of all predicted fundamental particles was completed in 2012, with the discovery of the Higgs boson at CERN [4]. Following the 2013 Nobel Prize award to François Englert and Peter W. Higgs "for the theoretical discovery of a mechanism that contributes to our understanding of the origin of mass of subatomic particles, and which recently was confirmed through the discovery of the predicted fundamental particle, by the ATLAS and CMS experiments at CERN's Large Hadron Collider", there was hope that this newly discovered particle would hint at the presence of some new physics (NP). However, its properties appear to be in agreement with the SM expectations, to increasing levels of accuracy. This result has, on the one hand, been received as one more SM victory but on the other hand, there has been some disappointment in the Higgs being exactly SM-like. The reason is that, despite its ongoing verification, the SM is widely viewed as the low energy limit of a more fundamental theory. There are solid arguments on an observational, as well as theoretical basis, that NP effects have to emerge around the TeV scale.

[1] Work of three independent groups: Robert Brout and Franois Englert; Peter Higgs; Gerald Guralnik, C. R. Hagen and Tom Kibble [2]

Interestingly enough, the most popular beyond the SM (BSM) scenario is supersymmetry (SUSY). Even though it predicts double the number of particles, none of which has yet been observed, it seems too "beautiful", too elegant and too predictive to give up on just yet. In the framework of Grand Unified Theories (GUTs), it allows for unification of the strong, electromagnetic and weak coupling constants. Furthermore, when SUSY is imposed as a local symmetry, the associated boson is identified with the graviton and therefore gravity is included automatically, in the form of supergravity (SUGRA). String theory, which attempts to unify all forces, is generally supersymmetric. There are many motivating arguments in favour of SUSY, such as the provision of a solution to the hierarchy problem and the provision of Dark Matter candidates. There is also a lot of disappointment in the null SUSY results of LHC Run 1. But, with the second Run having just begun, it is the time to focus on, rather than abandon SUSY.

Some theoretical puzzles within the SM and its supersymmetric extension remain. The main focus of this thesis is to tackle our lack of knowledge on the dynamics governing the flavour sector. Following the award of the 2015 Nobel Prize for "the discovery of neutrino oscillations which shows that neutrinos have mass", we still have no more understanding of flavour than back in 1936, when Rabi famously asked of the muon "who ordered that?". Part of the reason for this impasse is the failure of experiment to measure any flavour and CP violation beyond that expected in the SM. In order to understand the nature of flavour within the SM and beyond, it is necessary to answer the following questions:

1. Why are there three families of quarks and leptons?
2. Why are charged-fermion masses so hierarchical (spanning many orders of magnitude)?
3. Why are neutrinos so much lighter than every other fermion?
4. Why is the flavour mixing in the quark sector so much smaller than in the leptonic sector?
5. What is the origin of CP violation?
6. Why is the amount of flavour violation induced by new physics so small?

Pursuing the path of symmetry, this work attempts to answer the above questions following the idea introduced by Froggatt and Nielsen [5]. The aim is to identify a predictive symmetry that acts on the three families/flavours, thereby putting them on the same footing. In the limit where this "family" or "horizontal" symmetry is exact, there are no Yukawa couplings. Those are generated when the symmetry is spontaneously broken by non-zero vacuum expectation values (vevs) of some Higgs-like heavy scalar fields, called "flavons". The matter fields and the flavons transform under non-trivial representations of the family symmetry group and can couple to form non-renormalisable operators (at the level of the effective theory approach), invariant under all symmetries. When the family symmetry is broken, the flavon vev, suppressed by the heavy UV cut-off scale, induces an expansion parameter, in terms of which effective Yukawa couplings can be written, resulting in the desired hierarchical charged-fermion Yukawa matrices. The relatively recent information concerning massive neutrinos and their large mixing, points towards non-Abelian discrete family symmetries, in order to account for such non-hierarchical family structures. Ever since, there has been a lot of effort to formulate a theory of flavour [6] which can account for the observed pattern of fermion masses and mixing, while providing

more accurate predictions for the less well measured (or unmeasured) flavour parameters in the neutrino sector [7]. The smallness of neutrino masses is explained via the see-saw mechanism [8], while CP violation originates from the imposition of a CP symmetry, which is only broken by complex flavon vevs.

When embedding such a model in a supersymmetric framework, where SUSY is spontaneously broken in some "hidden" sector that respects the family symmetry, then the latter automatically controls the generation of the soft SUSY breaking masses. Just like the Yukawas, the trilinear A-terms vanish in the family symmetry limit, while the soft scalar masses are universal (assuming a canonical Kähler potential [9]). The goal then is to find a suitable family symmetry, which, combined with the appropriate set of flavon fields that acquire convenient vacuum alignments, generates the correct masses and mixing angles for the fermions and at the same time forces the soft SUSY breaking masses to be approximately diagonal. That way, the SUSY contributions to flavour violating processes are suppressed, exactly as observed. An interesting model should of course be viable with regard to the current experimental limits but it is also expected to generate signatures that can be tested in the future.

Observations of lepton flavour violation (LFV), Electric Dipole Moments (EDMs) or rare B decays at rates beyond that predicted by the SM, could in principle provide insight into the nature of the BSM theory of flavour. While evidence of LFV and EDMs, which are essentially zero in the SM, would be a clear NP signal, B decays, particularly the semileptonic ones, have also always been considered as a powerful NP probe. They allow to indirectly measure decays of the b quark, which is the heaviest quark that lives long enough to hadronise, resulting to multiple decay channels, where independent tests of the SM can be performed. As the size of the NP scale increases, indirect B physics measurements provide sensitivity to a much larger range of scales than direct production. This comes with requirement for increasingly higher both experimental and theoretical accuracy. Within the framework of an effective field theory, any BSM effects manifest themselves through changes to the Wilson coefficients (encoding the high energy/short distance (SD) dynamics), or through new operators (encoding the low energy/long distance (LD) dynamics) becoming relevant. In order to set constraints on the Wilson coefficients, such that NP models can in turn be constrained, the contribution of each effective operator to the observables under consideration needs to be known.

The outline of this thesis is as follows:

Chapter 2 A brief overview of the basic SM features is given, along with its minimal extension to incorporate neutrino masses. After highlighting the main motivations to go beyond the SM and consider a supersymmetric scenario, the basic formal aspects of SUSY are reviewed, before introducing the Minimal Supersymmetric Standard Model (MSSM). Finally, the flavour puzzle and the idea of a family symmetry are discussed, together with the fundamental aspects of model building, in particular when considering a SUSY GUT background.

Chapter 3 The supersymmetric $SU(5) \times S_4 \times U(1)$ family symmetry model is analysed. The model was first introduced in [10, 11], where only the fermionic sector was studied and found to be providing a good description of the SM masses, mixing angles and CP violation. As that analysis ignored effects of canonical normalisation that can significantly perturb

the Yukawa structure [12], in the present work the fermionic sector is revisited, with those effects included. The main focus though is on the flavour and CP violation induced by the soft SUSY breaking sector. It is found that this model can achieve approximate Minimal Flavour Violation (MFV) and the results are given in terms of mass insertion parameters [13], explicit expressions of which are provided. This work has been published in [14].

Chapter 4 Here, the focus is on the phenomenological implications of the model's low energy deviations from MFV. The low energy mass insertion parameters are numerically estimated for well-defined ranges of SUSY parameters and the "naive" model expectations are compared to the results of a numerical scan and the experimental bounds available in the literature. The results are then used to estimate the predictions for EDMs, B and K meson mixing, $\mathrm{BR}(\mu \to e\gamma)$, as well as rare B decays. It is found that the largest observable deviations from MFV come from the LFV process $\mu \to e\gamma$ and the electron EDM. This work has recently been submitted for publication [15].

Chapter 5 A different project, though still related to the flavour sector, is outlined. The contribution of the chromomagnetic operator to semileptonic B decays is computed, using the method of light cone sum rules (LCSRs) [16]. The results are compared with the QCD factorisation (QCDF) computation [17], which however suffers from end-point divergences. This work has been published in [18, 19].

Chapter 6 The conclusions of each Chapter are summarised.

Chapter 2

Theoretical Background

2.1 The Standard Model (SM) of Particle Physics

In what follows, the main features of the Standard Model of Particle Physics are summarised, in the context of a four-dimensional relativistic quantum field theory that, in addition to the space-time symmetry of the Poincaré group, exhibits a local gauge symmetry that describes all known elementary particles and their interactions, excluding gravity.

The field content of the SM is assigned to irreducible representations of the unitary gauge group, under which the electroweak (EW) and the strong nuclear interactions, the latter being described by the theory of quantum chromodynamics (QCD), are symmetric. The EW interactions are described through the Nobel Prize-winning (1979)"Glashow-Salam-Weinberg" model [3], the renormalisability of which was shown by 't Hooft and Veltman, whose work was also honoured with the Nobel prize (1999) [20]. The QCD theory is characterised by two unique features, known as "asymptotic freedom" and "confinement". The strong nuclear force between two particles increases with increasing distance, keeping them confined, while at very short distances it becomes negligible and the particles are considered to be asymptotically free. D. Gross, F. Wilczek and D. Politzer were awarded the Nobel Prize (2004) for their description of asymptotic freedom [21].

The EW symmetry is spontaneously broken to the smaller symmetry of electromagnetism, through the Higgs mechanism [2]. As a result, the unified electromagnetic and weak forces are separated and the matter fields as well as the weak force carriers gain their measured masses. The matter content, consisting of quarks that bind into hadrons and leptons that do not, comes in three flavours/families/generations that only differ in mass. The copies of each first generation particle that belong to the second and third generations have the same properties, like charges and spin but are significantly heavier. In principle, there is no reason why they should exist, as ordinary matter is only made up of particles that belong to the first generation. Their existence, along with the lack of a mechanism that dictates the size of their masses, are part of the still persistent SM flavour puzzle.

2.1.1 Gauge sector and particle content

All known elementary particles seem to exhibit three internal symmetries and their interactions can be described through the corresponding gauge theories:

- The $U(1)_Y$ symmetry of the weak hypercharge Y_W, with its associated gauge field B_μ, where $\mu = 0, 1, 2, 3$ is a Minkowski index.
- The $SU(2)_L$ symmetry of the weak isospin I_W, with three gauge fields W^i_μ, $i = 1, 2, 3$, transforming in a triplet representation, $I_W = 1$. Adopting the chiral Weyl spinor notation for the fermions, the right-handed components transform as singlets, with $I_W = 0$, while the left-handed ones transform as doublets, with $I_W = 1/2$.
- Finally, the $SU(3)_c$ symmetry of colour, known as QCD, with its eight gauge fields G^α_μ, $\alpha = 1, .., 8$, the gluons, that transform in an **8**-plet of the gauge group. There are three colours: red, blue and green and quarks transform in the fundamental triplet representation of $SU(3)_c$, while the colourless leptons are singlets.

The Standard Model of particle physics is therefore a Yang-Mills theory based on the gauge group:

$$G_{SM} = SU(2)_L \times U(1)_Y \times SU(3)_c, \tag{2.1.1}$$

that describes the electroweak and strong nuclear interactions between matter and radiation, with respective coupling constants: g, g' and g_s. The interaction terms are incorporated in the covariant derivative:

$$D_\mu = \partial_\mu - ig' Y_W B_\mu - igW^i_\mu T_i - ig_s G^\alpha_\mu \mathcal{T}_\alpha, \tag{2.1.2}$$

with T_i and $\mathcal{T}_\alpha$ being the generators of $SU(2)_L$ and $SU(3)_c$ respectively. Including the kinetic terms for the gauge bosons, the gauge part of the SM Lagrangian is written as:

$$\mathcal{L}_g = \sum_f \bar{f} i\gamma^\mu D_\mu f - \frac{1}{4} B_{\mu\nu} B^{\mu\nu} - \frac{1}{4}\mathrm{Tr}(W_{\mu\nu} W^{\mu\nu}) - \frac{1}{4}\mathrm{Tr}(G_{\mu\nu} G^{\mu\nu}), \tag{2.1.3}$$

where the sum runs over all fermions, coming in three identical copies (families/generations) and whose properties under G_{SM} are summarised in Table 2.1. The electromagnetic charge operator is given by the Gell-Man-Nishijima formula [22]:

$$Q = I^3_W + Y_W. \tag{2.1.4}$$

2.1.2 Higgs sector

The Lagrangian (2.1.3) describes massless particles, as in an exact gauge theory the underlying symmetries forbid mass terms for the gauge bosons. However, the ones associated with the weak force have been observed to have masses of the order of a hundred GeV. The required dynamics for breaking the EW symmetry and giving mass to the weak gauge bosons are obtained by introducing the Higgs field.

	Quarks			Leptons		Gauge bosons		
	$Q^I = \begin{pmatrix} u_L^I \\ d_L^I \end{pmatrix}$	u_R^I	d_R^I	$L^I = \begin{pmatrix} \nu_L^I \\ e_L^I \end{pmatrix}$	e_R^I	B_μ	W_μ^i	G_μ^α
$SU(3)_c$	**3**	$\bar{\mathbf{3}}$	$\bar{\mathbf{3}}$	**1**	**1**	**1**	**1**	**8**
$SU(2)_L$	**2**	**1**	**1**	**2**	**1**	**1**	**3**	**1**
$U(1)_Y$	1/6	2/3	$-1/3$	$-1/2$	-1	0	0	0

TABLE 2.1: Matter and gauge field content of the SM. I=1,2,3: matter family index, i=1,2,3, α=1,...,8: weak and colour gauge indices, μ=0,..,3: Minkowski index.

The Higgs part of the Lagrangian is:

$$\mathcal{L}_H = (D_\mu H)^\dagger (D^\mu H) - V(H), \qquad V(H) = \mu^2 H^\dagger H + \lambda (H^\dagger H)^2, \tag{2.1.5}$$

where the Higgs field H is a complex $SU(2)$ doublet,

$$H = \begin{pmatrix} \phi^+ \\ \phi^0 \end{pmatrix} = \frac{1}{\sqrt{2}} \begin{pmatrix} \phi_1 + i\phi_2 \\ \phi_3 + i\phi_4 \end{pmatrix} \tag{2.1.6}$$

with ϕ_i being real scalar fields. For $\mu^2 < 0$ and $\lambda > 0$, the minimum of the potential $V(H)$ is located not at the origin of the field configuration but at:

$$H^\dagger H = -\frac{\mu^2}{2\lambda}. \tag{2.1.7}$$

Since electromagnetism is observed as an exact symmetry in nature, this non-zero value should be reached in the neutral direction. Breaking the $SU(2)_L$ symmetry by making the choice: $\phi_1 = \phi_2 = \phi_4 = 0$, $\phi_3 = \upsilon = \sqrt{-\mu^2/\lambda}$ and the $U(1)_Y$ by assigning the charge $Y_W = 1/2$, the non-zero vacuum expectation value of the field:

$$\langle H \rangle = \frac{1}{\sqrt{2}} \begin{pmatrix} 0 \\ \upsilon \end{pmatrix}, \tag{2.1.8}$$

is given to the neutral component, such that the symmetry of electromagnetism with the generator Q is preserved: $Q\langle H \rangle = 0$. In other words, the EW symmetry is broken down to the smaller symmetry of $U(1)_{\text{em}}$,

$$SU(2)_L \times U(1)_Y \to U(1)_{\text{em}}. \tag{2.1.9}$$

The spectrum of the theory is analysed by plugging the Higgs field expanded around its vev into $\mathcal{L}_H$. Since W_μ^3 and B_μ have the same quantum numbers under $U(1)_{\text{em}}$, they mix. The resulting mass eigenstates are:

$$Z_\mu = -\sin\theta_W B_\mu + \cos\theta_W W_\mu^3, \tag{2.1.10}$$

$$A_\mu = \cos\theta_W B_\mu + \sin\theta_W W_\mu^3, \tag{2.1.11}$$

$$W_\mu^\pm = \left(W_\mu^1 \mp W_\mu^2\right)/\sqrt{2}, \tag{2.1.12}$$

where $\cos\theta_W = g/\sqrt{g^2+g'^2}$. The EW gauge bosons acquire mass terms (dropping the $\pm$ index from M_W) [23]:

$$M_W = \frac{g\,\upsilon}{2} \approx 80.39 \text{ GeV}, \quad M_Z = \frac{M_W}{\cos\theta_W} \approx 91.19 \text{ GeV}, \tag{2.1.13}$$

while the photon A_μ remains massless. The relation of M_W with the Fermi constant G_F [23]:

$$G_F = \frac{\sqrt{2}}{8}\frac{g^2}{M_W^2} \approx 1.1667 \times 10^{-5}\text{GeV}^{-2}, \tag{2.1.14}$$

fixes the vacuum expectation value:

$$\upsilon = \left(\sqrt{2}G_F\right)^{-1/2} \approx 246 \text{ GeV}. \tag{2.1.15}$$

The Higgs boson also has a mass term of $\upsilon/\sqrt{2\lambda}$ and the experimentally measured value of ~ 125 GeV [4] implies the tree-level value for the quartic self-coupling: $\lambda \approx 0.13$.

2.1.3 Yukawa sector

Adding by hand fermionic mass terms of the form $m_f \bar{f} f = m_f(\bar{f}_L f_R + \bar{f}_R f_L)$ in (2.1.3) would also be forbidden by the EW gauge symmetry. It is though possible to write the gauge invariant combinations:

$$\mathcal{L}_Y = -Y^e_{ij}\,\bar{L}_i\,H\,e_{R_j} - Y^d_{ij}\,\bar{Q}_i\,H\,d_{R_j} - Y^u_{ij}\,\bar{Q}_i\,\tilde{H}\,u_{R_j} + \text{h.c.}, \tag{2.1.16}$$

where:

$$\tilde{H} \equiv i\tau_2 H^* = \begin{pmatrix} \phi^{0*} \\ -\phi^- \end{pmatrix}, \quad \tau_2 = \begin{pmatrix} 0 & -i \\ i & 0 \end{pmatrix}, \tag{2.1.17}$$

Y^f_{ij} are the Yukawa couplings of the Higgs-fermion interactions and $i,j = 1,2,3$ are generation indices. When the Higgs field develops its non-zero vev, the fermions acquire masses proportional to the eigenvalues of the 3×3 matrices Y^f. Those are found through the singular value decomposition method, that is, by performing bi-unitary rotations as:

$$\text{Diag}\{m^f_1, m^f_2, m^f_3\} = \frac{\upsilon}{\sqrt{2}}(U^f_L)^\dagger Y^f U^f_R. \tag{2.1.18}$$

The unitary matrices $U^f_{L,R}$ rotate the matter fields from the flavour basis to the physical mass basis: $f^{\text{mass}}_{L_i} = (U^f_L)^\dagger_{ij} f^{\text{flav.}}_{L_j}$, $f^{\text{mass}}_{R_i} = (U^f_R)^\dagger_{ij} f^{\text{flav.}}_{R_j}$.

2.1.4 Flavour and CP violation

Unlike the Higgs field, the gauge bosons couple to the matter fields in the flavour basis. The interaction terms, arising from the $\bar{f} i\gamma^\mu D_\mu f$ terms in the Lagrangian in Eq. (2.1.3), in the EW

broken phase, can be written in terms of the currents:

$$\mathcal{L}_g \supset -eJ^\mu_{em}A_\mu - \frac{e}{\sin\theta_W\cos\theta_W}J^\mu_{NC}Z_\mu - \frac{e}{\sqrt{2}\sin\theta_W}J^\mu_{CC}\left(W^+_\mu + \text{h.c.}\right), \tag{2.1.19}$$

with the electromagnetic current given by:

$$J^\mu_{em}{=}Q_u\left(\bar{u}_L\gamma^\mu u_L + \bar{u}_R\gamma^\mu u_R\right) + Q_d\left(\bar{d}_L\gamma^\mu d_L + \bar{d}_R\gamma^\mu d_R\right) + Q_e\left(\bar{e}_L\gamma^\mu e_L + \bar{e}_R\gamma^\mu e_R\right), \tag{2.1.20}$$

where Q_f are the electric charges of the fermions $f = u, d, e$, the weak neutral current being:

$$J^\mu_{NC} = -\frac{1}{2}\bar{d}_L\gamma^\mu d_L - \frac{1}{2}\bar{e}_L\gamma^\mu e_L + \frac{1}{2}\bar{u}_L\gamma^\mu d_L + \frac{1}{2}\bar{\nu}_L\gamma^\mu\nu_L - \sin^2\theta_W J^\mu_{em} \tag{2.1.21}$$

and the weak charged current:

$$J^\mu_{CC} = \bar{u}_L\gamma^\mu d_L + \nu_L\gamma^\mu e_L. \tag{2.1.22}$$

When moving to the mass basis by redefining the matter fields by the unitary matrices $U^f_{L,R}$, the electromagnetic and weak neutral currents remain invariant. The charged current however, is now written as:

$$J^\mu_{CC} = \bar{u}_L\gamma^\mu(U^u_L)^\dagger U^d_L d_L + \nu_L\gamma^\mu(U^\nu_L)^\dagger U^e_L e_L. \tag{2.1.23}$$

Since neutrinos are massless in the SM due to the absence of right-handed components, it is possible to make the choice $U^\nu_L = U^e_L$, leaving invariant the above interaction in the lepton sector. In the quark sector on the other hand, the matrix:

$$V_{CKM} \equiv (U^u_L)^\dagger U^d_L, \tag{2.1.24}$$

known as the Cabibbo-Kobayashi-Maskawa (CKM) matrix [24], is different than the unit matrix, allowing for weak transitions between quarks of different flavours. In the so called "standard parametrisation" [23, 25], it is written in terms of three mixing angles θ_{12}, θ_{23} θ_{13} and one complex phase δ as:

$$V_{CKM}{\equiv}\begin{pmatrix} V_{ud} & V_{us} & V_{ub} \\ V_{cd} & V_{cs} & V_{cb} \\ V_{td} & V_{ts} & V_{tb} \end{pmatrix} = \begin{pmatrix} c_{12}c_{13} & s_{12}c_{13} & s_{13}e^{-i\delta} \\ -s_{12}c_{23} - c_{12}s_{23}s_{13}e^{i\delta} & c_{12}c_{23} - s_{12}s_{23}s_{13}e^{i\delta} & s_{23}c_{13} \\ s_{12}s_{23} - c_{12}c_{23}s_{13}e^{i\delta} & -c_{12}s_{23} - s_{12}c_{23}s_{13}e^{i\delta} & c_{23}c_{13} \end{pmatrix}, \tag{2.1.25}$$

where $c_{ij} \equiv \cos\theta_{ij}$, $s_{ij} \equiv \sin\theta_{ij}$. The angles θ_{ij} parametrise the amount of mixing between the quarks of the i-th and j-th flavours and the Dirac phase δ is the source of parity and charge conjugation (CP) violation, first discovered in the decays of neutral Kaon [26], that resulted in the Nobel Prize being awarded to J. Cronin and Val Fitch in 1980. The experimental measurements of the V_{CKM} elements proves that there is flavour violation in the $W^\pm$ vertex in the SM, as the up- and down-quark Yukawa matrices can not be diagonalised simultaneously. Even though $V_{CKM} \neq \mathbb{1}$, it is strongly hierarchical. This becomes apparent when writing Eq. (2.1.25) in the Wolfstein expansion [27], in terms of a small parameter λ, as:

$$V_{CKM} = \begin{pmatrix} 1-\lambda^2/2 & \lambda & A\,\lambda^3(\rho - i\eta) \\ -\lambda & 1-\lambda^2/2 & A\,\lambda^2 \\ A\,\lambda^3(1-\rho-i\eta) & -A\,\lambda^2 & 1 \end{pmatrix} + \mathcal{O}(\lambda^4), \tag{2.1.26}$$

where:

$$\lambda \equiv \frac{|V_{us}|}{\sqrt{|V_{ud}|^2 + |V_{us}|^2}} = s_{12}, \quad A \equiv \frac{1}{\lambda}\left|\frac{V_{cb}}{V_{us}}\right| = \frac{s_{23}}{\lambda^2}, \quad \rho + i\eta \equiv \frac{V_{ub}^*}{A\,\lambda^3} = \frac{s_{13}e^{i\delta}}{A\,\lambda^3}, \tag{2.1.27}$$

with numerical values [23]:

$$\begin{aligned} \lambda &= 0.22537 \pm 0.00061, \quad A = 0.814^{+0.023}_{-0.024}, \\ \rho\left(1 - \frac{\lambda^2}{2}\right) &= 0.117 \pm 0.021, \quad \eta\left(1 - \frac{\lambda^2}{2}\right) = 0.353 \pm 0.013. \end{aligned} \tag{2.1.28}$$

The amount of CP violation is measured through Jarlskog invariant [28], which is a phase-convention-independent quantity, defined as:

$$\mathrm{Im}[V_{ij}V_{kl}V_{il}^*V_{kj}^*] = J_{CP}\sum_{m,n}\epsilon_{ikm}\epsilon_{jln}, \tag{2.1.29}$$

with the numerical value of [23]:

$$J_{CP} = (3.06^{+0.21}_{-0.20}) \times 10^{-5}. \tag{2.1.30}$$

In the SM, flavour changing neutral currents (FCNC) are forbidden are tree level, whereas the flavour changing charged currents (FCCC) are suppressed, as they can only occur in loops with the $W^{\pm}$ bosons and the CKM matrix is very close to the unit matrix.

2.1.5 Incompleteness of the SM

To this day, experiments keep confirming the Standard Model as a successful theory describing the electroweak and strong nuclear forces. Every particle predicted has been observed, with the last missing piece, the Higgs boson, discovered in July of 2012 at CERN [4]. However, the only observation for physics beyond the SM has been the neutrino oscillations, implying that neutrinos are not massless. This discovery is of great importance for our understanding of the universe and Takaaki Kajita and Arthur B. McDonald were awarded the Nobel Prize in 2015 for their contributions.

- **Neutrino masses and mixing**
  In the SM, the fermionic mass terms arise from interactions of the left- and right-handed fermionic components with the Higgs field. Neutrinos were assumed to be only of the left-handed type, as only those interact via the weak nuclear force, the only observed interaction involving neutrinos. In the absence of right-handed components, neutrinos are strictly massless, in agreement with the experimental data at the time of the SM formulation.

  Since 1998, a number of experiments involving solar [29], atmospheric [30] and reactor [31] neutrinos have established that those particles can change flavour, just like quarks do and therefore have small but non-zero mass. A straightforward way of accommodating

massive neutrinos in the SM, is to extend it with a set of right-handed neutrinos, which are singlets under the SM gauge group. One can then write down a Yukawa term for neutrinos, to be added in Eq. (2.1.16), leading to Dirac masses of the type (2.1.18), once EW symmetry is broken. Such a term would violate the lepton numbers L_e, L_μ, L_τ that distinguish the different flavours of neutrinos but still preserve the total lepton number $L = L_e + L_\mu + L_\tau$. For the masses generated by a neutrino Dirac term to be of the order of 0.1 eV, in accordance with experimental observations, the Yukawa couplings should be as small as 10^{-12}, many orders of magnitude smaller than the corresponding couplings of the rest of the SM fermions.

An alternative approach is to also allow for violation of the total lepton number L at some high energy scale Λ_L. Then, one can write the five-dimensional, non-renormalisable Weinberg operator [32]:

$$-\frac{Y^{\nu}_{ij}}{\Lambda_L}(L_i H)(L_j H) + \text{h.c.} \tag{2.1.31}$$

which generates a Majorana mass term for the neutrinos:

$$-\frac{1}{2}(M_\nu)_{ij}\nu_{L_i}\nu_{L_j} + \text{h.c.}, \tag{2.1.32}$$

where the masses $M_\nu = Y_\nu\, v/\Lambda_L$ arise from the eigenvalues of Y^{ν}_{ij}. Then, the lightness of the neutrinos implies that the scale Λ_L is of the order of 10^{14} GeV, allowing for the couplings Y_ν to be of order one.

Generating the Majorana masses described above in a renormalisable extension of the SM, requires the presence of some heavy neutral particles, identified with right-handed neutrinos. Allowing for tree-level exchange of these heavy particles, reduces to the effective operator in Eq. (2.1.31), once they are integrated out. Then, the light neutrino mass matrix is given by:

$$m_\mu = -m_D^T M_R^{-1} m_D, \tag{2.1.33}$$

where m_D is the Dirac type mass matrix and M_R is the symmetric Majorana mass matrix for the right-handed neutrinos. In this framework, the lightness of the left-handed neutrinos is nicely explained, as they are suppressed by the heavy right-handed neutrino mass scale. Hence, this mechanism is called the "see-saw mechanism" [8].

The fact that neutrinos "oscillate" amongst the three flavour species ν_e, ν_μ, ν_τ, means that their mass matrix is non-diagonal and, in fact, a matrix with large mixing angles is needed for the extraction of its eigenvalues. As a result, the leptonic part of the charged current in Eq. (2.1.23) is brought to a non-diagonal form. In analogy with the quark sector, the product of the matrices that diagonalise the charged-lepton and neutrino mass matrices, is identified with the leptonic mixing matrix, named after Bruno Pontecorvo, Ziro Maki, Masami Nakagawa and Shoichi Sakata (PMNS) [33] and defined as:

$$U_{PMNS} \equiv (U^e_L)^\dagger U^\nu_L. \tag{2.1.34}$$

It can be parametrised in terms of the leptonic mixing angles and the leptonic CP violating phase in analogy to V_{CKM} in Eq. (2.1.25) and if neutrinos are Majorana, it is further post-multiplied by a phase matrix $P \equiv \text{Diag.}\{1, e^{i\beta_{21}/2}, e^{i\beta_{31}/2}\}$. According to the global fit [34],

the mixing angles lie in the 3σ range:

$$\sin^2\theta_{12} \in [0.270, 0.344], \quad \sin^2\theta_{23} \in [0.385, 0.644], \quad \sin^2\theta_{13} \in [0.0188, 0.0251]. \quad (2.1.35)$$

- **Gravity**
  Even minimally extended to incorporate neutrino masses, it is commonly agreed that the SM can not be the whole story. For a start, it does not incorporate gravity and gravitational effects become important near the Planck scale $M_P = \sqrt{8\pi G_{\text{Newton}}} = 2.4 \times 10^{18}$ GeV. We therefore know that some new physics has to be present around that scale. There is though strong theoretical motivation, accompanied with observations that the SM cannot explain, to believe that new physics will be discovered soon, well below the Planck scale.

- **Gauge hierarchy problem**
  The "gauge hierarchy problem" [35], associated with the sensitivity of the Higgs mass to the scale of new physics, is one of them. It arises when computing the quantum corrections to the Higgs bare mass. Introducing a cut-off scale Λ_{NP} at which some new physics is present, the Higgs bare mass receives corrections from higher order Feynman diagrams, involving any particle that couples to the Higgs, propagating in a loop. Schematically, the loop correction due to a fermion f that couples to the Higgs through the Yukawa term $-\lambda_f \bar{f} f H$, is of the form:

$$\delta m_h^2 = -\frac{|\lambda_f|^2}{8\pi^2}\Lambda_{\text{NP}}^2 + \text{log div.} + \text{finite}, \quad (2.1.36)$$

  where the second term in Eq. (2.1.36) grows only logarithmically with Λ_{NP} but the first term, being quadratic in Λ_{NP} is the source of the problem. Assuming that the SM is valid all the way up to the Planck scale, such that $\Lambda_{\text{NP}} = M_P$ and considering the largest contribution to (2.1.36), stemming from the top quark, $\lambda_f \approx 1$, results to radiative corrections δm_h^2 that are about 30 orders of magnitude larger than the Higgs mass squared itself. In other words, the tree-level Higgs mass squared should be of the same order as the radiative corrections $\delta m_h^2 \approx 10^{34}$ GeV^2, such that they cancel at a precision of about 30 digits, to yield $m_h^2 \approx 125^2$ GeV^2! Such an "unnatural" cancellation could be prevented if the new physics scale is not much larger than the measured Higgs mass or if there are some extra contributions to Eq. (2.1.36) which, due to some symmetry, would be able to cancel the quadratic in Λ_{NP} term.

- **Dark matter**
  An astrophysical observation for which the SM provides no explanation is the abundance of Dark Matter (DM). Since the 1930's, when Fritz Zwicky first discovered that the vast majority of the Coma cluster's mass was non-luminous [36], hence "dark", there has been compelling evidence that the ordinary, visible baryonic matter, consisting of protons and neutrons, constitutes less than 5% of the total mass-energy content of the universe. Studies of galaxy rotation curves, gravitational lensing effects, data from the cosmic microwave background radiation, all point towards the existence of some electrically neutral, massive

and stable particles that interact weakly with the ordinary matter. The only possible DM candidate that the SM can provide are the neutrinos. However, neutrinos are relativistic and a dominating DM particle with this property would lead to an unrealistic structure formation [37] of the universe. In addition to this argument, neutrino masses less than 1 eV, are too light to account for the cosmological matter density. Right-handed "sterile" neutrinos though, with masses in the keV range could account for all the dark matter of the universe [38].

- **Matter-antimatter asymmetry**
  The fact that our universe is matter dominated is an ongoing puzzle. Since the SM model is built upon symmetries, it is assumed that at the big-bang there were equal amounts of matter and antimatter. Had there been no mechanism to be held responsible for shifting that balance in favour of matter, all that would be left today after matter-antimatter annihilations, would be a universe of photons. The SM in its minimal form provides no such mechanism but when equipped with right-handed neutrinos, the leading candidate is "leptogenesis", a process that produces an asymmetry between leptons and anti-leptons in the early universe [39].

- **The flavour puzzle**
  There are already 19 free parameters in the SM and with the inclusion of neutrino masses, 7 (if neutrinos are Dirac fields) or 9 (if they are Majorana) new parameters are added. 13 of those are related to the flavour sector, which seems to demand a deeper understanding. The number of generations/flavours is not explained by first principles. The fermionic masses span many orders of magnitude, with the top quark being more than 10^{11} times heavier than the neutrinos. Furthermore, the quarks appear to change flavour/mix only mildly, whereas the leptonic sector exhibits the opposite behaviour. Although we do have a parametrisation to account for the observed masses and mixing angles, a lot of theoretical work has been done towards describing these patterns within a concrete theory based on symmetries.

2.2 Supersymmetry (SUSY)

2.2.1 Motivation

In the 1950s and '60s, with the advances in particle accelerators and detectors, hundreds of subatomic particles were discovered, urging for some classification scheme to put order in the chaos. In 1962, Murray Gell-Mann and Yuval Ne'eman independently proposed the "Eightfold Way" [40], that arranged mesons and baryons into geometrical shapes, based on their baryon number, spin and parity. It was an organisation of the already observed particles in multiplets of the $SU(3)_f$ symmetry of flavour, that also lead to the theoretical prediction of particles that were yet unseen. The natural question that followed was whether it was possible to unify particles of different spin in one multiplet of a symmetry group.

According to a no-go theorem of Coleman and Mandula in 1967 [41], under certain physically reasonable assumptions, the most general symmetry group of the scattering matrix S that describes relativistic particle interactions, is a direct product of the Poincaré group and some

internal symmetry groups, that does not allow for mixing of particles with different spins when the interactions are required to be non-vanishing. In other words, the internal symmetry generators commute with the space-time translation and the rotation and Lorentz boost generators, thus, acting on physical states by multiplying them with momentum- and spin-independent Hermitian matrices. However, in their proof, Coleman and Mandula had only considered bosonic generators. A few years later [42, 43], it was realised that relaxing the assumption that the symmetry generators only satisfy commutation relations, this no-go theorem can be circumvented. Extending the Poincaré algebra by including fermionic generators that satisfy anti-commutation relations, it is possible to unify states with spin differing by 1/2 in a single multiplet.

Such symmetries are called supersymmetries and constitute the only possible non-trivial extension of the Poincaré symmetry, putting the fermionic and bosonic degrees of freedom on the same footing and mixing internal (spin) and space-time states. The famous work of Wess and Zumino in 1974 on four-dimensional supersymmetric field theories [44] established the interest in their systematic study.

Even though no hint of supersymmetry has been experimentally observed so far, it is still a particularly favoured area of research on beyond the SM physics for a number of reasons. One of the most significant ones, is that it provides a solution to the gauge hierarchy problem, as for every fermionic loop correction to the Higgs mass in Eq. (2.1.36), there is a bosonic one contributing with the opposite sign, resulting to a perfect cancellation of the quadratic divergences and naturally allowing for a light Higgs. Supersymmetry also provides for weakly interacting, massive and stable neutral particles, which would be suitable Dark matter candidates. Another important point is that supersymmetry allows the three coupling constants of the SM gauge groups to unify around the energy scale of 10^{16} GeV. On the contrary, within the SM alone, the coupling constants approach one another at around 10^{14} GeV but they do not unify. Finally, when supersymmetry is gauged, i.e. imposed as a local symmetry where the transformations are space-time dependent, gravity is accounted for in the context of supergravity. For these and many more reasons that make this theory attractive, its main features are reviewed in what follows. More details and references can be found in [45–47].

2.2.2 SUSY algebra

In SUSY, bosons are turned into fermions and vice-versa through the fermionic generator Q:

$$Q|\text{boson}\rangle \propto |\text{fermion}\rangle, \qquad Q|\text{fermion}\rangle \propto |\text{boson}\rangle. \tag{2.2.1}$$

This is achieved by the generalisation of a Lie algebra to a graded algebra, where, for a group generator O_α,

$$O_\alpha O_\beta - (-1)^{\eta_\alpha \eta_\beta} O_\beta O_\alpha = i C^\gamma_{\alpha\beta} O_\gamma, \quad \eta_\alpha = \begin{cases} 0 & \text{if } O_\alpha \text{ is bosonic} \\ 1 & \text{if } O_\alpha \text{ is fermionic} \end{cases}. \tag{2.2.2}$$

The bosonic generators are those of the Poincaré group: P_μ for space-time translations and $M_{\mu\nu}$ for Lorentz transformations and the fermionic generators are the Weyl spinors $Q^{\mathcal{A}}_\alpha$, $\bar{Q}^{\mathcal{A}}_{\dot{\alpha}}$, $\mathcal{A} = 1, .., \mathcal{N}$. We shall restrict our discussion to $\mathcal{N} = 1$ SUSY, with only one copy of Qs. Those

commute with the generators of the SM gauge group, while the rest of the relations constituting the SUSY algebra read:

$$\{Q_\alpha, Q_\beta\} = \{\bar{Q}_{\dot{\alpha}}, \bar{Q}_{\dot{\beta}}\} = 0, \tag{2.2.3}$$

$$\{Q_\alpha, \bar{Q}_{\dot{\beta}}\} = 2(\sigma^\mu)_{\alpha\dot{\beta}} P_\mu, \tag{2.2.4}$$

$$[Q_\alpha, P_\mu] = \left[\bar{Q}_{\dot{\alpha}}, P_\mu\right] = 0, \tag{2.2.5}$$

$$[Q_\alpha, M_{\mu\nu}] = -\frac{1}{2} 2(\sigma^\mu)^\beta_\alpha Q_\beta, \tag{2.2.6}$$

$$\left[\bar{Q}_{\dot{\alpha}}, M_{\mu\nu}\right] = -\frac{1}{2} 2(\bar{\sigma}^\mu)^{\dot{\beta}}_{\dot{\alpha}} Q_\beta, \tag{2.2.7}$$

where the spinor indices $\alpha, \beta = 1, 2$ and $\dot{\alpha}, \dot{\beta} = 1, 2$ are raised and lowered by the totally antisymmetric tensor $\epsilon_{\alpha\beta} = \epsilon_{\dot{\alpha}\dot{\beta}} = -\epsilon^{\alpha\beta} = -\epsilon^{\dot{\alpha}\dot{\beta}}$, $\epsilon_{12} = 1$ and the four-vectors of the Pauli matrices are defined as $(\sigma^\mu)_{\alpha\dot{\beta}} \equiv (\mathbb{1}, \sigma^i)_{\alpha\dot{\beta}}$, $(\bar{\sigma}^\mu)^{\dot{\alpha}\beta} \equiv (\mathbb{1}, -\sigma^i)^{\dot{\alpha}\beta}$.

2.2.3 Superspace and Superfields

The single-particle states are organised into supermultiplets, the irreducible representations of the SUSY algebra. Each supermultiplet contains both fermions and bosons which are called superpartners of each other, such that the number of fermionic degrees of freedom (dof) is equal to the number of the bosonic ones. The Poincaré Casimir operator P^2 also commutes with the fermionic operators Q and therefore all states lying within a supermultiplet have equal P^2 eigenvalues, i.e. equal masses.

Just like our familiar fields are functions of the Minkowski space-time coordinates x^μ, supersymmetric fields (superfields) are functions of the superspace coordinates which include two additional Grassmann valued coordinates θ_α, $\bar{\theta}^{\dot{\alpha}}$. A generic superfield $S(x^\mu, \theta_\alpha, \bar{\theta}^{\dot{\alpha}})$ can be expanded in powers of $\theta_\alpha, \bar{\theta}^{\dot{\alpha}}$ and since Grassmann numbers are nilpotent, it is given by a finite number of terms:

$$\begin{aligned} S(x^\mu, \theta^\alpha, \bar{\theta}^{\dot{\alpha}}) = {} & \varphi(x) + \theta\psi(x) + \bar{\theta}\bar{\chi}(x) + \theta\theta M(x) + \bar{\theta}\bar{\theta} N(x) + (\theta\sigma^\nu\bar{\theta}) V_\nu(x) \\ & + (\theta\theta)\bar{\theta}\bar{\lambda}(x) + (\bar{\theta}\bar{\theta})\theta\rho(x) + (\theta\theta)(\bar{\theta}\bar{\theta}) D(x), \end{aligned} \tag{2.2.8}$$

where φ, M, N are complex scalar fields, V_ν is a complex vector field and $\phi_\alpha, \bar{\chi}^{\dot{\alpha}}, \rho_\alpha, \bar{\lambda}^{\dot{\alpha}}$ are Weyl spinors. Thus, S has 16 bosonic and 16 fermionic dof. Let us define the infinitesimal SUSY transformation:

$$S \to \left(1 + i\xi\mathcal{Q} + i\bar{\xi}\bar{\mathcal{Q}}\right) S = S + \delta S, \tag{2.2.9}$$

where $\xi, \bar{\xi}$ are Grassmann variables and

$$\mathcal{Q}_\alpha = -i\partial_\alpha - (\sigma^\mu\bar{\theta})_\alpha \partial_\mu, \qquad \bar{\mathcal{Q}}_{\dot{\alpha}} = i\bar{\partial}_{\dot{\alpha}} + (\theta\sigma^\mu)_{\dot{\alpha}} \partial_\mu, \tag{2.2.10}$$

with $\partial_\alpha \equiv \partial/\partial\theta^\alpha$, $\bar{\partial}_{\dot{\alpha}} \equiv \partial/\partial\bar{\theta}^{\dot{\alpha}}$, $\partial_\mu \equiv \partial/\partial x^\mu$, are representations of the fermionic generators. Then, if S_1, S_2 are superfields, so is their product, as $\delta(S_1\, S_2) = i(\xi\mathcal{Q} + \bar{\xi}\bar{\mathcal{Q}})(S_1\, S_2)$. Any linear combination of superfields is also a superfield and so is $\partial_\mu S$. However, $\partial_\alpha S$ is not, as $\delta(\partial_\alpha S) = \partial_\alpha(\delta S) = i\partial_\alpha\left[(\xi\mathcal{Q} + \bar{\xi}\bar{\mathcal{Q}})S\right] \neq i(\xi\mathcal{Q} + \bar{\xi}\bar{\mathcal{Q}})(\delta S)$. For that reason, the covariant

derivatives are defined as:

$$D_\alpha = i\partial_\alpha + (\sigma^\mu\bar{\theta})_\alpha\partial_\mu, \qquad \bar{D}_{\dot{\alpha}} = -i\bar{\partial}_{\dot{\alpha}} - (\theta\sigma^\mu)_{\dot{\alpha}}\partial_\mu, \tag{2.2.11}$$

satisfying:

$$\{D_\alpha, \bar{D}_{\dot{\beta}}\} = -2(\sigma^\mu)_{\alpha\dot{\beta}}P_\mu, \qquad \{D_\alpha, D_\beta\} = \{\bar{D}_{\dot{\alpha}}, \bar{D}_{\dot{\beta}}\} = 0, \tag{2.2.12}$$

$$\{D_\alpha, \mathcal{Q}_\beta\} = \{D_\alpha, \bar{\mathcal{Q}}_{\dot{\beta}}\} = \{\bar{D}_{\dot{\alpha}}, \mathcal{Q}_\beta\} = \{\bar{D}_{\dot{\alpha}}, \bar{\mathcal{Q}}_{\dot{\beta}}\} = 0, \tag{2.2.13}$$

such that $D_\alpha S$ and $\bar{D}_{\dot{\alpha}} S$ are superfields.

The generic superfield S, defined in Eq.(2.2.8), is not an irreducible representation of the supersymmetric algebra. Those are found by imposing certain constraints upon S, eliminating some of its dof. The simplest supermultiplet consist of a single Weyl fermion and a complex scalar field, having in total four dof. It is called the left-handed chiral or matter scalar supermultiplet, usually denoted by Φ and it is constructed by imposing the constraint:

$$\bar{D}_{\dot{\alpha}}\Phi = 0. \tag{2.2.14}$$

Analogously, the right-handed anti-chiral supermultiplet is defined as:

$$D_\alpha\Phi = 0. \tag{2.2.15}$$

Solving Eq.(2.2.16), a left-handed chiral superfield is written in terms of components as:

$$\begin{aligned}\Phi(x^\mu, \theta^\alpha, \bar{\theta}^{\dot{\alpha}}) = {} & \varphi(x) + \sqrt{2}\theta\psi(x) + \theta\theta F(x) + i\theta\sigma^\mu\bar{\theta}\partial_\mu\varphi(x) \\ & - \frac{i}{\sqrt{2}}(\theta\theta)\partial_\mu\psi(x)\sigma^\mu\bar{\theta} - \frac{1}{4}(\theta\theta)(\bar{\theta}\bar{\theta})\partial_\mu\partial^\mu\varphi(x).\end{aligned} \tag{2.2.16}$$

The scalar part φ can accommodate the Higgs and the superpartners of the SM fermions, called squarks and sleptons. The SM fermions and Higgs' superpartner, the Higgsino, would be contained into the spinor part ψ, while the scalar component F is a non-dynamical auxiliary field, added to match the bosonic and fermionic dof. The SUSY algebra then closes off-shell, while on-shell, F can be eliminated by using its equation of motion. Any holomorphic function of Φ is also a left-handed chiral superfield, while $\bar{\Phi} = \Phi^\dagger$ is a right-handed anti-chiral superfield.

The next irreducible representation of the SUSY algebra is obtained by applying the condition:

$$V = V^\dagger \tag{2.2.17}$$

on the superfield V. This is real vector supermultiplet, comprising by the components:

$$\begin{aligned}V(x^\mu, \theta^\alpha, \bar{\theta}^{\dot{\alpha}}) = {} & C(x) + i\theta\chi(x) - i\bar{\theta}\bar{\chi}(x) + \theta\sigma^\mu\bar{\theta}V_\mu(x) \\ & + \frac{i}{2}\theta\theta\left(M(x) + iN(x)\right) - \frac{i}{2}\bar{\theta}\bar{\theta}\left(M(x) - iN(x)\right) \\ & + i(\theta\theta)\bar{\theta}\left(\bar{\lambda}(x) + \frac{i}{2}\bar{\sigma}^\mu\partial_\mu\chi(x)\right) - i(\bar{\theta}\bar{\theta})\theta\left(\lambda(x) + \frac{i}{2}\sigma^\mu\partial_\mu\bar{\chi}(x)\right) \\ & + \frac{1}{2}(\theta\theta)(\bar{\theta}\bar{\theta})\left(D(x) - \frac{1}{2}\partial^\mu\partial_\mu C(x)\right),\end{aligned} \tag{2.2.18}$$

with C, M, N, D being real scalar fields, χ, λ complex Weyl spinors and V_μ a real spin-one vector field, amounting to eight bosonic and eight fermionic dof. If Λ is a chiral superfield, then $\Lambda + \Lambda^\dagger$, $\Lambda\Lambda^\dagger$,$i(\Lambda - \Lambda^\dagger)$ are real vector superfields, allowing us to consider a general $U(1)$ gauge transformation of the form:

$$V \to V + i(\Lambda - \Lambda^\dagger). \tag{2.2.19}$$

We then have the freedom to choose the components of $i(\Lambda - \Lambda^\dagger)$ such that some of the dof of V are eliminated or "gauged away". Choosing the Wess-Zumino gauge [44]: $C = M = N = 0$, $\chi = 0$, V takes the simple form:

$$V(x^\mu, \theta^\alpha, \bar{\theta}^{\dot{\alpha}})_{|\mathrm{WZ}} = \theta\sigma^\mu\bar{\theta}V_\mu(x) + (\theta\theta)(\bar{\theta}\bar{\lambda}(x)) + (\bar{\theta}\bar{\theta})(\theta\lambda(x)) + \frac{1}{2}(\theta\theta)(\bar{\theta}\bar{\theta})D(x). \tag{2.2.20}$$

The gauge field V_μ can accommodate the SM gauge bosons, λ is its superpartner, called gaugino and the auxiliary field D plays as similar role to the one that F plays in a chiral supermalutiplet.

2.2.4 SUSY Lagrangians

Let us consider a supersymmetric theory that incorporates the SM fermions within chiral supermultiplets. The action has to be invariant under the whole superspace. Thus, it would be sufficient to construct a Lagrangian density, which is obtained by only integrating over the fermionic coordinates, that, under an infinitesimal SUSY transformation, transforms up to a total space-time derivative.

The D-term of a general superfield $S = ... + (\theta\theta)(\bar{\theta}\bar{\theta})D(x)$ and the F-term of a chiral superfield $\Phi = ... + \theta\theta F(x)$ do have this property, as their transformations under (2.2.9) are:

$$\begin{aligned} \delta D &= \frac{i}{2}\partial_\mu\left(\xi\sigma^\mu\bar{\lambda} - \rho\bar{\sigma}^\mu\lambda\right), \\ \delta F &= i\sqrt{2}\bar{\xi}\bar{\sigma}^\mu\theta_\mu\psi. \end{aligned} \tag{2.2.21}$$

Recalling that integrals over Grassmann variables behave like derivatives:

$$\int d^2\theta\,(\theta\theta) = 1, \qquad \int d^2\theta \int d^2\bar{\theta}\,(\theta\theta)(\bar{\theta}\bar{\theta}) = 1, \tag{2.2.22}$$

we see that the most general supersymmetric Lagrangian density for a number of chiral superfields Φ_i, would have the form:

$$\begin{aligned} \mathcal{L} &= \int d^2\theta \int d^2\bar{\theta}\, K(\Phi_i, \Phi_i^\dagger) + \left(\int d^2\theta\, W(\Phi_i) + \mathrm{h.c.}\right) \\ &= K(\Phi_i, \Phi_i^\dagger)_{|D} + \left(W(\Phi_i)_{|F} + \mathrm{h.c.}\right), \end{aligned} \tag{2.2.23}$$

where K is a real function, called the Kähler potential and W is chiral holomorphic function, called the superpotential. The integrations over the Grassmann variables select the D-term (whatever multiplies $(\theta\theta)(\bar{\theta}\bar{\theta})$) of the Kähler potential and the F-term (whatever multiplies $(\theta\theta)$) of the superpotential.

In view of Eq.(2.2.16), a chiral superfield has the same mass dimension as its scalar component, $[\Phi] = [\varphi] = 1$. Furthemore, requiring that the fermions have mass dimension of 3/2, $[\psi] = 3/2$, we are lead to assign the Grassmann variables the dimensions: $[\theta_\alpha] = [\bar{\theta}_{\dot{\alpha}}] = -1/2$. Then, for the Lagrangian density to have mass dimension of four, it follows that $[K] = 2$ and $[W] = 3$.

The simplest renormalisable Kähler potential is:

$$K = \sum_i \Phi_i^\dagger \Phi_i, \tag{2.2.24}$$

which gives rise to the kinetic terms:

$$\mathcal{L}_K = \int d^2\theta \int d^2\bar{\theta}\, K = \sum_i \left(|\partial_\mu \varphi_i|^2 - i\bar{\psi}_i \bar{\sigma}^\mu \partial_\mu \psi_i + |F_i|^2 \right) \tag{2.2.25}$$

A more general form of K would lead to more complicated kinetic terms of the form:

$$\mathcal{L}_K \supset \mathcal{K}^{ij} \left(\partial_\mu \varphi_i \partial^\mu \varphi_j - i\bar{\psi}_i \bar{\sigma}^\mu \partial_\mu \psi_j + F_i F_j^\dagger \right), \tag{2.2.26}$$

where

$$\mathcal{K}^{ij} = \frac{\partial^2 K}{\partial \Phi_i^\dagger \partial \Phi_j}\Big|_{\Phi=\varphi}, \tag{2.2.27}$$

with $\mathcal{K}_{ij} = (\mathcal{K}^{ij})^{-1}$ is the Kähler metric. When $\mathcal{K}_{ij} = \delta_{ij}$, we say that the Kähler potential is canonical, leading to canonical kinetic terms. In order to extract any physically meaningful properties of a theory, the kinetic terms have to be brought to a canonical form through a basis transformation which is known as canonical normalisation.

The most general form of the superpotential is:

$$W = \sum_i \alpha_i \Phi_i + \frac{1}{2} \sum_{ij} m_{ij} \Phi_i \Phi_j + \frac{1}{3!} \sum_{ijk} y_{ijk} \Phi_i \Phi_j \Phi_k, \tag{2.2.28}$$

encoding all renormalisable interactions amongst the scalar and fermionic components of the supermultiplets. Then,

$$\mathcal{L}_W = \sum_i \frac{\partial W}{\partial \Phi_i}\Big|_{\Phi=\varphi} F_i - \frac{1}{2} \sum_{ij} \frac{\partial^2 W}{\partial \Phi_i \partial \Phi_j}\Big|_{\Phi=\varphi} \psi_i \psi_j + \text{h.c.} \tag{2.2.29}$$

and solving the F-term equations of motion, we find the scalar potential of the theory:

$$V = \frac{\partial \bar{W}}{\partial \Phi_i^\dagger} \mathcal{K}_{ij} \frac{\partial W}{\partial \Phi_j^\dagger}\Big|_{\Phi=\varphi}, \tag{2.2.30}$$

where $\mathcal{K}_{ij} = \delta_{ij}$ in the canonical basis.

Making the Lagrangian invariant under some abelian gauge $U(1)$ transformation is achieved by introducing a vector superfield in the Kähler potential, which transforms in the adjoint representation, as shown in Eq.(2.2.19). Φ_i on the other hand transform in the fundamental

representation as:

$$\Phi_i \to e^{-2igq_i\Lambda}\Phi_i, \tag{2.2.31}$$

where q_i are their charges under the $U(1)$ symmetry and g is the gauge coupling. Then, the Kähler potential:

$$K = \Phi_i^\dagger e^{2gq_iV}\Phi_i \tag{2.2.32}$$

is gauge invariant and when expanding the exponential and extracting the $D-$term, in addition to the kinetic terms of the components of the chiral superfields, it gives rise to their interactions with the vector and fermionic components of the vector superfield:

$$\begin{aligned}\mathcal{L}_K &= \int d^2\theta \int d^2\bar{\theta}\, K = (\Phi_i^\dagger e^{2gq_iV}\Phi_i)_{|D} \\ &= \sum_i \Big(|\partial_\mu\varphi_i|^2 - i\bar{\psi}_i\bar{\sigma}^\mu\partial_\mu\psi_i + |F_i|^2 + \sqrt{2}q_i\left(\varphi_i\bar{\lambda}\psi_i + \varphi_i^*\lambda\psi_i\right) \\ &+ g\, q_iV^\mu\left(-\bar{\psi}_i\bar{\sigma}_\mu\psi_i + i\varphi_i^*\partial_\mu\varphi_i - i\varphi_i\partial_\mu\varphi_i^*\right) + q_i(D + q_iV_\mu V^\mu)|\varphi_i|^2\Big).\end{aligned} \tag{2.2.33}$$

Note that if there was only one superfield Φ with non-zero charge under the gauge group, then the superpotential W would be zero. In the case where several superfields Φ_i are involved in the theory, then W can only consist of terms in which the net-charge cancels (gauge singet terms).

We also need to include the kinetic terms for the gauge fields. Introducing the field strength:

$$W_\alpha = -\frac{1}{4}(\bar{D}\bar{D})D_\alpha V, \tag{2.2.34}$$

which is a chiral superfield, such that $W^\alpha W_\alpha$ is also chiral, its F-term transforms as a total spacetime derivative and we can therefore add to the Lagrangian the term:

$$\mathcal{L}_{G_{kin}} = \frac{1}{4}\int d^2\theta\, W^\alpha W_\alpha + \text{h.c.} = \frac{1}{2}D^2 - \frac{1}{4}F_{\mu\nu}F^{\mu\nu} - i\lambda\sigma^\mu\partial_\mu\bar{\lambda}. \tag{2.2.35}$$

Collecting all the terms in the Lagrangian that involve the auxiliary field D,

$$\mathcal{L}_D = \frac{1}{2}D^2 + D\left(\sum_i q_i|\varphi_i|^2\right)^2 \tag{2.2.36}$$

and eliminating D by using its equations of motion, we arive at an additional D-term contribution to the scalar potential:

$$V_D = \frac{1}{2}\left(\sum_i q_i|\varphi_i|^2\right)^2. \tag{2.2.37}$$

2.2.5 The Minimal Supersymmetric Standard Model (MSSM)

It is understood that the SM can only be an effective theory that does not describe physics up to energy scales as large as the Planck scale. As we have seen, SUSY has many attractive features,

making the extension of the SM to a supersymmetric theory a compelling task. There are many ways this can be done, with the simplest possibility being the minimal extension of the SM, known as MSSM, where the SM is extended by one set of fermionic generators ($N = 1$ SUSY) and the particle content is minimal, in the sense that there is no introduction of "unnecessary" fields.

The MSSM is invariant under the SM gauge group $SU(3)_c \times SU(2)_L \times U(1)_Y$ and hence the fields that fall into the same supermultiplet have the same quantum numbers. Each SM fermion, being chiral, is accomodated within a chiral superfield, transforming in the fundamental representation of the gauge group. Since in the SM bosons have different quantum numbers from the fermions, new complex scalar particles are introduced as their superpartners. Those are named by putting an "s" in front of the associated fermion's name, in abbreviation for "scalar". For example, the electron's superpartners are two selectrons, one for each of the electron's handedness. The SM gauge bosons, being vectors, fall into vector superfields that transform in the adjoint representation of the gauge group and their fermionic superpartners therein are called gauginos.

Finally, the Higgs boson has no flavour while the fermions do, so it would fall into a seperate chilar supermultiplet, with its fermionic superpartner called Higgsino. Note though that within the MSSM, one Higgs superfield can not account for the masses of the up-type quarks as well as those of the down-type quarks and the charged leptons. In the SM model, the Yukawa interactions consist of the up-type quarks coupled to the Higgs field and the down-type quarks and the charged leptons coupled to its conjugate. In the MSSM however, these interactions arise from the superpotential, which is a holomorphic function, prohibiting a field and its complex conjugate to appear at the same time. Therefore, two Higgs superfields: H_u and H_d, with opposite hypercharges are required such that all fermions aquire their masses through the Higgs mechanism. Then, the MSSM physical Higgs' bosons are five rather than one. An advantageous consequence of this, is anomaly cancellation. The fermionic component of a Higgs superfield contributes to the SM anomalous triangle diagrams. Having a second Higgs superfield with opposite hypercharge, adds a contribution that cancells the first one, leaving the theory anomally-free.

A further addition to the SM symmetries is a discrete symmetry called R-parity or matter parity. It is introduced in order to forbid some interaction terms in the superpotential that violate either baryon or lepton number and lead to fast proton decay. Under R-parity, each particle is assigned a quantum number:

$$P_R = (-1)^{3(B-L)+2s}, \tag{2.2.38}$$

were B is the baryon number, L is the lepton number and s is the spin. Then, the SM particles are even under P_R whereas their superpartners are odd. Some inportant consequences of R-parity conservation, other than suppressing proton decay, are that superparticles are always produced in pairs, that the lightest supersymmetric particle (LSP), if electrically and colour-neutral, constitutes a dark matter candidate and that every other superparticle will always decay to an odd number of LSPs plus some SM particles.

In summary, the MSSM particle spectrum consists of one superfield per SM field plus an extra Higgs H_u superfield, all shown in Table 2.2. All superfields $\hat{f}$ are labelled by a hat and the

superpartners $\tilde{f}$ of the SM particle f are labelled by a tilde. Note that the $SU(2)_L$ singlets are conjugated and placed into left-handed chiral superfields, denoted as $\hat{f}^c$.

Superfield	Label	Bosonic part	Fermionic part	$SU(3)_c$	$SU(2)_L$	$U(1)_Y$
left-handed chiral	$\hat{Q}_i$	$\tilde{Q}_i = \begin{pmatrix} \tilde{u}_{L_i} \\ \tilde{d}_{L_i} \end{pmatrix}$	$Q_i = \begin{pmatrix} u_{L_i} \\ d_{L_i} \end{pmatrix}$	**3**	**2**	1/6
left-handed chiral	$\hat{U}_i^c$	$\tilde{u}_i^c$	u_i^c	$\bar{\mathbf{3}}$	**1**	−2/3
left-handed chiral	$\hat{D}_i^c$	$\tilde{d}_i^c$	d_i^c	$\bar{\mathbf{3}}$	**1**	1/3
left-handed chiral	$\hat{L}_i$	$\tilde{L}_i = \begin{pmatrix} \tilde{\nu}_{L_i} \\ \tilde{e}_{L_i} \end{pmatrix}$	$L_i = \begin{pmatrix} \nu_{L_i} \\ e_{L_i} \end{pmatrix}$	**1**	**2**	−1/2
left-handed chiral	$\hat{E}_i^c$	$\tilde{e}_i^c$	e_i^c	**1**	**1**	1
left-handed chiral	$\hat{H}_u$	$H_u = \begin{pmatrix} H_u^+ \\ H_u^0 \end{pmatrix}$	$\tilde{H}_u = \begin{pmatrix} \tilde{H}_u^+ \\ \tilde{H}_u^0 \end{pmatrix}$	**1**	**2**	1/2
left-handed chiral	$\hat{H}_d$	$H_d = \begin{pmatrix} H_d^0 \\ H_d^- \end{pmatrix}$	$\tilde{H}_d = \begin{pmatrix} \tilde{H}_d^0 \\ \tilde{H}_d^- \end{pmatrix}$	**1**	**2**	−1/2
vector	$\hat{G}^a$	g^a	$\tilde{g}^a$	**8**	**1**	0
vector	$\hat{W}^k$	W^k	$\tilde{W}^k$	**1**	**3**	0
vector	$\hat{B}$	B	$\tilde{B}$	**1**	**1**	0

TABLE 2.2: MSSM field content and transformation properties. The index $i = 1, 2, 3$ labels the three generations, $a = 1, .., 8$ enumarates the vector superfields of $SU(3)_c$ and $k = 1, 2, 3$ enumerates the vector superfiels of $SU(2)_L$.

2.2.6 The soft SUSY breaking sector

Since one of the main features of a supersymmetric theory is that particles falling in the same supermultiplet have the same mass, we know that SUSY cannot be an exact symmetry in nature. No sfermions or gauginos of equal masses to their SM partners have been observed so far in experiment, necessitating the formulation of a SUSY breaking mechanism. Without reference to the specifics of such a mechanism, the MSSM incorporates all possible renormalisable SUSY breaking terms that respect gauge and $R-$parity invariance, within the Lagrangian:

$$\begin{aligned} -\mathcal{L}_{\text{soft}} = & \frac{1}{2}\left(M_3\tilde{g}\tilde{g} + M_2\tilde{W}\tilde{W} + M_1\tilde{B}\tilde{B} + \text{h.c.}\right) \\ & + m_{H_u}^2|H_u|^2 + m_{H_d}^2|H_d|^2 + m_{Q_{ij}}^2\tilde{Q}_i^\alpha\tilde{Q}_j^{\alpha *} + m_{L_{ij}}^2\tilde{L}_i^\alpha\tilde{L}_j^{\alpha *} \\ & + m_{u_{ij}^c}^2\tilde{u}_i^{c*}\tilde{u}_j^c + m_{d_{ij}^c}^2\tilde{d}_i^{c*}\tilde{d}_j^c + m_{e_{ij}^c}^2\tilde{e}_i^{c*}\tilde{e}_j^c \\ & + \epsilon_{\alpha\beta}\left(-bH_d^\alpha H_u^\beta - A_{ij}^u H_u^\alpha\tilde{Q}_i^\beta\tilde{u}_j^c + A_{ij}^d H_d^\alpha\tilde{Q}_i^\beta\tilde{d}_j^c + A_{ij}^e H_d^\alpha\tilde{L}_i^\beta\tilde{e}_j^c + \text{h.c.}\right), \end{aligned} \quad (2.2.39)$$

where α, β are spinor indices and $i, j = 1, 2, 3$ are family indices. The first line of Eq.(2.2.39) contains the gaugino mass terms and the second and third lines the mass terms for the scalar

partners of the SM fermions and for the two Higgses. The last line introduces Yukawa-like trilinear A-terms and a Higgs mixing term. They all break supersymmetry, as they explicitly contribute only to the particles appearing therein but not to their superpartners. They are described as "soft" because all couplings are of positive mass dimension and the cancellation of quadratic divergences in the theory is preserved.

$\mathcal{L}_{\text{soft}}$ not only introduces a vast number of new parameters [48] the origin of which has to be explained but also gives rise to flavour and CP violating transitions. The soft trilinear and scalar masses are matrices in family space and the symmetries of the MSSM alone do not restrict their structure. Any off-diagonal elements can contribute to FCNC and face severe bounds from experimental measurements which, so far, are in agreement with the SM expectations. Also, the soft parameters introduce many complex phases that are constrained by flavour changing as well as flavour conserving transitions, such as CP asymmetries in rare decays or electric dipole moments. These issues are the source of the so-called SUSY flavour and CP problems.

In order to reduce the SUSY parameter space, the MSSM can be embedded in a Grand Unified Theory (GUT) background, where the gauge couplings unify at the high energy scale M_{GUT}. Then, all three gaugino masses are considered to be equal to the parameter $M_{1/2}$ and there are correlations amongst the matter sectors that transform in the same multiplets of the GUT group. A further simplified scenario is the constrained MSSM (CMSSM), inspired by minimal supergravity [49], which also assumes that all scalar masses are equal to m_0 at the high scale, stemming from diagonal and universal mass matrices. At the same time, the trilinear matrices are aligned with the Yukawas, with a proportionality constat A_0, while requiring EWSB fixes the absolute value of the μ parameter. Then, the theory only is formulated in terms of $M_{1/2}$, m_0, A_0, $\text{sgn}(\mu)$ and the ratio of the Higgs'vevs: $\tan_\beta \equiv t_\beta = \upsilon_u/\upsilon_d$. However, such assumptions are not fully justified by symmetry arguments.

2.3 Family symmetries

2.3.1 Motivation

A lot of effort has been put into trying to understand the flavour structure of the Standard Model. Its peculiar features involve hierarchical fermion masses, with the down-type quark and charged-lepton masses showing a similar pattern which differs from that of the up-type quarks, while neutrinos are signicantly lighter than all other particles. Flavour mixing in the lepton sector appears to be much larger than in the quark sector and the number of generations is not explained.

The explanation of the origin of mass comes through the Higgs mechanism. Particles that interact with the Higgs field aquire a mass that is proportional to the strength of that interaction. The masses of the SM particles have been well measured over the years and the Higgs discovery in the summer of 2012 sealed that description. What determines the strength of such interactions though, is still unknown.

As we have seen, the quark and charged-lepton mass terms are generated through Yukawa couplings to the Higgs doublet and the neutrino masses through the see-saw mechanism. Since

there are three generations/families for each fermion, those couplings are 3×3 matrices in family space and, when diagonalised, they result to fermionic masses that span many orders of magnitude. It has been observed that the mass and flavour bases are misaligned, allowing particles of different families to mix. Even though the amount of this misalignment has been measured, there is no confirmed theory that predicts it.

If we wish to understand the pattern of the fermionic masses and mixing angles, we need to reveal what dictates the structure of the Yukawa and Majorana matrices, when they are formulated in the flavour basis. Of course, one can always argue that Nature has simply chosen the observed patterns for no apparent reason; but ever since the ancient times, the quest for insight in physical reality and methodologies of physical inquiries has been based upon symmetry arguments. Making use of the phenomenological consequences that a successful unification theory can have, the strategy that has been extensively used in the literature is to unify the three families of matter within irreducible representations of a family symmetry. This symmetry is subsequently broken by some Higgs-like fields that develop non-zero vacuum expectation values. Then, the non-trivial structures that are observed at the low energy scales where experiments are performed, can be interpreted and analysed as the remaining traces of the family symmetry.

2.3.2 Model building

The idea of the family symmetry is based on extending the Standard Model gauge group by a family symmetry group G_F, which admits triplet representations, under which the three families of matter unify. The field content of the theory is enlarged, by introducing a set of heavy scalar fields Φ, called flavons, that are neutral under the SM gauge group but can couple to the usual matter fields. The operators that are allowed by all symmetries are typically non-renormalisable, of the form:

$$O_Y = f_i \frac{\Phi_i \, \Phi_j}{M^2} f_j^c H, \tag{2.3.1}$$

where i, j are generation indices, f is a left-handed fermion, f^c is a CP conjugated right-handed fermion, H is the Higgs field and M is a heavy mass scale that acts as an ultraviolet (UV) cut-off. The flavon fields aquire non-vanishing vacuum expectation values, spontaneously breaking G_F and giving rise to effective Yukawa couplings [1]:

$$Y_{ij} = \frac{\langle \Phi_i \rangle \langle \Phi_j \rangle}{M^2}, \tag{2.3.2}$$

in terms of the small parameter:

$$\lambda = \frac{\langle \Phi \rangle}{M}, \tag{2.3.3}$$

which can serve as an expansion parameter that is used to build the desired hierarchical Yukawa matrices. The goal is to find an appropriate set of symmetries which, combined with a suitable vacuum alignment for the flavons, will give rise to acceptable masses and mixing angles.

[1] It is more convenient in what follows to use the convention in Eq. (2.3.1) for the extraction of the Yukawa couplings. Then, the coupling in Eq. (2.3.2) corresponds to the conjugate of the couplings in Eq. (2.1.16).

This approach was first introduced in 1979 by Froggatt and Nielsen [5], who considered a $U(1)_{\rm FN}$ symmetry, broken by a single flavon field, carrying a $U(1)_{\rm FN}$ charge of -1. The objective was to explain the structure of the quark sector only. The charge assignment of quarks of different generations was chosen such that each element of the effective Yukawa matrices could be written as a power of λ times some order-one undetermined coefficient. The result was Yukawa matrices with the appropriate hierarchical structure but the predictability of the masses and mixing angles was hindered by the unspecified coefficients.

The Froggatt-Nielsen mechanism has since been extended to involve non-Abelian symmetries, which are more predictive, as they provide relations between different Yukawa couplings and are more successful in explaining the non-hierarchical leptonic mixing pattern. There have been extensive studies on family symmetries based on the continuous groups $U(2)$ [50], $SO(3)$ [51] and $SU(3)$ [9, 52–54]. However, when a continuous symmetry is spontaneously broken by the flavon vevs, one has to deal with the appearance of Goldstone modes. The use of a discrete symmetry instead, is safe from such effects and also offers smaller irreducible representations that can accommodate the flavon fields, simplifying their vacuum alignment. Furthermore, discrete symmetries are more suitable for describing particular mixing patterns of the leptonic mixing matrix. Together with the requirement for triplet irreducible representations that could justify the number of fermionic generations, the greatest interest in the last decade has been shown in discrete subgroups of $SU(3)$, with particular attention drawn to the groups A_4 [55, 56] and S_4 [10, 11, 57–59].

Until 2012, the neutrino tribimaximal (TB) mixing pattern proposed by Harrison, Perkins and Scott [60]:

$$U_{\rm TB} = \begin{pmatrix} \frac{2}{\sqrt{3}} & \frac{1}{\sqrt{3}} & 0 \\ -\frac{1}{\sqrt{6}} & \frac{1}{\sqrt{3}} & -\frac{1}{\sqrt{2}} \\ -\frac{1}{\sqrt{6}} & \frac{1}{\sqrt{3}} & \frac{1}{\sqrt{2}} \end{pmatrix}, \tag{2.3.4}$$

was in good agreement with the experimental data. the entries of $U_{\rm TB}$ correspond to $\sin^2\theta_{12} = \frac{1}{3}$, i.e. the three states $|\nu_e\rangle$, $|\nu_\mu\rangle$, $|\nu_\tau\rangle$ mix equally, $\sin^2\theta_{23} = \frac{1}{2}$, i.e. the $|\nu_\mu\rangle$ and $|\nu_\tau\rangle$ states mix maximally and $\sin^2\theta_{13} = 0$ due to no observation of electron neutrino disappearance at the time. These fractional numbers could be arising from the Clebsch-Gordan coefficients of a symmetry group. On the contrary, the neutrino mass squared differences (and the masses of the charged leptons) are not characterised by such distinct fractional relations amongst each-other. This suggests that the effective neutrino mass matrix m_ν is diagonalised by a matrix with mixing angles that are independent of the eigenvalues, i.e. m_ν is a "form diagonalisable" matrix [61]. Such a property is known to be realised in the context of discrete flavour groups.

Assuming that neutrinos are Majorana, their mass matrix, in the basis of diagonal charged leptons, is invariant under a Klein group $Z_2^S \times Z_2^U$, with generators denoted by S and U. In the case of TB mixing, they have the simple representation:

$$S = \frac{1}{3}\begin{pmatrix} -1 & 2 & 2 \\ 2 & -1 & 2 \\ 2 & 2 & -1 \end{pmatrix}, \quad U = -\begin{pmatrix} 1 & 0 & 0 \\ 0 & 0 & 1 \\ 0 & 1 & 0 \end{pmatrix}. \tag{2.3.5}$$

If the flavour symmetry of neutrinos is a residual symmetry of the family symmetry and it is preserved to leading order in the neutrino sector, then the family symmetry should contain both S and U. The smallest group with this property is S_4. It is the group of permutations of four objects, having $4! = 24$ elements [62].

In 2012, $\theta_{13} \neq 0$ was measured from RENO [63], MINOS [64], Daya Bay [65] and T2K [66] experiments, with a current fit value of $[7.87, 9.11]^o$ in the 3σ range [34]. However, this mixing angle is still a lot smaller than the other two, which are still consistent with TB mixing (see Eq. (2.1.35)) and therefore such a mixing pattern would be a good first approximation of a flavour model. Of course, deviations are needed, which can arise from charged lepton corrections or from the neutrino sector, by partly breaking the Klein symmetry at higher orders. For reviews on how discrete symmetry models can be modified to account for a non-zero θ_{13}, see [6].

2.3.3 Extension to SUSY GUTs

The family symmetry formalism can be extended to include supersymmetry. In the context of a supersymmetric field theory, all fields become superfields and the Yukawa operators arise from the superpotential of the theory, while the kinetic terms and the soft scalar masses, come from the Kähler potential. Now the flavour problem increases dramatically, as the superpartner masses and mixing angles must also be explained, while facing severe experimental constraints on the off-diagonal elements of the soft mass matrices.

In principle, when one writes the soft SUSY breaking Lagrangian, there is nothing that forces the mass matrices to be approximately diagonal. When those matrices are rotated into the mass basis of the SM fermions, the so called super-CKM (SCKM) basis [47], they participate in loop diagrams inducing FCNC. So, the extra issue to be taken care of is to control these off-diagonalities, as well as the new sources of CP violation, in order to stay in agreement with experiment.

One of the most important aspects in building a model of flavour by means of a family symmetry, is the appropriate alignment of the flavon vevs in flavour space. Supersymmetry provides a convenient mechanism for this [55]. A new set of fields is introduced, called "driving fields", together with a $U(1)_R$ symmetry. Under this symmetry, the Higgs superfields and the flavons are uncharged, the superfields containing the SM fields and the right-handed neutrinos have a charge of $+1$ and the driving fields carry a charge of $+2$. In that way, driving fields do not interact directly with the SM particles but can couple to the flavons and appear only linearly in the so called "driving piece" of the superpotential. By requiring that supersymmetry is unbroken at the scale of family symmetry braking, the F-terms of the driving fields have to vanish, leading to a particular alignment of the flavon vevs.

Let us now consider a supersymmetric theory supplemented with a family symmetry and see how the Yukawa and soft mass matrices are constructed. The first step is to write down all operators that couple them to the Higgs and matter fields, in order to generate the Yukawa piece of the superpotential (dropping the "hat" superfield notation for simplicity and including right-handed neutrinos):

$$W_Y = \epsilon_{\alpha\beta} \left(Y^u_{ij} H^\alpha_u Q^{\beta i} u^{c\,j} + Y^d_{ij} H^\alpha_d Q^{\beta i} d^{c\,j} + Y^\nu_{ij} H^\alpha_u L^{\beta i} \nu^{c\,j} + Y^e_{ij} H^\alpha_d L^{\beta i} e^{c\,j} \right). \tag{2.3.6}$$

The flavon expansion that, once the family symmetry is broken, will lead to W_Y in Eq. (2.3.6), can be schematically represented as:

$$H\, f \sum_{\Phi\,\Phi'} y^{f\,f^c}_{\Phi\,\Phi'} \frac{\Phi \otimes \Phi'}{M^2} f^c, \tag{2.3.7}$$

where $y^{f\,f^c}_{\Phi\,\Phi'}$ are some order-one coefficients. Demanding that CP is only broken by complex flavon vevs, all flavon expansion coefficients are real.

In the soft SUSY breaking sector, the piece of Eq. (2.2.39) containing the trilinear scalar couplings has a similar form to Eq. (2.3.6). Assuming that SUSY breaking is triggered at some mass scale M_X by some "hidden sector" superfield(s) X, which acquires a non-zero vev on its auxiliary F-component: $\langle F_X \rangle \neq 0$, then the trilinear piece comes from the F-terms of operators of the form:

$$\frac{X}{M_X} H\, f \sum_{\Phi\,\Phi'} a^{f\,f^c}_{\Phi\,\Phi'} \frac{\Phi \otimes \Phi'}{M^2} f^c. \tag{2.3.8}$$

In a supergravity framework, if the superpotential contains no direct couplings of X to the Yukawa sector and the Kähler potential is canonical, "picking up" the F-term of X in Eq. (2.3.8), would lead to (once the relevant fields develop their vevs) $A_f \propto Y_f$ [52, 67], as $a^{f\,f^c}_{\Phi\,\Phi'}$ would be equal to $y^{f\,f^c}_{\Phi\,\Phi'}$ up to a global factor. However, it has been shown that any superfield with a non-zero vev on its scalar component $\langle \Phi \rangle$, is expected to also develop a non-zero $\langle F_\Phi \rangle$, of the order of $m_{3/2} \times \langle \Phi \rangle$, where $m_{3/2}$ is the gravitino mass; and so do the flavons [53, 68]. As a result, when taking the F-terms of Eq. (2.3.8), there are additional, flavon-induced contributions to the trilinears A_{ij}, of the form: $\langle F_\Phi \partial_\Phi W_Y \rangle_{ij}$. In a family symmetry model with multiple effective operators, these contributions cause each of the coefficients $a^{f\,f^c}_{\Phi\,\Phi'}$ in Eq. (2.3.7) to differ from the corresponding ones in Eq. (2.3.6) by a different order-one factor [68]. In other words, any universality between the trilinear and the Yukawa matrices is inevitably lost. As discussed in [52], there are mechanisms for suppressing $\langle F_\Phi \rangle$, such that they are a lot smaller than $m_{3/2} \times \langle \Phi \rangle$, in order to keep flavour violating effects under control.

However, in the context of a global SUSY model that does not refer to a specific SUSY breaking mechanism, the vacuum alignment of the flavon F-terms and their contribution to the generation of the SUSY breaking terms can be derived through the minimization of the scalar potential, after promoting the mass parameters and the coupling constants of the theory to constant superfields with non-zero F-terms. This procedure is thoroughly described in [69], where it is found that $\langle F_\Phi \rangle$ are indeed of the order of $m_{SUSY} \times \langle \Phi \rangle$ and the orientations of these two types of vevs in flavour space are aligned to LO in the expansion parameter $\langle \Phi \rangle / M$.

Turning to the Kähler potential, to include the SUSY breaking effects, one can add a non-renormalisable operator involving the hidden sector superfield and write the effective potential as:

$$K_f = \sum_f f^\dagger \left[\left(c^f_0 + b^f_0 \frac{X^\dagger X}{M_X^2} \right) \mathbb{1} + \alpha \sum_\Phi \left(c^f_\Phi + b^f_\Phi \frac{X^\dagger X}{M_X^2} \right) \frac{\Phi \otimes \Phi^\dagger}{M^2} \right] f, \tag{2.3.9}$$

where $c^f_{0(\Phi)}$, $b^f_{0(\Phi)}$ are some order-one coefficients and α is a constant. Let us first consider $\alpha = 0$. Taking the D-term of (2.3.9), we obtain the kinetic terms in Eq. (2.2.25) (as the factor $1 + c^f_0 \langle |X|^2 \rangle / M_X^2$ can be absorbed into a simple redefinition of the matter superfields), while the term proportional to b^f_0 gives rise to effective soft scalar mass squared terms that are universal in flavour space and of the order of $\langle |F_X|^2 \rangle / M_X^2$. However, when we allow for couplings between the matter superfields and the flavons by turning on $\alpha \neq 1$, these non-renormalisable terms inevitably lead to a complicated Kähler metric once the relevant fields develop their non-zero vevs. Not only it is different from the unit matrix but also develops off-diagonal entries. We therefore need to go through the "canonical normalisation" procedure [12] and make a change of basis by redefining the superfields, such that $\tilde{K}_{ij} = \mathbb{1}$ in flavour space, leading to the standard kinetic terms. Then, the Yukawa, trilinear and soft scalar matrices have to be rotated into that basis.

In general, the Yukawa and trilinear terms vanish in the family symmetry limit, while the soft scalar masses are universal. When this symmetry is broken, any universality is lost. Since the soft scalar mass squared matrices and the non-canonical Kähler metrics arise from a similar flavon expansion, they acquire a similar structure in flavour space. In complete analogy, the flavour structure of the trilinear matrices is similar to the one of the Yukawas. The fact that c^f_Φ and b^f_Φ are different to account for SUSY breaking effects, means that the scalar masses will remain off-diagonal in the canonical basis. Similarly, as $a^{f\,f^c}_{\Phi\,\Phi'} \neq y^{f\,f^c}_{\Phi\,\Phi'}$ the trilinear matrices will not be diagonal in the mass basis of the SM fermions (SCKM basis). It is these off-diagonalities that a successful flavour model has to control, in addition to providing a good description of the SM fermionic masses and mixing angles.

Since Renormalisation Group (RG) running down to the electroweak scale is not expected to significantly alter these off-diagonal entries, the model should not predict large scalar mixings at the high energy scale. This scale could be the unification scale when SUSY is embedded in a GUT background. In such a case, quarks and leptons, as well as squarks and sleptons, fall into the same supermultiplets, providing us with correlations between the hadronic and leptonic sectors, which, after a computable RG running, can be inferred at the low energy scale where experiments are performed.

The simplest GUT group that can be used to make a model of flavour more constraining, is $SU(5)$ [70]. $SU(5)$ unification implies that the matter superfields fall into (three copies of) the $F = \bar{\mathbf{5}}$ and $T = \mathbf{10}$ representations as follows:

$$T = \frac{1}{\sqrt{2}} \begin{pmatrix} 0 & -u^c_G & u^c_B & -u_R & -d_R \\ u^c_G & 0 & -u^c_R & -u_B & -d_B \\ -u^c_B & u^c_R & 0 & -u_G & -d_G \\ u_R & u_B & u_G & 0 & -e^c \\ d_R & d_B & d_G & e^c & 0 \end{pmatrix} \quad \text{and} \quad F = (d^c_R \; d^c_B \; d^c_G \; e \; -\nu)\,, \tag{2.3.10}$$

where r, b, g correspond to the $SU(3)_c$ charges: red, blue and green. The decompositions into representations of the SM gauge group $SU(3)_c \times SU(2)_L \times U(1)_Y$ read:

$$\bar{\mathbf{5}} = (\bar{\mathbf{3}}, \mathbf{1}, 1/3) \oplus (\mathbf{1}, \bar{\mathbf{2}}, -1/2), \quad \mathbf{10} = (\bar{\mathbf{3}}, \mathbf{1}, -2/3) \oplus (\mathbf{3}, \mathbf{2}, 1/6) \oplus (\mathbf{1}, \mathbf{1}, 1), \tag{2.3.11}$$

with $F = (d^c, L)$ and $T = (u^c, Q, e^c)$, while right-handed neutrinos can be added as $SU(5)$ singlets. The Higgs doublets H_u and H_d fall within the $SU(5)$ multiplets $H_{\mathbf{5}}$ and $H_{\bar{\mathbf{5}}}$, such that the Yukawa terms for one family are written as:

$$y_u H_{\mathbf{5}_i} T_{jk} T_{lm} \epsilon^{ijklm} + y_\nu H_{\mathbf{5}_i} F^i \nu^c + y_d H^i_{\bar{\mathbf{5}}} T_{ij} F^j, \tag{2.3.12}$$

where ϵ^{ijklm} is the $SU(5)$ totally antisymmetric tensor with $i, j, k, l, m = 1, ..., 5$. Those terms correspond to the SM couplings:

$$y_u H_u Q u^c + y_\nu H_u L \nu^c + y_d (H_d Q d^c + H_d e^c L). \tag{2.3.13}$$

The unification of the down-quark and electron Yukawa coupling implied in (2.3.13) is consistent with the measurements of the down and electron masses but such a relation can not hold for the the other two generations. This difficulty is bypassed by considering the Higgs representation $H_{\bar{\mathbf{45}}}$, coupling to the second generation, through the $SU(5)$ singlet $(Y^d)_{22} H_{\bar{\mathbf{45}}} T_2 F_2$, corresponding to $(Y^d)_{22}(H_d Q_2 d^c_2 - 3 H_d e^c_2 L_2)$. Now H_d is actually a linear combination of the electroweak doublets contained in $H_{\bar{\mathbf{5}}}$ and $H_{\bar{\mathbf{45}}}$ and the factor -3 is an $SU(5)$ Clebsch-Gordan coefficient. For hierarchical Yukawa matrices with a zero (11) element, this set up results in the Georgi-Jarlskog relations [71]:

$$y_b = y_\tau, \quad y_s = \frac{y_\mu}{3}, \quad y_d = 3 y_e \tag{2.3.14}$$

at the GUT scale, which lead to acceptable low energy scale mass relations.

Chapter 3

Approaching Minimal Flavour Violation from an $SU(5) \times S_4 \times U(1)$ SUSY GUT

3.1 Introduction

This chapter details my research on a model of flavour, using a family symmetry in a supersymmetric GUT background. The work presented here has been published in [14].

As discussed in Chapter 2, the SM should be viewed as an effective field theory and some new physics is required, in particular in view of the Higgs naturalness problem. In the absence of any observed beyond the SM flavour and CP violation, strong restrictions are imposed on the flavour sector of any new physics model. In order to tackle this issue, a sort of "straw man" ansatz for flavour has emerged, known as Minimal Flavour Violation (MFV) [72–75]. In this scenario, all flavour and CP violating transitions are postulated to originate in the SM Yukawa matrices, so that they are governed by the CKM matrix.

When considering supersymmetry softly broken at the TeV scale, then in general large deviations from SM flavour and CP violation are expected. SUSY models include one-loop diagrams that lead to FCNC processes, such as e.g. $b \to s\gamma$ and $\mu \to e\gamma$, at rates which are proportional to the size of the off-diagonal elements of the scalar mass matrices, when the latter have been rotated to the SCKM basis where the Yukawa matrices are diagonal [47]. These SUSY contributions are tamed in the CMSSM, which postulates that, at the high energy scale, the SUSY breaking squark and slepton mass squared matrices are proportional to the unit matrix and the trilinear A-terms are additionally aligned with the Yukawa matrices, resulting in an (approximate) MFV-like structure at low energy [47], which is of course exactly what is observed.

The CMSSM framework always provides a safe haven from unwanted flavour violation, although CP violation in the form of Electric Dipole Moments (EDMs) remains a challenge [47]. However, with SUSY and SUSY GUTs, the real challenge is to justify the assumptions of MFV or the CMSSM, while at the same time providing a realistic explanation of quark and lepton (including

neutrino) masses, mixing and CP violation. This non-trivial balancing act is the concern of this chapter.

The discovery of neutrino mass and mixing has spurred a lot of work aiming to describe flavour in terms of a family symmetry of some kind, in particular a discrete non-Abelian family symmetry [6]. It was realised early on that in such models, the idea of spontaneous flavour and CP violation could effectively tame the flavour and CP problems of the SM [53, 68] without any *ad hoc* assumptions about MFV or the CMSSM. The main point is that the same family symmetry introduced to understand the Yukawa sector will also automatically control the flavour structures of the soft SUSY breaking sector. The only requirement is that the SUSY breaking hidden sector must respect the family symmetry, which means that the family (and CP) symmetry breaking scale must be below the mass scale of the messengers which mediate SUSY breaking to the visible sector. SUSY breaking in the framework of supergravity provides one attractive example for such a situation.

The idea of using family symmetry to solve the SUSY favour and CP problems has been fully explored in the framework of an $SU(3)$ family symmetry [9, 52, 53], where it was shown that the flavons that spontaneously break the family and CP symmetries will perturb the SUSY breaking sector, leading to tell-tale signatures of flavour and CP violation beyond MFV or the CMSSM. Unfortunately, these signatures which were expected to appear in Run1 of the LHC [76] did not in fact materialise, and indeed the allowed parameter space has been much reduced [77].

In the set-up discussed in [9, 52], the extra flavour violation can be understood as follows. At leading order, the CMSSM is enforced by the $SU(3)$ family symmetry acting on the squark and slepton mass squared matrices. However, the fact that $SU(3)$ is broken by flavons, as it must be to generate the quark and lepton masses, means that flavons appearing in the Kähler potential will give important contributions to the kinetic terms, requiring extra canonical normalisation (CN) [12]. Since SUSY breaking also originates from the Kähler potential, the flavons will also modify the couplings of squarks and sleptons to the fields with SUSY breaking F-terms. The resulting corrections to the soft mass squared matrices from unity will be similar to the corrections of the corresponding Kähler metrics, yet both are not aligned due to independent coefficients of the relevant operators. Likewise, the trilinear soft SUSY breaking A-terms will replicate the flavour structure of the Yukawa matrices prior to CN but exact alignment is not realised. All of this occurs at the high scale. Additional flavour violation is generated by renormalisation group (RG) running down to low energy, taking into account the see-saw mechanism [8] which will involve thresholds at an intermediate scale, see e.g. [78, 79].

In this chapter, it will be shown how approximate MFV can emerge from an $SU(5)$ SUSY GUT, supplemented by an $S_4 \times U(1)$ family symmetry. The fermionic sector of this model has been studied in [10, 11], where it was found that it provides a good description of all quark and lepton (including neutrino) masses, mixings and CP violation. The aim of the work presented here is to introduce the model's soft SUSY breaking sector, which is assumed to respect the family symmetry and investigate the flavour and CP violating (as well as conserving) effects that emerge.

One of the foremost steps in doing so, is to formulate the flavon expansion of the Kähler potential, which gives rise to the soft scalar mass matrices and the kinetic terms of the theory. As already pointed out, the breaking of the family symmetry necessarily leads to non-canonical kinetic

Field	T_3	T	F	N	H_5	$H_{\overline{5}}$	$H_{\overline{45}}$	Φ_2^u	$\widetilde{\Phi}_2^u$	Φ_3^d	$\widetilde{\Phi}_3^d$	Φ_2^d	$\Phi_{3'}^\nu$	Φ_2^ν	Φ_1^ν	η
$SU(5)$	**10**	**10**	$\overline{\mathbf{5}}$	**1**	**5**	$\overline{\mathbf{5}}$	$\overline{\mathbf{45}}$	**1**	**1**	**1**	**1**	**1**	**1**	**1**	**1**	**1**
S_4	**1**	**2**	**3**	**3**	**1**	**1**	**1**	**2**	**2**	**3**	**3**	**2**	**3′**	**2**	**1**	$\mathbf{1}^{(\prime)}$
$U(1)$	0	5	4	-4	0	0	1	-10	0	-4	-11	1	8	8	8	7

TABLE 3.1: The matter, Higgs and flavon superfields of the model in [11] together with their transformation properties under the imposed $SU(5) \times S_4 \times U(1)$ symmetry.

terms, such that a change of basis is required in order to make any meaningful predictions for the physical implications of the model. In fact, [12] highlights that the change to the canonical basis can significantly perturb the structure of the Yukawa matrices. These CN effects were ignored in [10, 11]. Therefore, the present work revisits the fermionic sector by including such corrections and it is advantageously found that the results of [10, 11] for the fermionic masses and mixing angles survive to leading order.

The vacuum alignment of the flavons is also revisited and calculated up to the eighth order in the expansion parameter (2.3.3), in order to keep track of different CP violating phases accompanying the higher order corrections. Also, there may be some notational differences with [10, 11] as, here, subleading terms are not absorbed into the corresponding leading ones, neither in the parametrisation of the flavon vevs nor in the parametrisation of the mass matrices, such that the series expansions can be performed in a systematic way.

The model's predictions for the SUSY contributions to any process, are given in terms of a set of dimensionless parameters, known as "mass insertion" parameters [13]. Those parameters are calculated in full detail and their low energy expressions are given in the SCKM basis, including effects of RG running. Remarkably, due to the peculiar flavour structure of the model, it is found that the small family symmetry $S_4 \times U(1)$ is sufficient to reproduce the effects of low energy MFV much more accurately than the previous $SU(3)$ family symmetry model.

3.2 Trimaximal $\boldsymbol{SU(5) \times S_4 \times U(1)}$ model

In this section, the basic ingredients of the supersymmetric model of flavour proposed in [11] are presented. It is capable of correctly describing a sizeable reactor neutrino mixing angle θ_{13}^l by generating a neutrino mass matrix of trimaximal form. The model represents a modification of an earlier tri-bimaximal model [10] with only minor changes.

Being formulated in a supersymmetric $SU(5)$ grand unified framework, the matter superfields fall into the **10** and $\overline{\mathbf{5}}$ representations, as shown in Eq. (2.3.10). Table 3.1 lists the matter, Higgs and flavon superfields together with their transformation properties under the imposed $SU(5) \times S_4 \times U(1)$ symmetry. Details of the non-Abelian finite group S_4 are provided in Appendix A. The $\overline{\mathbf{5}}$-plets, labelled by F, are assigned to a triplet representation of S_4, while the **10**-plets are split into an S_4 doublet T for the first two generations and an S_4 singlet T_3 for the third generation. In addition, right-handed neutrinos N are introduced, transforming

in the same S_4 triplet representation as F. The $SU(5)$ Higgs fields $H_{\mathbf{5}}$, $H_{\bar{\mathbf{5}}}$ and $H_{\mathbf{\bar{45}}}$ are all S_4 singlets. Note that each of these GUT Higgs representations contains an $SU(2)_L$ Higgs doublet. Therefore, the low energy doublet H_u originates from $H_{\mathbf{5}}$, while H_d arises from a linear combination of $H_{\bar{\mathbf{5}}}$ and $H_{\mathbf{\bar{45}}}$ [45, 47][1] . In addition, a number of flavon fields Φ_ρ^f are introduced, which are labelled by the corresponding S_4 representation ρ, as well as the fermion sector f to which they couple at leading order (LO). Two flavons, Φ_2^u and $\tilde{\Phi}_2^u$, generate the LO up-type quark mass matrix. Three flavon multiplets, Φ_3^d, $\tilde{\Phi}_3^d$ and Φ_2^d, are responsible for the down-type quark and charged lepton mass matrices. Finally, the right-handed neutrino mass matrix is generated from the flavon multiplets $\Phi_{3'}^\nu$, Φ_2^ν and Φ_1^ν, as well as the flavon η which is responsible for breaking the tri-bimaximal pattern of the neutrino mass matrix to a trimaximal one at subleading order [11]. The additional $U(1)$ symmetry has been introduced in order to control the coupling of the flavon fields to the matter fields in a way which avoids significant perturbations of the LO flavour structure by higher-dimensional operators [10].

The vacuum structure of the flavon fields arises from the F-term alignment mechanism [55]. Introducing a set of so-called driving fields, the corresponding F-term conditions give rise to particular flavon alignments as described in Appendix B. To LO, these are given as [10, 11]:

$$\frac{\langle\Phi_2^u\rangle}{M} = \begin{pmatrix} 0 \\ 1 \end{pmatrix} \phi_2^u \, \lambda^4, \qquad \frac{\langle\tilde{\Phi}_2^u\rangle}{M} = \begin{pmatrix} 0 \\ 1 \end{pmatrix} \tilde{\phi}_2^u \, \lambda^4, \tag{3.2.1}$$

$$\frac{\langle\Phi_3^d\rangle}{M} = \begin{pmatrix} 0 \\ 1 \\ 0 \end{pmatrix} \phi_3^d \, \lambda^2, \qquad \frac{\langle\tilde{\Phi}_3^d\rangle}{M} = \begin{pmatrix} 0 \\ -1 \\ 1 \end{pmatrix} \tilde{\phi}_3^d \, \lambda^3, \qquad \frac{\langle\Phi_2^d\rangle}{M} = \begin{pmatrix} 1 \\ 0 \end{pmatrix} \phi_2^d \, \lambda \ , \tag{3.2.2}$$

$$\frac{\langle\Phi_{3'}^\nu\rangle}{M} = \begin{pmatrix} 1 \\ 1 \\ 1 \end{pmatrix} \phi_{3'}^\nu \, \lambda^4, \qquad \frac{\langle\Phi_2^\nu\rangle}{M} = \begin{pmatrix} 1 \\ 1 \end{pmatrix} \phi_2^\nu \, \lambda^4, \qquad \frac{\langle\Phi_1^\nu\rangle}{M} = \phi_1^\nu \, \lambda^4, \qquad \frac{\langle\eta\rangle}{M} = \phi^\eta \, \lambda^4, \tag{3.2.3}$$

where $\lambda \approx 0.225$ is the Wolfenstein parameter [27] and the ϕs are dimensionless order one parameters. Imposing CP symmetry of the underlying theory, all coupling constants can be taken as real [58, 59], so that CP is broken spontaneously by generally complex values for the ϕs. M denotes a generic messenger scale which is common to all the non-renormalisable effective operators and assumed to be around the scale of grand unification. Considering also subleading terms in the flavon potential, these LO vacuum alignments receive corrections which are parametrised by small shifts as discussed in Appendix B and shown explicitly in Eq. (B.4). Throughout the calculations, such shifts have been taken into account, as well as all other subleading effects. As the LO results for the mass insertion parameters depend solely on the LO structure of the model, only the LO analysis is reported in the main part of this chapter. When giving explicit expressions, only the leading contributions will be shown and the additional higher order corrections will be omitted for the sake of simplicity. Such approximations will be indicated by $\approx$ throughout the chapter. Finally, the vevs of the two neutral Higgses are:

[1] As $H_{\bar{\mathbf{5}}}$ and $H_{\mathbf{\bar{45}}}$ transform differently under $U(1)$, it is clear that the mechanism which spawns the low energy Higgs doublet H_d must necessarily break $U(1)$. Although the discussion of any details of the $SU(5)$ GUT symmetry breaking (which, e.g., could even have an extra dimensional origin) is beyond the scope of this work, it is remarked that a mixing of $H_{\bar{\mathbf{5}}}$ and $H_{\mathbf{\bar{45}}}$ could be induced by introducing the pair $H_{\mathbf{24}}^{\pm}$ with $U(1)$ charges ± 1 in addition to the standard $SU(5)$ breaking Higgs $H_{\mathbf{24}}^0$.

$$v_u = v\ t_\beta/\sqrt{1+t_\beta^2}, \qquad v_d = v/\sqrt{1+t_\beta^2}, \tag{3.2.4}$$

where $t_\beta \equiv \tan(\beta) = \frac{v_u}{v_d}$ and $v = \sqrt{v_u^2 + v_d^2} = 174$ GeV [2].

3.3 Kähler potential

A characteristic feature of any effective theory is the presence of non-renormalisable operators which are only constrained by the imposed symmetries. In the context of supersymmetry, this is the case for both the superpotential and the Kähler potential. The effective coupling of flavons to the Kähler potential gives rise to kinetic terms with a non-canonical Kähler metric $\mathcal{K} \neq \mathbb{1}$,

$$\mathcal{L}_{\text{kin}} \;=\; \mathcal{K}_{ij}\left(\partial_\mu \tilde{f}_i^* \partial^\mu \tilde{f}_j + i\, f_i^* \partial_\mu \bar{\sigma}^\mu f_j\right), \tag{3.3.1}$$

where $\tilde{f}$ and f are, respectively, the scalar and fermionic components of a generic chiral superfield $\hat{f}$. In order to extract physically meaningful properties of a model, the kinetic terms have to be brought to a canonical form via a basis transformation [12].

In the context of $SU(5)$, a Kähler metric is encountered for each of the three GUT representations containing the matter fields. These will be denoted by $\mathcal{K}_T$, $\mathcal{K}_F$ and $\mathcal{K}_N$, respectively. Using the symmetries of Table 3.1, the expansions of these 3×3 matrices in terms of flavon fields can be obtained from:

$$\left(T^\dagger\ T_3^\dagger\right)(\mathcal{K}_T - \mathbb{1})\begin{pmatrix} T \\ T_3 \end{pmatrix} = \sum_n \left(T^\dagger\ T_3^\dagger\right)\begin{pmatrix} c_n^{K_{T_{22}}}\left(\mathcal{R}_2\right)_n & c_n^{K_{T_{i3}}}\left(\mathcal{R}_4\right)_n \\ \left[c_n^{K_{T_{i3}}}\left(\mathcal{R}_4\right)_n\right]^\dagger & c_n^{K_{T_{33}}}\left(\mathcal{R}_3\right)_n \end{pmatrix}\begin{pmatrix} T \\ T_3 \end{pmatrix}, \tag{3.3.2}$$

$$F^\dagger(\mathcal{K}_F - \mathbb{1})F = \sum_n F^\dagger\left[c_n^{K_F}\left(\mathcal{R}_1\right)_n\right]F\ , \tag{3.3.3}$$

$$N^\dagger(\mathcal{K}_N - \mathbb{1})N = \sum_n N^\dagger\left[c_n^{K_N}\left(\mathcal{R}_1\right)_n\right]N\ , \tag{3.3.4}$$

where c_n are order one coefficients which can be assumed to be real thanks to the imposed CP symmetry. Products of flavons which are allowed to couple in the Kähler potential are collected in the tuples $\mathcal{R}_i$, which in turn are unions of tuples $\mathcal{S}_i$. They contain all possible combinations of up to eight flavons with a minimum contribution of order λ^8 and are defined as:

$$\mathcal{R}_1 = \mathcal{S}_1 \cup \mathcal{S}_2 \cup \mathcal{S}_3\,, \qquad \mathcal{R}_2 = \mathcal{S}_1 \cup \mathcal{S}_2\,, \qquad \mathcal{R}_3 = \mathcal{S}_1\,, \qquad \mathcal{R}_4 = \mathcal{S}_4\,, \tag{3.3.5}$$

$$\begin{aligned}\mathcal{S}_1 = \Bigg\{ & \frac{\Phi_2^d\Phi_2^{d\dagger}}{M^2}, \frac{\Phi_3^d\Phi_3^{d\dagger}}{M^2}, \frac{\tilde{\Phi}_3^d\tilde{\Phi}_3^{d\dagger}}{M^2}, \frac{\Phi_2^u\Phi_2^{u\dagger}}{M^2}, \frac{\tilde{\Phi}_2^u\tilde{\Phi}_2^{u\dagger}}{M^2}, \frac{(\tilde{\Phi}_2^u)^2}{M^2}, \frac{\Phi_{3'}^\nu\Phi_{3'}^{\nu\dagger}}{M^2}, \frac{\Phi_2^\nu\Phi_2^{\nu\dagger}}{M^2}, \frac{\Phi_1^\nu\Phi_1^{\nu\dagger}}{M^2}, \frac{\eta\eta^\dagger}{M^2}, \\ & \frac{(\Phi_3^d)^2\Phi_1^\nu}{M^3}, \frac{(\Phi_3^d)^2\Phi_2^\nu}{M^3}, \frac{(\Phi_3^d)^2\Phi_{3'}^\nu}{M^3}, \frac{\Phi_2^d\Phi_2^{d\dagger}\tilde{\Phi}_2^u}{M^3}, \frac{\Phi_2^{d\dagger}\tilde{\Phi}_3^{d\dagger}\Phi_2^u}{M^3}, \frac{(\Phi_2^d\Phi_2^{d\dagger})^2}{M^4}, \frac{(\Phi_3^d\Phi_3^{d\dagger})^2}{M^4}, \\ & \frac{\Phi_2^d\Phi_2^{d\dagger}\Phi_3^d\Phi_3^{d\dagger}}{M^4}, \frac{\Phi_2^d\Phi_2^{d\dagger}\tilde{\Phi}_3^d\tilde{\Phi}_3^{d\dagger}}{M^4}, \frac{(\Phi_2^d\Phi_2^{d\dagger})^2\tilde{\Phi}_2^u}{M^5}, \frac{(\Phi_2^d\Phi_2^{d\dagger})^3}{M^6}, \frac{(\Phi_2^d\Phi_2^{d\dagger})^4}{M^8} + \text{all h.c.}\Bigg\}, \end{aligned} \tag{3.3.6}$$

[2] Absorbing the factor of $\sqrt{2}$ in Eq. (2.1.15) into v.

$$\mathcal{S}_2 = \left\{ \frac{\tilde{\Phi}_2^u}{M}, \frac{\Phi_1^\nu \Phi_2^{\nu\dagger}}{M^2}, \frac{\Phi_2^{d\dagger} \tilde{\Phi}_3^{d\dagger} \Phi_2^u}{M^3} + \text{all h.c.} \right\}, \tag{3.3.7}$$

$$\mathcal{S}_3 = \left\{ \frac{(\Phi_2^d)^4 \Phi_3^d}{M^5}, \frac{\Phi_1^\nu \Phi_{3'}^{\nu\dagger}}{M^2}, \frac{\Phi_2^\nu \Phi_{3'}^{\nu\dagger}}{M^2}, \frac{\Phi_3^d \Phi_3^{d\dagger} \tilde{\Phi}_2^u}{M^3}, \frac{(\Phi_2^d)^5 \Phi_2^{d\dagger} \Phi_3^d}{M^7} + \text{all h.c.} \right\}, \tag{3.3.8}$$

$$\mathcal{S}_4 = \left\{ \frac{(\Phi_2^d)^5}{M^5}, \frac{\eta (\Phi_2^{d\dagger})^2}{M^3}, \frac{\Phi_2^d \Phi_3^d \Phi_{3'}^\nu}{M^3}, \frac{\Phi_2^d \Phi_3^d (\Phi_3^{d\dagger})^2}{M^4}, \frac{(\Phi_2^{d\dagger})^2 \Phi_3^d \Phi_3^{d\dagger}}{M^4}, \frac{(\Phi_2^{d\dagger})^3 \Phi_2^\nu}{M^4}, \right.$$
$$\left. \frac{(\Phi_2^{d\dagger})^3 (\Phi_3^{d\dagger})^2}{M^5}, \frac{\eta \Phi_2^d (\Phi_2^{d\dagger})^3}{M^5}, \frac{(\Phi_2^d)^6 \Phi_2^{d\dagger}}{M^7} \right\}. \tag{3.3.9}$$

$\mathcal{S}_1$ and $\mathcal{S}_2$ contain combinations of flavons with $U(1)$ charges that sum up to zero. They come form S_4 invariants when contracted with two doublets or two triplets. Therefore, $\mathcal{S}_1$ and $\mathcal{S}_2$ contribute to $\mathcal{K}_F$, $\mathcal{K}_N$ and the upper-left 2×2 block of $\mathcal{K}_T$ in Eq. (3.3.2). Moreover, the combinations in $\mathcal{S}_1$ can be contracted to S_4 invariants so that they additionally contribute to the lower-right 1×1 block of $\mathcal{K}_T$. $\mathcal{S}_3$ gives further contributions to $\mathcal{K}_F$ and $\mathcal{K}_N$ but not to $\mathcal{K}_T$. Finally, the combinations contained in $\mathcal{S}_4$ have $U(1)$ charges which add up to 5 and allow for S_4 contractions to a doublet. Hence, they contribute to the off-diagonal upper-right block of $\mathcal{K}_T$. Note that the effects of the operators involving the flavon field η are independent of its S_4 transformation properties as a $\mathbf{1}$ or a $\mathbf{1}'$.

When calculating the Kähler metric from the expressions of Eqs. (3.3.2-3.3.4), it is important to take into account all invariant S_4 contractions of two matter fields with a given product of flavons.

3.3.1 Kähler metric with LO corrections

It is straightforward though tedious to determine the matrices $\mathcal{K}_T$, $\mathcal{K}_F$ and $\mathcal{K}_N$ from Eqs. (3.3.2-3.3.4). Keeping only the LO corrections to the unit matrix, for the $\mathbf{10}$ of $SU(5)$ it is found that:

$$\mathcal{K}_T - \mathbb{1} \approx \begin{pmatrix} (k_5 + k_1)\,\lambda^2 & k_2\,\lambda^4 & k_4\, e^{-i\theta_4^k} \lambda^6 \\ \cdot & (k_5 - k_1)\,\lambda^2 & k_3\, e^{-i\theta_3^k} \lambda^5 \\ \cdot & \cdot & k_6\,\lambda^2 \end{pmatrix}, \tag{3.3.10}$$

where k_i denote real order one coefficients, and θ_i^k are phases associated with the generally complex flavon vevs. Here and throughout the chapter, the dots in the lower-left corner of the matrix represent the complex conjugates of the corresponding entries in the upper-right part of the matrix. The operator $T^\dagger \Phi_2^d \Phi_2^{d\dagger} T/M^2$ gives rise to the parameters k_1 and k_5 through different S_4 contractions, while k_6 is due to $T_3^\dagger \Phi_2^d \Phi_2^{d\dagger} T_3/M^2$. Being associated with $T^\dagger \tilde{\Phi}_2^u T/M$, the parameter k_2 carries no phase factor because $\tilde{\phi}_2^u \in \mathbb{R}$, see Appendix B. Finally, the (13) and (23) elements originate from $T^\dagger \eta (\Phi_2^{d\dagger})^2 T_3/M^3$ and $T^\dagger (\Phi_2^d)^5 T_3/M^5$, respectively. Making use of the phases of the LO flavon vevs, given explicitly in Eq. (B.2), the phases of Eq. (3.3.10) can be written as:

$$\theta_4^k = \theta_3^d - \theta_2^d \qquad \text{and} \qquad \theta_3^k = -5\theta_2^d\,, \tag{3.3.11}$$

where θ_2^d and θ_3^d are the phases of the LO vevs ϕ_2^d and ϕ_3^d, respectively.

Analogously, one obtains the matrix $\mathcal{K}_F$:[3]

$$\mathcal{K}_F - \mathbb{1} \approx \begin{pmatrix} 2K_1 & K_3 & K_3 \\ \cdot & K_2 - K_1 & K_3 \\ \cdot & \cdot & -(K_2 + K_1) \end{pmatrix} \lambda^4 \,, \tag{3.3.12}$$

where $K_i \in \mathbb{R}$. The parameters on the diagonal, K_1 and K_2, originate from different contractions of the term $F^\dagger \Phi_3^d \Phi_3^{d\dagger} F/M^2$. The off-diagonal elements, parametrised by K_3, are derived from the operator $F^\dagger \tilde{\Phi}_2^u F/M$ and are real due to $\tilde{\phi}_2^u \in \mathbb{R}$. Hence the LO correction to $\mathcal{K}_F$ from unity is given by a real matrix.

The corresponding Kähler metric $\mathcal{K}_N$ for the right-handed neutrinos is identical to $\mathcal{K}_F$ up to a difference in the order one coefficients of the individual corrections. Therefore,

$$\mathcal{K}_N - \mathbb{1} \approx \begin{pmatrix} 2K_1^N & K_3^N & K_3^N \\ \cdot & K_2^N - K_1^N & K_3^N \\ \cdot & \cdot & -(K_2^N + K_1^N) \end{pmatrix} \lambda^4 \,, \tag{3.3.13}$$

where the coefficients K_i^N are again real.

3.3.2 Canonical normalisation

The expansion of the Kähler potentials in terms of flavon insertions leads to non-canonical kinetic terms. In order to bring the Kähler potential back to its canonical form, a non-unitary transformation has to be applied on the matter superfields. The canonical normalisation procedure introduces the 3×3 matrices P_A which transform the matter superfields $A = T, F, N$ as $A = P_A^{-1} A'$ so that

$$(P_A^\dagger)^{-1} \mathcal{K}_A P_A^{-1} = \mathbb{1} \quad \Longrightarrow \quad \mathcal{K}_A = P_A^\dagger P_A \,. \tag{3.3.14}$$

A prescription for deriving the matrices P_A can be found in Appendix C.1. To LO, they take the simple form

$$P_T \approx \begin{pmatrix} 1 & \frac{k_2}{2}\lambda^4 & \frac{k_4}{2} e^{-i\theta_4^k} \lambda^6 \\ \cdot & 1 & \frac{k_3}{2} e^{-i\theta_3^k} \lambda^5 \\ \cdot & \cdot & 1 \end{pmatrix}, \qquad P_{F(N)} \approx \begin{pmatrix} 1 & \frac{K_3^{(N)}}{2}\lambda^4 & \frac{K_3^{(N)}}{2}\lambda^4 \\ \cdot & 1 & \frac{K_3^{(N)}}{2}\lambda^4 \\ \cdot & \cdot & 1 \end{pmatrix}. \tag{3.3.15}$$

In the following sections, the structure of the Yukawa matrices is studied as well as the soft supersymmetry breaking sectors. The CN transformations of Eq. (3.3.15) have to be applied to these before aiming at a physical interpretation of the resulting patterns.

[3] There are also flavour universal λ^2 and λ^4 contributions to the diagonal elements of $\mathcal{K}_F$ which, however, do not effect the LO results.

3.4 Yukawa sector after CN

In this section, the fermionic sector of the model is studied, completing the analysis of [10, 11] by including the effects of canonical normalisation. The parametrisation differs slightly from the one used in [10, 11] as, in this work, none of the higher order corrections to the mass matrices or the flavon vevs are absorbed into the associated leading order terms. See Appendix B for more details.

3.4.1 Charged fermions

3.4.1.1 Up-type quarks

The Yukawa matrix of the up-type quarks can be constructed by considering all the possible combinations of a product of flavons with TTH_5 for the upper-left 2×2 block, with TT_3H_5 for the $(i3)$ elements, and with $T_3T_3H_5$ for the (33) element. The operators which generate a contribution to the Yukawa matrix of order up to and including λ^8 are

$$\begin{aligned} &y_t T_3 T_3 H_5 + \frac{1}{M} y_1^u TT\Phi_2^u H_5 + \frac{1}{M^2} y_2^u TT\Phi_2^u \tilde{\Phi}_2^u H_5 \\ &+ \frac{1}{M^3} y_{3,4}^u T_3 T_3 (\Phi_3^d)^2 \Phi_{2,3'}^\nu H_5 + \frac{1}{M^5} y_5^u TT(\Phi_2^d)^2 (\Phi_3^d)^3 H_5 + \frac{1}{M^5} y_6^u TT_3 (\Phi_2^d)^3 (\Phi_3^d)^2 H_5 \ , \end{aligned} \tag{3.4.1}$$

where the parameters y_t and y_i^u are real order one coefficients. Inserting the flavon VEVs and expanding the S_4 contractions of Eq. (3.4.1) using the Clebsch-Gordan coefficients that can be found in [10] , gives rise to the up-type Yukawa matrix at the GUT scale:

$$\mathcal{Y}^u_{\text{GUT}} \approx \begin{pmatrix} y_u e^{i\theta_u^y} \lambda^8 & 0 & 0 \\ 0 & y_c e^{i\theta_c^y} \lambda^4 & z_2^u e^{i\theta_2^{zu}} \lambda^7 \\ 0 & z_2^u e^{i\theta_2^{zu}} \lambda^7 & y_t \end{pmatrix} \ , \tag{3.4.2}$$

where the relation to the flavon vevs, see Eqs. (3.2.1-3.2.3) as well as Appendix B, is given by:

$$y_u e^{i\theta_u^y} = y_2^u \phi_2^u \tilde{\phi}_2^u + y_1^u \delta_{2,1}^u, \qquad y_c \, e^{i\theta_c^y} = y_1^u \phi_2^u, \qquad z_2^u e^{i\theta_2^{zu}} = y_6^u (\phi_2^d)^3 (\phi_3^d)^2 \ . \tag{3.4.3}$$

Applying the phases of the LO flavon vevs as given in Eq. (B.2), it is found moreover that

$$\theta_u^y = \theta_c^y = 2\theta_2^d + 3\theta_3^d, \qquad \theta_2^{z_u} = 3\theta_2^d + 2\theta_3^d, \tag{3.4.4}$$

where the fact that the shift $\delta_{2,1}^u$ of the flavon vev$\langle \Phi_2^u \rangle$ in the first component is of order λ^8 and proportional to $(\phi_2^d)^2 (\phi_3^d)^3$ has also been used, see. Eq. (B.5). It is worth noting that the (12), (13) and (21), (31) elements of Eq. (3.4.2) remain zero up to order λ^8.

Changing to the basis with canonical kinetic terms, $(P_T^{-1})^T \mathcal{Y}^u_{\text{GUT}} P_T^{-1}$ is calculated. For convenience an extra phase redefinition on the right-handed superfields is applied,

$$Q_u = \text{diag}(e^{i\theta_u^y}, e^{i\theta_u^y}, 1). \tag{3.4.5}$$

As a result, the up-type quark Yukawa matrix in the canonical basis is obtained:

$$Y^u_{\rm GUT} \approx \begin{pmatrix} y_u\,\lambda^8 & -\frac{1}{2}k_2\,y_c\,\lambda^8 & -\frac{1}{2}k_4\,y_t e^{i\theta^k_4}\,\lambda^6 \\ -\frac{1}{2}k_2\,y_c\lambda^8 & y_c\,\lambda^4 & -\frac{1}{2}k_3\,y_t e^{i\theta^k_3}\lambda^5 \\ -\frac{1}{2}k_4\,y_t e^{i(\theta^k_4-\theta^y_u)}\,\lambda^6 & -\frac{1}{2}k_3\,y_t e^{i(\theta^k_3-\theta^y_u)}\lambda^5 & y_t \end{pmatrix} . \tag{3.4.6}$$

Compared to Eq. (3.4.2), the canonical normalisation has significantly modified the off-diagonal entries: the texture zeros are filled in; moreover, the (23) and (32) elements feature a reduced λ-suppression.

3.4.1.2 Down-type quarks and charged leptons

The Yukawa matrices of the down-type quarks and the charged leptons can be deduced from the superpotential operators:

$$\begin{aligned} &y^d_1\frac{1}{M}FT_3\Phi^d_3H_{\bar5} + y^d_2\frac{1}{M^2}(F\tilde\Phi^d_3)_1(T\Phi^d_2)_1H_{4\bar5} + y^d_5\frac{1}{M^3}(F(\Phi^d_2)^2)_3(T\tilde\Phi^d_3)_3H_{\bar5} \\ &+ y^d_3\frac{1}{M^2}FT_3\Phi^d_3\tilde\Phi^u_2H_{\bar5} + y^d_4\frac{1}{M^2}FT_3\eta\tilde\Phi^d_3H_{\bar5} + y^d_6\frac{1}{M^3}FT\Phi^d_2\tilde\Phi^d_3\tilde\Phi^u_2H_{4\bar5} \\ &+ y^d_7\frac{1}{M^5}FT(\Phi^d_2)^2(\Phi^d_3)^3H_{4\bar5} + y^d_8\frac{1}{M^5}FT_3(\Phi^d_2)^3(\Phi^d_3)^2H_{4\bar5} + y^d_9\frac{1}{M^6}FT_3(\Phi^d_2)^4(\Phi^d_3)^2H_{\bar5}\,, \end{aligned} \tag{3.4.7}$$

where the y^d_i are real order one coefficients. For the operators proportional to y^d_2 and y^d_5, specific contractions have been chosen as described in [10, 11], such that the Gatto-Sartori-Tonin (GST) [80] and Georgi-Jarlskog (GJ) [71] relations are satisfied at LO. The contractions for all other operators are not restricted to special choices; however, it was checked that in all cases, the LO result can simply be parametrised by an effective coupling constant which is given as a combination of the individual contributions from each contraction. It is worth noting that the operator proportional to y^d_4 is only allowed if η transforms as a trivial singlet under S_4. Separating the contributions of $H_{\bar5}$ and $H_{4\bar5}$, the S_4 contractions give rise to:

$$\mathcal{Y}_{\bar5} \approx \begin{pmatrix} 0 & \tilde x_2 e^{i\theta^{\tilde x}_2}\lambda^5 & -\tilde x_2 e^{i\theta^{\tilde x}_2}\lambda^5 \\ -\tilde x_2 e^{i\theta^{\tilde x}_2}\lambda^5 & 0 & \tilde x_2 e^{i\theta^{\tilde x}_2}\lambda^5 \\ z^d_3 e^{i\theta^{z_d}_3}\lambda^6 & z^d_2 e^{i\theta^{z_d}_2}\lambda^6 & y_b e^{i\theta^y_b}\lambda^2 \end{pmatrix}, \quad \mathcal{Y}_{4\bar5} \approx \begin{pmatrix} z^d_1 e^{i\theta^{z_d}_1}\lambda^8 & 0 & 0 \\ 0 & y_s e^{i\theta^y_s}\lambda^4 & -y_s e^{i\theta^y_s}\lambda^4 \\ 0 & 0 & 0 \end{pmatrix}. \tag{3.4.8}$$

The parameters in these expressions are related to the flavon vevs as defined in Eqs. (3.2.1-3.2.3) and Appendix B via:

$$\tilde x_2 e^{i\theta^{\tilde x}_2} = y^d_5(\phi^d_2)^2\tilde\phi^d_3\,, \quad y_b e^{i\theta^y_b} = y^d_1\phi^d_3\,, \quad z^d_2 e^{i\theta^{z_d}_2} = y^d_1\delta^d_{3,3} + y^d_3\phi^d_3\tilde\phi^u_2\,, \quad z^d_3 e^{i\theta^{z_d}_3} = y^d_1\delta^d_{3,1}\,,$$

$$y_s e^{i\theta^y_s} = y^d_2\phi^d_2\tilde\phi^d_3\,, \quad z^d_1 e^{i\theta^{z_d}_1} = y^d_7(\phi^d_2)^2(\phi^d_3)^3 - y^d_6\phi^d_2\tilde\phi^d_3\tilde\phi^u_2\,. \tag{3.4.9}$$

Using Eqs. (B.2,B.6), the following relations for the phases are deduced:

$$\theta^{\tilde x}_2 = 3(\theta^d_2+\theta^d_3)\,, \quad \theta^y_s = \theta^{z_d}_1 = 2\theta^d_2 + 3\theta^d_3\,, \quad \theta^y_b = \theta^{z_d}_2 = \theta^{z_d}_3 = \theta^d_3\,. \tag{3.4.10}$$

The Yukawa matrices of the down-type quarks and the charged leptons are linear combinations of the two structures in Eq. (3.4.8). Following the construction proposed by Georgi and Jarlskog [71], one has: $\mathcal{Y}^d_{\rm GUT} = \mathcal{Y}_{\bar{5}} + \mathcal{Y}_{\bar{45}}$ and $\mathcal{Y}^e_{\rm GUT} = (\mathcal{Y}_{\bar{5}} - 3\mathcal{Y}_{\bar{45}})^T$, respectively.

Performing the canonical normalisation on the Yukawa matrices $(P_T^{-1})^T \mathcal{Y}^d_{\rm GUT} P_F^{-1}$ and $(P_F^{-1})^T \mathcal{Y}^e_{\rm GUT} P_T^{-1}$ as well as an additional rephasing of the right-handed superfields by:

$$Q_d = Q_e = \text{diag}(e^{i\theta^{\tilde{x}}_2}, e^{i\theta^{\tilde{x}}_2}, e^{i\theta^y_b}), \tag{3.4.11}$$

results in:

$$Y^d_{\rm GUT} \approx \begin{pmatrix} e^{i(\theta^{z_d}_1 - \theta^{\tilde{x}}_2)} z^d_1 \lambda^8 & \tilde{x}_2 \lambda^5 & -e^{i(\theta^{\tilde{x}}_2 - \theta^y_b)} \tilde{x}_2 \lambda^5 \\ -\tilde{x}_2 \lambda^5 & e^{i(\theta^y_s - \theta^{\tilde{x}}_2)} y_s \lambda^4 & -e^{i(\theta^y_s - \theta^y_b)} y_s \lambda^4 \\ e^{-i\theta^{\tilde{x}}_2} \left(z^d_3 e^{i\theta^{z_d}_3} - \frac{K_3}{2} e^{i\theta^y_b} y_b \right) \lambda^6 & e^{-i\theta^{\tilde{x}}_2} \left(z^d_2 e^{i\theta^{z_d}_2} - \frac{K_3}{2} e^{i\theta^y_b} y_b \right) \lambda^6 & y_b \lambda^2 \end{pmatrix}, \tag{3.4.12}$$

$$Y^e_{\rm GUT} \approx \begin{pmatrix} -3 e^{i(\theta^{z_d}_1 - \theta^{\tilde{x}}_2)} y_d \lambda^8 & -\tilde{x}_2 \lambda^5 & e^{-i\theta^y_b} \left(z^d_3 e^{i\theta^{z_d}_3} - \frac{K_3}{2} e^{i\theta^y_b} y_b \right) \lambda^6 \\ \tilde{x}_2 \lambda^5 & -3\, e^{i(\theta^y_s - \theta^{\tilde{x}}_2)} y_s \lambda^4 & e^{-i\theta^y_b} \left(z^d_2 e^{i\theta^{z_d}_2} - \frac{K_3}{2} e^{i\theta^y_b} y_b \right) \lambda^6 \\ -\tilde{x}_2 \lambda^5 & 3\, e^{i(\theta^y_s - \theta^{\tilde{x}}_2)} y_s \lambda^4 & y_b \lambda^2 \end{pmatrix}. \tag{3.4.13}$$

Note that the canonical normalisation modifies the down-type quark and charged lepton Yukawa matrices solely by additional contributions of the same order in the (31), (32) and (13), (23) elements, respectively. Comparing Eq, (3.4.12) with Eq. (3.4.6) suggests that the CKM mixing is dominated by the diagonalisation of the down-type quark Yukawa matrix. This will be explicitly verified when calculating the SCKM transformations in Section 3.6.

3.4.2 Neutrinos

3.4.2.1 Dirac neutrino coupling

Having introduced right-handed neutrinos N in Table 3.1, their Dirac coupling to the left-handed SM neutrinos originates from the superpotential terms:

$$\begin{aligned} & y_D F N H_5 + y^D_1 \frac{1}{M} F N \tilde{\Phi}^u_2 H_5 + y^D_2 \frac{1}{M^2} F N (\tilde{\Phi}^u_2)^2 H_5 + y^D_{3,4,5} \frac{1}{M^3} F N (\Phi^d_3)^2 \Phi^\nu_{1,2,3'} H_5 \\ & + y^D_6 \frac{1}{M^5} F N (\Phi^d_2)^4 \Phi^d_3 H_5, \end{aligned} \tag{3.4.14}$$

where y_D and y^D_i are real order one parameters. The corresponding Yukawa matrix is determined as:

$$\mathcal{Y}^\nu \approx \begin{pmatrix} y_D & z^D_2 e^{i\theta^{z_D}_2} \lambda^6 & z^D_1 \lambda^4 \\ z^D_2 e^{i\theta^{z_D}_2} \lambda^6 & z^D_1 \lambda^4 & y_D \\ z^D_1 \lambda^4 & y_D & z^D_2 e^{i\theta^{z_D}_2} \lambda^6 \end{pmatrix}, \tag{3.4.15}$$

with

$$z^D_1 = y^D_1 \tilde{\phi}^u_2 \,, \qquad z^D_2 e^{i\theta^{z_D}_2} = y^D_1 \tilde{\delta}^u_{2,1} \,, \qquad \theta^{z_D}_2 = 4\theta^d_2 + \theta^d_3 \,. \tag{3.4.16}$$

Here, the phase can be deduced from Eq. (B.5).

Applying the CN transformation $(P_F^{-1})^T \mathcal{Y}^\nu P_N^{-1}$, the corresponding Yukawa matrix in the basis with canonical kinetic terms takes the form:

$$Y^\nu \approx \begin{pmatrix} y_D & -\frac{y_D(K_3+K_3^N)}{2}\lambda^4 & \left(z_1^D - \frac{y_D(K_3+K_3^N)}{2}\right)\lambda^4 \\ -\frac{y_D(K_3+K_3^N)}{2}\lambda^4 & \left(z_1^D - \frac{y_D(K_3+K_3^N)}{2}\right)\lambda^4 & y_D \\ \left(z_1^D - \frac{y_D(K_3+K_3^N)}{2}\right)\lambda^4 & y_D & -\frac{y_D(K_3+K_3^N)}{2}\lambda^4 \end{pmatrix} . \tag{3.4.17}$$

Compared to Eq. (3.4.15), an additional contribution of the same order arises in the (13), (22) and (31) entries. Moreover, the λ-suppression of the (12), (21) and (33) elements is reduced.

3.4.2.2 Majorana neutrino mass

The mass matrix of the right-handed neutrinos is obtained from the superpotential terms:

$$w_{1,2,3} N N \Phi^\nu_{1,2,3'} + w_4 \frac{1}{M} N N \Phi_2^d \eta + w_{5,6,7} \frac{1}{M} N N \tilde{\Phi}_2^u \Phi^\nu_{1,2,3'} + w_8 \frac{1}{M^7} N N (\Phi_2^d)^8 \,, \tag{3.4.18}$$

where w_i denote real order one coefficients. This results in a right-handed Majorana neutrino mass matrix $\mathcal{M}_R$ of the form:

$$\frac{\mathcal{M}_R}{M} \approx \begin{pmatrix} A+2C & B-C & B-C \\ B-C & B+2C & A-C \\ B-C & A-C & B+2C \end{pmatrix} e^{i\theta_A}\lambda^4 + \begin{pmatrix} 0 & 0 & D \\ 0 & D & 0 \\ D & 0 & 0 \end{pmatrix} e^{i\theta_D}\lambda^5 \,, \tag{3.4.19}$$

with

$$A e^{i\theta_A} = w_1 \phi_1^\nu \,, \quad B e^{i\theta_A} = w_2 \phi_2^\nu \,, \quad C e^{i\theta_A} = w_3 \phi_{3'}^\nu \,, \quad D e^{i\theta_D} = w_2(\delta^\nu_{2,1} - \delta^\nu_{2,2}) + w_4\, \eta\, \phi_2^d \,. \tag{3.4.20}$$

According to Eqs. (B.2,B.5,B.6), the phases are given by:

$$\theta_A = -2\theta_3^d \,, \qquad \theta_D = 4\theta_2^d - \theta_3^d \,. \tag{3.4.21}$$

The first matrix of Eq. (3.4.19) arises from terms involving only $\Phi^\nu_{1,2,3'}$. As their VEVs respect the tri-bimaximal (TB) Klein symmetry $Z_2^S \times Z_2^U \subset S_4$, this part is of TB form. The second matrix of Eq. (3.4.19), proportional to D, is due to the operator $w_4 \frac{1}{M} N N \Phi_2^d \eta$. As the product of both flavon VEVs involved is not an eigenvector of U, half of the TB Klein symmetry is broken at a relative order of λ. The resulting trimaximal TM_2 [81] structure can accommodate the sizeable value of the reactor neutrino mixing angle θ_{13}^l as explained in [11] in the context of the original model [10].

Performing the CN basis transformation $(P_N^{-1})^T \mathcal{M}_R P_N^{-1}$ does not alter the matrix in Eq. (3.4.19) at the given order, so that $M_R = \mathcal{M}_R + \mathcal{O}(\lambda^6) M$.

3.4.2.3 Effective light neutrino mass matrix

Calculating the effective light neutrino mass matrix which arises via the type I see-saw mechanism $v_u^2\, Y^\nu M_R^{-1} (Y^\nu)^T$, the LO result can be parametrized as:

$$m_\nu^{\text{eff}} \approx \frac{y_D^2 v_u^2}{\lambda^4 M} \left[\begin{pmatrix} b^\nu + c^\nu - a^\nu & a^\nu & a^\nu \\ a^\nu & b^\nu & c^\nu \\ a^\nu & c^\nu & b^\nu \end{pmatrix} e^{-i\theta_A} + \begin{pmatrix} 0 & 0 & d^\nu \\ 0 & d^\nu & 0 \\ d^\nu & 0 & 0 \end{pmatrix} \lambda\, e^{i(\theta_D - 2\theta_A)} \right], \tag{3.4.22}$$

with a^ν, b^ν, c^ν and d^ν being functions of the real parameters A, B, C and D. The deviation from tri-bimaximal neutrino mixing is controlled by $d^\nu \propto D$. Due to the three independent LO input parameters ($w_1 \propto A$,$w_2 \propto B$,$w_3 \propto C$), any neutrino mass spectrum can be accommodated in this model. At this order, the canonical normalisation does not modify the effective light neutrino mass matrix as obtained without the CN transformations. Hence, concerning the results on light neutrino masses and mixing, the reader is simply referred to the corresponding discussion in [11].

3.5 Soft SUSY breaking sector after CN

Having applied the CN basis transformation of the matter superfields to the Yukawa sector, the focus will now turn to the soft SUSY breaking terms. In the context of the general MSSM with R-parity, these are parametrised as[4] [47]

$$\begin{aligned} -\mathcal{L}_{\text{soft}} \supset\ & A^u_{ij} H_u \tilde{Q}_i \tilde{u}^c_j + A^d_{ij} H_d \tilde{Q}_i \tilde{d}^c_j + A^e_{ij} H_d \tilde{L}_i \tilde{e}^c_j + A^\nu_{ij} H_u \tilde{L}_i \tilde{N}_j + \text{h.c.} \\ & + m^2_{Q_{ij}} \tilde{Q}^\alpha_i \tilde{Q}^{\alpha *}_j + m^2_{L_{ij}} \tilde{L}^\alpha_i \tilde{L}^{\alpha *}_j + m^2_{u^c_{ij}} \tilde{u}^{c*}_i \tilde{u}^c_j + m^2_{d^c_{ij}} \tilde{d}^{c*}_i \tilde{d}^c_j + m^2_{e^c_{ij}} \tilde{e}^{c*}_i \tilde{e}^c_j + m^2_{N_{ij}} \tilde{N}^*_i \tilde{N}_j \\ & + m^2_{H_u} |H_u|^2 + m^2_{H_d} |H_d|^2 \ , \end{aligned} \tag{3.5.1}$$

and contain trilinear scalar couplings (A-terms) as well as bilinear scalar masses. A tilde indicates the scalar partner $\tilde{f}$ of a SM fermion f. Taking into account the $SU(5)$ framework, in this section the effective soft SUSY breaking operators are constructed, assuming that the mechanism of SUSY breaking is practically independent of the family symmetry breaking.

3.5.1 Trilinear soft couplings

The flavour structure of the trilinear A-terms is similar to the corresponding Yukawa matrices, as both originate from the same set of superpotential terms. In the case of the soft terms, these are coupled to a hidden sector superfield X with independent real order one coupling constants and suppressed by a mass scale M_X. When X develops its SUSY breaking F-term VEV, the scalar components of the Higgs and matter superfields are projected out, thereby generating the trilinear soft terms. There exist in fact extra contributions to the A-terms from superpotential operators involving flavons but no X field. These can be traced back to non-vanishing vevs for the auxiliary F-components of the flavon fields, which are zero in the SUSY limit but develop a

[4] Dropping the spinor indeces in Eq. (2.2.39) and including the right-handed neutrino terms.

non-trivial value when SUSY breaking terms are included. It turns out that such F-term vevs are aligned with the LO flavon vevs in many situations [68, 69]. Hence, these extra contributions to the A-terms do not give rise to new flavour structures.

Defining the mass parameters $m_0 \equiv \langle F_X \rangle / M_X$ and $A_0 \equiv \alpha_0\, m_0$, with α_0 being a real constant, one obtains the expressions for the trilinear matrices $\mathcal{A}^f_{\rm GUT}/A_0$ by copying the Yukawas matrices of Eqs. (3.4.2,3.4.8,3.4.15) with different order-one coefficients and phases: $y_f \to a_f$, $\tilde{x}_2 \to \tilde{x}^a_2$, $z^f_i \to z^{f_a}_i$, $y_D \to \alpha_D$ as well as $\theta^y_f \to \theta^a_f$, $\theta^{\tilde{x}}_2 \to \theta^{\tilde{x}_a}_2$, $\theta^{z_f}_i \to \theta^{z_{f_a}}_i$. With these replacements, it is found that

$$\frac{\mathcal{A}^u_{\rm GUT}}{A_0} \approx \begin{pmatrix} a_u\, e^{i\theta^a_u}\lambda^8 & 0 & 0 \\ 0 & a_c\, e^{i\theta^a_c}\lambda^4 & z^{u_a}_2 e^{i\theta^{z_{u_a}}_2}\lambda^7 \\ 0 & z^{u_a}_2 e^{i\theta^{z_{u_a}}_2}\lambda^7 & a_t \end{pmatrix} , \tag{3.5.2}$$

and similarly for $\mathcal{A}^d_{\rm GUT}$, $\mathcal{A}^e_{\rm GUT}$ and $\mathcal{A}^\nu$. Applying the CN transformation as well as the rephasing of the right-handed superfields proceeds analogously to the Yukawa sector. The resulting trilinear matrices $A^f_{\rm GUT}/A_0$ in the basis of canonical kinetic terms are thus derived from Eqs. (3.4.6,3.4.12,3.4.13,3.4.17) by simply replacing $y_u \to a_u\, e^{i(\theta^a_u - \theta^y_u)}$, $y_c \to a_c\, e^{i(\theta^a_c - \theta^y_u)}$, $y_t \to a_t$, $y_s \to a_s\, e^{i(\theta^a_s - \theta^y_s)}$, $y_b \to a_b\, e^{i(\theta^a_b - \theta^y_b)}$, $\tilde{x}_2 \to \tilde{x}^a_2\, e^{i(\theta^{\tilde{x}_a}_2 - \theta^{\tilde{x}}_2)}$, $z^f_i \to z^{f_a}_i\, e^{i(\theta^{z_{f_a}}_i - \theta^{z_f}_i)}$ and $y_D \to \alpha_D$. For example, the up-type quark trilinear matrix takes the form:

$$\frac{A^u_{\rm GUT}}{A_0} \approx \begin{pmatrix} a_u\, e^{i(\theta^a_u - \theta^y_u)}\,\lambda^8 & -\frac{1}{2}k_2\, a_c\, e^{i(\theta^a_c - \theta^y_u)}\,\lambda^8 & -\frac{1}{2}k_4\, a_t e^{i\theta^k_4}\,\lambda^6 \\ -\frac{1}{2}k_2\, a_c\, e^{i(\theta^a_c - \theta^y_u)}\lambda^8 & a_c\, e^{i(\theta^a_c - \theta^y_u)}\,\lambda^4 & -\frac{1}{2}k_3\, a_t e^{i\theta^k_3}\lambda^5 \\ -\frac{1}{2}k_4\, a_t e^{i(\theta^k_4 - \theta^y_u)}\,\lambda^6 & -\frac{1}{2}k_3\, a_t e^{i(\theta^k_3 - \theta^y_u)}\lambda^5 & a_t \end{pmatrix} . \tag{3.5.3}$$

3.5.2 Soft scalar masses

The scalar mass terms of the soft supersymmetry breaking Lagrangian originate from the Kähler potential. Non-renormalisable couplings of the matter superfields to the square $X^\dagger X/M^2_X$ of the SUSY breaking field X generate soft masses when the F-term of X develops a vev. The structure of the soft mass matrices is therefore similar to the Kähler metric $\mathcal{K}$ of the corresponding GUT multiplet. As for the trilinear soft terms, all order one coefficients are independent of those appearing in $\mathcal{K}$. The scalar masses before canonical normalisation are then obtained from $\mathcal{K}_T$, $\mathcal{K}_F$ and $\mathcal{K}_N$ of Eqs. (3.3.10,3.3.12,3.3.13) by replacing $k_i \to b_i$, $\theta^k_i \to \theta^b_i$, $K_i \to B_i$ and $K^N_i \to B^N_i$. Moreover, the ones on the diagonal of $\mathcal{K}$ have to be rescaled by a new factor of order one. In the case of the **10** of $SU(5)$, the 2+1 structure requires the introduction of two extra parameters, b_{01} and b_{02}. Explicitly, one gets:

$$\frac{\mathcal{M}^2_{T_{\rm GUT}}}{m^2_0} \approx \begin{pmatrix} b_{01} + (b_5 + b_1)\lambda^2 & b_2\lambda^4 & b_4\, e^{-i\theta^k_4}\lambda^6 \\ \cdot & b_{01} + (b_5 - b_1)\lambda^2 & b_3\, e^{-i\theta^k_3}\lambda^5 \\ \cdot & \cdot & b_{02} + b_6\lambda^2 \end{pmatrix} , \tag{3.5.4}$$

$$\frac{\mathcal{M}^2_{F(N)_{\rm GUT}}}{m^2_0} \approx \begin{pmatrix} B^{(N)}_0 + 2B^{(N)}_1\lambda^4 & B^{(N)}_3\lambda^4 & B^{(N)}_3\lambda^4 \\ \cdot & B^{(N)}_0 + (B^{(N)}_2 - B^{(N)}_1)\lambda^4 & B^{(N)}_3\lambda^4 \\ \cdot & \cdot & B^{(N)}_0 - (B^{(N)}_2 + B^{(N)}_1)\lambda^4 \end{pmatrix} . \tag{3.5.5}$$

Performing the transformations to the basis of canonical kinetic terms results in soft scalar mass matrices of the form:

$$\frac{M^2_{T_{\rm GUT}}}{m_0^2} \approx \begin{pmatrix} b_{01} & (b_2 - b_{01}k_2)\lambda^4 & e^{-i\theta_4^k}(b_4 - \frac{k_4(b_{01}+b_{02})}{2})\lambda^6 \\ \cdot & b_{01} & e^{-i\theta_3^k}(b_3 - \frac{k_3(b_{01}+b_{02})}{2})\lambda^5 \\ \cdot & \cdot & b_{02} \end{pmatrix} , \tag{3.5.6}$$

$$\frac{M^2_{F(N)_{\rm GUT}}}{m_0^2} \approx \begin{pmatrix} B_0^{(N)} & (B_3^{(N)} - K_3^{(N)})\lambda^4 & (B_3^{(N)} - K_3^{(N)})\lambda^4 \\ \cdot & B_0^{(N)} & (B_3^{(N)} - K_3^{(N)})\lambda^4 \\ \cdot & \cdot & B_0^{(N)} \end{pmatrix} . \tag{3.5.7}$$

For convenience, the order one parameter B_0 is absorbed into the soft SUSY breaking mass m_0, so that the leading contribution on the diagonal of $M^2_{F_{\rm GUT}}/m_0^2$ is nothing but unity. For the right-handed fields contained in the GUT multiplets, an additional rephasing has to be applied. This will be revisited when calculating the soft terms in the SCKM basis in Section 3.6.2. Notice that all λ-suppressed corrections of the diagonal elements have been dropped. This simplification is justified as FCNC processes are induced by loop diagrams involving the off-diagonal entries of the sfermion mass matrices. The simplification of the diagonal elements in Eqs. (3.5.6,3.5.7) does not affect these off-diagonals in the LO analysis, even when going to the SCKM basis.

3.6 SCKM basis

Predictions relating a theoretical model with its phenomenological implications are typically given in the basis in which the Yukawa matrices are diagonal and positive, corresponding to the physical quark and lepton mass eigenstates. The so-called SCKM basis is the analogue in a supersymmetric framework. Changing to the SCKM basis, all canonically normalised quantities undergo a unitary transformation of the superfields which diagonalises the effective Yukawa couplings in the superpotential. In this basis it is convenient to define a set of dimensionless parameters, known as the "mass insertion parameters", which directly enter the expressions of phenomenological flavour observables.

In principle, the SCKM transformation should be performed after electroweak symmetry breaking. The canonically normalised Yukawa, trilinear and soft mass matrices should be evolved from the GUT scale $M_{\rm GUT}$ to the weak scale M_W using the corresponding renormalisation group equations (RGEs). Only at that point, the diagonalisation of the Yukawa matrices should take place, leading to the definition of a SCKM basis. Following this procedure, there is obviously no notion of mass insertion parameters at the scale $M_{\rm GUT}$ as there is no proper definition of the SCKM basis.

An alternative approach which is commonly used consists in diagonalising the Yukawa matrices at (or rather just below) the GUT scale. The so-obtained basis is approximately identical to the SCKM basis provided the RGE contributions to the off-diagonal elements of the Yukawa matrices remain negligible. This is the case as long as the RGE effects can be absorbed into a redefinition of the (unknown) order one coefficients. It is then possible to introduce mass insertion parameters already at $M_{\rm GUT}$. Their low energy values have to be determined from the corresponding RG evolution. In this work, the latter approach is adopted as it allows for a

semi-analytical study of the relations between the high and low energy parameters by means of a perturbative λ-expansion.

3.6.1 SCKM transformations

The SCKM transformations are applied on the matter superfields $\hat{f}_{L,R} \to U^f_{L,R}\hat{f}_{L,R}$, where $U^f_{L,R}$ denote unitary 3×3 matrices. These diagonalise the canonically normalised Yukawa matrices Y^f

$$(U^f_L)^\dagger Y^f U^f_R \;=\; \tilde{Y}^f_{\text{diag}} \;, \tag{3.6.1}$$

where the tilde denotes the SCKM basis. The derivation and the explicit form of the unitary transformations can be found in Appendix C.2. Applying this change of basis to the Yukawa matrices yields:

$$\tilde{Y}^u_{\text{GUT}} \approx \begin{pmatrix} y_u\lambda^8 & 0 & 0 \\ 0 & y_c\lambda^4 & 0 \\ 0 & 0 & y_t \end{pmatrix}, \qquad \tilde{Y}^d_{\text{GUT}} \approx \begin{pmatrix} \frac{\tilde{x}_2^2}{y_s}\lambda^6 & 0 & 0 \\ 0 & y_s\lambda^4 & 0 \\ 0 & 0 & y_b\lambda^2 \end{pmatrix}, \tag{3.6.2}$$

$$\tilde{Y}^e_{\text{GUT}} \approx \begin{pmatrix} \frac{\tilde{x}_2^2}{3y_s}\lambda^6 & 0 & 0 \\ 0 & 3y_s\lambda^4 & 0 \\ 0 & 0 & y_b\lambda^2 \end{pmatrix}. \tag{3.6.3}$$

These results, which are valid at the high scale, agree with the LO results derived in [10, 11]. This shows that the canonical normalisation does not affect the LO expressions of the quark and charged lepton masses.

Up to phase convention, the CKM matrix is given by $V_{\text{CKM}_{\text{GUT}}} = (U^u_L)^T U^{d*}_L$ (see Appendix C.2 for explicit expressions). Extracting the mixing angles

$$\sin(\theta^q_{13})_{\text{GUT}} \approx \frac{\tilde{x}_2}{y_b}\lambda^3 \;, \qquad \tan(\theta^q_{23})_{\text{GUT}} \approx \frac{y_s}{y_b}\lambda^2 \;, \qquad \tan(\theta^q_{12})_{\text{GUT}} \approx \frac{\tilde{x}_2}{y_s}\lambda \;, \tag{3.6.4}$$

shows that the LO CKM mixing arises purely from the down-type quark sector, incorporating the GST relation [80] $\theta^q_{12} \approx \sqrt{m_d/m_s}$, and agrees with the results obtained in [10, 11]. Concerning the CP violation, it is found that the Jarlskog invariant [28] to be

$$J^q_{\text{CP}_{\text{GUT}}} \approx \lambda^7 \frac{\tilde{x}_2^3}{y_b^2 y_s}\sin(\theta^d_2) \;. \tag{3.6.5}$$

The PMNS matrix is dominated by the trimaximal TM_2 neutrino mixing V_ν which diagonalises the effective light neutrino mass matrix of Eq. (3.4.22). Including the charged lepton corrections,

one has $U_{\mathrm{PMNS}_{\mathrm{GUT}}} = (U_L^e)^T V_\nu^*$ with mixing angles given as:

$$\tan(\theta_{23}^l)_{\mathrm{GUT}} \approx 1 + \lambda \frac{d^\nu}{2(a^\nu - c^\nu)} \cos(4\theta_2^d + \theta_3^d) \ , \tag{3.6.6}$$

$$\tan(\theta_{12}^l)_{\mathrm{GUT}} \approx \frac{1}{\sqrt{2}} - \lambda \frac{\tilde{x}_2}{2\sqrt{2} y_s} \cos(\theta_2^d) \ , \tag{3.6.7}$$

$$\begin{aligned} \sin(\theta_{13}^l)_{\mathrm{GUT}} \approx \frac{\lambda}{6\sqrt{2} y_s} \Bigg[& \left(\frac{3 d^\nu y_s \cos(4\theta_2^d + \theta_3^d) + 2(a^\nu - c^\nu)\tilde{x}_2 \cos(\theta_2^d)}{a^\nu - c^\nu} \right)^2 \\ & + \left(\frac{3 d^\nu y_s \sin(4\theta_2^d + \theta_3^d) + 2(a^\nu - b^\nu)\tilde{x}_2 \sin(\theta_2^d)}{a^\nu - b^\nu} \right)^2 \Bigg]^{\frac{1}{2}} , \end{aligned} \tag{3.6.8}$$

and a leptonic Jarlskog invariant of the form:

$$J_{\mathrm{CP}_{\mathrm{GUT}}}^l \approx -\frac{\lambda}{36} \left(\frac{2\tilde{x}_2}{y_s} \sin(\theta_2^d) + \frac{3 d^\nu}{a^\nu - b^\nu} \sin(4\theta_2^d + \theta_3^d) \right) \ .$$

3.6.2 Soft terms in the SCKM basis

In order to obtain the flavour structure of the soft SUSY breaking terms in a basis which is suitable for physical interpretations, one has to apply the SCKM transformations on the canonical trilinear soft couplings and soft scalar masses, see Section 3.5. The action of the $U_{L,R}^f$ matrices on the A-terms is identical to the transformation of the Yukawa matrices:

$$(U_L^f)^\dagger A_{\mathrm{GUT}}^f U_R^f \ = \ \tilde{A}_{\mathrm{GUT}}^f . \tag{3.6.9}$$

However, due to different order one coefficients, the A-terms remain non-diagonal in the SCKM basis. The soft masses of Eqs. (3.5.6,3.5.7) are transformed differently for different components of the $SU(5)$ multiplets. Moreover, one has to associate the mass matrices of the effective soft Lagrangian in Eq. (3.5.1) with $M_{T_{\mathrm{GUT}}}^2$ and $M_{F_{\mathrm{GUT}}}^2$ and take into account the additional rephasing transformations of the right-handed superfields, see Eqs. (3.4.5,3.4.11), that were performed after CN. Then, the soft masses in the SCKM basis are:

$$(\tilde{m}_u^2)_{LL_{\mathrm{GUT}}} = (U_L^u)^\dagger M_{T_{\mathrm{GUT}}}^{2\,*} U_L^u, \quad (\tilde{m}_u^2)_{RR_{\mathrm{GUT}}} = (U_R^u)^\dagger Q_u \, M_{T_{\mathrm{GUT}}}^2 Q_u^\dagger \, U_R^u, \tag{3.6.10}$$

$$(\tilde{m}_d^2)_{LL_{\mathrm{GUT}}} = (U_L^d)^\dagger M_{T_{\mathrm{GUT}}}^{2\,*} U_L^d, \quad (\tilde{m}_d^2)_{RR_{\mathrm{GUT}}} = (U_R^d)^\dagger Q_d \, M_{F_{\mathrm{GUT}}}^2 Q_d^\dagger \, U_R^d, \tag{3.6.11}$$

$$(\tilde{m}_e^2)_{LL_{\mathrm{GUT}}} = (U_L^e)^\dagger M_{F_{\mathrm{GUT}}}^{2\,*} U_L^e, \quad (\tilde{m}_e^2)_{RR_{\mathrm{GUT}}} = (U_R^e)^\dagger Q_d \, M_{T_{\mathrm{GUT}}}^2 Q_d^\dagger \, U_R^e. \tag{3.6.12}$$

The following leading order expressions are found, where the order one coefficients are defined in Eqs. (D.4,D.5). Note that the order one coefficient B_0 into m_0 is absorbed, see. Eq. (3.5.7), so that $(\tilde{m}_d^2)_{RR_{\mathrm{GUT}}}/m_0^2$ and $(\tilde{m}_e^2)_{LL_{\mathrm{GUT}}}/m_0^2$ have 1s on the diagonal.

Up-type quark sector:

$$\frac{\tilde{A}^u_{\rm GUT}}{A_0} \approx \begin{pmatrix} \tilde{a}^u_{11}\lambda^8 & 0 & 0 \\ 0 & \tilde{a}^u_{22}\lambda^4 & e^{i\theta^d_2}\tilde{a}^u_{23}\lambda^7 \\ 0 & e^{i(3\theta^d_2+\theta^d_3)}\tilde{a}^u_{23}\lambda^7 & \tilde{a}^u_{33} \end{pmatrix} , \tag{3.6.13}$$

$$\frac{(\tilde{m}^2_u)_{LL_{\rm GUT}}}{m_0^2} \approx \begin{pmatrix} b_{01} & e^{-i\theta^d_2}\tilde{b}_{12}\,\lambda^4 & e^{-i(4\theta^d_2+\theta^d_3)}\tilde{b}_{13}\,\lambda^6 \\ \cdot & b_{01} & e^{-i(7\theta^d_2+2\theta^d_3)}\tilde{b}_{23}\,\lambda^5 \\ \cdot & \cdot & b_{02} \end{pmatrix} , \tag{3.6.14}$$

$$\frac{(\tilde{m}^2_u)_{RR_{\rm GUT}}}{m_0^2} \approx \begin{pmatrix} b_{01} & e^{-i\theta^d_2}\tilde{b}_{12}\,\lambda^4 & \tilde{b}_{13}\,\lambda^6 \\ \cdot & b_{01} & e^{i(5\theta^d_2+\theta^d_3)}\tilde{b}_{23}\,\lambda^5 \\ \cdot & \cdot & b_{02} \end{pmatrix} . \tag{3.6.15}$$

Down-type quark sector:

$$\frac{\tilde{A}^d_{\rm GUT}}{A_0} \approx \begin{pmatrix} \tilde{a}^d_{11}\,\lambda^6 & \tilde{a}^d_{12}\,\lambda^5 & \tilde{a}^d_{12}\,\lambda^5 \\ -\tilde{a}^d_{12}\,\lambda^5 & \tilde{a}^d_{22}\,\lambda^4 & \tilde{a}^d_{23}\,\lambda^4 \\ e^{-i\theta^d_2}\tilde{a}^d_{31}\,\lambda^6 & \tilde{a}^d_{32}\,\lambda^6 & \tilde{a}^d_{33}\,\lambda^2 \end{pmatrix} , \tag{3.6.16}$$

$$\frac{(\tilde{m}^2_d)_{LL_{\rm GUT}}}{m_0^2} \approx \begin{pmatrix} b_{01} & \tilde{B}_{12}\,\lambda^3 & e^{i\theta^d_2}\tilde{B}_{13}\,\lambda^4 \\ \cdot & b_{01} & \tilde{B}_{23}\,\lambda^2 \\ \cdot & \cdot & b_{02} \end{pmatrix} , \tag{3.6.17}$$

$$\frac{(\tilde{m}^2_d)_{RR_{\rm GUT}}}{m_0^2} \approx \begin{pmatrix} 1 & e^{i\theta^d_2}\tilde{R}_{12}\,\lambda^4 & -\,e^{i\theta^d_2}\tilde{R}_{12}\,\lambda^4 \\ \cdot & 1 & -\,\tilde{R}_{12}\,\lambda^4 \\ \cdot & \cdot & 1 \end{pmatrix} . \tag{3.6.18}$$

Charged lepton sector:

$$\frac{\tilde{A}^e_{\rm GUT}}{A_0} \approx \begin{pmatrix} \frac{1}{3}\tilde{a}^d_{11}\,\lambda^6 & e^{i\theta^d_2}\tilde{a}^d_{12}\,\lambda^5 & \tilde{a}^d_{31}\,\lambda^6 \\ -e^{-i\theta^d_2}\tilde{a}^d_{12}\,\lambda^5 & 3\tilde{a}^d_{22}\,\lambda^4 & \tilde{a}^e_{23}\,\lambda^6 \\ -e^{-i\theta^d_2}\tilde{a}^d_{12}\,\lambda^5 & 3\tilde{a}^d_{23}\,\lambda^4 & \tilde{a}^d_{33}\,\lambda^2 \end{pmatrix} , \tag{3.6.19}$$

$$\frac{(\tilde{m}^2_e)_{LL_{\rm GUT}}}{m_0^2} \approx \begin{pmatrix} 1 & \tilde{R}_{12}\,\lambda^4 & -\,\tilde{R}_{12}\,\lambda^4 \\ \cdot & 1 & -\,\tilde{R}_{12}\,\lambda^4 \\ \cdot & \cdot & 1 \end{pmatrix} , \tag{3.6.20}$$

$$\frac{(\tilde{m}^2_e)_{RR_{\rm GUT}}}{m_0^2} \approx \begin{pmatrix} b_{01} & -\,e^{i\theta^d_2}\frac{1}{3}\tilde{B}_{12}\,\lambda^3 & \frac{1}{3}\tilde{B}_{13}\,\lambda^4 \\ \cdot & b_{01} & 3\tilde{B}_{23}\,\lambda^2 \\ \cdot & \cdot & b_{02} \end{pmatrix} . \tag{3.6.21}$$

3.7 Mass insertion parameters

In supersymmetry, flavour changing processes are induced by the mismatch of fermion and sfermion mass eigenstates. Having changed the basis of the superfields to the SCKM basis, the Yukawa matrices are diagonal. Thus, the off-diagonal entries of the scalar mass matrices determine the size of the resulting FCNCs. As both the left- and the right-handed fermions have their own scalar partners, there are three types of scalar mass matrices:

$$m^2_{\tilde{f}_{LL}} = (\tilde{m}^2_f)_{LL} + \tilde{Y}_f \tilde{Y}_f^\dagger v^2_{u,d} \,, \quad m^2_{\tilde{f}_{RR}} = (\tilde{m}^2_f)_{RR} + \tilde{Y}_f^\dagger \tilde{Y}_f v^2_{u,d} \,, \quad m^2_{\tilde{f}_{LR}} = \tilde{A}_f v_{u,d} - \mu \tilde{Y}_f v_{d,u} \,, \tag{3.7.1}$$

where μ is the higgsino mass which is taken to be real. In Eq. (3.7.1), the first contribution on the right-hand sides originates from the soft breaking Lagrangian, while the second term is the supersymmetric F-term contribution to the scalar masses. Note that it is formally possible to define $m^2_{\tilde{f}_{RL}} \equiv (m^2_{\tilde{f}_{LR}})^\dagger$.

From the model building perspective, a convenient measure of flavour violation is provided by a set of dimensionless parameters, known as the mass insertion parameters. These are defined as [13]:

$$(\delta^f_{LL})_{ij} = \frac{(m^2_{\tilde{f}_{LL}})_{ij}}{\langle m_{\tilde{f}} \rangle^2_{LL}} \,, \qquad (\delta^f_{RR})_{ij} = \frac{(m^2_{\tilde{f}_{RR}})_{ij}}{\langle m_{\tilde{f}} \rangle^2_{RR}} \,, \qquad (\delta^f_{LR})_{ij} = \frac{(m^2_{\tilde{f}_{LR}})_{ij}}{\langle m_{\tilde{f}} \rangle^2_{LR}} \,, \tag{3.7.2}$$

where the average masses in the denominators are:

$$\langle m_{\tilde{f}} \rangle^2_{AB} = \sqrt{(m^2_{\tilde{f}_{AA}})_{ii} (m^2_{\tilde{f}_{BB}})_{jj}} \,. \tag{3.7.3}$$

3.7.1 Mass insertion parameters δ at the GUT scale

Inserting the results of Section 3.6, it is straightforward to calculate the mass insertion parameters at the GUT scale. The full LO expressions are given in Appendix D. In the following, only the flavour structure of the various δs in terms of their λ-suppression is reported.

$$\delta^u_{LL_{\rm GUT}} \sim \begin{pmatrix} 1 & \lambda^4 & \lambda^6 \\ \cdot & 1 & \lambda^5 \\ \cdot & \cdot & 1 \end{pmatrix}, \quad \delta^u_{RR_{\rm GUT}} \sim \begin{pmatrix} 1 & \lambda^4 & \lambda^6 \\ \cdot & 1 & \lambda^5 \\ \cdot & \cdot & 1 \end{pmatrix}, \quad \delta^u_{LR_{\rm GUT}} \sim \begin{pmatrix} \lambda^8 & 0 & 0 \\ 0 & \lambda^4 & \lambda^7 \\ 0 & \lambda^7 & 1 \end{pmatrix}, \tag{3.7.4}$$

$$\delta^d_{LL_{\rm GUT}} \sim \begin{pmatrix} 1 & \lambda^3 & \lambda^4 \\ \cdot & 1 & \lambda^2 \\ \cdot & \cdot & 1 \end{pmatrix}, \quad \delta^d_{RR_{\rm GUT}} \sim \begin{pmatrix} 1 & \lambda^4 & \lambda^4 \\ \cdot & 1 & \lambda^4 \\ \cdot & \cdot & 1 \end{pmatrix}, \quad \delta^d_{LR_{\rm GUT}} \sim \begin{pmatrix} \lambda^6 & \lambda^5 & \lambda^5 \\ \lambda^5 & \lambda^4 & \lambda^4 \\ \lambda^6 & \lambda^6 & \lambda^2 \end{pmatrix}, \tag{3.7.5}$$

$$\delta^e_{LL_{\rm GUT}} \sim \begin{pmatrix} 1 & \lambda^4 & \lambda^4 \\ \cdot & 1 & \lambda^4 \\ \cdot & \cdot & 1 \end{pmatrix}, \quad \delta^e_{RR_{\rm GUT}} \sim \begin{pmatrix} 1 & \lambda^3 & \lambda^4 \\ \cdot & 1 & \lambda^2 \\ \cdot & \cdot & 1 \end{pmatrix}, \quad \delta^e_{LR_{\rm GUT}} \sim \begin{pmatrix} \lambda^6 & \lambda^5 & \lambda^6 \\ \lambda^5 & \lambda^4 & \lambda^6 \\ \lambda^5 & \lambda^4 & \lambda^2 \end{pmatrix}. \tag{3.7.6}$$

3.7.2 Effects of RG running

Having calculated the GUT scale mass insertion parameters, it is now necessary to consider their evolution down to the electroweak scale. Only then is one able to compare the predictions

of the model to experimental measurements of flavour observables. This evolution is described by the RG equations which are given explicitly in Appendix E in the SCKM basis. Technically, the RG running is performed in two stages, first from $M_{\rm GUT}$ to M_R where the right-handed neutrinos are integrated out, and then from M_R to $M_{\rm SUSY} \sim M_W$. In order to derive analytical results, the effects of the running is estimated using the leading logarithmic approximation. As the Yukawa matrices themselves are also affected by the running, it is necessary to apply further basis transformations on the superfields which diagonalise the low energy Yukawas matrices.

Details of the various steps involved in calculating the low energy mass insertion parameters can be found in Appendix F. For the down-type squarks and the charged sleptons, the resulting effects can simply be absorbed into new order one coefficients. It is interesting to see that this is not the case for the up-type squarks, where the order of the (13) and (23) elements of δ^u_{LR} get modified. For completeness, the flavour structure of the low energy δs is presented in terms of their λ-suppression, which should be compared to Eqs. (3.7.4-3.7.6).

$$\delta^u_{LL} \sim \begin{pmatrix} 1 & \lambda^4 & \lambda^6 \\ \cdot & 1 & \lambda^5 \\ \cdot & \cdot & 1 \end{pmatrix}, \quad \delta^u_{RR} \sim \begin{pmatrix} 1 & \lambda^4 & \lambda^6 \\ \cdot & 1 & \lambda^5 \\ \cdot & \cdot & 1 \end{pmatrix}, \quad \delta^u_{LR} \sim \begin{pmatrix} \lambda^8 & 0 & \lambda^7 \\ 0 & \lambda^4 & \lambda^6 \\ 0 & \lambda^7 & 1 \end{pmatrix}, \tag{3.7.7}$$

$$\delta^d_{LL} \sim \begin{pmatrix} 1 & \lambda^3 & \lambda^4 \\ \cdot & 1 & \lambda^2 \\ \cdot & \cdot & 1 \end{pmatrix}, \quad \delta^d_{RR} \sim \begin{pmatrix} 1 & \lambda^4 & \lambda^4 \\ \cdot & 1 & \lambda^4 \\ \cdot & \cdot & 1 \end{pmatrix}, \quad \delta^d_{LR} \sim \begin{pmatrix} \lambda^6 & \lambda^5 & \lambda^5 \\ \lambda^5 & \lambda^4 & \lambda^4 \\ \lambda^6 & \lambda^6 & \lambda^2 \end{pmatrix}, \tag{3.7.8}$$

$$\delta^e_{LL} \sim \begin{pmatrix} 1 & \lambda^4 & \lambda^4 \\ \cdot & 1 & \lambda^4 \\ \cdot & \cdot & 1 \end{pmatrix}, \quad \delta^e_{RR} \sim \begin{pmatrix} 1 & \lambda^3 & \lambda^4 \\ \cdot & 1 & \lambda^2 \\ \cdot & \cdot & 1 \end{pmatrix}, \quad \delta^e_{LR} \sim \begin{pmatrix} \lambda^6 & \lambda^5 & \lambda^6 \\ \lambda^5 & \lambda^4 & \lambda^6 \\ \lambda^5 & \lambda^4 & \lambda^2 \end{pmatrix}. \tag{3.7.9}$$

3.8 Conclusion

The main aim of this Chapter was to study the amount of flavour and CP violation that can be generated through the soft SUSY breaking sector of the $SU(5) \times S_4 \times U(1)$ supersymmetric GUT model of flavour, which was proposed in [11]. The model's objective is to address the number of quark and lepton families, provide an explanation for the structure of the fermionic masses and mixing angles and at the same time describe the mechanism that suppresses flavour and CP violation induced by the SUSY sector.

The existence of three families emerges through the furnishing of the only faithful irreducible representations of S_4, the triplet representations. Working in an expansion in powers of the Wolfenstein parameter λ, the structure of the Yukawa and Majorana matrices, including CP violating phases, stems from the controlled way in which the family and CP symmetries are broken by the non-zero complex flavon vevs. This aspect was studied in [10, 11] where it was shown to provide a good description of all quark and lepton masses, mixings and CP violation. In this Chapter, the Yukawa sector was revisited, in order to examine whether canonical normalisation effects, which were ignored in [10, 11], considerably perturb the original matrix structures. It was found that those effects significantly alter the up-quark Yukawa matrix, by filling the zero textures and suppressing the (23) and (32) elements by two orders in λ. The (12), (21) and (33) elements of the Dirac Yukawa matrix are also reduced by two orders in λ. On the other hand, the down-quark and charged lepton Yukawas are solely modified by

additional contributions that are of the same order in λ as the non-canonical matrices. The structure of the effective neutrino mass matrix is also not alter to LO. As a result, the fermionic masses and mixing angles survive the canonical transformation effects and, to LO, they are in agreement with those obtained in [10, 11].

The study of the SUSY sector was based on the assumptions that the soft SUSY breaking mechanism respects the family and CP symmetries. Expressing the operators that contribute to the soft mass matrices as flavon expansions, after the family and CP symmetry breaking, the trilinear and scalar mass squared matrices were also expressed as power series in λ. Moving to the canonical and then to the SCKM basis, the results were presented in terms of mass insertion parameters at the GUT scale. When considering the effects of RG running down to the low scales, the Yukawa matrices developed off-diagonal entries anew. Therefore, a further basis transformation was required to render them diagonal again. Explicit expressions for the low mass insertion parameters in that basis are provided in Appendix F.3, while their λ-structure (dropping any coefficients) is summarised in Eqs. (3.7.7-3.7.9).

It was found that δ^f_{LL} and δ^f_{RR} are approximately equal to the identity, with only small off-diagonal entries. The δ^f_{LR} parameters feature the same hierarchies in the diagonal entries as the corresponding diagonal Yukawa matrices $\tilde{Y}^f$, while the off-diagonal elements are strongly suppressed. These results show that the $S_4 \times U(1)$ SUSY GUT approximately reproduces the effects of low energy MFV, where one would simply impose $\delta^f_{LL} = \delta^f_{RR} = \mathbb{1}$ and $\delta^f_{LR} \propto \tilde{Y}^f$. The phenomenological implications of the deviations form MFV are discussed quantitatively in Chapter 4, where the model's predictions with respect to a number of different flavour observables are discussed in detail.

Chapter 4

Phenomenological Implications of an $\mathbf{SU(5) \times S_4 \times U(1)}$ SUSY GUT of Flavour

4.1 Introduction

This chapter details my research on the exploration of the phenomenology implied by the $SU(5) \times S_4 \times U(1)$ SUSY GUT model of flavour that was studied in Chapter 3. The work presented in this chapter was recently submitted for publication [15] as a separate follow up to [14].

In Chapter 3 it was shown how MFV emerges approximately in the model. However, there are important phenomenological differences which can provide tell-tale signatures of the model, and it is the main purpose of this chapter to discuss these in detail. In other words, this work exploits the low energy mass insertion parameters of the model calculated in Chapter 3 to analyse a panoply of rare and flavour changing processes as well as EDMs in both the lepton and quark sectors. The results are quite illuminating: while only small new effects in B physics are found, very large effects arise for Lepton Flavour Violation (LFV) and the EDMs which are therefore predicted to be observed soon.

The layout of the remainder of the Chapter is as follows. Section 4.2 discusses numerical estimates of the low energy mass insertion parameters for ranges of SUSY parameters which are consistent with the bounds from direct searches for squarks and sleptons at LHC Run 1. The naive model expectations are compared to the numerical scans and the experimental bounds. In Section 4.3 these results are then used to estimate the predictions for EDMs, LFV, B and K meson mixing as well as rare B decays. The largest observable deviations from MFV come from the LFV process $\mu \to e\gamma$ and the EDMs. Section 4.4 concludes the Chapter.

4.2 Numerical analysis

4.2.1 Parameter range

Numerical results for the running quark and charged lepton masses as well as for the quark mixing angles at the GUT scale can be found in [83]. The matching conditions from the SM to the MSSM, imposed at the SUSY scale, take the form

$$\begin{aligned} y_{u,c,t}^{\rm SM} &\approx y_{u,c,t}^{\rm MSSM} \sin\bar{\beta}, \\ y_{d,s}^{\rm SM} &\approx (1+\bar{\eta}_q)\, y_{d,s}^{\rm MSSM} \cos\bar{\beta}, \\ y_{b}^{\rm SM} &\approx (1+\bar{\eta}_b)\, y_{b}^{\rm MSSM} \cos\bar{\beta}, \\ y_{e,\mu}^{\rm SM} &\approx (1+\bar{\eta}_l)\, y_{e,\mu}^{\rm MSSM} \cos\bar{\beta}, \\ y_{\tau}^{\rm SM} &\approx y_{\tau}^{\rm MSSM} \cos\bar{\beta}, \end{aligned} \tag{4.2.1}$$

for the singular values of the Yukawa matrices. Similarly, for the CKM mixing

$$\theta_{i3}^{q,\rm SM} \approx \frac{1+\bar{\eta}_q}{1+\bar{\eta}_b}\theta_{i3}^{q,\rm MSSM}, \qquad \theta_{12}^{q,\rm SM} \approx \theta_{12}^{q,\rm MSSM}, \qquad \delta^{q,\rm SM} \approx \delta^{q,\rm MSSM}. \tag{4.2.2}$$

Here

$$\bar{\eta}_q = \eta_q - \eta_l', \qquad \bar{\eta}_b = \eta_q' + \eta_A - \eta_l', \qquad \bar{\eta}_l = \eta_l - \eta_l', \tag{4.2.3}$$

represent SUSY radiative threshold corrections that are parametrised by $\eta_i = \epsilon_i \tan\beta$, with explicit expressions for ϵ_i available in [84]. The unprimed η parameters correspond to corrections to the first two generations, the primed ones to the third generation, and the one with index "A" to a correction due to the soft SUSY breaking trilinear terms. The parameter $\bar{\beta}$ follows from the absorption of η_l' into β,

$$\cos\bar{\beta} \equiv (1+\eta_l')\cos\beta, \qquad \sin\bar{\beta} \approx \sin\beta, \tag{4.2.4}$$

with the approximation being valid for $\tan\beta \gtrsim 5$. In the limit where threshold effects for the charged leptons are neglected, $\tan\bar{\beta}$ simply reduces to $\tan\beta$.

The model presented in Chapter 3 predicts $\hat{y}_{b,\tau} = y_b\,\lambda^2$, where the hat indicates the diagonalised Yukawa sector at the GUT scale. As a consequence, very large values of $\tan\beta$ are excluded, and this work will only study the parameter space in which $\tan\beta \in [5, 25]$, keeping the value of y_b below four. In order to obtain viable ranges for the Yukawa input parameters, $y_{u,c,t,b}$, $(\tilde{x}_2/y_s)^2$ and $(1+\bar{\eta}_l)y_s$ are plotted against $\tan\bar{\beta}$ using the results for the diagonalised Yukawa sector at the GUT scale provided in [83]. Note that y_b, y_s and $\tilde{x}_2$ are extracted from the lepton sector. The resulting curves are fitted using the relative uncertainties $\sigma(y_u)/y_u = 31\%$, $\sigma(y_c)/y_c = 3.5\%$, $\sigma(y_t)/y_t = 10\%$, $\sigma(y_b)/y_b = 0.6\%$, see [83]. Concerning y_s and $\tilde{x}_2$, here it is taken that $\sigma(y_s)/y_s = 10\%$ and $\sigma(\tilde{x}_2)/\tilde{x}_2 = 10\%$, allowing for higher order corrections to the mass ratios that would reduce the discrepancy between the values of $\tilde{x}_2/y_s$ predicted from the lepton and the quark sectors and maximise the GUT scale value of $(\hat{y}_\mu\,\hat{y}_d)/(\hat{y}_s\,\hat{y}_e)$. Due to the implementation of the Georgi-Jarlskog relation [71], it is equal to 9 in the model at LO, while

its preferred range is $10.7^{+1.8}_{-0.8}$ [83], which is independent of threshold corrections and also not sensitive to a change of the SUSY scale.

The low energy Yukawa couplings are estimated using the leading logarithmic approximation as described in Chapter 3. Clearly, the resulting low energy Yukawa matrices will only be valid up to that approximation. Mindful of such limitations, one has

$$\tilde{Y}^u_{\rm low} \approx {\rm Diag}\left[(1+R^y_u)\,y_u\,\lambda^8, (1+R^y_u)\,y_c\,\lambda^4, (1+R^y_t)\,y_t\right], \tag{4.2.5}$$

$$\tilde{Y}^d_{\rm low} \approx {\rm Diag}\left[(1+R^y_d)\frac{\tilde{x}_2^2}{y_s}\lambda^6, (1+R^y_d)\,y_s\,\lambda^4, (1+R^y_b)\,y_b\,\lambda^2\right], \tag{4.2.6}$$

$$\tilde{Y}^e_{\rm low} \approx {\rm Diag}\left[(1+R^y_e)\frac{\tilde{x}_2^2}{3\,y_s}\lambda^6, (1+R^y_e)3y_s\,\lambda^4, (1+R^y_e)\,y_b\,\lambda^2\right], \tag{4.2.7}$$

where the corrections from the RG running are encoded in the parameters R^y_f, defined in Eq. (F.1.6). The scan produces the following values for the right-hand sides of Eq. (4.2.1):

$$\begin{aligned}
&\tilde{Y}^u_{\rm low_{11}} \sin\bar{\beta} \in [3.4, 6.9]\times 10^{-6},\ \tilde{Y}^u_{\rm low_{22}} \sin\bar{\beta} \in [2.34, 2.65]\times 10^{-3},\ \tilde{Y}^u_{\rm low_{33}} \sin\bar{\beta} \in [0.77, 0.89],\\
&\tilde{Y}^d_{\rm low_{11}} \cos\bar{\beta}(1+\bar{\eta}_q) \in [0.9, 1.6]\times 10^{-5}, \qquad \tilde{Y}^d_{\rm low_{22}} \cos\bar{\beta}(1+\bar{\eta}_q) \in [2.2, 3.5]\times 10^{-4},\\
&\tilde{Y}^d_{\rm low_{33}} \cos\bar{\beta}(1+\bar{\eta}_b) \in [1.17, 1.6]\times 10^{-2},\\
&\tilde{Y}^e_{\rm low_{11}} \cos\bar{\beta}(1+\bar{\eta}_l) \in [2.4, 3.8]\times 10^{-6}, \qquad \tilde{Y}^e_{\rm low_{22}} \cos\bar{\beta}(1+\bar{\eta}_l) \in [5.6, 7.7]\times 10^{-4},\\
&\tilde{Y}^e_{\rm low_{33}} \cos\bar{\beta} \in [1.06, 1.14]\times 10^{-2},
\end{aligned} \tag{4.2.8}$$

which have to be compared to the SM values, taken from Table 2 of [83],

$$\begin{aligned}
&y_u^{\rm SM} \in [3.40, 7.60]\times 10^{-6}, \quad y_c^{\rm SM} \in [2.69, 3.20]\times 10^{-3}, \quad y_t^{\rm SM} \in [0.78, 0.88],\\
&y_d^{\rm SM} \in [1.15, 1.56]\times 10^{-5}, \quad y_s^{\rm SM} \in [2.29, 2.84]\times 10^{-4}, \quad y_b^{\rm SM} \in [1.21, 1.42]\times 10^{-2},\\
&y_e^{\rm SM} \in [2.85, 2.88]\times 10^{-6}, \quad y_\mu^{\rm SM} \in [6.01, 6.08]\times 10^{-4}, \quad y_\tau^{\rm SM} \in [1.02, 1.03]\times 10^{-2}.
\end{aligned} \tag{4.2.9}$$

The corresponding ranges of the order one input parameters of the Yukawa sector are listed in the first five rows of the first column of Table 4.1. All other coefficients that are not fixed by this fit, are scanned over the interval $\pm[0.5, 2]$, with the following exceptions: the absolute value of the Dirac neutrino Yukawa coupling y_D is allowed to be as small as 0.2 but not larger than 0.6, such that it does not exceed the maximum allowed value of y_t. The lower bounds on $|\tilde{x}^a_2|$, $|a_s|$ and $|a_u|$ are also relaxed and the upper bound on $|a_b|$ is extended, such that they are allowed to get the same values as the corresponding Yukawa coefficients. The coefficients c_{H_u} and c_{H_d} of the soft Higgs mass squares,

$$m^2_{H_u{\rm GUT}} = c_{H_u}\,m_0^2, \qquad m^2_{H_d{\rm GUT}} = c_{H_d}\,m_0^2\,, \tag{4.2.10}$$

are taken to be positive, just like the coefficients b_{01}, b_{02} and $B_0^{(N)}$ of the leading order diagonal elements of the soft scalar mass squared matrices. Phases are generally allowed to take arbitrary values within $[0, 2\pi]$. As mentioned earlier, $\tan\beta \equiv t_\beta$ is varied between 5 and 25. Concerning the CMSSM parameters, the following are defined:

$$\alpha_0 \equiv A_0/m_0, \qquad x \equiv (M_{1/2}/m_0)^2, \tag{4.2.11}$$

Yukawa terms	Range	Soft trilinear terms	Range
$\tilde{x}_2, y_s$	$[0.2, 1.6]$	$\tilde{x}_2^a, a_s$	$\pm[0.2, 2]$
y_b	$[0.7, 3.8]$	a_b	$\pm[0.5, 4]$
y_u	$[0.3, 0.6]$	a_u	$\pm[0.3, 2]$
y_c	$[0.5, 0.6]$	a_c	$\pm[0.5, 2]$
y_t	$[0.46, 0.6]$	a_t	
y_D	$\pm[0.2, 0.6]$	α_D	
z_i^f	$\pm[0.5, 2]$	$z_i^{f_a}$	
Kähler metric	Range	Soft mass terms	Range
$k_2, k_3, k_4, K_3^{(N)}$	$\pm[0.5, 2]$	$b_2, b_3, b_4, B_3^{(N)}$	$\pm[0.5, 2]$
		$b_{01}, b_{02}, B_0^{(N)}, c_{H_u}, c_{H_d}$	$[0.5, 2]$
SUSY masses	Range	SUSY ratios	Range
$M_{1/2}$	$[0.3, 5]$ TeV	$\tan\beta$	$[5, 25]$
m_0	$[0.05, 5]$ TeV	α_0	$[-3, 3]$

TABLE 4.1: Ranges of the input parameters used in the scan.

and scanned over $M_{1/2} \in [0.3, 5]$ TeV, $m_0 \in [0.05, 5]$ TeV as well as $\alpha_0 \in [-3, 3]$ in order to avoid charge and colour breaking minima.[1]

The μ parameter, which is taken as real, is given at the electroweak scale by the relation [86]

$$\frac{M_Z^2}{2} = \frac{m_{H_d}^2 + \Sigma_d^d - (m_{H_u}^2 + \Sigma_u^u) t_\beta^2}{t_\beta^2 - 1} - \mu^2, \tag{4.2.12}$$

where M_Z denotes the Z boson mass. Σ_u^u and Σ_d^d are radiative corrections, with the most important contributions coming from the stops,

$$\Sigma_u^u(\tilde{t}_{1,2}) = \frac{3}{16\pi^2} F(m_{\tilde{t}_{1,2}}^2) \left(Y_t^2 - g_Z^2 \mp \frac{A_t^2 - 8 g_Z^2 \left(\frac{1}{4} - \frac{2}{3} x_W\right) \Delta_t}{m_{\tilde{t}_2}^2 - m_{\tilde{t}_1}^2} \right), \tag{4.2.13}$$

$$\Sigma_d^d(\tilde{t}_{1,2}) = \frac{3}{16\pi^2} F(m_{\tilde{t}_{1,2}}^2) \left(g_Z^2 \mp \frac{Y_t^2 \mu^2 + 8 g_Z^2 \left(\frac{1}{4} - \frac{2}{3} x_W\right) \Delta_t}{m_{\tilde{t}_2}^2 - m_{\tilde{t}_1}^2} \right). \tag{4.2.14}$$

In these expressions, Y_t, A_t and μ denote the low energy Yukawa and trilinear couplings and the low energy μ parameter, respectively. Moreover,

$$\begin{aligned} m_{\tilde{t}_{1,2}}^2 &= \frac{1}{2} \left(m_{\tilde{t}_{LL}}^2 + m_{\tilde{t}_{RR}}^2 \mp \sqrt{4 m_{\tilde{t}_{LR}}^2 + (m_{\tilde{t}_{LL}}^2 - m_{\tilde{t}_{RR}}^2)^2} \right), \\ F(m^2) &= m^2 \left(\log\left(\frac{m^2}{M_S^2}\right) - 1 \right), \qquad \Delta_t = \frac{1}{2} \left(m_{\tilde{t}_{LL}}^2 - m_{\tilde{t}_{RR}}^2 \right) + M_Z^2 \cos(2\beta) \left(\frac{1}{4} - \frac{2}{3} x_W \right), \\ x_W &= \sin^2\theta_W, \qquad g_Z^2 = \frac{M_Z^2}{4v^2}, \qquad M_S = \sqrt{m_{\tilde{t}_1} m_{\tilde{t}_2}}, \end{aligned} \tag{4.2.15}$$

with θ_W denoting the Weinberg angle. $m_{\tilde{t}_{LL}}^2$, $m_{\tilde{t}_{RR}}^2$ and $m_{\tilde{t}_{LR}}^2$ are the low energy (33) elements of the squark mass matrices defined in Eq. (3.7.1).

[1] In the numerical scan, it was checked that the potentials are always bounded from below and that the corresponding minima do not break charge nor colour [85].

The so-determined μ parameter can then be used to calculate the physical Higgs mass. The estimation of the intrinsic theoretical uncertainties when including the full one-loop and dominant two-loop corrections to the tree level mass is of the order of 3 GeV [88]. Considering the $t/\tilde{t}$ sector, the one-loop effect leads to the by far most important positive contribution to the Higgs mass, while the two-loop $\mathcal{O}(\alpha_t\alpha_s)$ and $\mathcal{O}(\alpha_t^2)$ effects, where α_t is defined as the superpotential top Yukawa coupling squared suppressed by 4π, cause a further reduction and a smaller enhancement respectively. Approximate formulae including the leading m_t^4 corrections (ignoring the $\mathcal{O}(\alpha_t^2)$ effects) within the Feynman diagrammatic (FD) approach, are provided in [87]. Eqs. (2.64-2.66) therein express the Higgs mass in terms of on-shell quantities. Rewritting this result in terms of the running top-quark mass in the $\overline{\text{MS}}$ scheme, as in Eqs. (2.67,2.68) of [87], an extra $\mathcal{O}(\alpha_t\alpha_s)$ contribution is induced, lifting the Higgs mass by a few GeV for $M_S \sim 1$ TeV and considerably more for growing M_S. When taking into account the $\mathcal{O}(\alpha_t^2)$ corrections, a several GeV increase is observed [87], while the (s)bottom effects only become important for large μ and $t_\beta > 30$. As pointed out in [88], an adequate estimation of the Higgs mass should properly account for the dependence on the SUSY scale. In particular, the few GeV uncertainty atributed in the $M_S \sim 1$ TeV study, corresponds to a significant underestimation of the higher order corrections for $M_S \gtrsim 2$ TeV. Interestingly, for a sufficiently high SUSY scale, the experimentally measured Higgs mass can be reached, even for vanishing mixing in the stop sector [88]. In view of the limitations of the available approximate analytic expressions, in this work, adopting the formulae (2.64-2.66) of [87], it is demanded that the resulting Higgs mass lies within the interval $[110, 135]$ GeV. A more precise fit, even though is expected to restrict any model's parameter space, would require the implementation of the appropriate numerical methods, an approach which is beyond the scope of the present work. However, it is worth commenting on the well known maximal mixing requirement for reaching the observed Higgs mass, when $M_S \sim 1$ TeV. In that case, due to the trilinear couplings being non-universal in family space, the mixing in the sectors other than the stop one, can still be relatively small, while, as already mentioned, with increasing SUSY scale, the maximal mixing requirement gets lifted.

Concerning cuts on the SUSY parameters from direct searches, it is required that the first and the second generation squark masses are larger than 1.4 TeV.

4.2.2 Estimates of the low energy mass insertion parameters

This section analyses the predictions for the low energy mass insertion parameters δ, whose explicit expressions are given in Appendix F.3. Tables 4.2-4.6 provide naive expectations for the individual δs, where the λ-suppression and the main effects of the RG running are accounted for, while any order one coefficients are set to one. Clearly, one still expects to see a spread within a few orders of magnitude due to the variation of the SUSY scale and the order one coefficients. The third columns of Tables 4.2-4.6 list existing experimental bounds. The full ranges of the δs arising from scanning over the input parameters given in Table 4.1, are depicted in Figures 4.1-4.6.

4.2.2.1 Up-type quark sector

Parameter	Naive expectation	Exp. bound
$\sqrt{\lvert\mathrm{Im}[(\delta^u_{LL,RR})^2_{12}]\rvert}$	$\mathcal{O}\left(\frac{\sqrt{\sin(2\theta^d_2)}\lambda^4}{1+6.3\,x} \approx 4\times10^{-4}\sqrt{\sin(2\theta^d_2)}\right)$	2.85×10^{-2} [89] $(1.65\times10^{-3})\vert_{LL=RR}$
$\sqrt{\lvert\mathrm{Im}[(\delta^u_{LR,RL})^2_{12}]\rvert}$	0	3.75×10^{-3}[89]
$\lvert(\delta^u_{LL})_{13}\rvert$	$\mathcal{O}\left(\frac{1+\eta\left(\frac{R_q}{1+6.5\,x}-y_t^2\right)}{1+6.5\,x}\lambda^6 \approx 2\times10^{-5}\right)$	$\mathcal{O}(10^{-1})$ [90]
$\lvert(\delta^u_{RR})_{13}\rvert$	$\mathcal{O}\left(\frac{1+2\eta\left(\frac{R_q}{1+6.15\,x}-y_t^2\right)}{1+6.15\,x}\lambda^6 \approx 2\times10^{-5}\right)$	
$\lvert(\delta^u_{LL})_{23}\rvert$	$\mathcal{O}\left(\frac{1+\eta\left(\frac{R_q}{1+6.5\,x}-y_t^2\right)}{1+6.5\,x}\lambda^5 \approx 8\times10^{-5}\right)$	
$\lvert(\delta^u_{RR})_{23}\rvert$	$\mathcal{O}\left(\frac{1+2\eta\left(\frac{R_q}{1+6.15\,x}-y_t^2\right)}{1+6.15\,x}\lambda^5 \approx 8\times10^{-5}\right)$	
$\lvert(\delta^u_{LR})_{13}\rvert$	$\mathcal{O}\left(\frac{\alpha_0\,v_u}{m_0}\frac{2\,\eta}{(1+6.3\,x)}\lambda^7 \approx 10^{-7}\right)$	
$\lvert(\delta^u_{LR})_{23}\rvert$	$\mathcal{O}\left(\frac{\alpha_0\,v_u}{m_0}\frac{2\,\eta}{(1+6.3\,x)}\lambda^6 \approx 5\times10^{-7}\right)$	$\mathcal{O}(10^{-1})$ [91]
$\lvert(\delta^u_{RL})_{13}\rvert$	0	
$\lvert(\delta^u_{RL})_{23}\rvert$	$\mathcal{O}\left(\frac{\alpha_0\,v_u}{m_0}\frac{1+\eta\left(\frac{46\,g_U^2}{5}-8y_t^2+\frac{R_q}{1+6.5\,x}\right)}{1+6.3\,x}\lambda^7 \approx 5\times10^{-7}\right)$	

TABLE 4.2: The naive numerical expectations for the low energy up-type mass insertion parameters as extracted from the model (second column), to be compared with experimental bounds in the literature (third column). The full ranges of the δs are shown in Figures 4.1 and 4.2. Note that the (12), (21) and (31) δ^u_{LR} parameters remain zero up to order λ^8.

The strongest constraints on the up-type mass insertion parameters involve the (12) sector and stem from $D^0 - \bar{D}^0$ mixing. The SM contribution to this amplitude conserves CP to a good approximation and provides significant constraints on the imaginary parts of $(\delta^u_{AB})_{12}$, $A, B = L, R$. These limits were derived in [89], assuming equal squark and gluino masses of 1 TeV. They are quoted in the third column of Table 4.2, rescaled to masses of 1.5 TeV. The limits on the RR and RL parameters are identical to the LL and LR ones due to the $L \leftrightarrow R$ symmetric form of the gluino-squark box diagram. The index $LL = RR$ refers to the assumption that $(\delta^u_{LL})_{12} \approx (\delta^u_{RR})_{12}$, as is the case in the model. In the second column of Table 4.2, naive estimates are given for $\sqrt{\lvert\mathrm{Im}[(\delta^u_{LL})^2_{12}]\rvert} \approx \sqrt{\lvert\mathrm{Im}[(\delta^u_{RR})^2_{12}]\rvert} \approx \sqrt{\lvert\mathrm{Im}[(\delta^u_{LL})_{12}(\delta^u_{RR})_{12}]\rvert}$. For $\theta^d_2 = \pi/2$, as suggested from maximising the Jarlskog invariant of Eq. (3.6.5), these quantities vanish to LO. Since $\sqrt{\lvert\mathrm{Im}[(\delta^u_{LL,RR})^2_{12}]\rvert}$ is at most $\sim \lvert(\delta^u_{LL})_{12}\rvert$, only the full range of the absolute value of that parameter is shown in Figure 4.1, plotted against the corresponding GUT scale coefficient $\tilde{b}_{12}$, defined in Eq. (D.4). This coefficient quantifies the mismatch between the Kähler metric and the soft mass matrix elements for the $SU(5)$ **10**-plets and can be as large as 6 when the associated parameters contribute constructively and receive their maximum values in the scan. The effects of the RG running are trivial and depend only on $x = (M_{1/2}/m_0)^2$; for $x \approx 1$ and $\tilde{b}_{12} \approx 1$, a value of around 4×10^{-4} is estimated, shown by the blue dashed line in Figure 4.1.

With increasing x, even smaller values are obtained, as the RG suppression is increased. The red dotted line shows the experimental limit, adapted from [89] and valid for $(\delta^u_{LL})_{12} \approx (\delta^u_{RR})_{12}$.

The LL and RR parameters of the $(i3)$ sector $(i = 1, 2)$ have GUT scale coefficients with the same range as the parameters of the (12) sector but a different RG suppression due to the milder running of the third generation sfermionic masses. This is represented by the factor $\eta\, R_q$ appearing in Eq. (F.3.14), where η and R_q are defined in Eqs. (F.1,F.2.14), respectively. Approximating these δs as shown in Table 4.2 and taking $x \approx 1$, $R_q \approx 3y_t^2 + 1$ as well as $y_t \approx 0.5$, one expects $|(\delta^u_{LL,RR})_{13}| \propto \lambda^6$ and $|(\delta^u_{LL,RR})_{23}| \propto \lambda^5$ to vary around 2×10^{-5} and 8×10^{-5}, respectively. The existing bounds on these variables from flavour changing effects are very weak, leaving them essentially unconstrained. B_d mixing can place a bound on $|(\delta^u_{LL})_{13}|$ of the order of 10^{-1} at most, as described in [90].

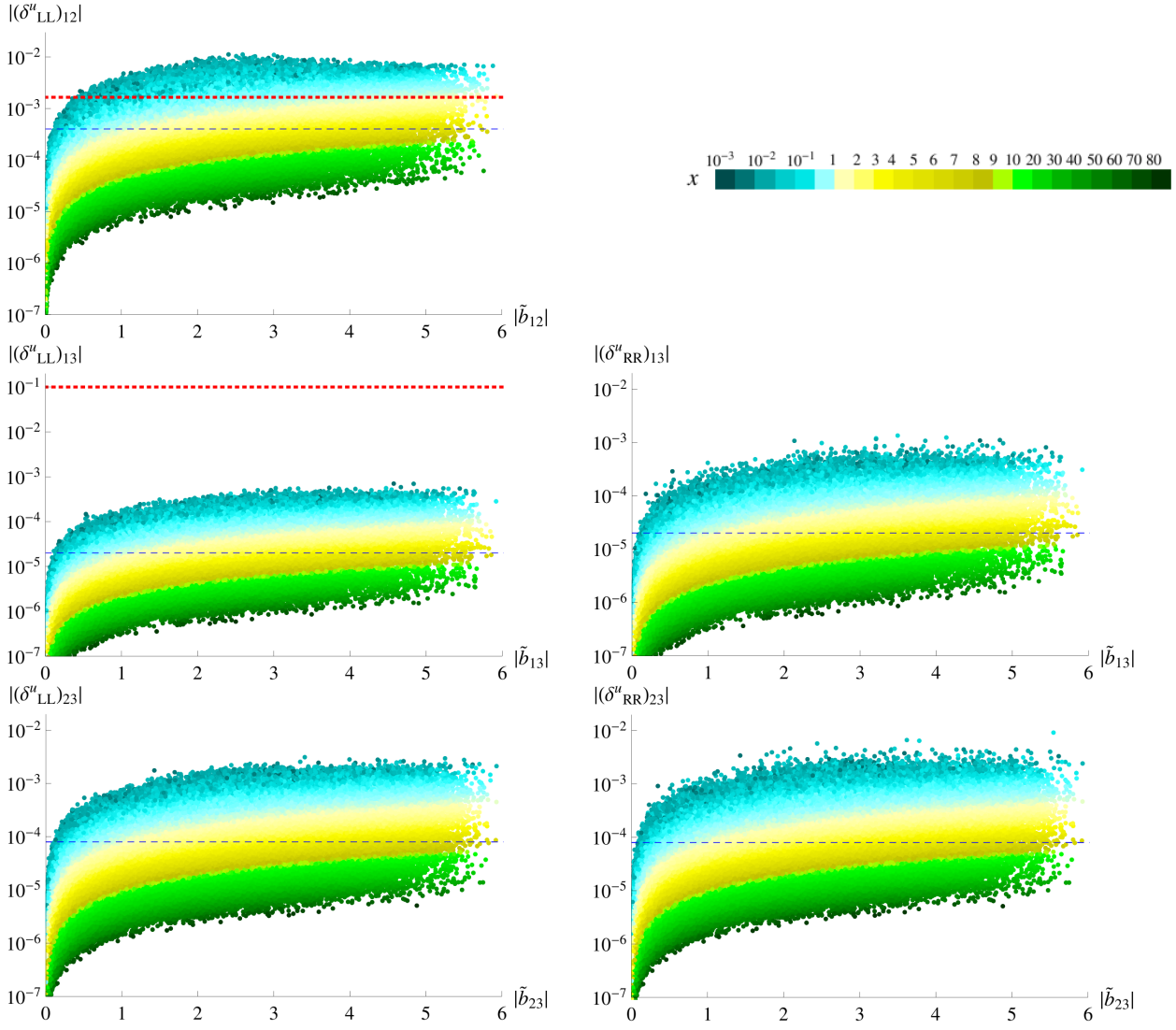

FIGURE 4.1: The low energy LL and RR up-type mass insertion parameters plotted against their GUT scale coefficients, defined in Eq. (D.4). The blue dashed lines represent the naive numerical expectations according to the second column of Table 4.2, while the red dotted lines (when available) represent the experimental limits shown in the third column of Table 4.2. Since $(\delta^u_{RR})_{12} \approx (\delta^u_{LL})_{12}$, only the LL parameter is plotted. The plots have been produced by scanning over the input parameters listed in Table 4.1.

The parameters of LR type have a slightly different behaviour. They are proportional to the factor $(\alpha_0\, v_u/m_0)$ which, for $|A_0| > 0.5$ TeV, can cause an extra suppression of up to $\mathcal{O}(10^{-3})$. Because of this factor, the LR parameters show a dependence on the mass scale, even at the GUT scale. $(\delta^f_{LR})_{ij}$ are also generally proportional to the mismatch of the ratios of soft trilinear over Yukawa sector coefficients for the i-th and the j-th generation and vanish, barring RG induced corrections, if those are aligned. To estimate the magnitude of these parameters in Table 4.2, $|\alpha_0|\, v_u/m_0 \approx 10^{-1}$, $x \approx 1$, $y_t \approx 0.5$ and $R_q \approx 1.75$ are taken, while their full ranges are shown in Figure 4.2.

The $(\delta^u_{LR})_{13}$ parameter was zero at the GUT scale but receives a contribution through the RG running of the order of $\eta\,\lambda^7$. Similarly, $(\delta^u_{LR})_{23}$, which was suppressed by λ^7 at the GUT scale, receives a similar running contribution which comes in at an even lower order, namely $\eta\,\lambda^6$. Such an effect is not found in any other δ parameter. Finally, note that $(\delta^u_{LR,RL})_{12}$ as well as $(\delta^u_{RL})_{13}$ are zero up to order λ^8, where the expansion is truncated.

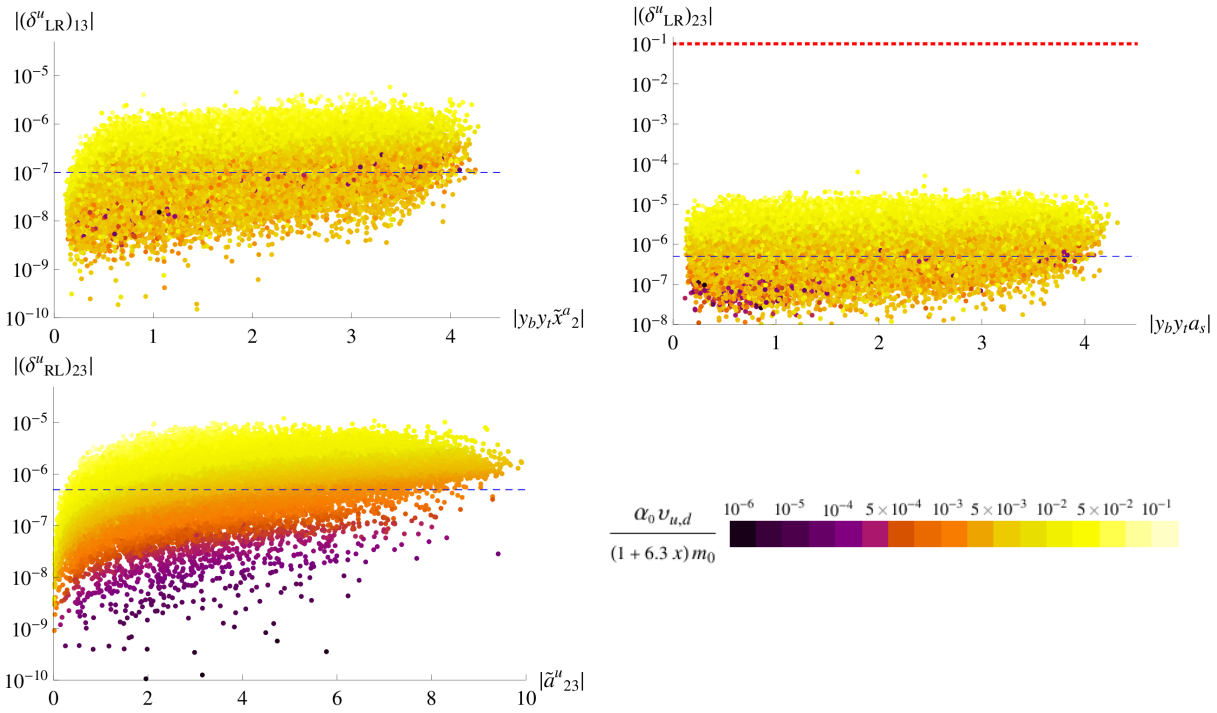

FIGURE 4.2: Low energy LR and RL up-type mass insertion parameters. $(\delta^u_{RL})_{23}$ is plotted against its GUT scale coefficient, defined in Eq. (D.5), while $(\delta^u_{LR})_{13,23}$ are plotted against a coefficient multiplying the RG running contribution, see Eqs. (F.3.11,F.3.12). The blue dashed lines represent the naive numerical expectations according to the second column of Table 4.2, while the red dotted line represents the experimental limit shown in the third column of Table 4.2. The plots have been produced by scanning over the input parameters listed in Table 4.1.

The limits on the LR parameters of the $(i3)$ sector $(i = 1, 2)$ originate mainly from the requirement that the potential be bounded from below with a vacuum that does not break charge nor colour [85]. Having already constrained the trilinear parameters accordingly, those effects shall not be discussed further. Other bounds on the LR off-diagonal parameters can be deduced by demanding that the supersymmetric radiative corrections to the CKM matrix elements do not

exceed their experimental values [92]. The limit for $|(\delta^u_{LR})_{23}|$ quoted in Table 4.2 has been obtained in [91] by considering chargino loop contributions to $b \to s l^+ l^-$. In the model, all up-type mass insertion parameters of the LR type turn out to be safely below any current bound.

4.2.2.2 Down-type quark sector

Parameter	Naive expectation	Exp. bound
$\sqrt{\lvert\mathrm{Re}\left[(\delta^d_{LL})^2_{12}\right]\rvert}$	$\mathcal{O}\left(\frac{1}{1+6.5\,x}\lambda^3 \approx 2\times10^{-3}\right)$	$[6.6\times10^{-2},$
$\sqrt{\lvert\mathrm{Re}\left[(\delta^d_{RR})^2_{12}\right]\rvert}$	$\mathcal{O}\left(\frac{\sqrt{\cos(2\theta^d_2)}}{1+6.1\,x}\lambda^4 \approx 4\times10^{-4}\sqrt{\cos(2\theta^d_2)}\right)$	$3.3\times10^{-1}]$
$\sqrt{\lvert\mathrm{Im}\left[(\delta^d_{LL})^2_{12}\right]\rvert}$	$\mathcal{O}\left(\frac{\sqrt{\sin(\theta^d_2)}}{1+6.5\,x}\lambda^{7/2} \approx 7\times10^{-4}\sqrt{\sin(\theta^d_2)}\right)$	$[8.7\times10^{-3},$
$\sqrt{\lvert\mathrm{Im}\left[(\delta^d_{RR})^2_{12}\right]\rvert}$	$\mathcal{O}\left(\frac{\sqrt{\sin(2\theta^d_2)}}{1+6.1\,x}\lambda^4 \approx 4\times10^{-4}\sqrt{\sin(2\theta^d_2)}\right)$	$4.2\times10^{-2}]$
$\sqrt{\lvert\mathrm{Re}\left[(\delta^d_{LR(RL)})^2_{12}\right]\rvert}$	$\mathcal{O}\left(\frac{\alpha_0\,v_d}{m_0}\frac{1+\eta\frac{44}{5}\frac{g_U^2}{}}{1+6.3\,x}\lambda^5\times\right.$	$[7.8, 12]\times10^{-3}$
$\lvert\mathrm{Im}\left[(\delta^d_{LR(RL)})_{12}\right]\rvert$	$\left.\mathrm{Re(Im)}\left[f(\theta_2^{\tilde{x}_a}-\theta_2^{\tilde{x}},\theta_s^a-\theta_s^y)\right] \approx 7\times10^{-7}\right)$	$[1, 5.7]\times10^{-4}$

TABLE 4.3: The naive expectation for the ranges of $(\delta^d_{AB})_{12}$, $A, B = L, R$, as extracted from the model (second column), to be compared with experimental bounds from [93] for $m_{\tilde{q}} \approx 1.5$ TeV and $(m_{\tilde{g}}/m_{\tilde{q}})^2 \in [0.3, 4]$ (third column). The full ranges of these δs as produced in the scan are shown in Figures 4.3 and 4.4.

The (12) elements of the down-type mass insertion parameters $(\delta^d_{AB})_{12}$ will be considered first, where $A, B = L, R$. The corresponding bounds are derived from the results of [93], which are rescaled to $m_{\tilde{q}} \approx 1.5$ TeV and $(m_{\tilde{g}}/m_{\tilde{q}})^2 \in [0.3, 4]$. These bounds are summarised in the third column of Table 4.3 and have been extracted using observables related to Kaon mixing. They are given separately for the real and imaginary parts due to a relative difference of an order of magnitude.

In the model, $(\delta^d_{LL})_{12} \sim \lambda^3$ is real at LO, while the NLO contribution is a linear combination of $e^{-i\theta^d_2}$ and $\cos(4\theta^d_2+\theta^d_3)$. Therefore, $\sqrt{\lvert\mathrm{Im}\left[(\delta^d_{LL})^2_{12_{\mathrm{NLO}}}\right]\rvert}$ is proportional to $\sqrt{\sin(\theta^d_2)}\lambda^{7/2}$. Setting $\theta^d_2 = \pi/2$, i.e. the value preferred by the Jarlskog invariant J^q_{CP}, one expects $\mathrm{Im}\left[(\delta^d_{LL})^2_{12_{\mathrm{NLO}}}\right]$ to take its maximum value. In Figure 4.3 only the absolute value of this mass insertion parameter is plotted versus its GUT scale coefficient $\tilde{B}_{12}$, see Eq. (D.4), which can take values between zero and twelve. The naive numerical estimate of $|(\delta^d_{LL})_{12}|$, approximated as shown in the second column of Table 4.3, is of the order of 10^{-3} for $x \approx 1$, visualised by the blue dashed line in Figure 4.3. Since the experimental limits are given as ranges, they are depicted by the red shaded region.

The parameter $(\delta^d_{RR})_{12}$ is proportional to $e^{i\theta^d_2}$, so that $\sqrt{\lvert\mathrm{Im}\left[(\delta^d_{RR})^2_{12}\right]\rvert}$ vanishes for $\theta^d_2 = \pi/2$, while the corresponding real part is maximised. The RG suppression is again trivial, only depending on x, while the GUT scale δ parameter is proportional to the misalignment of the coefficients of the Kähler metric and the soft squared mass for the $SU(5)$ $\bar{\mathbf{5}}$-plets: $\tilde{R}_{12} = (B_3 - K_3)$, see Eq. (D.4). When $B_3 = -K_3 = 2$ and $x \ll 1$, the absolute value of this mass

insertion reaches its maximum of 10^{-2}, as can be seen in the associated plot in Figure 4.3. On the other hand, for $B_3 = 0.5$, $K_3 = 1$ and $x \gg 1$, it can scale down to about 10^{-6}. Note that $|(\delta^d_{RR})_{12}| = |(\delta^d_{RR})_{23}| = |(\delta^d_{RR})_{13}|$, as can be seen in Eqs. (F.3.20,F.3.21).

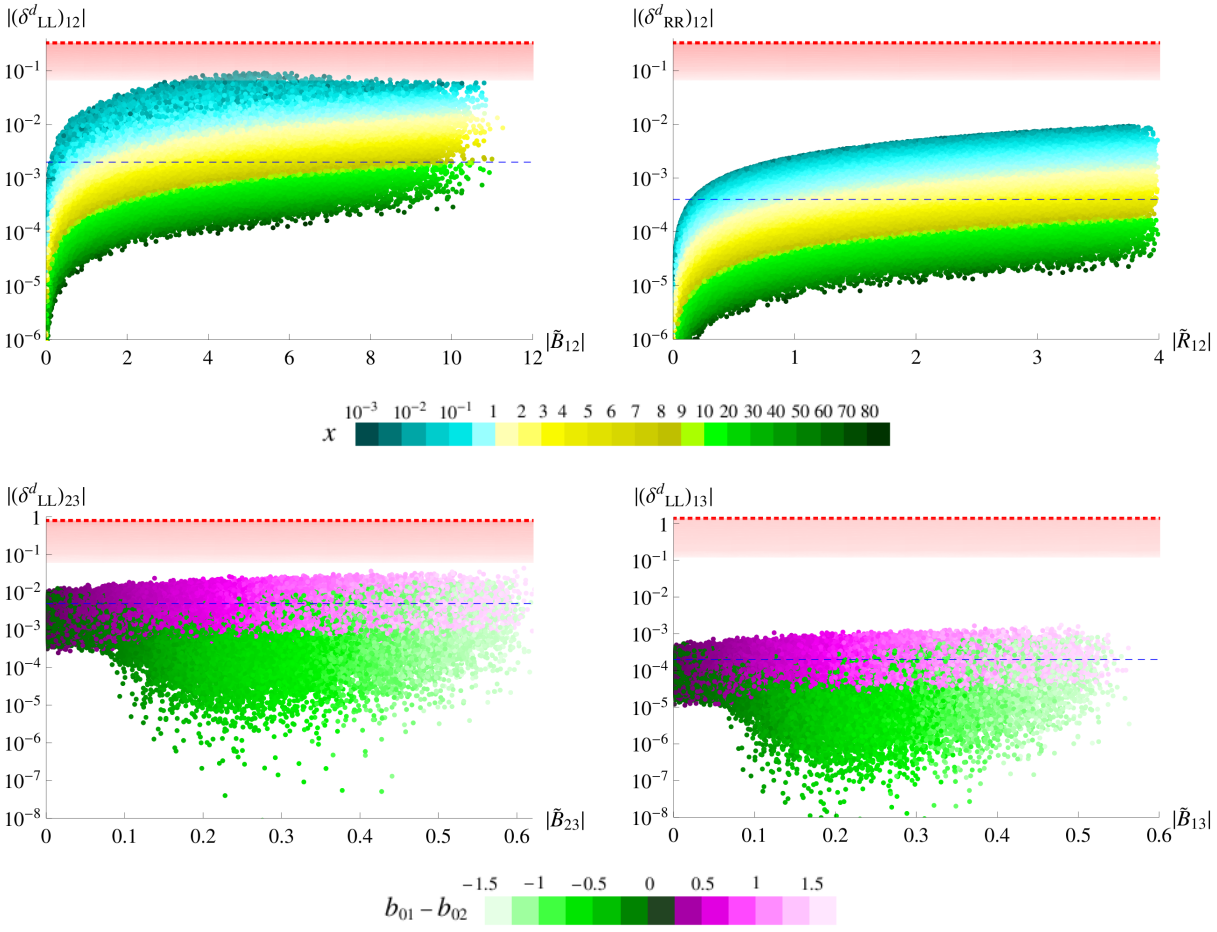

FIGURE 4.3: Low energy LL and RR down-type mass insertion parameters plotted against their GUT scale coefficients, defined in Eqs. (D.4). The blue dashed lines represent the naive numerical expectation according to the second columns of Tables 4.3-4.5. The red shaded areas cover the parameter space bounded by the limits shown in the third column of the corresponding tables, with the red dotted lines denoting the weakest limit in each case. The absolute values of δ^d_{RR} are equal in the (12),(23) and (13) sectors; therefore only the bound stemming from the (12) sector is shown, as it is the strongest one. The plots have been produced by scanning over the input parameters shown in Table 4.1.

As parts of the parameter space place the down-type mass insertion parameter $|(\delta^d_{LL})_{12}|$ within a region possibly excluded by Kaon mixing observables, the relevant contributions will be studied in Section 4.3 in more detail. Due to additional strong constraints on the product of LL and RR mass insertion parameters, it will be shown that actually a large fraction of the parameter space will be excluded.

The mass insertion parameters $(\delta^d_{LR})_{12} = -(\delta^d_{RL})_{12} = (\delta^d_{LR})_{13}$ receive an extra suppression from the factor $\alpha_0\, v_d/m_0$, for which the value of 5×10^{-3} is used in naive numerical estimates. Then, for $x \approx 1$, one expects these δ parameters to vary around 7×10^{-7}, see the last two

rows of Table 4.3. As can be seen in Figure 4.4, the model predictions lie well below the limits. Furthermore, if the Yukawa and soft trilinear phase structures are aligned, the phases within $\tilde{a}^d_{12}$ cancel and $(\delta^d_{LR})_{12}$ becomes real at the given order in λ.

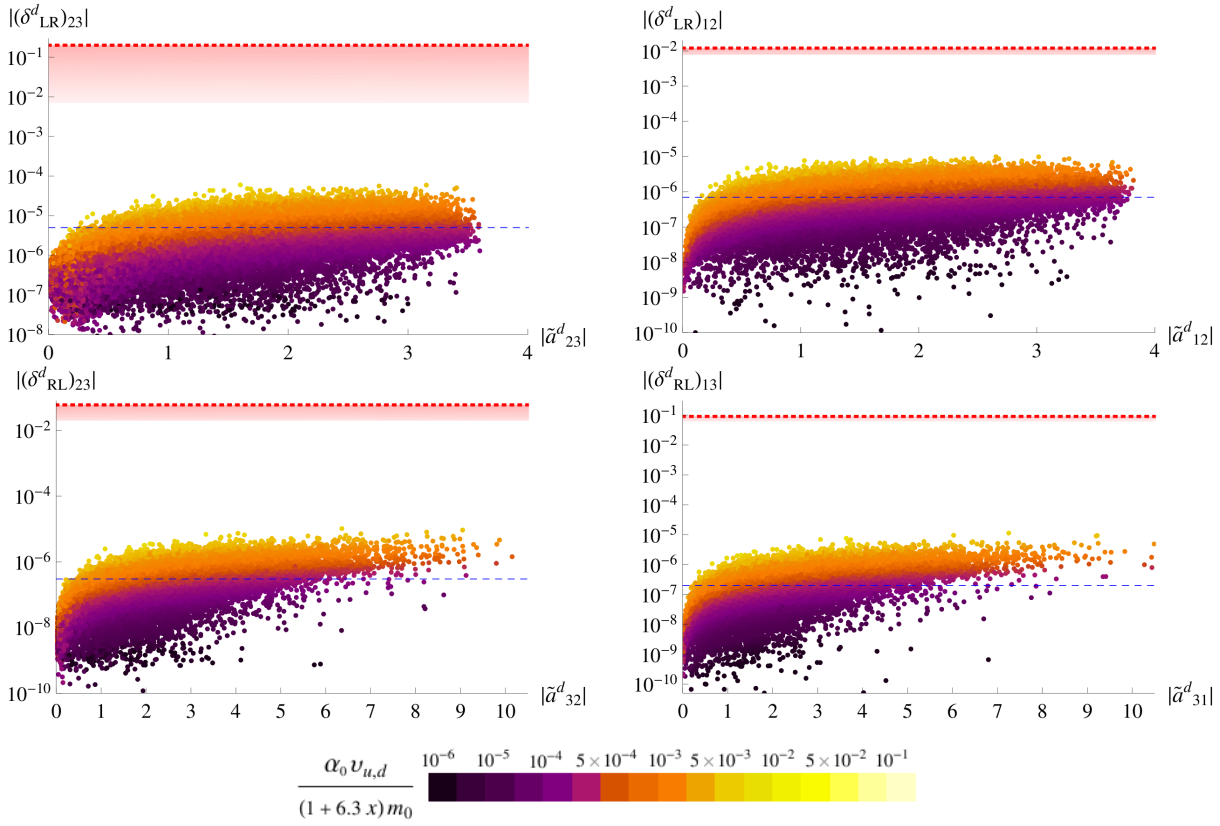

FIGURE 4.4: Low energy LR and RL down-type mass insertion parameters plotted against their GUT scale coefficients, defined in Eqs. (D.5). The blue dashed lines represent the naive numerical expectation according to the second columns of Tables 4.3-4.5. The red shaded areas cover the parameter space bounded by the limits shown in the third column of the corresponding tables, with the red dotted lines denoting the weakest limit in each case. Since$|(\delta^d_{LR})_{12}| = |(\delta^d_{RL})_{12}| = |(\delta^d_{LR})_{13}|$, only the bound stemming from the (12) sector is shown, as it is the strongest one. All plots have been produced by scanning over the input parameters shown in Table 4.1.

The bounds on $(\delta^d_{AB})_{23}$, $A, B = L, R$, are related to $b \to s$ transitions. They are taken from [94] and were derived by demanding that the contribution of each individual mass insertion parameter to the flavour observables $\mathrm{BR}(B \to X_s\gamma)$, $\mathrm{BR}(B_s \to \mu^+\mu^-)$ and ΔM_{B_s} does not exceed the current experimental limits. The analysis was performed for six representative points of the MSSM parameter space which are compatible with LHC SUSY and Higgs searches as well as an explanation of the discrepancy of $(g-2)_\mu$ from its SM value in terms of one-loop SUSY contributions from charginos and neutralinos. The extracted bounds are presented in the third column of Table 4.4, where the intervals arise due to the dependence on the SUSY spectra. Note that, for simplicity, all δs were assumed to be real in [94].

Parameter	Naive expectation	Exp. bound
$\lvert(\delta^d_{LL})_{23}\rvert$	$\mathcal{O}\left(\frac{2\eta\, R_q}{1+6.5\,x}\lambda^2\rvert_{b_{01}=b_{02}} \approx 5\times10^{-3}\right)$	$[6\times10^{-2}, 8\times10^{-1}]$
$\lvert(\delta^d_{RR})_{23}\rvert$	$\mathcal{O}\left(\frac{1}{1+6.1\,x}\lambda^4 \approx 4\times10^{-4}\right)$	$[6.3, 9.7]\times10^{-1}$
$\lvert(\delta^d_{LR})_{23}\rvert$	$\mathcal{O}\left(\frac{\alpha_0\, v_d}{m_0}\frac{1+\eta\left(\frac{44\, g_U^2}{5}+2a_t\, y_t\right)}{1+6.3\,x}\lambda^4 \approx 5\times10^{-6}\right)$	$[7\times10^{-3}, 2\times10^{-1}]$
$\lvert(\delta^d_{RL})_{23}\rvert$	$\mathcal{O}\left(\frac{\alpha_0\, v_d}{m_0}\frac{1+\eta\left(\frac{44\, g_U^2}{5}+2a_t\, y_t+\frac{R_q}{1+6.5\,x}\right)}{1+6.3\,x}\lambda^6 \approx 3\times10^{-7}\right)$	$[2, 6]\times10^{-2}$

TABLE 4.4: The naive expectation for the ranges of $(\delta^d_{AB})_{23}$, $A, B = L, R$, as extracted from the model (second column), to be compared with experimental bounds from [94] (third column). The full ranges of each δ parameter, produced by scanning over the input parameters as shown in Table 4.1, are shown in Figures 4.3 and 4.4.

At the GUT scale, the parameter $(\delta^d_{LL})_{23} \sim \lambda^2$ is proportional to $(b_{01} - b_{02})$; it can therefore vanish at that order if $b_{02} \to b_{01}$. In that case, it would still receive a non-zero contribution through the running, as can be seen in Eq. (F.3.19), through the factor R_q, defined in Eq. (F.2.14). To see this effect, $(\delta^d_{LL})_{23}$ is expanded to first order in the running parameter η, defined in Eq. (F.1), taking the limit $b_{02} \to b_{01}$. Then, for $R_q \approx 3y_t^2 + 1$, $y_t \approx 0.5$ and $x \approx 1$, the absolute value of $(\delta^d_{LL})_{23}$ is expected to vary around 5×10^{-3} for $\tilde{B}_{23} \propto b_{01} - b_{02} \to 0$, as shown by the blue dashed line in Figure 4.3. The spread towards smaller values of $(\delta^d_{LL})_{23}$ as $\tilde{B}_{23}$ deviates from zero, is mainly due to the parameter space where $b_{01} - b_{02}$ is negative, thereby partly cancelling the R_q contribution. As can be seen in Figures 4.3 and 4.4, all generated points lie below the limits of the corresponding (23) sector.

Parameter	Naive expectation	Exp. bound
$\lvert(\delta^d_{LL})_{13}\rvert$	$\mathcal{O}\left(\frac{2\eta\, R_q}{1+6.5\,x}\lambda^4\rvert_{b_{01}=b_{02}} \approx 2\times10^{-4}\right)$	$[1.2, 14]\times10^{-1}$
$\lvert(\delta^d_{RR})_{13}\rvert$	$\mathcal{O}\left(\frac{1}{1+6.1\,x}\lambda^4 \approx 4\times10^{-4}\right)$	
$\lvert(\delta^d_{LR})_{13}\rvert$	$\mathcal{O}\left(\frac{\alpha_0\, v_d}{m_0}\frac{1+\eta\frac{44\, g_U^2}{5}}{1+6.3\,x}\lambda^5 \approx 7\times10^{-7}\right)$	$[6, 9]\times10^{-2}$
$\lvert(\delta^d_{RL})_{13}\rvert$	$\mathcal{O}\left(\frac{\alpha_0\, v_d}{m_0}\frac{1+\eta\left(\frac{44\, g_U^2}{5}+\frac{R_q}{1+6.5\,x}-y_t^2\right)}{1+6.3\,x}\lambda^6 \approx 2\times10^{-7}\right)$	

TABLE 4.5: The naive expectation for the ranges of $(\delta^d_{AB})_{13}$, $A, B = L, R$, as extracted from the model (second column), to be compared with experimental bounds from [93] for $m_{\tilde{q}} \approx 1$ TeV and $(m_{\tilde{g}}/m_{\tilde{q}})^2 \in [0.25, 4]$ (third column). The full ranges of the δs as produced in the scan are shown in Figures 4.3 and 4.4.

In the model, $\lvert(\delta^d_{LL})_{13}\rvert$ is expected to have a similar behaviour as $\lvert(\delta^d_{LL})_{23}\rvert$ but with an extra suppression of λ^2. Furthermore, $\lvert(\delta^d_{LR})_{23}\rvert$ mimics $\lvert(\delta^d_{LR})_{12}\rvert = \lvert(\delta^d_{RL})_{12}\rvert = \lvert(\delta^d_{LR})_{13}\rvert$ with an extra enhancement factor of λ^{-1}. The RL parameters (13) and (23) sectors are of the same order in λ

and should therefore have a similar numerical range. All (13) sector mass insertion parameters δ^d_{AB} lie below the limits set by B_d mixing, as can be seen in Figures 4.3 and 4.4.

4.2.2.3 Charged lepton sector

Parameter	Naive expectation	Exp. bound
$\lvert(\delta^e_{LL})_{12}\rvert$	$\mathcal{O}\left(\frac{2\,R_l\eta_N}{1+0.5\,x}\lambda^4\rvert_{B_3=K_3} \approx 2\times10^{-4}\right)$	$[1.5, 60]\times10^{-5}$
$\lvert(\delta^e_{LL})_{23,13}\rvert$		$[0.7, 35]\times10^{-2}$
$\lvert(\delta^e_{RR})_{12}\rvert$	$\mathcal{O}\left(\frac{\lambda^3}{1+0.15\,x} \approx 10^{-2}\right)$	$[0.35, 25]\times10^{-3}$
$\lvert(\delta^e_{RR})_{23}\rvert$	$\mathcal{O}\left(\frac{\lambda^2}{1+0.15\,x} \approx 4\times10^{-2}\right)$	$[2, 10]\times10^{-1}$
$\lvert(\delta^e_{RR})_{13}\rvert$	$\mathcal{O}\left(\frac{\lambda^4}{1+0.15\,x} \approx 2\times10^{-3}\right)$	
$\lvert(\delta^e_{LR(RL)})_{12}\rvert$	$\mathcal{O}\left(\frac{\alpha_0\,v_d}{m_0}\frac{1+\eta\frac{24g_U^2}{5}+\eta_N\left(\frac{R_l}{1+0.5\,x}-y_D^2\right)}{1+0.3\,x}\lambda^5 \approx 3\times10^{-6}\right)$	$[1.2, 22]\times10^{-6}$
$\lvert(\delta^e_{RL})_{13}\rvert$		$[1, 22]\times10^{-2}$
$\lvert(\delta^e_{LR})_{13}\rvert$	$\mathcal{O}\left(\frac{\alpha_0\,v_d}{m_0}\frac{1+\eta\frac{24g_U^2}{5}+\eta_N\left(\frac{R_l}{1+0.5\,x}-y_D^2\right)}{1+0.3\,x}\lambda^6 \approx 8\times10^{-7}\right)$	
$\lvert(\delta^e_{LR})_{23}\rvert$		
$\lvert(\delta^e_{RL})_{23}\rvert$	$\mathcal{O}\left(\frac{\alpha_0\,v_d}{m_0}\frac{1+\eta\frac{24g_U^2}{5}+\eta_N\left(\frac{R_l}{1+0.5\,x}-y_D^2\right)}{1+0.3\,x}\lambda^4 \approx 10^{-5}\right)$	

TABLE 4.6: The naive expectation for the ranges of $(\delta^e_{AB})_{ij}$, $A, B = L, R$, as extracted from the model (second column), to be compared with experimental bounds from [95] (third column). The full ranges of the δ parameters produced in the scan are shown in Figures 4.5 and 4.6.

The bounds on the mass insertion parameters $(\delta^e_{AB})_{ij}$, $A, B = L, R$, of the charged lepton sector are taken from [95]. They were derived by studying radiative, leptonic and semileptonic LFV decays as well as $\mu \to e$ conversion in heavy nuclei. The analysis was performed for six representative points in the MSSM parameter space, which are in agreement LHC SUSY and Higgs searches as well as data on $(g-2)_\mu$. Moreover, four additional, more general two-dimensional scenarios, characterised by universal squark and slepton mass scales, were considered in [95]. The derived limits vary within an order of magnitude in all cases and are summarised in the third column of Table 4.6. Note that all δs were assumed to be real in [95] for simplicity.

At the GUT scale, the mass insertion parameter $(\delta^e_{LL})_{12} \sim \lambda^4$ is proportional to $\tilde{R}_{12} = B_3 - K_3$. Its absolute value is equal to $\lvert(\delta^d_{RR})_{12}\rvert$ due to the $SU(5)$ framework. However, the parameter of the lepton sector, given in Eq. (F.3.31), receives large RG corrections which encode see-saw effects. At the low energy scale, it is non-zero even for $B_3 = K_3$, due to the term proportional to the small parameter η_N which is defined in Eq. (F.1) and originates from the running between the GUT scale and the scale of the right-handed neutrinos. In the second column of Table 4.6, this effect is estimated by considering $B_3 = K_3$. Expanding to first order in η_N, $R_l \approx R'_l$ is then considered, where R_l and R'_l are defined in Eqs. (F.2.16,F.2.17). For $x \approx 1$, $R_l \approx 3y_D^2 + 1$ and $y_D \approx 0.5$, one expects the low energy $\lvert(\delta^e_{LL})_{12}\rvert$ to vary around 2×10^{-4}. However, the non-trivial expression of $\tilde{E}_{12}$, see Eqs. (F.2.15,F.3.31), creates a spread of about two orders of magnitude around this value. As $\lvert\tilde{R}_{12}\rvert$ increases, the mass insertion parameter lies above the limits given in Table 4.6. As can be seen in Figure 4.5, the non-observation of $\mu \to e\gamma$ places

stronger constraints on the down-type quark δs than the direct bounds from the quark sector. Analogous to the down-type RR parameters, the absolute values of the (12), (23) and (13) lepton LL parameters are identical, see Eqs. (F.3.31,F.3.32).

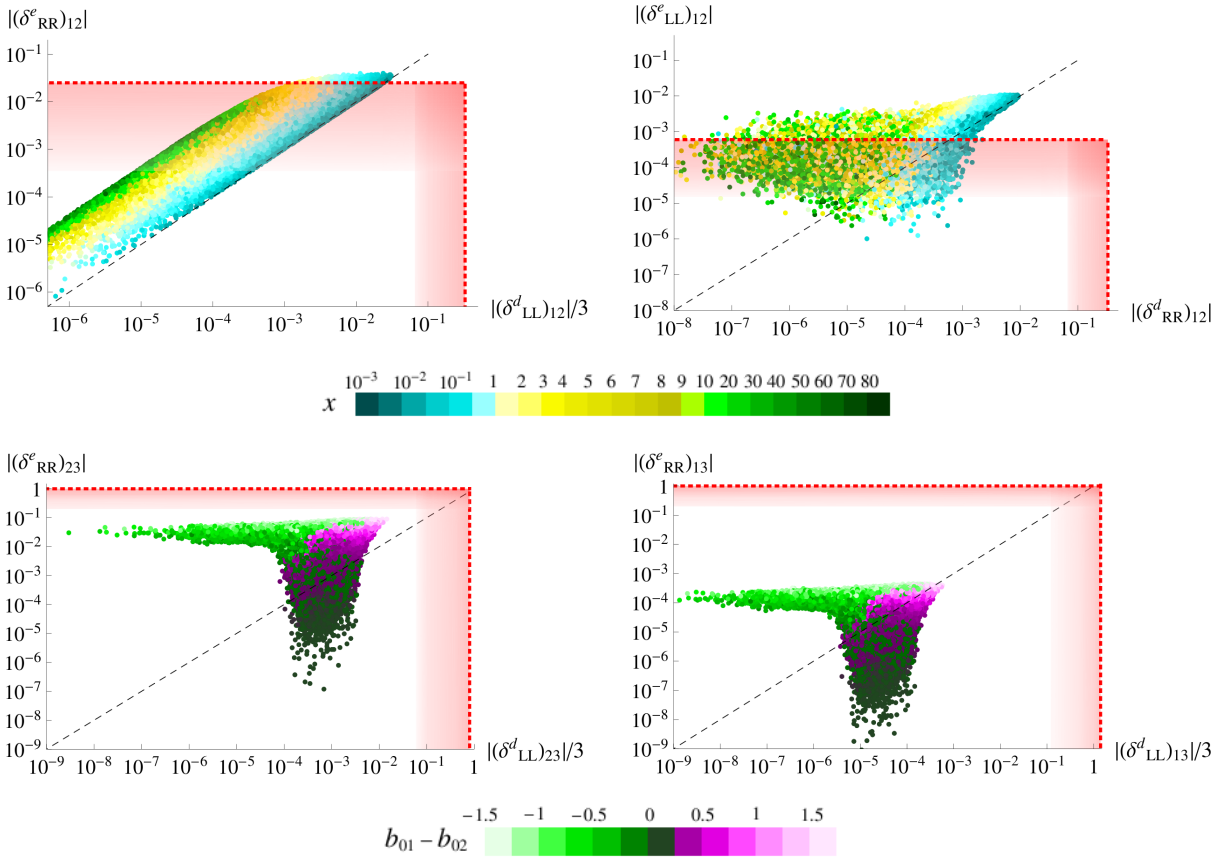

FIGURE 4.5: Low energy LL and RR charged lepton mass insertion parameters plotted against the down-type δs to which they are related via the $SU(5)$ framework. The dashed lines represent their GUT scale relations, while the red shaded areas denote experimental limits on the parameter space according to the third columns of Tables 4.3-4.6. Scanning over the input parameters within the ranges shown in Table 4.1, it is found that in particular $|(\delta^e_{LL})_{12}|$ exceeds its limit for much of the parameter space. Note that $|(\delta^e_{LL})_{12}| = |(\delta^e_{LL})_{23}| = |(\delta^e_{LL})_{13}|$.

Similarly, at the GUT scale, the absolute values of the RR parameters in the lepton sector are equal to the LL ones of the down-type sector times the Georgi-Jarlskog factor of 1/3. For the (12) δs, the RG running effects are trivial, consisting only of a suppression through x, which is milder in the lepton sector where the numerical prefactor of x is 0.15, as compared to a factor of 6.5 in the quark one. For the (13) and (23) parameters, the non-trivial running effects in the quark sector are obvious in Figure 4.5, where it is seen that even though $|(\delta^d_{LL})_{23,13}|$ can get very small for negative $b_{01} - b_{02}$, $|(\delta^e_{RR})_{23,13}|$ can only receive such small values when $b_{01} \to b_{02}$, see e.g. Eqs. (F.3.18,F.3.34).

Finally, the variation of the LR parameters can be understood in an analogous way to the one described in the quark sector. $|(\delta^e_{LR})_{ij_{\rm GUT}}| = |(\delta^d_{RL})_{ij_{\rm GUT}}|$, with the exception of the (23) parameters which are not equal due to a term which involves a $H_{\bar{45}}$, thereby receiving an extra factor of 9 for the leptons, see Eqs. (D.2,D.3,D.5). As in the down-type sector, $|(\delta^e_{RL})_{12}| =$

$|(\delta^e_{LR})_{12}| = |(\delta^e_{RL})_{13}|$ and only the (12) parameter is shown in Figure 4.6 which features the strongest experimental constraint.

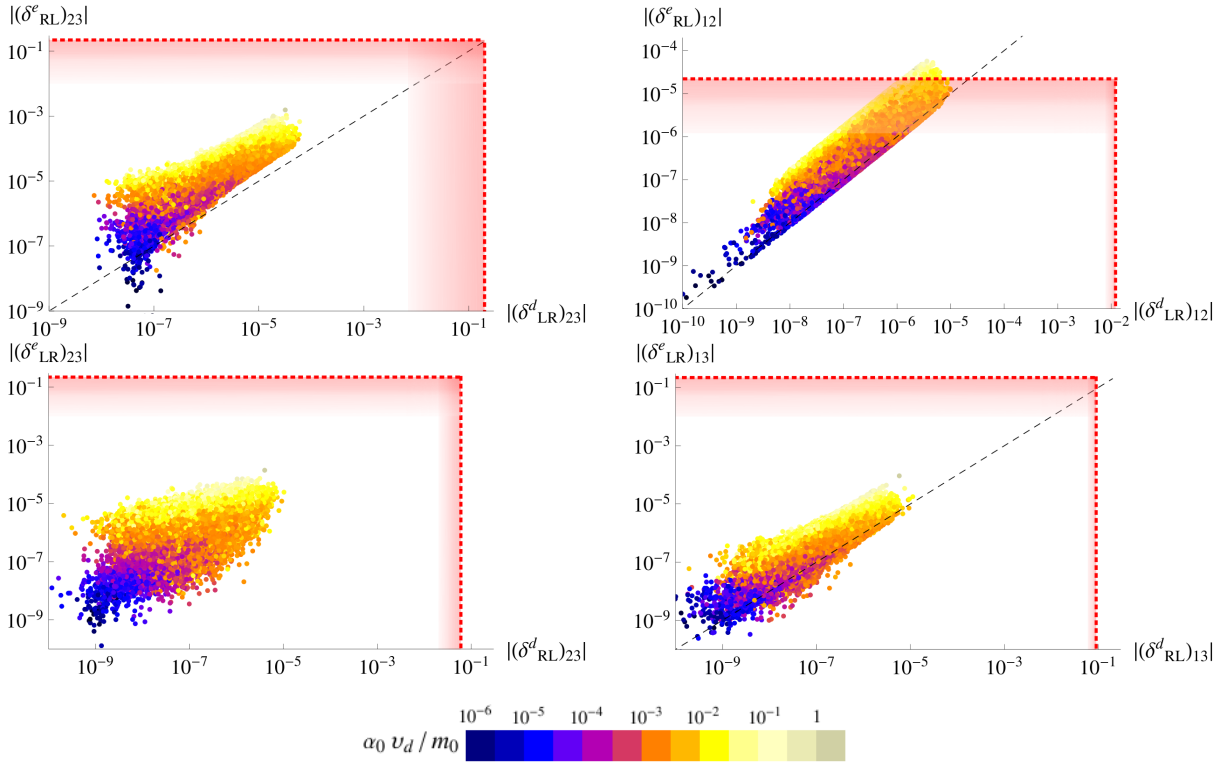

FIGURE 4.6: Low energy LR and RL charged lepton mass insertion parameters plotted against the down-type δs to which they are related via the $SU(5)$ framework. Note that $|(\delta^e_{RL})_{12}| = |(\delta^e_{LR})_{12}| = |(\delta^e_{RL})_{13}|$. The dashed lines represent their GUT scale relations, while the red shaded areas denote experimental limits on the parameter space according to the third column of Tables 4.3-4.6. The plots have been produced by scanning over the input parameters within the ranges shown in Table 4.1

4.3 Phenomenological implications

In the preceding section, it was found that parts of the parameter space spanned by the (12) mass insertion parameters of the down-type and charged lepton sector are excluded due to experimental limits set by $\mu \to e\gamma$ and Kaon mixing observables. The corresponding bounds are available in the literature and their derivation is highly dependent on the assumed SUSY mass spectra. Possible interference effects between contributions from multiple δ parameters to a given observable can additionally have significant effects. These are usually ignored when setting "model independent" limits on mass insertion parameters.

This section therefore investigates the phenomenological implications of the deviations of the model from MFV. In particular, the focus is on predictions for $BR(\mu \to e\gamma)$ and ϵ_K and whether the phase structure of the model can survive the strong limits set by electric dipole moments.

Since the analysis in [94], which provides the limits on $(\delta^d_{AB})_{23}$, assumes real parameters throughout, how the model contributes to the time-dependent CP asymmetry associated with the decay

$B_s \to J/\psi\phi$ is also studied. For completeness, it is checked that the limits set by the decay $B_d \to J/\psi K_S$ and the mass differences $\Delta M_{B_{s,d}}$ are satisfied. Finally, the branching ratios of $b \to s\gamma$ and $B_{s,d} \to \mu^+\mu^-$ will be considered.

Adopting the leading logarithmic approximation, the low energy gaugino masses [45]:

$$M_i = \frac{g_i^2}{g_U^2} M_{1/2} \approx \frac{M_{1/2}}{1 + 2\,\eta\, g_U^2\, \beta_i}, \qquad i = 1, 2, 3, \tag{4.3.1}$$

with $\beta_1 = 33/5$, $\beta_2 = 1$ and $\beta_3 = -3$, are given by:

$$M_1 \approx 0.43\, M_{1/2}, \qquad M_2 \approx 0.83\, M_{1/2}, \qquad M_3 \approx 2.53\, M_{1/2}. \tag{4.3.2}$$

4.3.1 Electron EDM

The current experimental limit for the electric dipole moment of the electron stems from the ACME collaboration [96] and is given by:

$$|d_e/e| \lesssim 8.7 \times 10^{-29}\,\text{cm} \approx 4.41 \times 10^{-15}\,\text{GeV}^{-1}. \tag{4.3.3}$$

This tiny value poses a strong constraint on the phases of any model. The supersymmetric contributions depend on the mass insertion parameters as follows [97][2] :

$$\begin{aligned} \frac{d_e}{e} = \frac{\alpha}{8\pi \cos^2\theta_W} 0.43 \frac{\sqrt{x}}{m_0^3}\, m_{\tilde{e}_{LL}} \text{Im}\Big[& -(\delta^e_{LR})_{11} C_B\, m_{\tilde{e}_{RR}} + \\ & + \Big\{ (\delta^e_{LL})_{1i} (\delta^e_{LR})_{i1} C'_{B,L} + (\delta^e_{LR})_{1i} (\delta^e_{RR})_{i1} C'_{B,R} \Big\} m_{R_{ii}} - \\ & - \Big\{ (\delta^e_{LL})_{1i} (\delta^e_{LR})_{ij} (\delta^e_{RR})_{j1} + (\delta^e_{LR})_{1j} (\delta^e_{RL})_{ji} (\delta^e_{LR})_{i1} \Big\} C''_B\, m_{R_{jj}} \Big], \end{aligned} \tag{4.3.4}$$

where $m_{\tilde{e}_{LL}}$ and $m_{\tilde{e}_{RR}}$ are given in Eq. (F.3.45). Moreover $m_{R_{ii}} = m_{\tilde{e}_{RR}}$ for $i = 1, 2$ and $m_{R_{33}} = m_{\tilde{\tau}_{RR}}$, with the latter being also defined in Eq. (F.3.45). The expression of Eq. (4.3.4) is actually proportional to the bino mass M_1, which is approximated by Eq. (4.3.2) using $x = (M_{1/2}/m_0)^2$. The dimensionless loop functions C_i, whose expressions can be found in Appendix G encode the contributions from the pure bino ($i = B$) and the bino-higgsino with left- ($i = B, L$) and right-handed ($i = B, R$) slepton diagrams. For $x \ll 1$, all ratios of different C_i functions are close to one. With increasing x, C_B takes slightly larger values than the rest of the functions, reaching up to twice the value of $C'_{B,L(R)}$ and three times the value of C''_B. This can be seen in the limit where the left- and right-type slepton masses are not very different,

[2] The corresponding expression in [76] also include triple mass insertions of type $(LR)(RR)(RR)$ and $(LL)(LL)(LR)$. In the model, these give suppressed contributions to d_e/e of order λ^{11} and λ^{13}, respectively, which can be safely neglected.

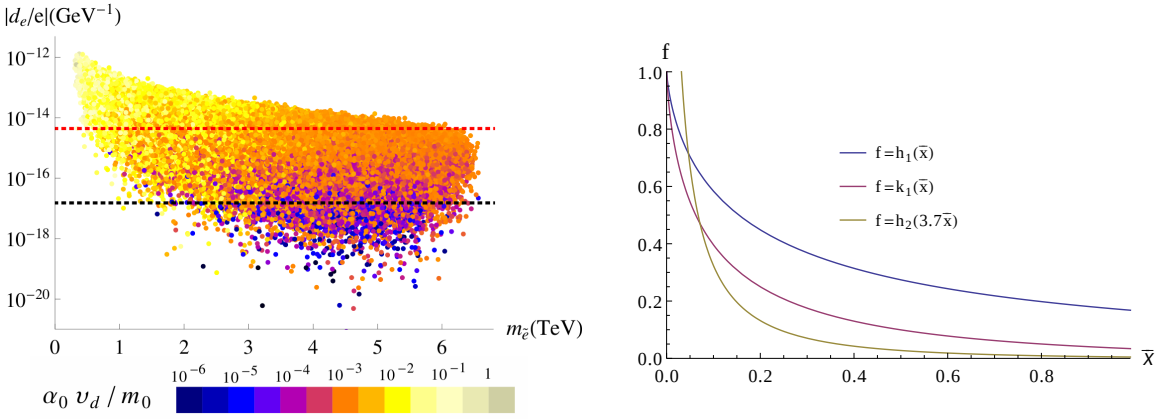

FIGURE 4.7: Left panel: the prediction for the SUSY contribution to the electron EDM versus $m_{\tilde{e}} = \sqrt{m_{\tilde{e}_{LL}} m_{\tilde{e}_{RR}}}$. The red dotted line represents the current experimental limit of Eq. (4.3.3), while the black dotted line corresponds to the expected future limit of $|d_e/e| \lesssim 3 \times 10^{-31}$ cm $\approx 1.52 \times 10^{-17}\,\text{GeV}^{-1}$ [98]. Right panel: the behaviour of the functions h_1, k_1 and (in anticipation of the discussion in Section 4.3.2) h_2.

such that the loop functions take the form [97]

$$C_B \approx \frac{m_0^4}{m_{\tilde{e}}^4} h_1(\bar{x}), \qquad C_B'' \approx \frac{m_0^4}{3m_{\tilde{e}}^4} \left(h_1(\bar{x}) + 2k_1(\bar{x})\right),$$
$$C'_{B,L} \approx C'_{B,R} \approx \frac{m_0^4}{2m_{\tilde{e}}^4} \left(h_1(\bar{x}) + k_1(\bar{x})\right), \tag{4.3.5}$$

where $m_{\tilde{e}} = \sqrt{m_{\tilde{e}_{LL}} m_{\tilde{e}_{RR}}}$ is considered as the average slepton mass[3] and $\bar{x} = (M_1/m_{\tilde{e}})^2$. The function h_1 is given in Appendix G while k_1 denotes the derivative $k_1(\bar{x}) \equiv d(\bar{x}h_1(\bar{x}))/d\bar{x}$. Their behaviour is shown in the right panel of Figure 4.7.

The dominant contribution to the electron EDM comes from the single chirality flipping diagonal mass insertion $(\delta^e_{LR})_{11} \propto \lambda^6$, such that the following approximation can be made

$$|d_e/e| \approx \frac{\alpha}{8\pi \cos^2\theta_W} 0.43\sqrt{x}\, \frac{|\alpha_0| v_d}{m_0^2} (1 + R_e^y) \frac{1}{3} \left|\text{Im}[\tilde{a}^d_{11}]\right| \lambda^6 C_B, \tag{4.3.6}$$

where R_e^y is an RG running factor defined in Eq. (F.1.6) and $\tilde{a}^d_{11}/3$, defined in Eq. (D.5), is the (11) element of $\tilde{A}^e_{\text{GUT}}/A_0$, with $\tilde{A}^e_{\text{GUT}}$ denoting the GUT scale soft trilinear matrix in the SCKM basis. Its imaginary part is non-zero when allowing the phases of the soft trilinear sector to be different from the phases of the corresponding Yukawa sector. Then, for $|\alpha_0 v_d/m_0| \approx 10^{-2}$, $m_0 \approx 1$ TeV and $x \approx 1$, one expects $|d_e/e|$ to vary around $10^{-13}\,\text{GeV}^{-1}$.

As can be seen in the left panel of Figure 4.7, which was produced using the full expression in Eq. (4.3.4), the numerical choice for the suppression factor $|\alpha_0\, v_d/m_0|$ corresponds to the yellow points and brings the prediction for the EDM above its current experimental limit, represented by the red dotted line.

[3] $m_{\tilde{e}_{RR}}$ and $m_{\tilde{\tau}_{RR}}$ only differ in the order one coefficients b_{01} and b_{02} which take values in the same range. Since the dominant term in Eq. (4.3.4) involves the first generation masses, $m_{\tilde{e}} = \sqrt{m_{\tilde{e}_{LL}} m_{\tilde{e}_{RR}}}$ is used rather than $m_{\tilde{e}} = \sqrt{m_{\tilde{e}_{LL}} \sqrt{m_{\tilde{e}_{RR}} m_{\tilde{\tau}_{RR}}}}$ as the average slepton mass.

In the case where the phases of the soft trilinear and Yukawa sectors are equal, $\tilde{a}^d_{11}$ and all factors in Eq. (D.5) become real. In that case, the dominant imaginary part originates from the NLO contribution[4] to $(\delta^e_{LR})_{11}$ and is proportional to $\sin(4\theta^d_2 + \theta^d_3)$. Setting $\theta^d_2 = \pi/2$, as is preferred by the Jarlskog invariant J^q_{CP}, given in Eq. (3.6.5), it is seen that also the NLO contribution vanishes for $\theta^d_3 = 0$, such that $|d_e/e|$ would only arise at order λ^8.

Concerning the terms of Eq. (4.3.4) with double mass insertions, they enter at orders $(\delta^e_{LR})_{12}(\delta^e_{RR})_{21} \sim \lambda^8$, $(\delta^e_{LR})_{13}(\delta^e_{RR})_{31} \sim \lambda^{10}$ and $(\delta^e_{LL})_{12}(\delta^e_{LR})_{21} \sim (\delta^e_{LL})_{13}(\delta^e_{LR})_{31} \sim \lambda^9$ in the model. In the situation described in the preceding paragraph, the first two terms are real, while the contributions of the latter two cancel against each other. Finally, the contributions of the triple mass insertions are further suppressed, with the largest one, $(\delta^e_{LL})_{13}(\delta^e_{LR})_{33}(\delta^e_{RR})_{31} \sim \lambda^{10}$, being real in the case at hand, while all other triple insertions entail contributions which lie below the experimental limit.

4.3.2 $BR(\mu \to e\gamma)$

According to Figures 4.5 anf 4.6, a large part of the parameter space in the (12) charged lepton sector appears to be excluded by the experimental limit set by the non-observation of $\mu \to e\gamma$. This section, therefore studies in detail the contributions to this LFV process within the model. The current experimental limit for the branching ratio

$$BR(\mu \to e\,\gamma) \;\lesssim\; 5.7 \times 10^{-13}\;, \tag{4.3.7}$$

is set by the MEG collaboration [99]. The expression for the corresponding SUSY contribution is given by [97]:

$$\begin{aligned} BR(\mu \to e\gamma) \;&=\; 3.4 \times 10^{-4} \times 0.43^2\, M_W^4\, x\, \frac{\mu^2\, t_\beta^2}{m_0^6} \times \\ \times \Bigg(&\left| (\delta^e_{LL})_{12} \left(-(\delta^e_{LR})_{22} \frac{m_{\tilde{e}_{LL}} m_{\tilde{e}_{RR}}}{\mu\, t_\beta\, m_\mu} C'_{B,L} + \frac{1}{2} C'_L + C'_2 \right) + (\delta^e_{LR})_{12} \frac{m_{\tilde{e}_{LL}} m_{\tilde{e}_{RR}}}{\mu\, t_\beta\, m_\mu} C_B \right|^2 \\ + &\left| (\delta^e_{RR})_{12} \left(-(\delta^e_{LR})^*_{22} \frac{m_{\tilde{e}_{LL}} m_{\tilde{e}_{RR}}}{\mu\, t_\beta\, m_\mu} C'_{B,R} - C'_R \right) + (\delta^e_{LR})^*_{21} \frac{m_{\tilde{e}_{LL}} m_{\tilde{e}_{RR}}}{\mu\, t_\beta\, m_\mu} C_B \right|^2 \Bigg). \end{aligned} \tag{4.3.8}$$

It is proportional to the bino mass squared, that has been approximated by Eq. (4.3.2) and expressed as $M_1^2 = 0.43^2 x\, m_0^2$, where $x = (M_{1/2}/m_0)^2$. The loop function C'_2 encodes the wino-higgsino contribution and is defined in Appendix G, along with the rest of the functions C_i.

In the model, $(\delta^e_{LL})_{12} \sim \lambda^4$, $(\delta^e_{RR})_{12} \sim \lambda^3$, $(\delta^e_{LR})_{12(21)} \sim \lambda^5$ and $(\delta^e_{LR})_{22} \sim \lambda^4$. To get an estimate of the dominant δs in Eq. (4.3.8), the $SU(2)$ ($\propto C'_2$) and the $U(1)$ ($\propto C'_{B,L}, C'_L$) contributions to the $(\delta^e_{LL})_{12}$ term are compared by studying the ratio:

$$R = \left| C'_2 \Big/ \left(\left(1 - \frac{A_0}{\mu\, t_\beta} \frac{\tilde{a}^d_{22}}{y_s} \right) C'_{B,L} + \frac{1}{2} C'_L \right) \right|, \tag{4.3.9}$$

[4] The SCKM rotation which renders the Yukawas sector diagonal and real does not do the same to the A-terms beyond leading order.

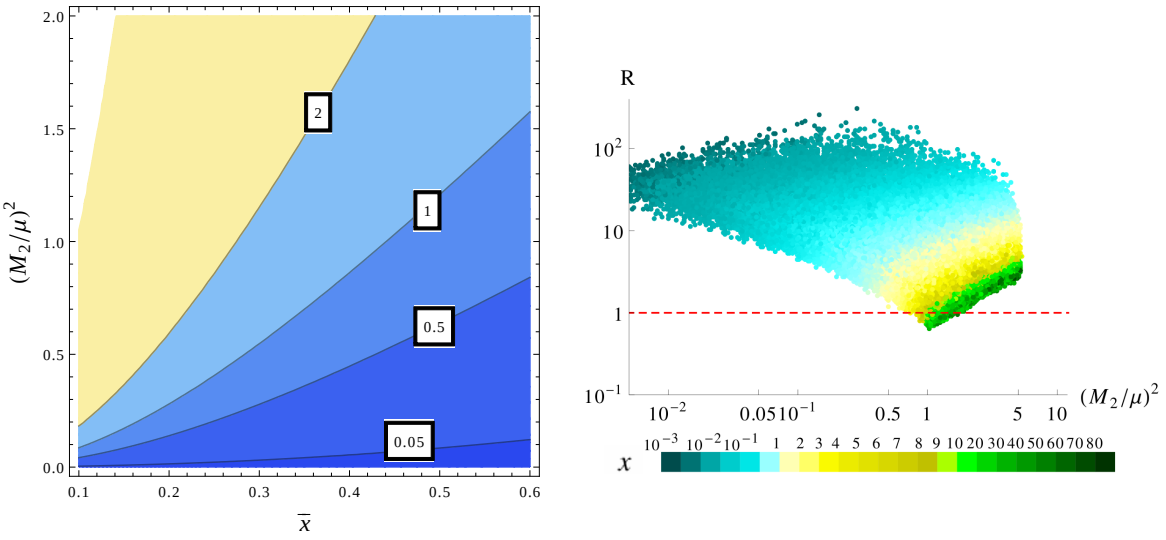

FIGURE 4.8: Left panel: the contour lines for $\bar{R}$, the approximate ratio of the $SU(2)$ over the $U(1)$ contributions to the $(\delta^e_{LL})_{12}$ term in Eq. (4.3.8), as defined in Eq. (4.3.10). For the average slepton mass $m_{\tilde{e}} = \sqrt{m_{\tilde{e}_{LL}} m_{\tilde{e}_{RR}}}$, $\bar{x} = (M_1/m_{\tilde{e}})^2 \approx 0.43^2 x/(1 + 0.3\,x)$, with $x = (M_{1/2}/m_0)^2$. Right panel: the ratio R (without approximation), as defined in Eq. (4.3.9) and produced in the scan. The dependence of $(M_2/\mu)^2$ and $\bar{x}$ on x is such that the $SU(2)$ contributions dominate for most of the parameter space.

which, in the limit where $m_{\tilde{e}_{RR}}$ and $m_{\tilde{e}_{LL}}$ are not very different, can be written as

$$R \;\approx\; \bar{R} = 2\frac{M_2}{M_1}\cot^2\theta_W \left| \frac{\frac{1}{\bar{y}-\bar{x}'}\left(h_2(\bar{x}') - h_2(\bar{y})\right)}{h_1(\bar{x}) + k_1(\bar{x}) + \frac{1}{\bar{y}-\bar{x}}\left(h_1(\bar{x}) - h_1(\bar{y})\right)} \right| . \tag{4.3.10}$$

The behaviour of the loop functions h_1 and h_2, which are defined in Appendix G, as well as $k_1(\bar{x}) \equiv d(\bar{x}h_1(\bar{x}))/d\bar{x}$ is shown in the right panel of Figure 4.7, and $\bar{x} = (M_1/m_{\tilde{e}})^2$, $\bar{x}' = (M_2/m_{\tilde{e}})^2$, $\bar{y} = (\mu/m_{\tilde{e}})^2$, with $m_{\tilde{e}} = \sqrt{m_{\tilde{e}_{LL}} m_{\tilde{e}_{RR}}}$. The contours in the left panel of Figure 4.8 show the dependence of $\bar{R}$, as defined in Eq. (4.3.10), on $(M_2/\mu)^2$ and $\bar{x}$. It is seen that for $(M_2/\mu)^2 \gtrsim 1.5$, $\bar{R}$ is larger than one for all $\bar{x} \approx 0.43^2 x/(1 + 0.3\,x) \lesssim 0.6$, while for $(M_2/\mu)^2 \sim \mathcal{O}(1)$ and smaller, the $U(1)$ contributions can dominate if $\bar{x}$ does not decrease faster than $(M_2/\mu)^2$. The right panel in Figure 4.8 is based on the scan and shows that the correlation of $(M_2/\mu)^2$ and $\bar{x}$ through x is such that R, as defined in Eq. (4.3.9), stays larger than one in most of the parameter space, making the $SU(2)$ contribution to the $(\delta^e_{LL})_{12}$ term in Eq. (4.3.8) the most important one.

Similarly, one can show that the RR contribution to $\mu \to e\gamma$ in Eq. (4.3.8) is comparable to the LL one only when $|(\delta^e_{RR})_{12}\lambda|/|(\delta^e_{LL})_{12}| \gtrsim 1$, although $(\delta^e_{LL})_{12}$ is suppressed by an order of λ with respect to $(\delta^e_{RR})_{12}$. This happens because the RR parameter has only two $U(1)$ contributions which come in with opposite signs, allowing even for a complete cancellation.

Finally, the relative size of the LL and LR contributions will now be studied by considering the ratio:

$$R' = \left| \frac{\mu\, t_\beta\, m_\mu (\delta^e_{LL})_{12}\, C_2'}{m_{\tilde{e}_{LL}} m_{\tilde{e}_{RR}} (\delta^e_{LR})_{12} C_B} \right| = \lambda^3 \kappa \left| \frac{\mu\, t_\beta}{A_0} \frac{C_2'}{C_B} \right| , \tag{4.3.11}$$

where $\kappa = \left|3\, y_s(\tilde{R}_{12} - 2\eta_N\, \tilde{E}_{12})/(\tilde{a}^d_{12}(p^e_L)^2)\right|$, with $\tilde{R}_{12}$, $\tilde{a}^d_{12}$, p^e_L, $\tilde{E}_{12}$ and η_N defined in Eqs. (D.4,D.5,F.3.44,F.2.15,F.1), respectively. The absolute value of the right-hand side of Eq. (4.3.11) exhibits a similar behaviour as the ratio R, defined in Eq. (4.3.9) and shown in the right panel of Figure 4.8. Taking into account the λ-suppression ($\lambda^3 \sim 10^{-2}$) and the range of κ which can vary within two orders of magnitude, it is found that the $(\delta^e_{LR})_{12}$ contribution to the branching ratio can be comparable to the $(\delta^e_{LL})_{12}$ one when $(M_2/\mu)^2 \sim 1$.

Considering situations in which the $(\delta^e_{LR})_{12}$ contribution to Eq. (4.3.8) dominates, one obtains the approximate expression

$$BR(\mu \to e\gamma)|_{(\delta^e_{LR})_{12}} \approx \mathcal{O}\left(10^2\, \alpha_0^2 \frac{m_0^4}{m_{\tilde{e}}^8} h_1^2(\bar{x})\right) \left(\frac{|\tilde{a}^d_{12}|}{3\, y_s}\right)^2 . \tag{4.3.12}$$

In the case where $(\delta^e_{LL})_{12}$ is more important, e.g. when $(M_2/\mu)^2 \ll 1$, see right panel of Figure 4.8, one obtains

$$BR(\mu \to e\gamma)|_{(\delta^e_{LL})_{12}} \approx \mathcal{O}\left(\frac{x\, t_\beta^2}{\mu^2} \frac{m_0^6}{m_{\tilde{e}_{LL}}^8} h_2^2(3.7\, x_L)\right) \left|\tilde{R}_{12} - 2\eta_N\, \tilde{E}_{12}\right|^2 . \tag{4.3.13}$$

For $x_L \equiv (M_1/m_{\tilde{e}_{LL}})^2 \approx \bar{x} \approx 0.1$, $x \approx 1$, $\alpha_0 \approx 1$, $t_\beta \approx 10$, $\mu \approx m_0 \approx 1$ TeV and $m_{\tilde{e}_{LL}} \approx 750$ GeV, the approximations of Eqs. (4.3.12,4.3.13) both produce a value of the order of 10^{-10} times the relevant order one coefficients squared. In order to gain an extra suppression of at least an order of magnitude, the latter are preferred to be smaller than one.

The total supersymmetric contribution to the branching ratio of $\mu \to e\gamma$ of Eq. (4.3.8) as produced in the scan is shown in Figure 4.9. There it is plotted against the average slepton mass (left panel) as well as $|d_e/e|$ (right panel). From the left panel, observe that the model requires rather heavy sleptons, in the TeV range, in order to survive the current experimental limit in Eq. (4.3.7), which is denoted by the red dotted line. As can be seen in Eqs. (4.3.8,4.3.13), there is also a strong μ dependence, with a preference for large values. The right panel of Figure 4.9 shows that the $\mu \to e\gamma$ branching ratio is correlated with the electron EDM, mainly through the slepton masses and the bino-slepton mass ratio. The combination of the current limits on both observables highly restricts the parameter space. Reaching the expected future limits, denoted by the black dotted lines, would nearly exclude the model.

In Figure 4.10 it is shown that the predictions for $BR(\mu \to e\gamma)$ in the plane of two (12) mass insertion parameters as produced in the scan. Comparing this to the discussion of Section 4.2.2.3 reveals that, with the present MEG bound, $|(\delta^e_{LL})_{12}| \lesssim 5 \times 10^{-3}$ and $|(\delta^e_{LR})_{12}| \lesssim 5 \times 10^{-6}$ are not excluded as it was suggested by the limits in Figure 4.5. On the other hand, $|(\delta^e_{RR})_{12}|$ can take its maximum values produced by the scan. The reason for these weaker bounds is twofold. Firstly, the analysis in [95] sets the limits on the mass insertion parameters by choosing t_β as large as 60, whereas here only maximum values of 25 are allowed. Secondly, the derivation in [95] requires that the discrepancy of $(g-2)_\mu$ from its SM value is explained by SUSY contributions.

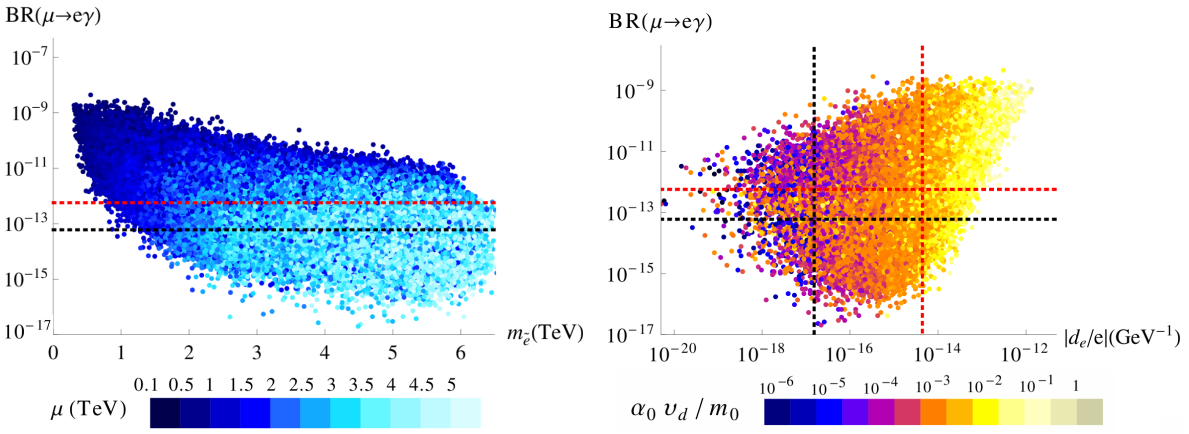

FIGURE 4.9: The supersymmetric contribution to the branching ratio of $\mu \to e\,\gamma$ versus the average slepton mass $m_{\tilde{e}} = \sqrt{m_{\tilde{e}_{LL}} m_{\tilde{e}_{RR}}}$ (left panel) as well as $|d_e/e|$ (right panel). The red dotted lines represent the current experimental limits given in Eqs. (4.3.3,4.3.7) while the black dotted lines show the expected future limits, that is $BR(\mu \to e\,\gamma) \lesssim 6 \times 10^{-14}$ [100] and $|d_e/e| \lesssim 1.52 \times 10^{-17}$ GeV^{-1} [98].

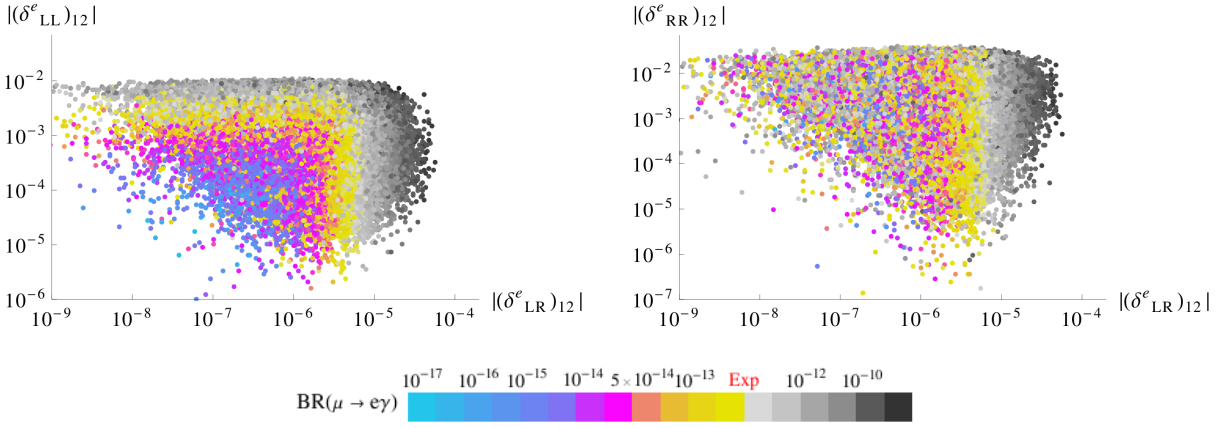

FIGURE 4.10: The range of the (12) lepton mass insertion parameters as produced in the scan, together with the resulting prediction for the branching ratio of $\mu \to e\gamma$. The grey points do not satisfy the current experimental limit given in Eq. (4.3.3).

4.3.3 Meson mixing

Turning to $\Delta F = 2$ transitions, the SUSY contributions to meson mixing are now studied. The dispersive part of the mixing for a meson P can be parametrised as [101]:

$$M_{12}^P = M_{12}^{P,\,\mathrm{SM}} + M_{12}^{P,\,\mathrm{NP}} = M_{12}^{P,\,\mathrm{SM}} \left(1 + h_P e^{2i\sigma_P}\right), \tag{4.3.14}$$

and the corresponding mass difference is given by:

$$\Delta M_P = 2|M_{12}^P|. \tag{4.3.15}$$

The SM contribution is expressed herein as $M_{12}^{P,\mathrm{SM}} = |M_{12}^{P,\mathrm{SM}}|\, e^{2i\phi_P^{\mathrm{SM}}}$. The New Physics (NP) contribution, $M_{12}^{P,\mathrm{NP}} = |M_{12}^{P,\mathrm{NP}}|\, e^{2i\theta_P}$, is encoded in the real parameters

$$h_P = \frac{|M_{12}^{P,\mathrm{NP}}|}{|M_{12}^{P,\mathrm{SM}}|}, \qquad \sigma_P = \theta_P - \phi_P^{\mathrm{SM}}. \tag{4.3.16}$$

The contributions of the gluino-squark box diagram in terms of mass insertion parameters read [13, 76]:

$$\begin{aligned} M_{12}^{P,(\tilde{g})} = A_1^{P,(\tilde{g})} \Bigg(& A_2^{P,(\tilde{g})} \left[(\delta^d_{LL})^2_{ji} + (\delta^d_{RR})^2_{ji} \right] + A_3^{P,(\tilde{g})} (\delta^d_{LL})_{ji} (\delta^d_{RR})_{ji} \\ & + A_4^{P,(\tilde{g})} \left[(\delta^d_{LR})^2_{ji} + (\delta^d_{RL})^2_{ji} \right] + A_5^{P,(\tilde{g})} (\delta^d_{LR})_{ji} (\delta^d_{RL})_{ji} \Bigg), \end{aligned} \tag{4.3.17}$$

where

$$\begin{aligned} A_1^{P,(\tilde{g})} &= -\frac{\alpha_s^2}{216\, m_{\tilde{q}}^2} \frac{1}{3} M_P f_P^2, \qquad A_2^{P,(\tilde{g})} = 24\, y f_6(y) + 66 \tilde{f}_6(y), \\ A_3^{P,(\tilde{g})} &= \left(384 \left(\frac{M_P}{m_j + m_i} \right)^2 + 72 \right) y f_6(y) + \left(-24 \left(\frac{M_P}{m_j + m_i} \right)^2 + 36 \right) \tilde{f}_6(y), \\ A_4^{P,(\tilde{g})} &= -132 \left(\frac{M_P}{m_j + m_i} \right)^2 y f_6(y), \quad A_5^{P,(\tilde{g})} = \left(-144 \left(\frac{M_P}{m_j + m_i} \right)^2 - 84 \right) \tilde{f}_6(y). \end{aligned} \tag{4.3.18}$$

M_P denotes the mass of the meson under consideration and f_P is the associated decay constant. m_i and m_j are the masses of the meson's constituent quarks while $m_{\tilde{q}}$ is an average squark mass defined herein as:

$$m_{\tilde{q}} = \begin{cases} \sqrt{m_{\tilde{d}_{LL}} m_{\tilde{d}_{RR}}}, & P = K, \\ \sqrt{\sqrt{m_{\tilde{d}_{LL}} m_{\tilde{b}_{LL}}}\, m_{\tilde{d}_{RR}}}, & P = B_{s,d}, \end{cases} \tag{4.3.19}$$

with $m_{\tilde{d}_{LL}}$, $m_{\tilde{b}_{LL}}$ and $m_{\tilde{d}_{RR}}$ defined in Eq. (F.3.30). The loop functions $f_6(y)$ and $\tilde{f}_6(y)$, where $y = (m_{\tilde{g}}/m_{\tilde{q}})^2$, are given in Appendix G and the gluino mass has been approximated by Eq. (4.3.2).

4.3.3.1 $B_q - \bar{B}_q$ mixing

The SM contribution to B_q, $q = s, d$ meson mixing given by [102]:

$$M_{12}^{B_q,\mathrm{SM}} = \frac{G_F^2 M_{B_q}}{12\pi^2} M_W^2 (V_{tb} V_{tq}^*)^2 \eta_B S_0(x_t) f_{B_q}^2 \hat{B}_{B_q}, \tag{4.3.20}$$

with:

$$V_{ts} = -|V_{ts}| e^{i\beta_s}, \qquad V_{td} = |V_{td}| e^{-i\beta}, \tag{4.3.21}$$

$$\phi_{B_s}^{\mathrm{SM}} = -\beta_s, \qquad \phi_{B_d}^{\mathrm{SM}} = \beta. \tag{4.3.22}$$

Here η_B is a QCD factor, $\hat{B}_{B_q}$ a perturbative parameter related to hadronic matrix elements and $S_0(x_t \equiv \bar{m}_t^2(\bar{m}_t)/M_W^2)$ is the Inami-Lim loop function [103]. The calculation of the pure SM contribution to the B_s mass difference gives [104]:

$$\Delta M_{B_s}^{(\mathrm{SM})} = 125.2^{+13.8}_{-12.7} \times 10^{-13}\ \mathrm{GeV}, \tag{4.3.23}$$

with the largest uncertainty stemming from the non-perturbative factor $f_{B_s}\sqrt{\hat{B}_{B_s}}$, for which the value 275 ± 13 MeV [105] has been used.[5] The SM prediction for ΔM_{B_d} can be deduced from the ratio [104]:

$$\frac{\Delta M_{B_d}^{(\mathrm{SM})}}{\Delta M_{B_s}^{(\mathrm{SM})}} = 0.02835 \pm 0.00187, \tag{4.3.24}$$

which is less sensitive to theoretical uncertainties. On the other hand, the associated experimental averages as of summer 2014, provided by the HFAG group, read [107]:

$$\Delta M_{B_s}^{(\mathrm{exp})} = (116.9 \pm 0.1) \times 10^{-13}\ \mathrm{GeV}\ , \tag{4.3.25}$$

$$\Delta M_{B_d}^{(\mathrm{exp})} = (3.357 \pm 0.020) \times 10^{-13}\ \mathrm{GeV}\ , \tag{4.3.26}$$

$$\frac{\Delta M_{B_d}^{(\mathrm{exp})}}{\Delta M_{B_s}^{(\mathrm{exp})}} = 0.02879 \pm 0.0002. \tag{4.3.27}$$

Comparing Eq. (4.3.23) with Eq. (4.3.25) leads to a negative central value for the experimentally allowed NP contribution to ΔM_{B_s}, with a similar result being obtained for ΔM_{B_d}. The main source for the errors are the uncertainties of the SM calculation.[6] In view of Eqs. (4.3.23-4.3.27), and in anticipation of reduced theoretical uncertainties, it is concluded that the largest NP effects that could still be allowed should be consistent with:

$$|\Delta M_{B_s}^{(\mathrm{NP})}| \leq 2 \times 10^{-12}\ \mathrm{GeV}\ , \qquad |\Delta M_{B_d}^{(\mathrm{NP})}| \leq 1 \times 10^{-13}\ \mathrm{GeV}\ . \tag{4.3.28}$$

Using Eqs. (4.3.15,4.3.17), one can estimate the effects of the gluino-squark box diagrams. Taking into account the λ-suppression of each δ parameter entering Eq. (4.3.17), one can write $\Delta M_{B_{s,d}}^{(\tilde{g})}$ in the schematic form:

$$\begin{aligned}
\Delta M_{B_s}^{(\tilde{g})} &\propto \lambda^4 \left(A_2^{B_s,(\tilde{g})} + A_3^{B_s,(\tilde{g})}\lambda^2 + A_4^{B_s,(\tilde{g})}\lambda^4 + A_5^{B_s,(\tilde{g})}\lambda^6 \right), \\
\Delta M_{B_d}^{(\tilde{g})} &\propto \lambda^8 \left(A_2^{B_d,(\tilde{g})} + A_3^{B_d,(\tilde{g})} + A_4^{B_d,(\tilde{g})}\lambda^2 + A_5^{B_d,(\tilde{g})}\lambda^3 \right).
\end{aligned} \tag{4.3.29}$$

Figure 4.11 shows the individual contributions as a function of $y = (m_{\tilde{g}}/m_{\tilde{q}})^2$. The largest contributions originate from the terms proportional to $A_2^{B_{s,d},(\tilde{g})}$ and $A_3^{B_{s,d},(\tilde{g})}$, i.e. the terms associated with the δ_{LL}^d and δ_{RR}^d, see Eq. (4.3.17). The contributions from the LR-type mass insertion parameters, proportional to $A_{4,5}^{B_{s,d},(\tilde{g})}$, are negligible. The maximum effect of the gluino-squark box diagrams is obtained when $x = (M_{1/2}/m_0)^2$ and y are smaller than one,

[5] Note that the 2014 average of the FLAG collaboration [106] corresponds to a lower central value but with a larger error: $f_{B_s}\sqrt{\hat{B}_{B_s}}\Big|_{\mathrm{FLAG}} = 266 \pm 18$ MeV.

[6] For a recent discussion on theoretical uncertainties and comparison with experimental results, see [108].

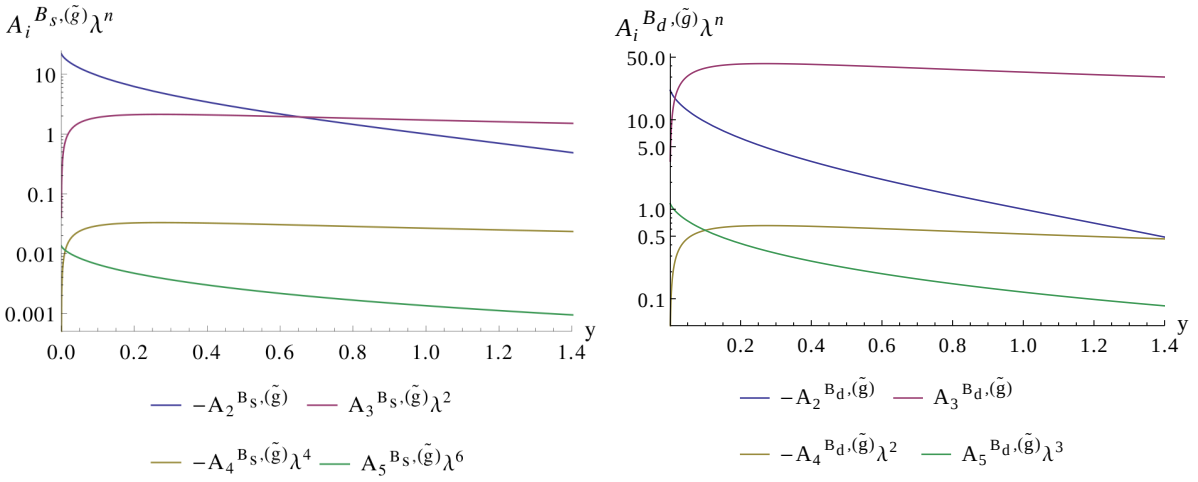

FIGURE 4.11: The dependence of the individual contributions in Eq. (4.3.29) on $y = (m_{\tilde{g}}/m_{\tilde{q}})^2$. The average squark mass $m_{\tilde{q}}$ is defined in Eq. (4.3.19) while the functions $A_i^{B_{s,d},(\tilde{g})}$ can be found in Eq. (4.3.18).

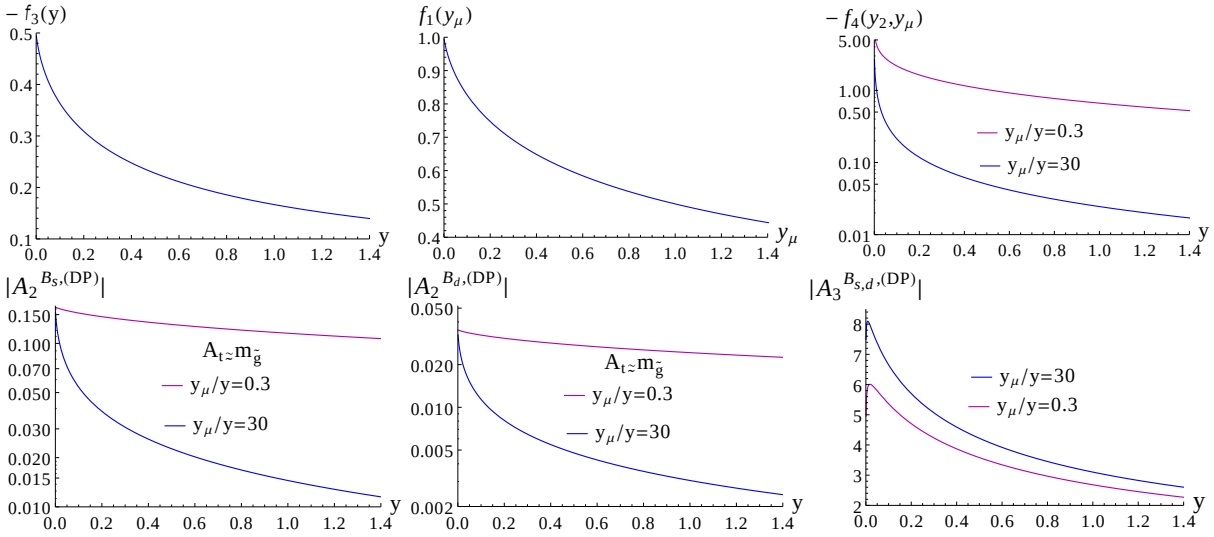

FIGURE 4.12: The dependence of the loop functions as well as $|A_{2,3}^{B_q,(\mathrm{DP})}|$ appearing in Eq. (4.3.30) on $y = (m_{\tilde{g}}/m_{\tilde{q}})^2$, $y_\mu = (\mu/m_{\tilde{q}})^2$ and $y_2 = (M_2/m_{\tilde{q}})^2 \approx 0.11\,y$. The blue lines correspond to $y_\mu/y = 30$ and the magenta ones to $y_\mu/y = 0.3$. In the plots for $|A_2^{B_q,(\mathrm{DP})}|$, it has been assumed that $A_t \approx m_{\tilde{q}}$.

with the $(\delta^d_{LL(RR)})^2_{i3}$ and $(\delta^d_{LL})_{i3}(\delta^d_{RR})_{i3}$ terms interfering constructively. For relatively light $m_{\tilde{q}}$ around 2 TeV, $|A_1^{B_{s,d},(\tilde{g})}|_{\max} \sim \mathcal{O}(10^{-12})$ GeV. Assuming furthermore $|(\delta^d_{LL})_{13}| \approx 10^{-3}$, $|(\delta^d_{LL})_{23}| \approx 2\times 10^{-2}$ and $|(\delta^d_{RR})_{13}| = |(\delta^d_{RR})_{23}| \approx 10^{-2}$ (see Figure 4.3) as well as $y \approx 0.3$, one can use Eqs. (4.3.15,4.3.17) together with Figure 4.11 to estimate the maximum gluino effects as $|\Delta M_{B_s}^{(\tilde{g})}|_{\max} \sim \mathcal{O}(10^{-14})$ GeV and $|\Delta M_{B_d}^{(\tilde{g})}|_{\max} \sim \mathcal{O}(10^{-15})$ GeV. This is about two orders of magnitude smaller than the corresponding SM and experimental values.

For relatively large values of t_β and a light CP-odd Higgs mass M_A, the contributions of the double penguin (DP) diagrams, which scale as $t_\beta^4\,\mu^2/M_A^2$, become important. Considering diagrams with (*i*) two gluino, (*ii*) one gluino and one Higgsino and (*iii*) one gluino and one Wino

loops, the associated part of $M_{12}^{B_q}$ can be approximated by [76]:

$$M_{12}^{B_q,(\mathrm{DP})} = A_1^{B_q,(\mathrm{DP})} (\delta^d_{RR})_{3i}\, t_\beta^4 \frac{\mu^2}{M_A^2} \left\{ A_2^{B_q,(\mathrm{DP})} + (\delta^d_{LL})_{3i} A_3^{B_q,(\mathrm{DP})} \right\}, \tag{4.3.30}$$

where $i = 1(2)$ for $q = d(s)$ and

$$\begin{aligned} A_1^{B_q,(\mathrm{DP})} &= \frac{\alpha_s\, \alpha_2^2}{16\pi} \frac{M_{B_q} f_{B_q}^2}{m_{\tilde{q}}^2} \left(\frac{M_{B_q}}{m_b + m_q} \right)^2 \frac{2 m_b^2}{3 M_W^2}\, y\, f_3(y), \\ A_2^{B_q,(\mathrm{DP})} &= \frac{A_t}{m_{\tilde{g}}} \frac{m_t^2}{M_W^2} V_{tb} V_{tq}^*\, f_1(y_\mu), \\ A_3^{B_q,(\mathrm{DP})} &= 2 \left(\frac{M_2}{m_{\tilde{g}}}\, f_4(y_2, y_\mu) - \frac{8}{3} \frac{\alpha_s}{\alpha_2} f_3(y) \right). \end{aligned} \tag{4.3.31}$$

$y_\mu = (\mu/m_{\tilde{q}})^2$ and $y_2 = (M_2/m_{\tilde{q}})^2$ where the latter is related to $y = (m_{\tilde{g}}/m_{\tilde{q}})^2$ via the approximations of Eq. (4.3.2). The loop functions $f_3(y)$, $f_1(y_\mu)$, $f_4(y_2, y_\mu)$ are given in Appendix G. Their behaviour is sketched in Figure 4.12, along with that of $|A_{2,3}^{B_q,(\mathrm{DP})}|$. For $|A_t| > 500$ GeV, the dominant contribution to Eq. (4.3.30) comes from $A_2^{B_d,(\mathrm{DP})}$ in the B_d sector, even for the maximum values of $|(\delta^d_{LL})_{13}|$, while for B_s, where $|(\delta^d_{LL})_{23}|$ assumes larger values (see Figure 4.3), the two terms in the curly brackets are comparable. For light average squark masses $m_{\tilde{q}}$ around 2 TeV, $A_1^{B_q,(\mathrm{DP})}$ can reach values up to $\mathcal{O}(10^{-16})$ GeV, while $|(\delta^d_{RR})_{i3}|_{\max} \approx 10^{-2}$ (see Figure 4.3). Then, for $A_t \gtrsim m_{\tilde{g}}$ and $\mu \ll m_{\tilde{q}}$, $|A_2^{B_{s(d)},(\mathrm{DP})}| \approx \mathcal{O}(10^{-1(-2)})$, such that $|\Delta M_{12}^{B_{s(d)},(\mathrm{DP})}| \approx 2 \times 10^{-19(-20)} \times t_\beta^4\, \mu^2/M_A^2$ GeV, barring contributions from the $A_3^{B_q,(\mathrm{DP})}$ term. When t_β takes its maximum value of 25 and $\mu \sim M_A$, the double penguin contributions to ΔM_{B_q} increase to about an order of magnitude above the gluino-box contributions, which is however still significantly below the SM and experimental values.

Figure 4.13 shows the predicted SUSY contributions to the B_q meson mixings as produced in the scan. They are plotted against the average squark mass defined in Eq. (4.3.19) and lie below both the experimental measurements (red dotted lines) and the NP limits (blue dotted lines) by at least an order of magnitude. This result is in agreement with the findings in Section 4.2.2.2, where the predictions for the mass insertion parameters are compared with existing limits in the literature.

The effects of the complex down-type mass insertion parameters of the (23) and (13) sectors can be studied through the time dependent CP asymmetries associated with the decays $B_s \to J/\psi\, \phi$ and $B_d \to J/\psi\, K_S$. Focusing on the mixing-induced CP asymmetries, one has [109]

$$S_f = \frac{2\, \mathrm{Im}(\lambda_f)}{1 + |\lambda_f|^2}, \tag{4.3.32}$$

with:

$$\lambda_f = \frac{q}{p} \frac{\bar{\mathcal{A}}(\bar{B}_q \to f)}{\mathcal{A}(B_q \to f)}, \qquad \frac{q}{p} = \sqrt{\frac{M_{12}^{B_q *} - \frac{i}{2}\Gamma_{12}^{B_q *}}{M_{12}^{B_q} - \frac{i}{2}\Gamma_{12}^{B_q}}}, \tag{4.3.33}$$

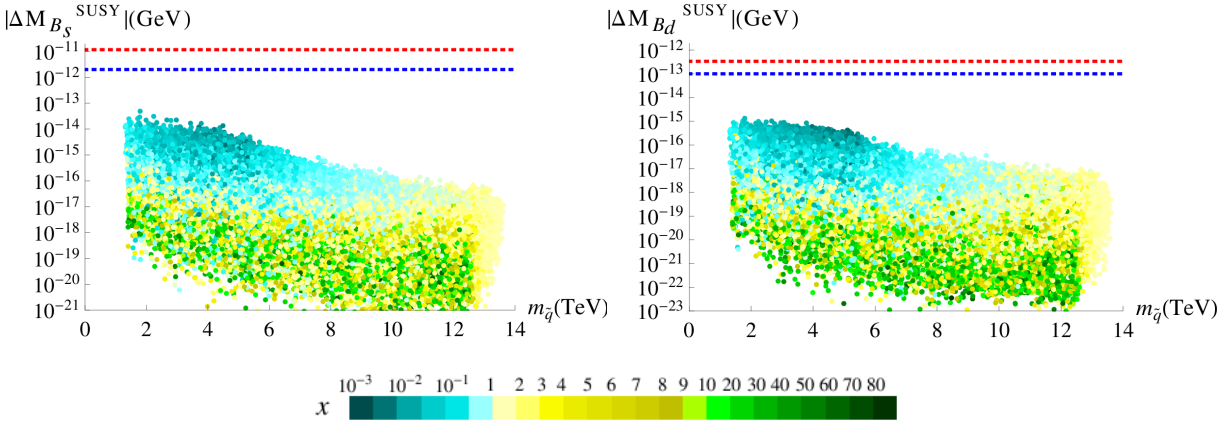

FIGURE 4.13: The absolute value of the gluino and double penguin contributions to $\Delta M_{B_{s(d)}}$ versus the average squark mass as defined in Eq. (4.3.19). The colour coding corresponds to different values of $x = (M_{1/2}/m_0)^2$. The red dotted lines denote the experimental central values of Eqs. (4.3.25,4.3.26), while the blue dotted lines indicate the maximum allowed NP contributions according to Eq. (4.3.28).

where f denotes the final state of the decay and $\mathcal{A}$ is the corresponding amplitude. As the absorptive part $\Gamma_{12}^{B_q}$ of the B_q meson mixing is much smaller than the dispersive one $M_{12}^{B_q}$, i.e. $\Gamma_{12}^{B_q} \ll M_{12}^{B_q}$, one can approximate $q/p \approx \sqrt{M_{12}^{B_q *}/M_{12}^{B_q}}$. Then, the λ_f factors associated with the decays $B_s \to J/\psi\,\phi$ and $B_d \to J/\psi\,K_S$ take the form:

$$\begin{aligned} \lambda_{J/\psi\phi} &= e^{-i\phi_s}, \qquad & \phi_s &= -2\beta_s + \arg\left(1 + h_{B_s} e^{2i\sigma_{B_s}}\right), \\ \lambda_{J/\psi K_S} &= -e^{-i\phi_d}, \qquad & \phi_d &= 2\beta + \arg\left(1 + h_{B_d} e^{2i\sigma_{B_d}}\right), \end{aligned} \tag{4.3.34}$$

where the parameters h_{B_q} and σ_{B_q} are defined in Eq. (4.3.16), while the SM phases β_s and β can be found in Eqs. (4.3.21,4.3.22). The mixing-induced time dependent asymmetries can then be simply written as:

$$S_{J/\psi\phi} = -\sin(\phi_s), \qquad S_{J/\psi K_S} = \sin(\phi_d). \tag{4.3.35}$$

The current measurements are [107][7]

$$S_{J/\psi\phi} = 0.015 \pm 0.035, \qquad S_{J/\psi K_S} = 0.682 \pm 0.019, \tag{4.3.36}$$

while the SM expectations read [111]:

$$S^{\rm SM}_{J/\psi\phi} = \sin(2\beta_s) = 0.0365^{+0.0012}_{-0.0013}, \qquad S^{\rm SM}_{J/\psi K_S} = \sin(2\beta) = 0.771^{+0.017}_{-0.041}. \tag{4.3.37}$$

$S^{\rm SM}_{J/\psi\phi}$ comes with a relatively small error, whereas $S^{\rm SM}_{J/\psi K_S}$ depends strongly on the value of $|V_{ub}|$, which differs significantly when extracted via inclusive or exclusive decays, see e.g. [102], with the above data preferring the lower exclusive result. The value of $S^{\rm SM}_{J/\psi K_S}$ quoted in Eq. (4.3.37) has been derived by averaging over inclusive and exclusive semileptonic determinations of the

[7] LHCb recently published their first measurements of $S_{J/\psi K_S} = 0.746 \pm 0.030$ [110] in the limit of a vanishing direct CP asymmetry, i.e. $\frac{1-|\bar{\mathcal{A}}(\bar{B}_q \to J/\psi K_S)/\mathcal{A}(B_q \to J/\psi K_S)|^2}{1+|\bar{\mathcal{A}}(\bar{B}_q \to J/\psi K_S)/\mathcal{A}(B_q \to J/\psi K_S)|^2} = 0$, thereby improving consistency with the SM expectation.

relevant CKM elements and using the value of the CP-violating parameter ϵ_K, see Eq. (4.3.45), amongst the input parameters but not the measurement of $\sin(2\beta)$ itself.

Comparing Eq. (4.3.36) and Eq. (4.3.37), one observes that the NP contributions to $S_{J/\psi\phi}$ and $S_{J/\psi K_S}$ can be as large as $\sim 100\%$ and $\sim 10\%$ of the respective SM values. In order to reach 10% deviations, h_{B_s} and h_{B_d} should be larger than $\sim 4 \times 10^{-3}$ and ~ 0.14 respectively, corresponding to $|\Delta M^{(\mathrm{NP})}_{B_{s,d}}| \gtrsim 5 \times 10^{-14}$. Here NP phases were assumed which maximise the effect. In view of Figure 4.13, one would expect a non-negligible contribution to $S_{J/\psi\phi}$ in a small part of the parameter space. However, at leading order, $(\delta^d_{LL})_{23}$ and $(\delta^d_{RR})_{23}$ are real, see Eqs. (F.3.19,F.3.21). They only receive non-trivial phase factors at order λ^5, suppressing the imaginary part of $\Delta M^{\mathrm{SUSY}}_{B_s}$ by one power of $\lambda \approx 10^{-1}$ with respect to the real part. As a result, any deviation from $S^{\mathrm{SM}}_{J/\psi\phi}$ is only of the order of 1%. In the B_d sector, $(\delta^d_{LL})_{13}$ and $(\delta^d_{RR})_{13}$ are already complex at leading order in λ, see Eqs. (F.3.18,F.3.20). But as can be seen from Figure 4.13, $|\Delta M^{\mathrm{SUSY}}_{B_d}|_{\max} \approx 10^{-15}$ is too small to be relevant. Even for $|\Delta M^{\mathrm{SUSY}}_{B_d}| \approx 10^{-14}$, the maximum deviation from $S^{\mathrm{SM}}_{J/\psi K_S}$ would be $\sim 3\%$ at most.

In conclusion, the model would not be able to explain any persistent deviations from SM expectations in observables related to B meson mixing.

4.3.3.2 $K - \bar{K}$ mixing

The SM contribution to the Kaon mixing reads [102]:

$$M_{12}^{K,\mathrm{SM}} = \frac{G_F^2 M_K}{12\pi^2} M_W^2 \Big((V_{cs}V_{cd}^*)^2 \eta_{cc} S_0(x_c) + (V_{ts}V_{td}^*)^2 \eta_{tt} S_0(x_t) + \\ + 2V_{cs}V_{cd}^* V_{ts}V_{td}^* \eta_{ct} S_0(x_c, x_t) \Big) f_K^2 \hat{B}_K, \tag{4.3.38}$$

where η_i are QCD factors, $\hat{B}_K$ denotes a perturbative parameter and $S_0(x_i \equiv \bar{m}_i^2(\bar{m}_i)/M_W^2)$ are the Inami-Lim loop functions [103]. From this, the SM value for the Kaon mass difference is numerically given by [112]:

$$\Delta M_K^{(\mathrm{SM})} = 3.30(34) \times 10^{-15} \ \mathrm{GeV}, \tag{4.3.39}$$

while the experimental measurement yields [113]:

$$\Delta M_K^{(\mathrm{exp})} = 3.484(6) \times 10^{-15} \ \mathrm{GeV}. \tag{4.3.40}$$

Therefore it is sensible to impose the constraint that the maximum allowed NP contribution should be limited by:

$$\Delta M_K^{(\mathrm{NP})} \leq 5 \times 10^{-16} \ \mathrm{GeV}. \tag{4.3.41}$$

For Kaon mixing, the relevant mass insertion parameters are those of the (12) sector. Taking into account their λ-suppression, one can write the gluino-box contribution to the mixing amplitude, given in Eq. (4.3.17), in the schematic form:

$$\Delta M_K^{(\tilde{g})} \propto \lambda^6 \left(A_2^{K,(\tilde{g})} + A_3^{K,(\tilde{g})} \lambda + A_4^{K,(\tilde{g})} \lambda^4 + A_5^{K,(\tilde{g})} \lambda^4 \right). \tag{4.3.42}$$

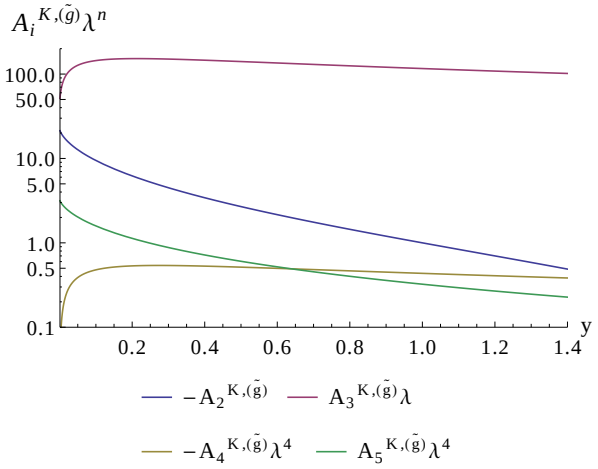

FIGURE 4.14: The dependence of the individual contributions in Eq. (4.3.42) on $y = (m_{\tilde{g}}/m_{\tilde{q}})^2$. The average squark mass $m_{\tilde{q}}$ is defined in Eq. (4.3.19) while the functions $A_i^{K,(\tilde{g})}$ can be found in Eq. (4.3.18).

Figure 4.14 depicts the individual contributions as a function of $y = (m_{\tilde{g}}/m_{\tilde{q}})^2$. It shows that the dominant contribution originates from the term proportional to $A_3^{K,(\tilde{g})}$, i.e. the term proportional to $(\delta^d_{LL})_{21}(\delta^d_{RR})_{21}$, see Eq. (4.3.17). The effects of the LR-type δs, proportional to $A_{4,5}^{K,(\tilde{g})}$, are negligible. Using Eqs. (4.3.15,4.3.17) together with Figure 4.14, one can estimate the maximum gluino contributions to $|\Delta M_K|$. Assuming $y \approx 0.3$, $A_1^{K,(\tilde{g})} \approx 10^{-13}$ GeV and $(\delta^d_{LL})_{21} \approx 5 \times 10^{-2}$, $(\delta^d_{RR})_{21} \approx 7 \times 10^{-3}$ (see Figure 4.3), it is expected that $|\Delta M_K^{(\tilde{g})}|_{\max} \approx 5 \times 10^{-14}$ GeV, which is about one order of magnitude larger than the experimental result of Eq. (4.3.40).

The double penguin (DP) contributions to ΔM_K arise at the level of four mass insertions, by effectively generating the $(s \to d)$ transitions through $(s \to b)$ followed by $(b \to d)$. The relevant part of the mixing amplitude takes the form [76]:

$$M_{12}^{K,(\mathrm{DP})} = \frac{\alpha_s^2\,\alpha_2}{16\pi} M_K f_K^2 \left(\frac{M_K}{m_s + m_d}\right)^2 \frac{32 m_b^2}{9 M_W^2} \frac{t_\beta^2\,\mu^2}{M_A^2\, m_{\tilde{q}}^2}\, y\,(f_5(y))^2 \times \tag{4.3.43}$$

$$\times\ (\delta^d_{LL})_{23}(\delta^d_{LL})_{31}(\delta^d_{RR})_{23}(\delta^d_{RR})_{31}, \tag{4.3.44}$$

with the loop function $f_5(y)$ given in Appendix G. It is found that this contribution is completely negligible, as it is proportional to λ^{14}. The upper left panel of Figure 4.15 shows the combined gluino and DP SUSY contribution to ΔM_K, as produced in the scan. It can exceed the NP limit quoted in Eq. (4.3.41) (blue dotted line) for small values of x, even shooting above the experimental value of Eq. (4.3.40) (red dotted line) for $x \ll 1$.

Turning now to the CP-violating parameter ϵ_K, defined as [102]:

$$\epsilon_K = \frac{\kappa_\epsilon e^{i\varphi_\epsilon}}{\sqrt{2}\Delta M_K^{\mathrm{exp.}}} \left(\mathrm{Im}(M_{12}^{K,\mathrm{SM}}) + \mathrm{Im}(M_{12}^{K,\mathrm{SUSY}})\right), \tag{4.3.45}$$

where the superweak phase[8] $\varphi_\epsilon = \arctan(2\Delta M_K/\Delta\Gamma) = (43.52 \pm 0.05)^\circ$ [113], and the factor

[8] $\Delta\Gamma$ denotes the difference of the widths.

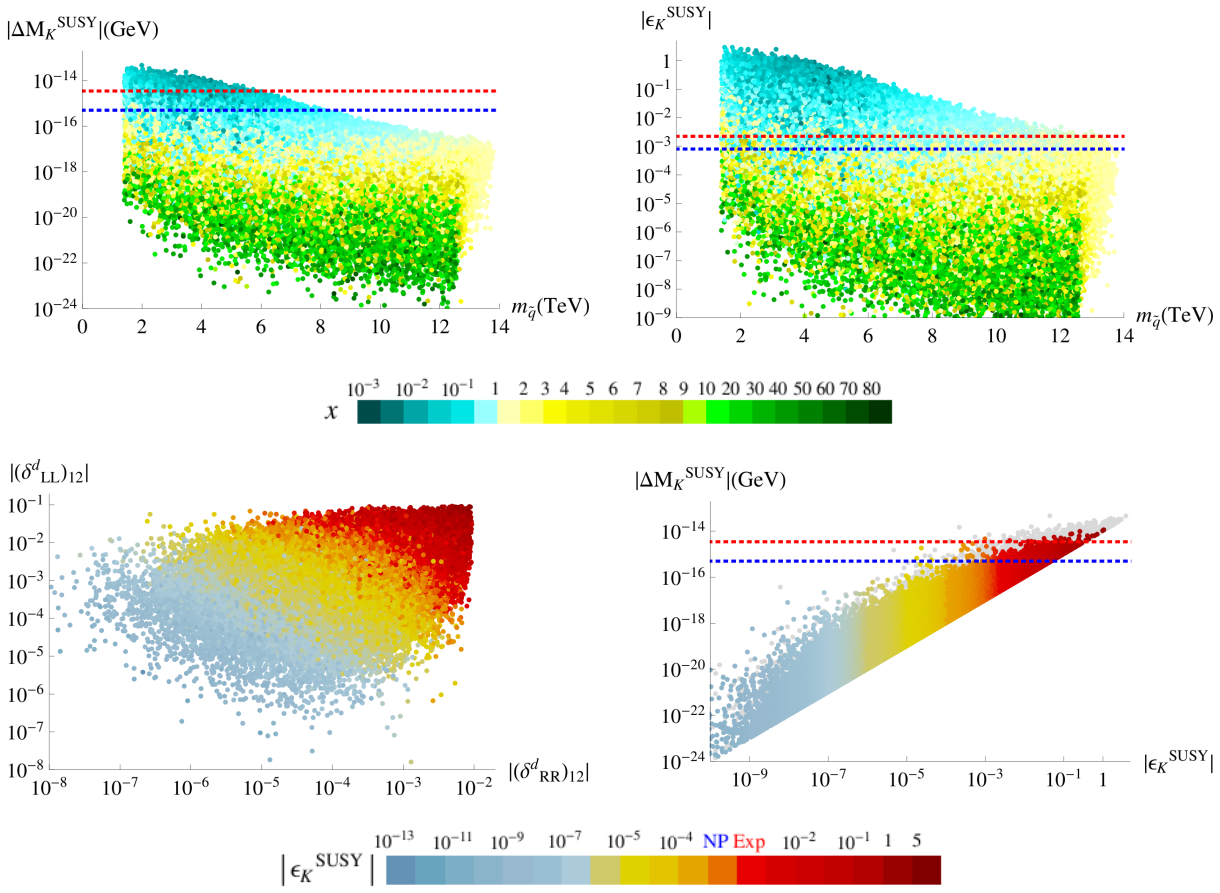

FIGURE 4.15: Upper panels: the absolute value of SUSY contributions to ΔM_K (left) and ϵ_K (right) plotted against the average squark mass defined in Eq. (4.3.19), with the different colours corresponding to different values of $x = (M_{1/2}/m_0)^2$. Lower panels: the most important mass insertion parameters, relevant for K mixing (left) with different colours representing the produced value of $|\epsilon_K^{\rm SUSY}|$; $|\Delta M_K^{\rm SUSY}|$ versus $|\epsilon_K^{\rm SUSY}|$ (right), with the grey shaded points being excluded by $BR(\mu \to e\gamma)$. The red dotted lines indicate the experimentally observed values, while the blue dotted lines show the limits on NP contributions.

$\kappa_\epsilon = 0.94 \pm 0.02$ [114] takes into account that $\varphi_\epsilon \neq \pi/4$ and includes long distance contributions. The experimentally measured value of ϵ_K is [113]:

$$\epsilon_K^{(\rm exp)} = (2.228 \pm 0.011) \times 10^{-3} \times e^{i\varphi_\epsilon}, \tag{4.3.46}$$

while the SM prediction depends highly on the value of V_{cb} [102]. According to [115] and for the input set from the angle-only fit [116], where the Wolfenstein parameters do not show an unwanted correlation with ϵ_K and $\hat{B}_K$, one finds

$$\begin{aligned} |\epsilon_K^{(\rm SM)}| &= 2.17(24) \times 10^{-3} \text{ (inclusive } V_{cb}), \\ |\epsilon_K^{(\rm SM)}| &= 1.58(18) \times 10^{-3} \text{ (exclusive } V_{cb}). \end{aligned} \tag{4.3.47}$$

Therefore, it is demanded that:

$$|\epsilon_K^{(\rm NP)}| \leq 0.8 \times 10^{-3}. \tag{4.3.48}$$

The upper right panel of Figure 4.15 shows the absolute value of the predicted SUSY contribution to ϵ_K, plotted against the average squark mass. This can exceed the limit of Eq. (4.3.48) by more than three orders of magnitude when $x < 1$. In view of Figure 4.3, one would not have expected such a big effect. However, the limits on the mass insertion parameters used in Section 4.2.2.2, only take into account one non-zero mass insertion at a time. As was seen in this section, the dominant contribution to the Kaon mixing amplitude stems from the multiple δ term $A_3^{K,(\tilde{g})}(\delta^d_{LL})_{21}(\delta^d_{RR})_{21}$ (see Figure 4.14). The non-zero phase of the RR parameter is the source of the prediction of a large $|\epsilon_K^{\rm SUSY}|$.

The lower left panel of Figure 4.15 shows $|\epsilon_K^{\rm SUSY}|$ in the $|(\delta^d_{LL})_{12}| - |(\delta^d_{RR})_{12}|$ plane. It indicates that for $|(\delta^d_{LL})_{12}| \sim 5 \times 10^{-2}$, i.e. towards the largest possible value according to Figure 4.3, $|(\delta^d_{RR})_{12}| \lesssim 10^{-5}$ is required. When $|(\delta^d_{RR})_{12}|$ takes its maximum value of $\sim 10^{-2}$, $|(\delta^d_{LL})_{12}|$ should stay below $\sim 10^{-4}$.

Finally, from the lower right panel of Figure 4.15 one observes that ϵ_K places stronger bounds on the mass insertion parameters than ΔM_K. Due to the $SU(5)$ framework of the model there is a correlation between the δ parameters relevant in Kaon mixing and the ones that enter the branching ratio of $(\mu \to e\gamma)$. Denoting the points excluded by $BR(\mu \to e\gamma)$ with a grey shade reveals that there still remains a small area of parameter space which is excluded by ϵ_K.

4.3.4 $BR(b \to s\gamma)$

This section will now consider the gluino contribution to the branching ratio of $b \to s\gamma$. In terms of the relevant mass insertion parameters it is given by [13]:

$$BR(b \to s\gamma) = \frac{\alpha_s^2\,\alpha}{81\pi^2 m_{\tilde{q}}^4} m_b^3 \tau_B \Big(|m_b\, M_3(y)(\delta^d_{LL})_{23} + m_{\tilde{g}}\, M_1(y)(\delta^d_{LR})_{23}|^2 + L \leftrightarrow R \Big), \tag{4.3.49}$$

where the loop functions $M_1(y)$, $M_3(y)$ are defined in Appendix G, τ_B denotes the mean life of the B meson and $y = (m_{\tilde{g}}/m_{\tilde{q}})^2$. This observable does not constraint the parameter space. Even for squark masses as low as 100 GeV and $y = 1$, the LL and RR mass insertion parameters would only need to be smaller than 0.4 to be consistent with the current experimental value of [107]:

$$BR(B \to X_s\gamma) = (3.43 \pm 0.21 \pm 0.07) \times 10^{-4}, \tag{4.3.50}$$

which is in good agreement with the SM prediction [117]. Similarly, the chirality flipping mass insertion parameters would need to be smaller than 3×10^{-3}. In the scan it is found that, see Figure 4.3, $(\delta^d_{LL})_{23} \lesssim 10^{-2}$, $(\delta^d_{RR})_{23} \lesssim 10^{-2}$, $(\delta^d_{LR})_{23} \lesssim 10^{-5}$ and $(\delta^d_{RL})_{23} \lesssim 10^{-6}$. Taking into account the squark mass dependence and the fact that the scan excludes such light squarks, it was found that the model predicts a contribution to $BR(b \to s\gamma)$ which is at least three orders of magnitude below the experimental measurement.

4.3.5 $BR(B_{s,d} \to \mu^+\mu^-)$

The most recent SM predictions for the branching ratios of $B_{s,d} \to \mu^+\mu^-$ are given by [118]:

$$\begin{aligned} BR(B_s \to \mu^+\mu^-)^{(\mathrm{SM})} &= (3.65 \pm 0.23) \times 10^{-9}, \\ BR(B_d \to \mu^+\mu^-)^{(\mathrm{SM})} &= (1.06 \pm 0.09) \times 10^{-10}, \end{aligned} \tag{4.3.51}$$

while the averages of the CMS and LHCb collaborations read [119]:

$$\begin{aligned} BR(B_s \to \mu^+\mu^-)^{(\mathrm{exp.})} &= 2.8^{+0.7}_{-0.6} \times 10^{-9}, \\ BR(B_d \to \mu^+\mu^-)^{(\mathrm{exp.})} &= 3.9^{+1.6}_{-1.4} \times 10^{-10}. \end{aligned} \tag{4.3.52}$$

The B_d sector therefore still allows for rather large relative deviations from the SM expectations. In the case of B_s the experimental measurement yields a value which is slightly lower than the SM prediction.[9] Therefore, the allowed room for contributions from new physics is quoted as:

$$\begin{aligned} BR(B_s \to \mu^+\mu^-)^{(\mathrm{NP})} &\leq 1.68 \times 10^{-9}, \\ BR(B_d \to \mu^+\mu^-)^{(\mathrm{NP})} &\leq 4.53 \times 10^{-10}. \end{aligned} \tag{4.3.53}$$

The chargino and gluino contributions to the branching ratio of $B_{s,d} \to \mu^+\mu^-$ can be expressed as [76]:

$$\begin{aligned} BR(B_q \to \mu^+\mu^-) = {} & \frac{\tau_{B_q} f_{B_q}^2 M_{B_q}^3}{32\pi} \sqrt{1 - 4\frac{m_\mu^2}{M_{B_q}^2}} \times \\ & \times \left\{ \left| \mathcal{A}_1^{B_q} \left[\mathcal{A}_2^{B_q} - \frac{\alpha_s}{\alpha_2} f_3(y) \left((\delta_{LL}^d)_{i3} - (\delta_{RR}^d)_{i3} \right) \right] \right|^2 \left(1 - 4\frac{m_\mu^2}{M_{B_q}^2} \right) \right. \\ & \left. + \left| 2\frac{m_\mu}{M_{B_q}} C_{10}^{\mathrm{SM}} + \mathcal{A}_1^{B_q} \left[\mathcal{A}_2^{B_q} - \frac{\alpha_s}{\alpha_2} f_3(y) \left((\delta_{LL}^d)_{i3} + (\delta_{RR}^d)_{i3} \right) \right] \right|^2 \right\}, \end{aligned} \tag{4.3.54}$$

where

$$\begin{aligned} \mathcal{A}_1^{B_q} &= \alpha_2^2 \, t_\beta^3 \frac{M_{B_q} m_\mu}{4 M_W^2} \frac{m_{\tilde{g}} \, \mu}{M_A^2 \, m_{\tilde{q}}^2}, \qquad \mathcal{A}_2^{B_q} = \frac{m_t^2}{M_W^2} \frac{A_t}{m_{\tilde{g}}} V_{tb} V_{tq}^* f_1(y_\mu) + \frac{M_2}{m_{\tilde{g}}} (\delta_{LL}^u)_{i3} \, f_4(y_2, y_\mu), \\ C_{10}^{\mathrm{SM}} &= \frac{\alpha_2}{4\pi} \frac{4 G_F}{\sqrt{2}} V_{tb} V_{tq}^* Y_0(x_t), \qquad Y_0(x) = \frac{x}{8} \left(\frac{x-4}{x-1} + \frac{3x}{(x-1)^2} \ln(x) \right), \end{aligned} \tag{4.3.55}$$

with $x_t = m_t^2/M_W^2$ and $i = 1(2)$ for $q = d(s)$. The loop functions $f_1(y_\mu)$, $f_3(y)$ and $f_4(y_2, y_\mu)$ are the ones which appear in the double penguin contributions to B_q mixing in Section 4.3.3.1. With $C_{10}^{\mathrm{SM}} = 0$ and $A_t \gtrsim 100$ GeV, the dominant contribution to Eq. (4.3.54) originates from the flavour blind term of $\mathcal{A}_2^{B_q}$, such that the following approximation can be made:

$$BR(B_{s(d)} \to \mu^+\mu^-) \approx \mathcal{O}\left(\frac{6 \times 10^{-6} (1 \times 10^{-7}) \mathrm{GeV}^4}{m_{\tilde{q}}^4} t_\beta^6 \frac{A_t^2 \, \mu^2}{M_A^4} f_1^2(y_\mu) \right). \tag{4.3.56}$$

[9] The calculations in [118] have been performed using the inclusive value of $|V_{cb}|$. Working with the exclusive one would result in a lower central value of $BR(B_s \to \mu^+\mu^-)^{(\mathrm{SM})} = 3.1 \times 10^{-9}$ which fully agrees with the data [120].

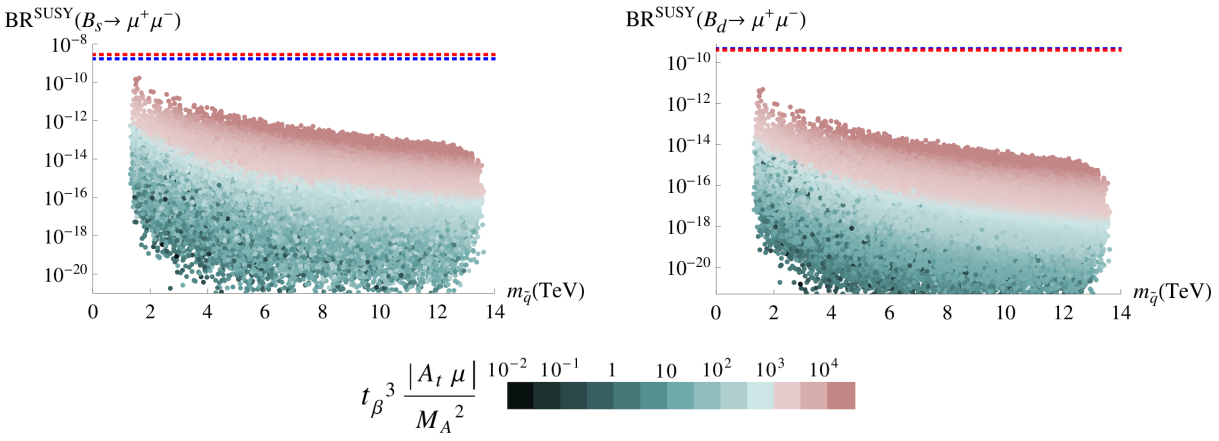

FIGURE 4.16: The SUSY contributions to the branching ratios of $B_q \to \mu^+\mu^-$ versus the average squark mass $m_{\tilde{q}}$, defined in Eq. (4.3.19). The red dotted lines denote the experimental measurements, while the blue dotted lines indicate the maximum NP contributions.

Then, for $|A_t\,\mu|/M_A^2 \approx \mathcal{O}(1)$, $m_{\tilde{q}} \approx 2$ TeV, $t_\beta \approx 25$ and $f_1(y_\mu)$ receiving its maximum value of order one (cf. Figure 4.12), one expects $BR(B_{s(d)} \to \mu^+\mu^-) \approx \mathcal{O}(10^{-10(-12)})$.

In Figure 4.16, the predicted SUSY contributions to the branching ratios of $B_q \to \mu^+\mu^-$ are plotted against the average squark mass $m_{\tilde{q}}$, defined in Eq. (4.3.19). The red dotted lines denote the experimental measurements, while the blue ones correspond to the limits for the NP contributions as given in Eq. (4.3.53). In both sectors, B_s and B_d, the maximum predictions fall about an order of magnitude below these limits.

4.3.6 Neutron and ^{199}Hg EDMs

CP-violating effects in the quark sector can manifest themselves through the quark EDMs as well as the quark Chromo Electric Dipole Moments (CEDMs). The gluino contributions read [76, 121, 122]:

$$\left\{\frac{d_{q_i}}{e}, d_{q_i}^C\right\} = \frac{\alpha_s}{4\pi}\frac{m_{\tilde{g}}}{m_{\tilde{q}}^2}\mathrm{Im}\left[(\delta_{LL}^q)_{ik}(\delta_{LR}^q)_{kj}(\delta_{RR}^q)_{ji}\right]\left\{Q_q\mathcal{F}_q(y), \mathcal{F}_q^C(y)\right\}, \tag{4.3.57}$$

with

$$\mathcal{F}_q(y) = -\frac{8}{3}N_1(y), \qquad \mathcal{F}_q^C(y) = \left(\frac{1}{3}N_1(y) + 3N_2(y)\right), \tag{4.3.58}$$

where Q_q denotes the electric charge of quark q and the loop functions $N_1(y)$, $N_2(y)$, with $y = (m_{\tilde{g}}/m_{\tilde{q}})^2$, are given in Appendix G. As the first generation squarks dominate Eq. (4.3.57), the average squark masses are used

$$m_{\tilde{u}} = \sqrt{m_{\tilde{u}_{LL}} m_{\tilde{u}_{RR}}}, \qquad m_{\tilde{d}} = \sqrt{m_{\tilde{d}_{LL}} m_{\tilde{d}_{RR}}}, \tag{4.3.59}$$

with $m_{\tilde{q}_{LL(RR)}}$ given in Eqs. (F.3.15,F.3.30).

Similar to the case of the electron EDM, the most general scenario is considered where the phases of the soft trilinear sector are different from the corresponding Yukawa ones. Then the dominant contributions of Eq. (4.3.57) arise from the single mass insertions with $i = j = k = 1$,

$$\mathrm{Im}\left[(\delta^u_{LR})_{11}\right] \propto \mathrm{Im}\left[\tilde{a}^u_{11}\right]\lambda^8, \qquad \mathrm{Im}\left[(\delta^d_{LR})_{11}\right] \propto \mathrm{Im}\left[\tilde{a}^d_{11}\right]\lambda^6, \tag{4.3.60}$$

where $\tilde{a}^f_{ij}$ is defined in Eq. (D.5). The double and triple mass insertions start contributing at orders λ^{12} and λ^8 for the up and down quark (C)EDMs, respectively.

If, however, the phases of the soft trilinear and Yukawa sectors are aligned, $\tilde{a}^f_{ij}$ is real. In the case of the up quark sector, one should then check[10] whether the NLO corrections to $\mathrm{Im}\left[(\delta^u_{LR})_{11}\right]$ also vanish, before assuming that the term $\mathrm{Im}\left[(\delta^u_{LL})_{13}(\delta^u_{LR})_{33}(\delta^u_{RR})_{31}\right] \propto \sin(4\theta^d_2 - \theta^d_3)\lambda^{12}$ dominates. The situation in the down sector is such that the NLO correction to $(\delta^d_{LR})_{11}$ gives a non-vanishing contribution to the (C)EDMs. Explicitly, it was found that $\mathrm{Im}\left[(\delta^d_{LR})_{11}\right]_{\mathrm{NLO}} \propto \sin(4\theta^d_2 + \theta^d_3)\lambda^7$, while the smallest contribution from multiple mass insertions is $\mathrm{Im}\left[(\delta^d_{LL})_{12_{\mathrm{NLO}}}(\delta^d_{LR})_{21}\right] \propto \sin(\theta^d_2)\lambda^9$.

In order to compare the gluino contributions of the model according to Eq. (4.3.57) with the experimental limits, the RG running is taken into account from the SUSY scale down to the hadronic scale, using the LO results of [123], for $\alpha_s(\mu_S \approx 1\mathrm{TeV}) \approx 0.089$ and $\alpha_s(\mu_H \approx 1\mathrm{GeV}) \approx 0.358$ [124]. Then,

$$\begin{aligned} d^C_{q_i}(\mu_H) &\approx 0.87\, d^C_{q_i}(\mu_S), \\ \frac{d_{q_i}}{e}(\mu_H) &\approx 0.38\, \frac{d_{q_i}}{e}(\mu_S) - 0.39\, Q_q\, d^C_{q_i}(\mu_S), \end{aligned} \tag{4.3.61}$$

with $d^{(C)}_{q_i}(\mu_S)$ as given in Eq. (4.3.57).

With these preparations, the predictions for the neutron and the ^{199}Hg EMDs can be studied. Adopting the QCD sum rules approach, the neutron EDM at the renormalisation scale $\mu = 1$ GeV, is given in terms of the QCD $\bar{\theta}$-term and the quark (C)EDMs by [98]:

$$\frac{d_n}{e} = 8.2 \times 10^{-17}\,\mathrm{cm}\,\bar{\theta} - 0.12\,\frac{d_u}{e} + 0.78\,\frac{d_d}{e} + \left(-0.3\, d^C_u + 0.3\, d^C_d - 0.014\, d^C_s\right), \tag{4.3.62}$$

while the current experimental limit is [125]:

$$|d_n/e| \leq 2.9 \times 10^{-26}\mathrm{cm} \approx 1.47 \times 10^{-12}\ \mathrm{GeV}^{-1}. \tag{4.3.63}$$

The quark (C)EDMs can also be probed through measurements of the EDMs of atomic systems, where ^{199}Hg provides the best upper limit amongst the diamagnetic systems [126]:

$$|d_{\mathrm{Hg}}/e| \leq 3.1 \times 10^{-29}\mathrm{cm} \approx 1.57 \times 10^{-15}\ \mathrm{GeV}^{-1}. \tag{4.3.64}$$

However, large theoretical uncertainties in the atomic and in particular the nuclear calculations prevent the extraction of bounds on $d^{(C)}_{q_i}$. Eq. (4.3.64) limits the nuclear Schiff moment as [127]:

$$S_{\mathrm{Hg}} \leq 1.45 \times 10^{-12} |e|\,\mathrm{fm}^3, \tag{4.3.65}$$

[10] The expansion was truncated at the order of λ^8.

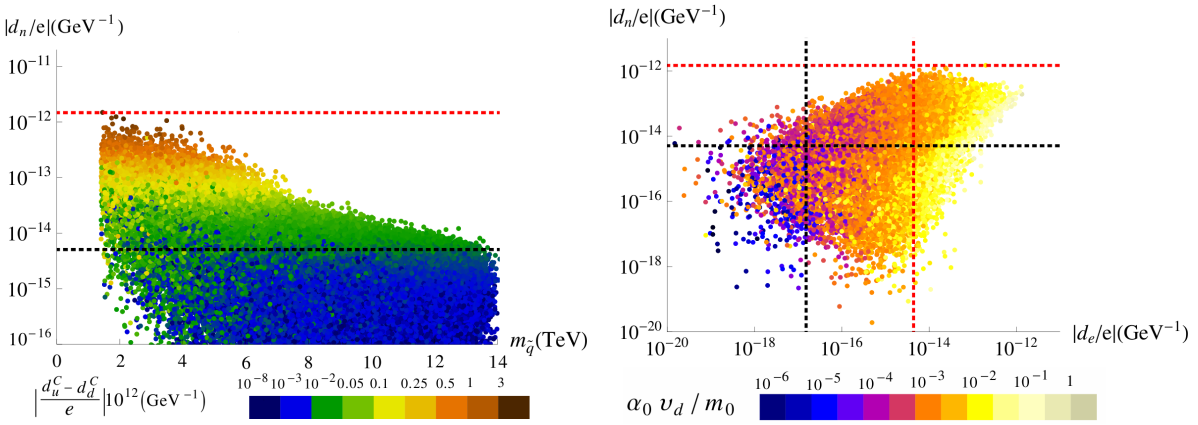

FIGURE 4.17: The neutron EDM versus the average squark mass $m_{\tilde{q}} = \sqrt{m_{\tilde{u}}\, m_{\tilde{d}}}$, with $m_{\tilde{u}}$ and $m_{\tilde{d}}$ as defined in Eq. (4.3.59) (left panel) and versus the electron EDM (right panel). The red dotted lines denote the current experimental limits as given in Eqs. (4.3.63,4.3.3) and the black dotted lines the future limits $|d_n/e| \lesssim 10^{-28}$ cm $\approx 5 \times 10^{-15}\,\mathrm{GeV}^{-1}$ and $|d_e/e| \lesssim 3 \times 10^{-31}$ cm $\approx 1.52 \times 10^{-17}\,\mathrm{GeV}^{-1}$ [98].

which, assuming it is dominated by pion-nucleon interactions, can be expressed as [128]:

$$S_{\mathrm{Hg}} = 13.5 \left(0.01\, \bar{g}^{(0)}_{\pi NN} + (\pm)0.02\, \bar{g}^{(1)}_{\pi NN} + 0.02\, \bar{g}^{(2)}_{\pi NN}\right). \tag{4.3.66}$$

In this equation, the $\bar{g}^{(i)}_{\pi NN}$ denote the pion-nucleon couplings. Their coefficients in Eq. (4.3.66) are the best fit values taken from the review article [128], which assesses the strengths and weaknesses of different, sometimes contradictory, nuclear calculations provided in the literature. Combining Eqs. (4.3.65,4.3.66) with the relation:

$$\bar{g}^{(1)}_{\pi NN} = 2 \times 10^{-12} \left(d_u^C - d_d^C\right), \tag{4.3.67}$$

which was derived in [129], it can be inferred that [127]:

$$|(d_u^C - d_d^C)/e| \leq 2.8 \times 10^{-26}\mathrm{cm} \approx 1.42 \times 10^{-12}\ \mathrm{GeV}^{-1}. \tag{4.3.68}$$

However, this bound only applies if the coefficient of $\bar{g}^{(1)}_{\pi NN}$ in Eq. (4.3.66) takes its best fit value. In principle, it could also be zero, in which case no bound on $|(d_u^C - d_d^C)/e|$ could be extracted.

In the left panel of Figure 4.17, the prediction for the neutron EDM is shown versus the average first generation squark mass $m_{\tilde{q}} = \sqrt{m_{\tilde{u}}\, m_{\tilde{d}}}$. For squark masses less than about 6 TeV, it lies just below the red line denoting the experimental limit in Eq. (4.3.63). For heavier squarks it stays below the limit by at least one order of magnitude. The colour coding corresponds to the predicted value of $|(d_u^C - d_d^C)/e| \times 10^{12}$ GeV, which can also reach the limit in Eq. (4.3.68) for large $|d_n/e|$ values. In the right panel of Figure 4.17, the neutron and electron EDMs are plotted against each other. They are of the same order of magnitude, but it is the current electron EDM limit that constrains the parameter space. When the future experimental limits are reached, only the small part lying in the lower left corner bounded by the black dotted lines would survive.

4.4 Conclusions

In Chapter 3 it was shown how MFV can emerge approximately from an $SU(5)$ SUSY GUT, whose flavour structure is controlled by the family symmetry $S_4 \times U(1)$ and provides a good description of all quark and lepton masses, mixings, as well as CP violation. It was seen that the model leads to mass insertion parameters in Eqs. (3.7.7,3.7.8,3.7.9) which very closely resemble the MFV forms, where $\delta^{u,d,e}_{LL,RR}$ are unit matrices and $\delta^{u,d,e}_{LR}$ are proportional to the Yukawa matrices.

Whereas Chapter 3 focused on the similarity to MFV, this chapter investigates the deviations, by considering the predictions for electric dipole moments, lepton flavour violation, B and K meson mixing, as well as rare B decays. It is found that many of the supersymmetric contributions lie below current limits, as anticipated. This is the case for example in B physics observables, where deviations are negligible (at the 1% level) making it unlikely for the model to explain any possible discrepancies between SM expectations and measurements in $\Delta M_{B_{s,d}}$ or in the time dependent asymmetries $S_{J/\psi\phi}$ and $S_{J/\psi K_S}$. On the contrary, the $SU(3)$ family symmetry models previously studied, predicted large effects in these observables.

However, there are still processes where the $S_4 \times U(1)$ SUSY GUT model could be probed. The (12) down-type quark and charged lepton sectors, show significant deviations from MFV, leading to large contributions to Kaon mixing observables and to the branching ratio of $\mu \to e\gamma$. In particular, $(\delta^e_{LL})_{12}$ provides the dominant contribution to $\mathrm{BR}(\mu \to e\gamma)$ and rather heavy sleptons, exceeding about 1 TeV, are required in order to satisfy the experimental bound. Furthermore, the model produces observable CP violating effects, predominantly in the prediction of the electron EDM, where again large (TeV scale) slepton masses are required for compatibility with current bounds. A signal is therefore expected to be observed in both $\mu \to e\gamma$ and the electron EDM, within the expected future sensitivity of the associated experiments.

Turning to CP violation in the Kaon system, an important contribution to ϵ_K is found, due to the phase of $(\delta^d_{RR})_{12}$. The SM prediction for this observable depends sensitively on $|V_{cb}|$, which differs when considering inclusive or exclusive decays, leading to a lower central value in the latter case. It is noted though, that even for inclusive values of $|V_{cb}|$, the SM expectation for ϵ_K is still about 10% below the measurement. That being the case, sufficient enhancement appears to be available from this flavour model, in order for experimentally observed value of ϵ_K to be explained.

Chapter 5

Exclusive Chromomagnetism in heavy-to-light FCNCs

5.1 Introduction

This Chapter reports on a different project, not directly related to Chapters 3 and 4. It describes the computation of the chomomagnetic matrix element for heavy-to-light semileptonic decays, using the method of light-cone sum rules (LCSRs). The work presented here has been published in [18, 19]. My contribution has been to the derivation of the analytical results; the numerical output presented in Tables 5.2, 5.3, H.1 and Figure 5.5 has been provided by my collaborators.

The study of exclusive flavour changing semileptonic decays, where the underlying quark level transition is of the $b \to s(d)l^+l^-$ type, are of particular interest, as they give rise to multiple observables, such as CP and isospin asymmetries. These "rare" decays are very suppressed in the SM and they can potentially provide invaluable information for the flavour structure of TeV scale physics. Identification of any BSM effects in the B-sector necessitates the improvement of the measurements of different independent observables, but also accurate theoretical estimation of how the operators of the weak effective Hamiltonian in Eq. (5.1.1) contribute to each one of them. There are ten operators contributing to the amplitudes of semileptonic B decays and with the present calculation of the chromomagnetic dipole operator $\mathcal{O}_8$ contribution, they are now all known.

The energy scales encountered in such a decay are both the electroweak scale of $\mathcal{O}(M_W)$, related to the underlying quark level flavour changing transition and the scale of the strong interactions Λ_{QCD}, related to meson formation. Since the mass of the W boson is a lot larger than the typical hadronic scale, the W propagator is of very short range and the charged currents, which it connects in a weak decay, can be considered to interact locally, as in the classical Fermi theory. In that sense, the W boson, as well as heavy quarks, can be integrated out as dynamical degrees of freedom and using the Operator Product Expansion (OPE), one can construct an effective weak Hamiltonian, appropriate for the low energy scales under consideration [132]:

$$\mathcal{H}_{eff} = \frac{G_F}{\sqrt{2}} \sum_i V^i_{\text{CKM}} C_i(\mu) \mathcal{O}_i(\mu) \tag{5.1.1}$$

In the above formula, the operators $\mathcal{O}_i(\mu)$ describe the low-energy/long distance (LD) dynamics of the system, while the Wilson coefficients $C_i(\mu)$ encode the high-energy/short distance (SD) structure of the theory and play the role of coupling constants for the effective interaction terms $\mathcal{O}_i(\mu)$. The factorisation scale at which the LD and SD contributions are separated is denoted by μ and the V^i_{CKM} factors denote the CKM structure of a particular operator. Then, the probability amplitude for an $I \to F$ transition factorises as:

$$\mathcal{A}(I \to F) = \langle F|\mathcal{H}_{eff}|I\rangle = \frac{G_F}{\sqrt{2}} \sum_i V^i_{\text{CKM}} C_i(\mu) \langle F|\mathcal{O}_i(\mu)|I\rangle. \tag{5.1.2}$$

Any new physics effects at a high scale manifest themselves at low energy through corrections to the Wilson coefficients (and/or introduction of additional operators). The Wilson coefficients are process independent perturbative objects that can be calculated once and for all. This is done by requiring that the "full" amplitude, where the W bosons have not been integrated out, is equal to the amplitude in the effective approach; this is done at the matching scale which is of the order of M_W. Subsequently, the Wilson coefficients can be evolved down to the low energy scale of the external momenta, typically of the order of the decaying meson.

On the other hand, the hadronic matrix elements $\langle \mathcal{O}_i \rangle$, depend on the external states and encode LD contributions. As exclusive processes suffer from non-perturbative QCD effects due to the hadronisation of the quarks participating in the $I \to F$ transition, these matrix elements are described in terms of hadronic "Form Factors" (FF), that are specific to the initial and final states and their calculation requires a non-perturbative method.

In a B meson decay, the b quark decays into a light quark (recoiling quark), which combines with the light quark contained in the B meson (spectator quark), to form the final state meson. There are two different parton configurations that need to be described [133]; one is the so-called hard-gluon exchange, where through the momentum transfer of an energetic gluon, all quarks have large momenta; the second one corresponds to the case where one quark is soft and interacts with the other partons only via soft-gluon exchange. The method used for the calculation of $\langle \mathcal{O}_i \rangle$ needs to treat these two mechanisms on the same footing. The light-cone sum rules (LCSRs) method is designed to do exactly that. In the context of weak-decay form factors, the main object of the calculation is the correlation function of the weak current and a current with the quantum numbers of the B-meson, sandwiched between the vacuum and the final state meson. For large (negative) virtualities of these currents (below any thresholds corresponding to physical states), the correlation function is (in coordinate-space) dominated by distances near the light-cone, such that it can be analysed within the framework of a "light-cone" expansion (LC-OPE) [16, 133], which allows consistent factorisation of perturbative and non-perturbative effects. This is briefly illustrated in what follows.

In order for the final meson to be formed, its two constituent quarks should have a small transverse separation. The light-cone expansion is based on integrating out the transverse momenta of the partons, up to some scale μ_F, and considering only the longitudinal ones as the relevant degrees of freedom. Then, the correlation function can be factorised as:

$$\sum_i T^{(i)} \circ \phi^{(i)}, \tag{5.1.3}$$

according to the so-called "collinear factorisation", as the momenta of the partons in the meson are collinear with its momentum. All momenta below the cut-off μ_F are included in the light-cone distribution amplitude (DA) ϕ, which is a non-perturbative object, while the larger ones are contained in the process-dependent amplitudes T, which are the analogues of the Wilson coefficients in Eq. (5.1.1) and can be calculated in perturbation theory. The sum runs over contributions with increasing "twist", which is defined as the difference between the spin and the dimension of the corresponding operators. With increasing twist, the terms in the sum are suppressed by increasing powers of the virtualities of the involved currents. The leading term is a twist-2 DA, which corresponds to the final state meson being in a 2-parton (quark-antiquark) state. It is then a dimensionless function of u that describes the probability to find the meson in a state where its quark has a collinear momentum fraction u and its antiquark $\bar{u} \equiv 1-u$. A twist-3 DA would describe a meson being in a 3-parton (quark-antiquark-gluon) state and so on.

Using the LCSRs method, a review of which can be found in [16], this Chapter describes the computation of the matrix elements:

$$\langle M(p)\gamma^*(q)|\mathcal{O}_8|H(p_H)\rangle\ , \qquad p_H = p+q\ , \tag{5.1.4}$$

of the chromomagnetic operator [1] :

$$\mathcal{O}_8 \equiv -\frac{g}{8\pi^2}\, m_b \bar{s}\sigma_{\mu\nu}G_a^{\mu\nu}\frac{\lambda^a}{2}(1+\gamma_5)b \equiv \left[-\frac{g m_b}{8\pi^2}\right]\ \tilde{\mathcal{O}}_8\ , \tag{5.1.5}$$

where H is a pseudoscalar heavy meson that decays into a pseudoscalar or vector meson M and a photon γ. Allowing the latter to be off-shell, leads to photon momentum invariant q^2-dependence of the matrix element. It is found that the matrix elements are suppressed by one(two) orders of magnitude for the $D(B)$-transitions w.r.t. to the penguin short-distance (SD) form factors. Their interest is thus for asymmetries rather than for branching ratios. One example is the isospin asymmetry, since the emission of the photon from the spectator quark is dependent on the charge of the decaying hadron.

The chapter is organised as follows: In section 5.2 the matrix elements are defined and the basic sum rule is presented. Section 5.3 describes the computation, including the final sum rule expression. Section 5.4 contains the numerics. In section 5.5 the results are compared with the estimate of the QCD Factorisation method (QCDF) [17], which suffered from end-point divergences, not encountered in the LCSRs approach. In section 5.6 the main points of the chapter are summarised. Some explicit results and definitions can be found in Appendices H to L. The analytic structure of the correlation functions in use, can be found in Appendix J.

[1] The normalisation of $\mathcal{O}_8$ goes with the effective Hamiltonian normalisation convention: $\mathcal{H}_{\text{eff}} = -G_F V_{ts}^* V_{tb} C_8 \mathcal{O}_8/\sqrt{2} + \ldots$

5.2 Matrix element and sum rule

5.2.1 Lorentz-decomposition of $\tilde{\mathcal{O}}_8$ matrix elements

For definiteness, throughout this chapter, the initial state meson is chosen to be of the $\bar{B}$ type and the final state meson to be a vector meson V[2] . The relevant transition amplitude reads:

$$\mathcal{A}^{*\rho}(V) \equiv \langle \gamma^*(q,\rho) V(p,\eta)|\tilde{O}_8|\bar{B}(p_B)\rangle = i\int_x \langle V|T j^\rho_{\rm em}(x)\tilde{\mathcal{O}}_8(0)|\bar{B}\rangle e^{iq\cdot x} + \dots \,, \tag{5.2.1}$$

where the dots stand for higher-twist contributions. The polarisation vector of V is denoted by η and the momenta of V, γ and B are denoted by p, q and $p_B \equiv p+q$ respectively. Also, the notation: $\int_x = \int d^4x$ is used. The star indicates that the photon is, generically, off-shell and the index ρ is due to the photon polarisation left uncontracted. The operator $\tilde{\mathcal{O}}_8 \equiv \bar{s}\sigma\cdot G(1+\gamma_5)b$ corresponds to $\mathcal{O}_8$ in Eq. (5.1.5) with the constant prefactor dropped.

The amplitude in Eq. (5.2.1) can be decomposed as: [3]

$$\begin{aligned} c_V\, \mathcal{A}^{*\rho}(V) &= k_G \left(G_1(q^2) P_1^\rho + G_2(q^2) P_2^\rho + G_3(q^2) P_3^\rho \right) \\ \mathcal{A}^{*\rho}(P) &= k_G \left(G_T(q^2) P_T^\rho \right) , \end{aligned} \tag{5.2.2}$$

where G_ι are the scalar functions that play the role of the form factors and $P_{i,T}$ are the Lorentz structures given in Appendix I. The normalisation constant $k_G \equiv -2e/g$ is chosen such that the G_ι-functions parallel the standard vector T_i and pseudoscalar f_T penguin form factors in the amplitude:

$$\begin{aligned} \langle \gamma^*(q,\rho) V(p,\eta)|H_{\rm eff}|\bar{B}\rangle &\propto \sum_i (C_7 T_i(q^2) + C_8 G_i(q^2)) P_i^\rho + \dots \\ \langle \gamma^*(q,\rho) P(p)|H_{\rm eff}|\bar{B}\rangle &\propto (C_7 f_T(q^2) + C_8 G_T(q^2)) P_T^\rho + \dots \end{aligned} \tag{5.2.3}$$

The physical domain of semileptonic transitions is $(2m_l)^2 \le q^2 \le (m_B - m_{P,V})^2$. Under exchange of chirality $(1+\gamma_5) \to (1-\gamma_5)$ in $\mathcal{O}_8$, often denoted as $\mathcal{O}_8'$, the G_ι-functions transform as follows:

$$\{G_1, G_2, G_2, G_T\} \overset{(1+\gamma_5)\to(1-\gamma_5)}{\to} \{G_1, -G_2, -G_3, G_T\} \,. \tag{5.2.4}$$

5.2.2 The sum rule

A characteristic feature of the LCSRs method is that the initial state meson features as an interpolating current, which can produce not only the ground state but also excited mesons and a continuum of states that have the same quantum numbers. The matrix elements (5.1.4) are

[2] The analogous relation for the pseudoscalar $\mathcal{A}^\rho(P)$ simply replaces V by P in the final state.

[3] The factor c_V is inserted to absorb trivial factors due to the $\omega \sim (\bar{u}u + \bar{d}d)/\sqrt{2}$ and $\rho^0 \sim (\bar{u}u - \bar{d}d)/\sqrt{2}$ wave functions. $c_V = -\sqrt{2}$ for ρ in $b \to d$ transitions, $c_V = \sqrt{2}$ in all other transitions into ω & ρ^0 and $c_V = 1$ otherwise.

extracted from the following correlation function[4]:

$$\Pi^V(q^2,p_B^2)=\epsilon^{*\rho}(q)\Pi^V_\rho(q^2,p_B^2)=i\int_x\langle\gamma^*(q)V(p)|TJ_B(x)\tilde{O}_8(0)|0\rangle e^{-ip_B\cdot x}\,, \tag{5.2.5}$$

$$J_B=im_b\bar{b}\gamma_5 q\,,\qquad \langle\bar{B}(p_B)|J_B|0\rangle=m_B^2 f_B\,. \tag{5.2.6}$$

where J_B is the interpolating current of the B-meson. The dispersion representation of the correlation function in the variable p_B^2 reads:

$$\Pi^V(q^2,p_B^2)=\frac{1}{2\pi i}\oint_{\overline{\Gamma}}\frac{ds\Pi^V(q^2,s)}{s-p_B^2}\,, \tag{5.2.7}$$

and is nothing but Cauchy's integral theorem: The closed path $\overline{\Gamma}$ is chosen such that no singularities[5] are crossed. An example is shown in Figure 5.1 for the analytic structure of the correlation function in QCD; $\overline{\Gamma}=\overline{\Gamma}_{\rm P}\cup\overline{\Gamma}_{\rm C}$. In a second step, advantage is taken of the isolated B-pole, encircled by $\overline{\Gamma}_{\rm P}$ in Figure 5.1, by splitting the dispersion integral into two parts as follows:

$$\Pi^V(q^2,p_B^2)=\frac{m_B^2 f_B}{m_B^2-p_B^2}\langle\gamma^*(q)V(p)|\tilde{O}_8|\bar{B}(p_B)\rangle+\frac{1}{2\pi i}\oint_{\overline{\Gamma}_{\rm C}}\frac{ds\Pi^V(q^2,s)}{s-p_B^2}\,. \tag{5.2.8}$$

Equating (5.2.7) and (5.2.8), one obtains the desired ground state contribution:

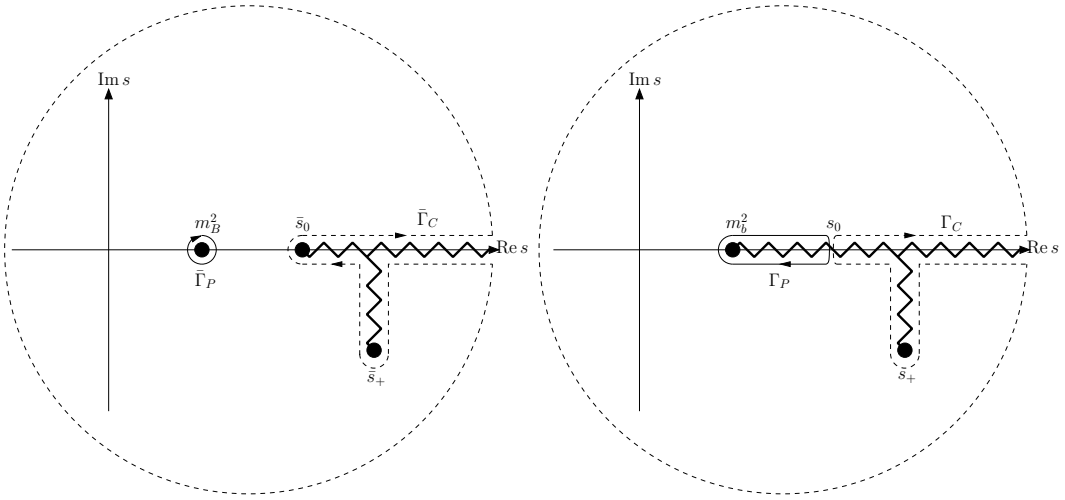

FIGURE 5.1: $\Gamma_{\rm P}[\overline{\Gamma}_{\rm P}]$ and $\Gamma_{\rm C}[\overline{\Gamma}_{\rm C}]$ correspond to the straight and dashed paths in the right[left] figure respectively. (left) Analytic structure of the correlation function in QCD. There is an isolated B-pole at $s=m_B^2$ and a branch point $\bar{s}_0=(m_B+2m_\pi)^2$ at the continuum threshold. The existence of a complex branch point $\bar{s}_+$, which corresponds to an anomalous threshold is discussed in Appendix J. The path $\overline{\Gamma}=\overline{\Gamma}_P\cup\overline{\Gamma}_{\rm C}$ is a possible path for Eq. (5.2.7). (right) Analytic structure of the correlation function as found in leading order perturbation theory. The branch point related to the normal threshold starts at m_b^2. The two branch points $\bar{s}_+$ and s_+ are expected to be close, but not identical, like m_B^2 is close to m_b^2.

[4]For the sake of notational simplicity the photon polarisation tensor is kept contracted here as with respect to (5.2.1), though from a physical point of view this does not make sense for an off-shell photon.

[5]including the anomalous branch-cut extending into the lower half plane in Figure 5.1, the existence of which is discussed in the next section

$$\frac{m_B^2 f_B}{m_B^2 - p_B^2}\langle\gamma^*(q)V(p)|\tilde{O}_8|\bar{B}(p_B)\rangle = \frac{1}{2\pi i}\left(\oint_{\overline{\Gamma}}\frac{ds\Pi^V(q^2,s)}{s-p_B^2} - \oint_{\overline{\Gamma}_C}\frac{ds\Pi^V(q^2,s)}{s-p_B^2}\right) . \tag{5.2.9}$$

For the purpose of numerical improvement, a Borel transformation [16, 134],

$$B_{s\to M^2}[\frac{1}{x-s}] = \frac{e^{-x/M^2}}{M^2} , \tag{5.2.10}$$

in the variable p_B^2 is applied to (5.2.9), yielding:

$$\langle\gamma^*(q)V(p)|\tilde{O}_8|\bar{B}(p_B)\rangle = D[\Pi^V,\overline{\Gamma}] - D[\Pi^V,\overline{\Gamma}_C] , \tag{5.2.11}$$

where the following shorthand notation is introduced:

$$D[f,\Gamma_f] \equiv \frac{1}{f_B m_B^2}\frac{1}{2\pi i}\oint_{\Gamma_f} ds\, e^{(m_B^2-s)/M^2} f(q^2,s) . \tag{5.2.12}$$

The expression in (5.2.11), up to neglecting the width of the B-meson, is exact although rather cryptic. Approximations enter the calculation of the correlation function Π^V, due to neglecting higher twist- and α_s-corrections and in estimating $D[\Pi^V,\overline{\Gamma}_C]$. More precisely, whereas $D[\Pi^V,\overline{\Gamma}] \approx D[\Pi^V|_{\text{LC-OPE}},\Gamma]$ is a good approximation for off-shell p_B^2 (up to the truncations in twist and α_s mentioned above), the approximation $D[\Pi^V,\overline{\Gamma}_C] \approx D[\Pi^V|_{\text{LC-OPE}},\Gamma_C]$, which goes under the name of *semi-global quark hadron duality*, is less transparent and usually the main limitation of a sum rule computation. In the full theory $\overline{\Gamma}_C$ marks the onset of the continuum threshold which corresponds to the lowest lying multi-particle state (e.g. $\bar{s}_0 = (m_B + 2m_\pi)^2$ in QCD. For the LC-OPE dispersion representation shown in Figure 5.1 (right), one introduces an effective continuum threshold s_0 [16, 134], which corresponds to the duality approximation mentioned above.

The crucial point in connection with the anomalous threshold which results in branch cuts extending into the complex plane, is that its real part is above the continuum threshold, $m_b^2 + m_B^2/2 > s_0$, and therefore it is entirely included in Γ_C and does not contribute to the final sum rule[6]. Therefore, the path Γ minus the path Γ_C corresponds to the path Γ_P that encircles the real line segment from m_b^2 to s_0. The final sum rule can be written as:

$$\begin{aligned}\langle\gamma^*(q)V(p)|\tilde{O}_8|\bar{B}(p_B)\rangle \quad &\simeq D[\Pi^V|_{\text{LC-OPE}},\Gamma] - D[\Pi^V_{\text{LC-OPE}},\Gamma_C] \\ &= D[\Pi^V|_{\text{LC-OPE}},\Gamma_P] = \frac{1}{f_B m_B^2}\int_{m_b^2}^{s_0} ds e^{(m_B^2-s)/M^2}\rho^V(q^2,s)\end{aligned} \tag{5.2.13}$$

where:

$$2\pi i\rho^V(q^2,s) = \text{Disc}_s\Pi^V(q^2,s) = \Pi^V(q^2,s+i0) - \Pi^V(q^2,s-i0) , \tag{5.2.14}$$

and the subscript LC-OPE in Eq. (5.2.14) has been dropped. Note that the radius of the path Γ_C and Γ (as well as for the barred quantities) does not enter the final relation (5.2.13). The important point is that the endpoint of the duality interval is much larger than the intrinsic scale of QCD: $s_0 \gg \Lambda^2_{\text{QCD}}$.

[6] It is also suppressed by the Borel transformation (5.2.10) (by at least of $e^{(m_B^2-s_0)/M^2}$ with respect to the B-pole part), both due to the large real part of s and the oscillation in the exponential due to $\Im s \neq 0$ along the associated branch cut.

5.2.2.1 Remarks on dispersion relations and anomalous thresholds

As the appearance of complex singularities in forms of anomalous thresholds is rather non-standard in sum rule computations, adding a few remarks may be worthwhile. For a two-point function, a dispersion representation is in one-to-one correspondence with the insertion of a complete set of states. Thus, the analytic structure in the complex plane of the four momentum invariant has a cut and poles on the real line, starting from the lowest state in the spectrum. For correlation functions with three and more fields, there is no such direct relation. The analytic structure can be more involved, as singularities other than those related to intermediate states might appear, known as anomalous thresholds e.g. [137, 138]. Singularities related to unitarity, that is to say to an insertion of a complete set of states, are called normal thresholds. From the viewpoint of a dispersion relation, normal and anomalous thresholds should be viewed as being on the same footing, as only the analytic structure counts. Which singularities are relevant for the physics in question is another matter. Clearly, the interest here is in the matrix element corresponding to the residue of the pole of the B-meson, which belongs to the normal part. It should be clear that the anomalous thresholds do no more harm to the extraction of the matrix element in question than any other continuum contribution.

5.3 The computation

This section provides some more details of the computation, with some explicit results deferred to the appendices. At leading order in α_s, there are twelve graphs in total. They can be split into those where the gluon connects to the spectator(s) and the ones where it connects to the non-spectator (ns) quark:

$$G_\iota(q^2) = G_\iota^{(s)}(q^2) + G_\iota^{(ns)}(q^2) \,. \tag{5.3.1}$$

The four diagrams denoted by A_1 to A_4 in Figure 5.2 (top, middle) contribute to $G_\iota^{(s)}$, whereas the diagrams at the bottom of the same figure correspond to the $G_\iota^{(ns)}$-contributions. Hereafter, $\bar{u} \equiv 1 - u$ is used. The $G_\iota^{(ns)}$-functions factorise into a function $f(q^2/m_b^2)$ times the standard vector, axial or tensor form factors. The function f has been obtained in the inclusive case in [139][7], in terms of an expansion in powers of q^2/m_b^2 and logarithmic terms. The two diagrams where the gluon connects to the non-spectator quark and the photon is emitted from the latter are not shown. These diagrams are expected to be small, since no fraction of the m_b-rest mass is transmitted to the energetic photon. They are therefore neglected. For the same reason and for being of higher twist, one expects the diagrams where the gluon is radiated into the final state meson to be suppressed [8].

[7] It is worth adding that it would be possible to compute these contribution within LCSR itself.

[8] A rough estimate can be given by comparing the similar case, where a gluon is radiated from a charm loop, instead of $\mathcal{O}_8$, to the hard spectator or the final state meson. Taking the estimates of [130] and [140, 141], a factor of roughly four is found between them.

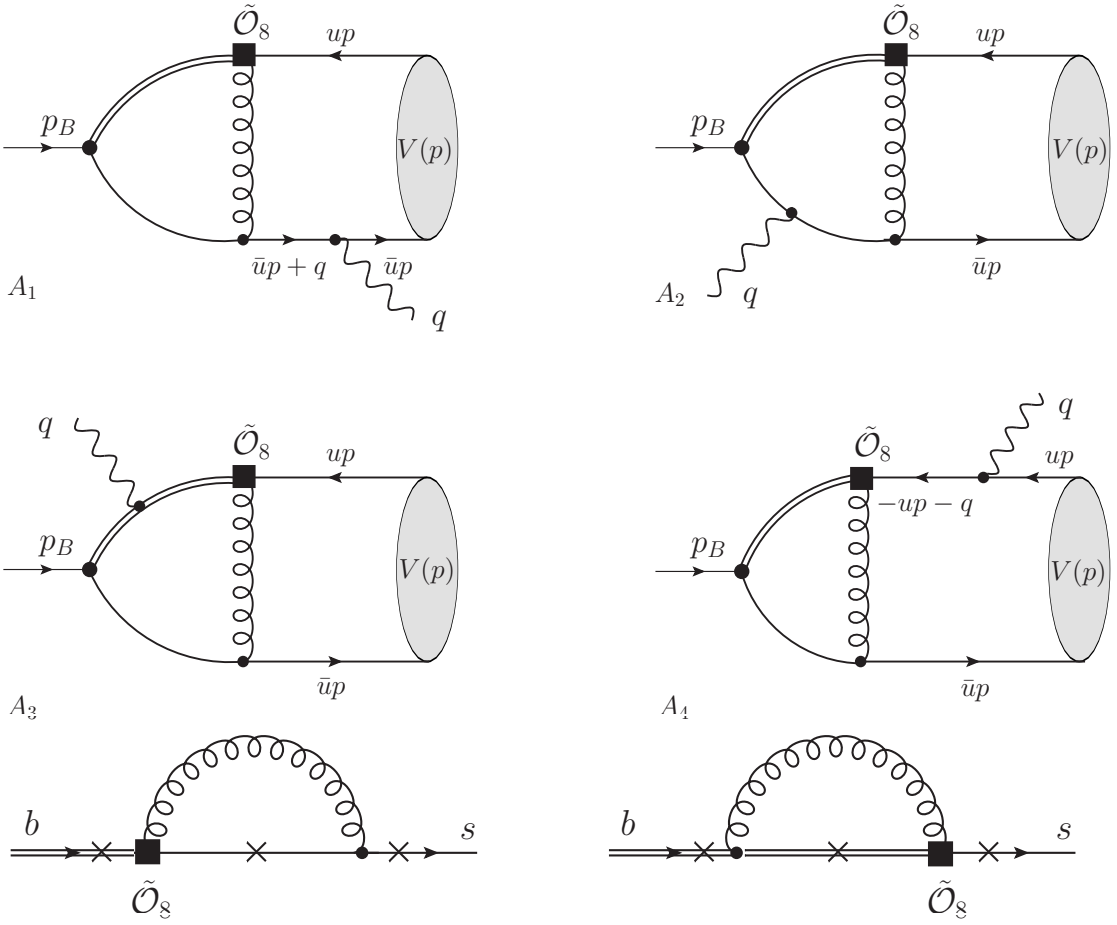

FIGURE 5.2: (top/middle) Diagrams A_1 to A_4, correspond to all four possibilities with the gluon from the weak vertex connecting to the spectator quark. (bottom) Non-spectator corrections. They have been computed in the inclusive case in [139]. The crosses indicate all possible photon insertions.

5.3.1 The problem of parasitic cuts

Due to the fact that there is no momentum flowing into the weak vertex at $\tilde{\mathcal{O}}_8$, there's an ambiguity in separating the cuts corresponding to the B-meson from other cuts. The general problem originates from the fact that the relation between correlation functions of higher degree and matrix elements is complicated by time ordering and a non-trivial analytic structure. The problem is best understood by first introducing its (partial) cure.

Following the method introduced by Khodjamirian for $B \to \pi\pi$ [143], a spurious momentum k is introduced into the weak vertex. This introduces two further momenta, denoted by $P = p_B - k$ and $Q = q - k$. Formally, the $1 \to 2$ decay is augmented by the spurious momentum k to a $2 \to 2$ scattering process, which has six independent kinematic variables: $\{q^2, Q^2, p_B^2, P^2, k^2, p^2\}$. For the purposes considered here, it is possible to set $q^2 = Q^2$ and $k^2 = 0$ without consequence. From now on, capital Q will only be used for the four momentum throughout the chapter. Recalling that $p^2 = m_{P,V}^2$ the six kinematical invariants are reduced to $\{q^2, P^2, p_B^2\}$. The variable P^2 remains the only trace of the spurious momentum at this stage. How it effectively disappears from the final result, is discussed in the next subsection after the light-like dominance of the

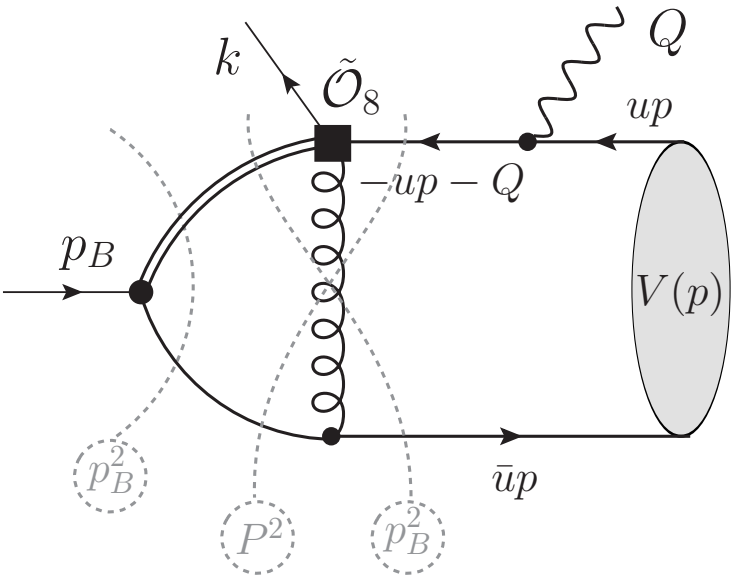

FIGURE 5.3: Various cuts in the variables p_B^2 and $P^2 \equiv (p_B - k)^2$. The cut in P^2 is of a parasitic type, in the sense that for $k \to 0$ it cannot be distinguished from p_B^2, yet it is clearly not associated with the B-meson, as it does not cut in the b-quark line. The two cuts in p_B^2 are of the 2-parton and 3-parton type and should and are both included. The double-line denotes the b-meson propagator.

correlation function is discussed. At the level of the correlation function (5.2.5), the change is implemented by changing the photon momentum $q \to Q$. The above mentioned cuts then branch into cuts in p_B^2 and P^2, see Figure 5.3, where the former correspond to the B-meson and the latter to parasitic ones.

The extension of the Lorentz-structures to the case where the spurious momentum k is included, is given in Appendix I.1. Denoting the photon polarization tensor by $\epsilon(Q)$, the correlation function is now parametrised as:

$$\Pi^V = \sum_{i=0}^{4} g_i(q^2)\epsilon(Q)\cdot p_i \,, \qquad \Pi^P = \sum_{i\in\{0,T,\bar{T}\}} g_i(q^2)\epsilon(Q)\cdot p_i \,. \tag{5.3.2}$$

5.3.2 The Light-Cone Expansion

The correlation function is expected to be dominated by light-like distances, in the case where the kinematical invariants k^2, q^2, p_B^2 and P^2 [9] are below the thresholds. In that case, the light-cone operator product expansion (LC-OPE), see [16] for a review article on the topic, is applicable. For the physical matrix element, q^2 and P^2 necessitate analytic continuation, an issue which is deferred to sections 5.3.3 and 5.4.2. Schematically the LC-OPE reads:

$$\Pi(q^2, p_B^2, P^2) = \sum_i T_H^{(i)}(q^2, p_B^2, P^2; \mu_F; u) \circ \phi^{(i)}(u, \mu_F) \,, \tag{5.3.3}$$

[9] The remaining two invariants are $Q^2 = q^2$ and $p^2 = m_{P,V}^2$. The former does not necessitate a separate statement, while the latter is on-shell, as it corresponds to the momentum of a physical state.

where i sums over different distribution amplitudes (DAs) of increasing twist. The twist corresponds to the dimension of the operator minus its spin. The terms in the sum are suppressed by $\Lambda_{\rm QCD}$ over the virtuality, to the power of the twist. This work is limited to the the leading twist-2. The relevant DAs are summarised in Appendix I.2. The variable u represents generic parton momentum fractions, the symbol $\circ$ stands for the integration over the latter and T_H is a perturbatively calculable hard kernel. The symbol μ_F denotes the collinear factorisation scale and separates, within the LC-OPE, the SD physics in the kernel T_H from the LD part in the DA. Using FeynCalc [145] to compute Dirac traces, Passarino-Veltman (PV) [146] reduction and basis projections, the results are obtained in terms PV functions and their corresponding dispersion relations, including the handling of the complex branch cuts, are given appendices H and J respectively.

5.3.3 Analytic continuation and appearance of strong phases

As previously stated, the LC-OPE is valid when all invariants take on values such that no thresholds are crossed. To obtain a physical result, two of those invariants: q^2 and P^2 need to be analytically continued; q^2 to enter the physical domain for $B \to V(P)ll$ transitions and P^2 to eliminate the spurious momentum k.

For $B \to V(P)ll$, the physical range for q^2 is between $(2m_l)^2$ and $(m_B - m_{P,V})^2$ and it has become customary to exclude the region below $1\,\text{GeV}^2$, in order to avoid the (ρ,ω)-resonance region. For $B \to V\gamma$, which corresponds to $q^2 = 0$, it can be argued that one is sufficiently below the (ρ,ω)-threshold region and therefore the LC-OPE is expected to work. It is once again highlighted, that the only trace of the spurious momentum is in $P^2 \equiv (p_B - k)^2 \neq p_B^2$. This trace can be lifted by analytically continuing $P^2 \to m_B^2 + i0$. Note that if the full solution of the correlation function was available, then $p_B^2 = m_B^2$ would lead to an exact projection by virtue of an LSZ reduction. In the sum rule approximation, the remnant of this is the fact that the integral representation (5.2.13) averages over a narrow range of m_B^2. On the level of the LC-OPE, this analytic continuation is expected to hold, as it is far above all thresholds; the variable P^2 does not cut through the b quark line (see Figure 5.3). Both analytic continuations lead to LD contributions, which in turn lead to strong phases. This is illustrated for a $P^2 = m_B^2$-cut in Figure 5.4 (left) and for a $q^2 \simeq m_\rho^2$ cut in Figure 5.4 (right). In summary, both q^2 and P^2 are analytically continued sufficiently far above the thresholds.

5.4 Results, summary and numerics

Note that in the sum rule the product $[m_B^2 f_B] \times \langle \gamma^*(q) V(p) | \tilde{O}_8 | \bar{B}(p_B) \rangle$, see Eq. (5.2.8), rather than the $G_i(q^2)$ functions themselves are extracted. This suggests that one should use a sum rule determination of the same order in the quantity $[m_B^2 f_B]$ [10] in order to extract the matrix element(s). Such a strategy has for example been proposed in [147]. From Figure 5.3, it is evident that the 2-particle cut corresponds to a decay constant of order $\mathcal{O}(\alpha_s^0)$. The 3-particle cut in the same figure corresponds partially to an $\mathcal{O}(\alpha_s)$-correction. The former is expected to be dominant, justifying the use of the sum rule result for $[m_B^2 f_B]$ [148] to $\mathcal{O}(\alpha_s^0)$,

[10] This quantity corresponds to the matrix element of the interpolating current (5.2.6).

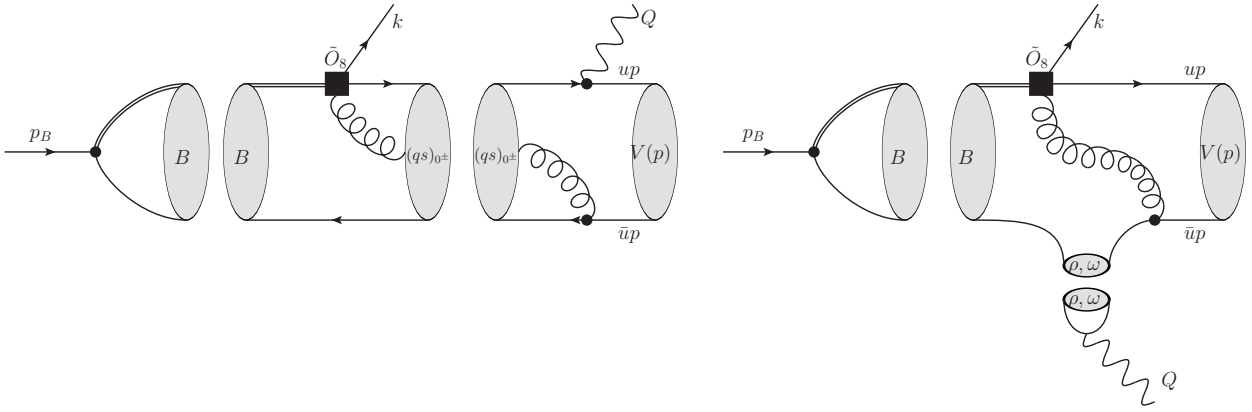

FIGURE 5.4: (left) Hadronic interpretation of the 3-particle cut in Figure 5.3 in terms of a LD hadronic process. The latter is a source for the strong (CP-even) phase obtained for the $G_\iota(q^2)$-functions. (right) Hadronic interpretation of the strong phase due to $q^2 > 0$, associated with $B \to V(\rho,\omega) \to V\gamma^* \to Vll$-type transitions.

$$[m_{B_q}^2 f_{B_q}]^2|_{SR_0} = (m_b+m_q)^2 e^{\frac{m_B^2-m_b^2}{M^2}}\Big(- m_b\langle\bar{q}q\rangle_\mu - \frac{m_b}{2M^2}(1-\frac{m_b^2}{2M^2})\langle\bar{q}Gq\rangle_\mu \\ + \frac{3}{8\pi^2}\int_{(m_b+m_q)^2}^{s_0} e^{\frac{m_b^2-s}{M^2}}(s-(m_b-m_q)^2)\sqrt{(s-m_b^2-m_q^2)^2-4m_b^2m_q^2}\frac{ds}{s}\Big) \tag{5.4.1}$$

The parameters $M^2 = M^2[f_{H_q}]$ and $s_0 = s_0[f_{H_q}]$ are not necessarily the same as the ones in the sum rule for G_ι-functions.

Following the decomposition (5.3.1), at twist-2, the spectator parts decompose for the vector and pseudoscalar final state as follows:

$$\begin{aligned} G_i^{(s)} &= G_i^{(\perp)}(q^2) + G_i^{(\parallel)}(q^2)\,, \\ G_T^{(s)} &= G_T^{(P)}(q^2)\,, \end{aligned} \tag{5.4.2}$$

The superscripts $\{\perp, \parallel, P\}$ refer to the projections onto the corresponding light-meson DA e.g. (I.2.11). Out of the seven functions (5.4.2), four satisfy relations, so that the full function can be reconstructed by three of them:

$$V:\ \ G_1^{(\perp)}(q^2), G_3^{(\parallel)}(q^2)\,, \qquad P:\ \ G_T^{(P)}(q^2)\,, \tag{5.4.3}$$

The four relations required are:

$$G_1^{(\parallel)}(q^2) = G_2^{(\parallel)}(q^2) = 0,\ \ G_2^{(\perp)} = (1-q^2/m_B^2)G_3^{(\perp)},\ \ G_2^{(\perp)} = (1-q^2/m_B^2)G_1^{(\perp)} \tag{5.4.4}$$

Furthermore, in the ultra-relativistic approximation $m_V^2 \to 0$, the projections $G_T^{(P)}(q^2)$ and $G_3^{(\parallel)}(q^2)$ are proportional to each other modulo a replacement of the corresponding DA, see Appendix H.

For the sake of completeness, the sum rule expression for $G_1^{(\perp)}(q^2)$ is given:

$$G_1^{(\perp)}(q^2) = \frac{1}{(m_B^2 f_B)|_{SR_0}} \int_{m_b^2}^{s_0} e^{\frac{m_B^2 - s}{M^2}} \rho_1^{(\perp)}(s)$$
$$\rho_1^{(\perp)}(s) = p \int_0^1 du \phi_\perp(u) \sum_{i=a}^{d} (b_i^\perp \rho_{B_i}(u,s) + c_i^\perp \rho_{C_i}(u,s)) \,, \tag{5.4.5}$$

where $p \equiv C_F(\alpha_s/4\pi) f_V^\perp m_b^2 Q_b/(-2)$ and and $\rho_{B(C)_i}$ and $b(c)_i^\perp$ are given in Eqs. (J.4) and (H.5) respectively.

The types of FCNC $b \to (d,s)$-, $c \to u$-transitions of $B(D)$ meson into a light $V(P)$ meson that have been considered are indicated in Table 5.1 This sums to a total of 19 transitions; 11 to a vector and 8 to a pseudoscalar.

		$\rho[\pi]^+$	$\rho[\pi]^0, \omega$	$\rho[\pi]^-$	$K^*[K]^+$	$K^*[K]^0$	$K^*[K]^-$	$\bar{K}^*[\bar{K}]^0$	ϕ
		$(u\bar{d})$	$(\bar{u}u) \pm (\bar{d}d)$	$(u\bar{d})$	$(u\bar{s})$	$(d\bar{s})$	$(s\bar{u})$	$(s\bar{d})$	$(s\bar{s})$
B^-	$(b\bar{u})$	–	–	$b \to d$	–	–	$b \to s$	–	–
$\bar{B}^0$	$(b\bar{d})$	–	$b \to d$	–	–	–	–	$b \to s$	–
$\bar{B}_s$	$(b\bar{s})$	–	–	–	–	$b \to d$	–	–	$b \to s$
D^0	$(c\bar{u})$	–	$c \to u$	–	–	–	–	–	–
D^+	$(c\bar{d})$	$c \to u$	–	–	–	–	–	–	–
D_s	$(c\bar{s})$	–	–	–	$c \to u$	–	–	–	–

TABLE 5.1: FCNC-transitions up to charge conjugation for $B(D) \to V(P)$ as indicated. The valence quark content of the mesons are indicated in brackets and the type of transition is also indicated. There are $11_V + 8_P = 19$ transitions in total.

The central hadronic input parameters and their uncertainties are given in Appendix K. The collinear factorisation scale is chosen to be $\mu_F^2 = m_b(m_c)\Lambda_{\rm had} \simeq m_b(m_c)\,0.8\,\text{GeV}$ for $B(D)$ transitions. This scale corresponds to the momentum transfer and is standard for hard-spectator contributions. Central values at $q^2 = 0$ for $G_1^{(\perp)}(0)$, as required for $B(D) \to V\gamma$-transitions and uncertainties are collected in Tab.5.2. The Borel parameters $M^2[G]$, $M^2[f_H]$, the continuum threshold s_0, the heavy quark mass m_b, the decay constants and the condensates are all varied as indicated in Appendix K. The major uncertainties come from varying s_0, m_h and μ_F which amount to about 11[15], 8[7], and 5[20]% for $B[D]$-transitions respectively. The uncertainties in the decay constants can be significant depending on the final state meson, as they enter linearly. One expects violation of quark-hadron duality to be accounted for by variations of s_0. There are two further sources of uncertainty which are not taken care of by varying parameters. First, the scale dependence of the operator $\tilde{O}_8(\mu_{\rm UV})$,[11] especially since proper radiative corrections in α_s are not included. At 1-loop level the diagonal anomalous dimension is $\gamma_{88} = C_F$ in conventions where $\gamma_m = 6C_F$ and is fortunately small. Evolving at leading log level from $\mu = 1\,\text{GeV}$ to

[11] In physical processes, such as $B \to K^*\gamma$, this is compensated by the Wilson coefficients.

m_b leads to a 7%-effect which shall be adapted as an estimate of this uncertainty. Second, the omission of twist-3 and higher twists: on grounds of past experience a 15% uncertainty is attributed to them. Note that the Borel mass is chosen to suppress the latter, yet keeping violations of quark-hadron duality acceptably small, as explained in Appendix K. Finally all the parametric variations, as described above, and the uncertainty of higher twist and $\mu_{\rm UV}$ are added in quadrature, as strong correlations are not anticipated. The final uncertainties along with the central values are collected in Table 5.2.

	$G_1^{(\perp)}(0)\cdot 10^2$	unc.%	type		$G_1^{(\perp)}(0)\cdot 10^2$	unc.%	type
$B^-\to\rho^-\gamma$	$0.29-0.39i$	25%	$(bD)^-$	$\bar{B}_s\to K^{*0}\gamma$	$0.21+0.18i$	27%	$(bD)^0$
$B^-\to K^{*-}\gamma$	$0.29-0.40i$	26%	$(bD)^-$	$\bar{B}_s\to\phi\gamma$	$0.26+0.23i$	26%	$(bD)^0$
$\bar{B}^0\to\rho^0\gamma$	$0.22+0.19i$	27%	$(bD)^0$	$D^0\to\rho^0\gamma$	$-7.0-5.0i$	32%	$(cu)^0$
$\bar{B}^0\to\omega\gamma$	$0.19+0.17i$	33%	$(bD)^0$	$D^0\to\omega\gamma$	$-6.1-4.3i$	34%	$(cu)^0$
$\bar{B}^0\to\bar{K}^{*0}\gamma$	$0.20+0.20i$	28%	$(bD)^0$	$D^+\to\rho^+\gamma$	$-1.9+2.5i$	32%	$(cu)^+$
				$D_s^+\to K^{*+}\gamma$	$-1.8+2.1i$	33%	$(cu)^+$

TABLE 5.2: Contribution of the diagrams A_1-A_4 in Figure 5.2 at $q^2=0$, for an on-shell photon. On a qualitative level, there are four types of transitions, the B or D and charged or uncharged. The notation $(bD)^0$ for instance means a $b\to(d,s)$ transition in a charge neutral meson. In all cases, the charge conjugate transition follows by simply reversing the sign, since all amplitudes are proportional to the charges of the valence quarks. Together with the non-spectator correction $G_i^{(ns)}$, this constitutes the relevant information for $B(D)\to V\gamma$ decays. Note that $G_1^{(\perp)}(0)=G_2^{(\perp)}(0)$. The uncertainties in the real and imaginary parts are very close and thus are not quoted separately.

5.4.1 Qualitative discussion

As discussed in the caption of Table 5.2, there are four qualitatively different transitions depending on whether the initial meson is either of b or c flavour and on whether it is charged or not, which is of course a manifestation of the sensitivity to isospin. The b-types are plotted in Figure 5.5. The q^2-dependence is somewhat more complex than the one of an ordinary form factor $B\to\pi$. In the latter case, the q^2-dependence is merely governed by a series of poles, starting at $q^2=m_{B^*}^2$, and higher multi-hadron cuts. For this reason, fitting that form factor is rather simple. In the case at hand, the photon couples to all kinds of flavours and thus poles in $q^2=m_\rho^2, m_{B^*}^2, \Upsilon(\bar{b}b)$ appear. Furthermore, there are genuine LD contributions which result in strong phases for $q^2, P^2>0$, as discussed in subsection 5.3.3 and illustrated in Figure 5.4. Moreover, note that the imaginary part decreases with q^2. This is to be expected as the process shown in Figure 5.4 (left) is more and more off-shell for higher q^2.

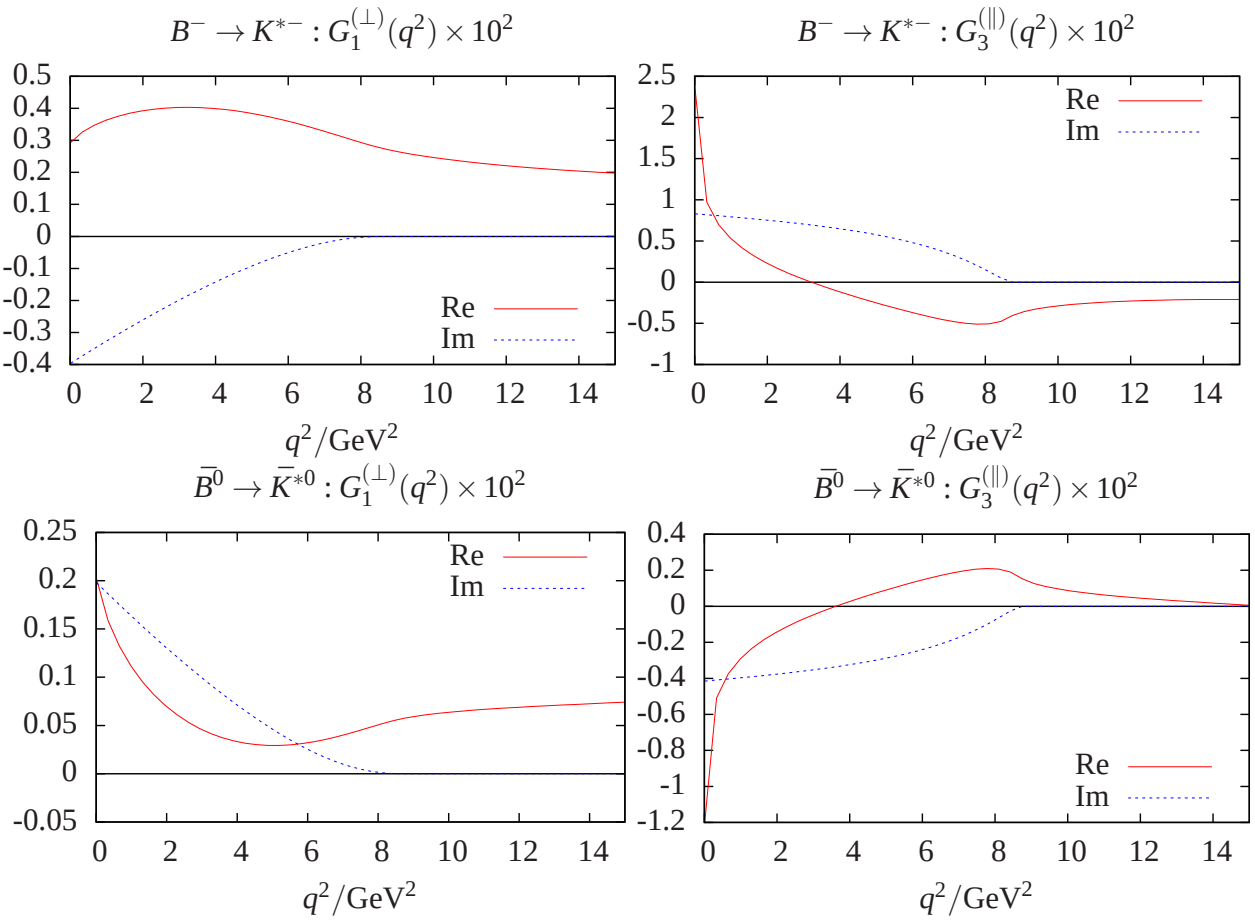

FIGURE 5.5: Plots of $G_1^{(\perp)}(q^2)$ and $G_3^{(\parallel)}(q^2)$ for charged and uncharged B mesons. Any other G_ι-function, where a U- or D-type flavour is exchanged, is qualitatively similar. As usual, U- and D-type stand for the u, c, t and d, s, b-flavours.

Table 5.3 reproduces values for $G_1(0)$ for the spectator contributions $G_1^{(s)}(0)$, the non-spectator contributions $G_1^{(ns)}(0)$, their sum $G_1(0) = G_1^{(s)}(0) + G_1^{(ns)}(0)$ as well as ratios between the latter and the SD penguin form factors $T_1(0)$. The ratios of $|G_1^{(\perp)}(0)/G_1^{(ns)}|$ are between 20% and 59% and vary considerably according to the charge and flavour of the heavy initial meson. The ratio of $|G_1^{(s)}(0)/T_1(0)|$ is around 2% for the B meson and considerably larger for the $D^{0(-)}$ at 5%(13%). The ratio of the total $G_1(0)$ to the SD part, $|G_1(0)/T_1(0)|$, is 7% for the B meson and rather sizeable for the $D^{0(-)}$: 21%(34%). Concerning the comparison of the B and D matrix elements themselves, to obtain a meaningful answer one has to use the decomposition:

$$G_1^{(s)}(0) = Q_h G_1^{h,(s)}(0) + Q_q G_1^{q,(s)}(0) \,, \qquad h \in \{b, c\} \,, q \in \{u, d, s\}. \tag{5.4.6}$$

Then,

$$R_h = \frac{G_1^{b,(\perp)}(0)[B \to \rho\gamma]}{G_1^{c,(\perp)}(0)[D \to \rho\gamma]} = 0.14 \,, \quad R_l = \frac{G_1^{q,(\perp)}(0)[B \to \rho\gamma]}{G_1^{q,(\perp)}(0)[D \to \rho\gamma]} = 0.05 + 0.04i \,. \tag{5.4.7}$$

type	$B^- \to \rho^-\gamma$	$\bar{B}^0 \to \rho^0\gamma$	$D^+ \to \rho^+\gamma$	$D^0 \to \rho^0\gamma$
$G_1^{(s)}(0)\cdot 10^{-2}$	$0.29-0.39i$	$0.22+0.19i$	$-1.9+2.5i$	$-7.0-5.0i$
$G_1^{(ns)}(0)\cdot 10^{-2}$	$0.90+1.3i$	$0.90+1.3i$	$-8.5-12i$	$-8.5-12i$
$G_1(0)\cdot 10^{-2}$	$1.2+0.91i$	$1.1+1.5i$	$-10-9.5i$	$-16-17i$
$\left\lvert G_1^{(s)}(0)/G_1^{(ns)}(0)\right\rvert$ [%]	31	18	21	58
$\left\lvert G_1^{(s)}(0)/T_1(0)\right\rvert$ [%]	2	1	4	12
$\lvert G_1(0)/T_1(0)\rvert$ [%]	6	7	20	33

TABLE 5.3: Comparison of various parts of the four characteristic types of G_ι-functions. See subsection 5.4.1 for comments. For the $T_1(0)$ form factors the following were used as reference values: $T_1^{B\to\rho}(0) = 0.27$ [154] for $B \to \rho$ and $T_1^{D\to\rho}(0) = 0.7$, e.g. [155], for $D \to \rho$. Note $G_1^{(s)}(0) = G_1^{(\perp)}(0)$ at this level of twist-approximation. The ratio of $G_1^{(ns)}$ to $T_1(0)$ can directly be inferred from the formula (5.4.9).

5.4.2 Validity of computation in q^2-range

The validity of the computation in the q^2-range will now be discussed in some more detail than in section 5.3.3. The computation cannot be trusted when either real QCD or perturbative QCD, as employed here[12], predicts the production of particles, which would be hadrons and quarks & gluons in the respective cases. This happens in real QCD when q^2 reaches the ρ-, $B^*_{d,s}$- and $\Upsilon(\bar{b}b)$ thresholds for $J^{PC} = 1^{--}$-mesons. The corresponding production thresholds for perturbative QCD are of the two-valence quark-type and occur at q^2: $(2m_q)^2$, $(m_b + m_{d,s})^2$ and $(2m_b^2)$ respectively. The ρ-threshold leads to the exclusion of the region $0 < q^2 < (\simeq 1\ \text{GeV}^2)$ for $B \to Vll$. The quark threshold at $(m_b + m_{d,s})^2$ indicates that the LC-OPE is not valid a few GeV below that value. This is the case for all diagrams except $A_1 - A_2$ which do not have these thresholds and therefore the validity ought to extend a few GeV below B^*-resonance and thus basically to the endpoint of the physical region.

5.4.3 Summary for $B(D) \to V\gamma$

For the reader's convenience, the essentials points for $B(D) \to V\gamma$ decay are briefly be summarised.

$$B(D) \to V\gamma: \quad G_1(0) = G_2(0) = G_1^{(\perp)}(0) + G_1^{(ns)}(0) \tag{5.4.8}$$

with

$$G_1^{(ns)}(0) = \left(\frac{3\alpha_s(m_h)}{4\pi}\right) Q_h F_8^{(7)} T_1(0)\ , \tag{5.4.9}$$

where $h = b(c)$, $Q_{b(c)} = -1/3(2/3)$ and $F_8^{(7)}$ are taken from [139]. The generic amplitude assumes the following form:[13]

$$\mathcal{A}(B(D) \to V\gamma) \sim \Big(\mathcal{A}_1(P_1\cdot\epsilon) + \mathcal{A}_2(P_2\cdot\epsilon)\Big)\ , \tag{5.4.10}$$

[12] By which it is meant that the LC-OPE with perturbatively computed hard scattering kernels.
[13] The amplitudes $\mathcal{A}_{1,2}$ up to normalisation are often denoted by $A_{\text{PC,PV}}$ in the literature.

where $\mathcal{A}_{L,R} = \mathcal{A}_1 \pm \mathcal{A}_2$ correspond to left- and right-handed photon polarisations. The result and the leading SD penguin read:

$$\mathcal{A}_1 = \mathcal{A}_2 = C_7 T_1(0) + C_8 G_1(0) + .. \,. \tag{5.4.11}$$

Using the notation $\mathcal{O}'_{7,8} = \mathcal{O}_{7,8}|_{\gamma_5 \to -\gamma_5}$ for the penguin operators with opposite chirality and the corresponding Wilson coefficients one gets:

$$\mathcal{A}_{1,2} = C_7 T_1(0) + C_8 G_1(0) \pm (C'_7 T_1(0) + C'_8 G_1(0)) + .. \,, \tag{5.4.12}$$

where $T_1(0) = T_2(0)$ and $G_1(0) = G_2(0)$ were used. The former is an equality and the latter is a result of the leading twist-2 computation.

5.5 Comparison with QCD factorisation

This section compares the results with QCDF [17]. More precisely the diagrams A_1 and A_2[14], in Figure 5.2, at $q^2 = 0$ corresponding to $Q_q G_1^{q,(s)}(0)$ (5.4.2) shall be considered, where the formulae take on a rather simple form. The G_1-function at $q^2 = 0$ is parametrised as follows:

$$G_1(0) = \Big[\underbrace{\frac{\alpha_s}{4\pi} \frac{C_F}{N_c} 12\pi^2 \frac{f_\perp f_B}{m_B^2}}_{\sim m_b^{-5/2}} \Big] (Q_q X_\perp + Q_b \overline{X}_\perp) \,, \tag{5.5.1}$$

with $X_\perp$ as in [17],

$$X_\perp = \int_0^1 \phi_\perp(u) x_\perp(u) \,, \tag{5.5.2}$$

$$x_\perp^{QCDF}(u) = \frac{1+\bar{u}}{3\bar{u}^2} \tag{5.5.3}$$

and likewise for the quantity $\overline{X}_\perp$. The LCSR result in this limit reads:

$$x_\perp^{LCSR}(u) = \int_{m_b^2}^{s_0} ds\, e^{\frac{m_B^2 - s}{M^2}} \rho(s,u) \,, \tag{5.5.4}$$

with

$$\rho(s,u) = \underbrace{\frac{m_b^2 N_c}{12\pi^2 f_B^2}}_{\equiv c m_b^3} \left[\frac{\log\left(\frac{\bar{u}s(m_b^2 + P^2 - s)}{P^2(m_b^2 - us)}\right)}{P^2 - \bar{u}s} - \frac{s - m_b^2}{\bar{u}sP^2} \right] ,$$

$$\bar{\rho}(s,u) = \frac{m_b^2 N_c}{12\pi^2 f_B^2} \left[- \left(\frac{s - m_b^2}{usP^2} - \theta(us - m_b^2) \left(\frac{us - m_b^2}{2u^2 sP^2} + \frac{\log\left(\frac{us}{m_b^2}\right)}{2uP^2} \right) \right) \right] . \tag{5.5.5}$$

It should be emphasised that the result in Eq. (5.5.3) was computed anew and found to be in agreement with reference [17]. The contributions of diagrams $A_{3,4}$, which correspond to

[14] Note the sum of these two diagrams is well-defined as they constitute the contribution proportional to the spectator charge.

$\overline{X}_\perp$, have been kept in the expression above. A few remarks about the m_b-behaviour are in order. The term in the bracket in Eq. (5.5.1) scales as $m_b^{-5/2}$, taking into account $f_B \sim m_b^{-1/2}$. The coefficient c in Eq.(5.5.5) is $\mathcal{O}(m_b^0)$. The expression $X_\perp^{QCDF}$ is $\mathcal{O}(1)$. The questions for investigation are:

a) The presence and absence of an endpoint divergence at leading order α_s, for $\bar{u} \to 0$, in $X_\perp^{QCDF}$ and $X_\perp^{LCSR}$ respectively.

b) In what respect $X_\perp^{QCDF}$ and $X_\perp^{LCSR}$ can be compared to each other.

c) The absence and presence of an imaginary part, to leading order in α_s, in $X_\perp^{QCDF}$ and $X_\perp^{LCSR}$ respectively.

The answers to these questions are, certainly, tied to each other. First, question a) will be discussed. Assuming the usual endpoint behaviour

$$\phi_\perp(u) \stackrel{u\simeq 1}{\to} 6\bar{u}u \,, \tag{5.5.6}$$

the most singular part in (5.5.3),

$$x_\perp^{QCDF} = \frac{1}{3\bar{u}^2} + \mathcal{O}(\bar{u}^{-1}) \quad \Rightarrow \quad X_\perp^{QCDF} = 2\int_0^1 \frac{du}{\bar{u}} + \text{finite} \tag{5.5.7}$$

convoluted as in (5.5.2) with (5.5.6) leads to logarithmic endpoint divergence. The endpoint configuration $u \simeq 1$ corresponds to the situation where the non-spectator quark carries all the momentum. On a purely technical level the divergent integral arises from the fact that two propagators assume the same form $1/(\bar{u}m_B^2)$, see Figure 5.6 (left), as the momentum fraction of the spectator quark is neglected due to $\Lambda_{\rm QCD}/m_b$ suppression. In view of this and potential transverse corrections, it was advertised in [156], that for $B \to \pi\pi$ and similar cases the replacement $1/(\bar{u}m_B^2) \to 1/((\bar{u}+\epsilon)m_B^2)$ should be made ($\epsilon = \Lambda_h/m_b$ with Λ_h some hadronic scale of the order of the QCD-scale) and a correction term included to account for missing soft contributions with possible strong phases. The endpoint divergent integral in (5.5.7) becomes,

$$x_\perp^{QCDF} \to (1+\rho e^{i\phi})\Theta\left(\bar{u} - \frac{\Lambda_h}{m_b}\right)\frac{1}{3\bar{u}^2} + \mathcal{O}(\bar{u}^{-1}) \tag{5.5.8}$$

$$\Rightarrow \quad X_\perp^{QCDF} = 2(1+\rho e^{i\phi})\,\ln\left(\frac{m_b}{\Lambda_h}\right) + \Lambda_h\text{-independent} \,, \tag{5.5.9}$$

with $\rho \in [0,1]$ and $\phi \in [0, 2\pi]$ being numbers parametrising the above mentioned corrections. Thus changes can be expected if the heavy quark limit is not assumed as is the case in LCSR. Yet the question to address is whether there are qualitative differences beyond the behaviour of the RHS in Eqs. (5.5.8, 5.5.9).

In the LCSR computation there is only one propagator with manifest $1/(\bar{u}m_B^2)$-behaviour, see Figure 5.6. Thus, to the question: Is there another one hidden in the loop? The answer is no, as it would correspond to a power IR-divergence whereas it is known that in four dimensions IR-singularities, be they soft or collinear, are at worst logarithmic in nature, e.g. [157]. Inspection of the graph Figure 5.6 reveals that there can at most be a collinear divergence in the limit

$\bar{u} \to 0$ and $p^2 = q^2 = 0$. The potential endpoint sensitive terms are parametrised as follows:

$$x_\perp^{LCSR} \sim \alpha_\perp \frac{\ln(\bar{u})}{\bar{u}} + \beta_\perp \ln(\bar{u}) + \gamma_\perp \frac{1}{\bar{u}} \,. \tag{5.5.10}$$

Note that they are all integrable assuming the DA Eq.(5.5.6). From Eq. (5.5.5) [15] it is found that: $\alpha_\perp = 0$, $\beta_\perp \neq 0$, $\gamma_\perp \neq 0$. The absence of the most singular term $\ln(\bar{u})/\bar{u}$ appears to be accidental; such terms are present in the $P/V^{\|}$-contribution. In summary, the endpoint behaviour of the $x_\perp^{LCSR}$ (5.5.10) differs from $x_\perp^{QCDF}$ (5.5.7) even when finite m_b-effects are added by hand (5.5.8).

Before attempting an interpretation of this difference one should try to reflect on question b), namely to what degree it makes sense to compare the QCDF and the LCSR result at face value.

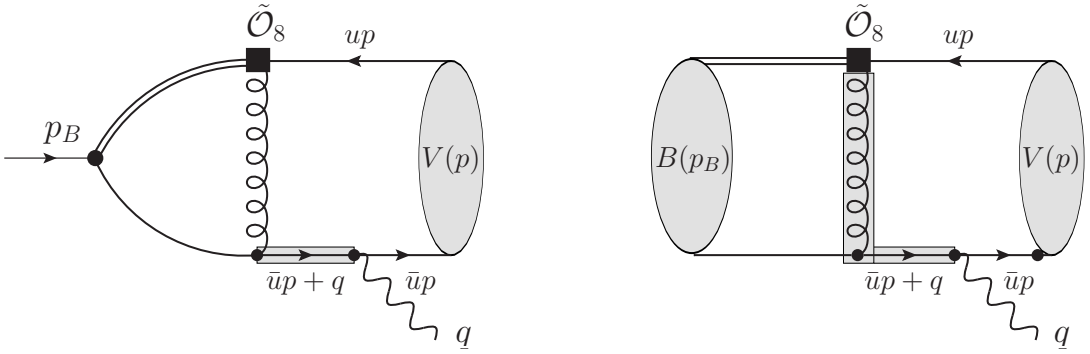

FIGURE 5.6: The shaded propagators that scale like $1/(\bar{u}m_B^2)$ in both figures. (left) Diagram of LCSR or the LC-OPE respectively (right) Diagram in QCDF. Thus $x_\perp^{QCDF} \sim 1/\bar{u}^2$ and $x_\perp^{LCSR} \sim \ln(\bar{u})/\bar{u}$ at worst, as explained in the text.

It is advocated here that, within the approximations, the QCDF contribution is contained in the LCSR result but the converse is not true. For example, the gluon in Figure 5.6 (right) is not necessarily the hard gluon of QCDF but can also be a gluon that hadronises into a 3-particle $(qs)_{0^\pm}$-state, as shown in Figure 5.4(left). Moreover there are cuts of the 3-particle type for the B-meson as well, see Figure 5.3. Possibly it is helpful, at this point, to note that there is a crucial difference between the two approaches. In QCDF one computes a specific sub-process and the corresponding scaling of the momenta leads to a clear physical picture of the dynamics of that sub-process, whereas in LCSR one computes a correlation function, in a domain where it is believed to be valid, and extracts the matrix element by suitable methods such as dispersion relation and Borel transformation. Thus, the physical parton configurations are, generically, not immediately deducible from the correlation function.

In summary, the LCSR result is not endpoint divergent, yet sensitive to the endpoint It is seen that the amendment (5.5.8) is not enough to obtain a similar qualitative behaviour of $x_\perp^{QCDF}$ and $x_\perp^{LCSR}$. Whether or not this is due to the fact that $x_\perp^{LCSR}$ constitutes in addition to the physics present in $x_\perp^{QCDF}$, a LD-part, see Figure 5.4 (left) is a question not addressed herein.

[15] Integration over ds is not going to change anything at this point.

5.6 Summary & conclusions

This chapter has reported on the computation of $\mathcal{O}_8$ matrix elements between heavy pseudoscalar B and D states and a light vector and pseudoscalar state plus an off-shell photon, by using the method of LCSRs, at leading twist-2 and leading α_s. Scalar functions of the photon momentum invariant $G_{1,2,3}(q^2)$ and $G_T(q^2)$ Eqs. (5.2.1,5.2.2) were defined such that they parallel the well-known penguin tensor form factors $T_{1,2,3}(q^2)$ and $f_T(q^2)$, see Eq. (5.2.3). Central values for interesting flavour transitions are presented in Table 5.2, as well as plots of the four characteristic cases in Figure 5.5 are presented in section 5.4. A remarkable feature is the large CP-even (strong) phase for which a LD interpretation was given in section 5.3.3 (see Figure 5.4). This fact, as well as the plots, make it clear why $G_\iota(q^2)$ should be referred to as matrix elements rather than form factors. Comparison of various contributions such as spectator, non-spectator, and SD penguin photon emission can be found in Table 5.3. Note that the $G_\iota(q^2)$-functions are relevant for asymmetries of isospin- [151] and CP-type (depending on new weak phases) [131], rather than branching ratios.

In section 5.5 the computation was compared with QCDF. The comparison is not straightforward as the LCSRs contain LD contributions of the type shown in Figure 5.4 (left) which are not present in leading order QCDF. The LCSR computation does not suffer from endpoint divergences like QCDF, which is attributed to the fact that IR-divergences are at worst logarithmic in four dimensions.

A remarkable feature on the technical side of the computation is the appearance of a complex anomalous threshold on the physical Riemann sheet, for which various viewpoints and derivations are given in Appendix J. The anomalous threshold is associated, in the three point-function, with all three propagators being on the mass shell and therefore is not related to the intermediate B-meson state. The crucial point, for the physics, is that the anomalous thresholds is well isolated from the m_B-pole. This results in an exponential as well as oscillatory suppression by the Borel parameter, such that the extraction of the matrix element is not affected considerably.

Chapter 6

Conclusions

To recap, despite its tremendous success, the Standard Model of particle physics is widely viewed as the low energy limit of a more fundamental theory. One of its long-standing puzzles is associated with the flavour sector, which is governed by free parameters, tuned to fit the experimental observation. There is still no mechanism that dictates their size. When considering a supersymmetric framework, the number of free parameters and, as a result, the flavour, as well as the CP problems increase dramatically. Even though there is no symmetry to force supersymmetric sources of flavour and CP violation to be small, experiment tells us that they have to be as all measurements so far are in agreement with the SM expectations. From the phenomenological point of view, this issue is usually addressed by means of *ad hoc* assumptions such as e.g. Minimal Flavour Violation (MFV), where all sources of flavour violation are intimately linked to the flavour structure of the Yukawa matrices. However, the concept of MFV is not a theory of flavour. Moreover, it does not seem to provide a framework in which the structure of the fermionic masses and mixing angles, the origin of CP violation and the number of generations can be addressed in a satisfactory way. Through all those concerns emanates the need for an underlying symmetry.

In Chapter 2, the main features of the SM were briefly reviewed and its perceived shortcomings were discussed. Motivating supersymmetry as a favourable new physics scenario, its basic ingredients were outlined. Finally, the idea of imposing a family symmetry was discussed in order to gain insight into the flavour sector of the SM and its supersymmetric extension, ideally in a GUT background.

In Chapter 3, the crux of the original research of this thesis was reached. Therein, the SM and SUSY flavour and CP problems were addressed, within an $SU(5)$ SUSY GUT model of flavour, based on the simple family symmetry $S_4 \times U(1)$ [11]. The existence of three families of quarks and leptons ensues from the non-Abelian factor of the family symmetry, whose triplets are the only faithful irreducible representations and they accommodate the matter superfields. Introducing a set of heavy Higgs-like scalars, called flavons, that can couple to the usual matter superfields and working in an effective theory approach, all operators involving flavons, matter and Higgs fields, that can form a singlet under all symmetries were identified. The structure of the Yukawa, Majorana and soft SUSY breaking mass matrices, as well as that of the Kähler metrics, is dictated by the controlled breaking of the family and CP symmetries, via non-zero

complex flavon vevs. Identifying the absolute value of these vevs, divided by the UV cut-off mass scale, with powers of the Wolfenstein parameter λ, all matrices were constructed up to and including the order λ^8. Taking into account effects of canonical normalisation and RG running, it is found that the model provides a good description of all quark and lepton masses, mixings and CP violation, in agreement with the LO results in [11](where canonical normalisation effects were ignored).

Concerning the soft SUSY breaking sector, which was the main focus in this work, the mass insertion parameters were derived, which parametrise the amount of flavour and CP violation beyond the SM. The calculation relied on the assumption that the SUSY breaking mechanism respects the family symmetry. The results for the low energy mass insertions were summarised in Eqs. (3.7.7-3.7.9) in terms of their λ-suppression, while their full expressions were given in Appendix F.3. It was found that δ^f_{LL} and δ^f_{RR} are approximately equal to the identity, with only small off-diagonal entries. Considering the parameters δ^f_{LR}, it was observed that the diagonal elements featured the same hierarchies as the corresponding diagonal Yukawa matrices $\tilde{Y}^f$, while the off-diagonal elements are strongly suppressed. Crucially, this shows that the $S_4 \times U(1)$ SUSY GUT model approximately reproduces the effects of low energy MFV, where one would simply impose $\delta^f_{LL} = \delta^f_{RR} = \mathbb{1}$ and $\delta^f_{LR} \propto \tilde{Y}^f$. The phenomenological implications of the deviations from MFV were left to be discussed quantitatively in Chapter 4, where the predictions of the model with respect to a number of different flavour observables were presented and discussed in detail.

Whereas in Chapter 3 the focus was on the similarity to MFV, Chapter 4 highlighted the differences. This was done by considering the predictions for electric dipole moments, lepton flavour violation, B and K meson mixing as well as rare B decays. As expected, it was found that many of the new physics contributions fall well below current limits. This is the case for example in B physics observables, where deviations are negligible (at the 1% level). Thus, the model would be unable to explain any discrepancies between SM expectations and measurements in $\Delta M_{B_{s,d}}$ or in the time dependent asymmetries $S_{J/\psi\phi}$ and $S_{J/\psi K_S}$. This is in marked contrast to the $SU(3)$ family symmetry models previously studied, where large effects were expected in these observables. Thus, neutrino physics which led to $S_4 \times U(1)$, appears to lead us towards models with small such deviations.

On the other hand, it was found that there were observable effects which would distinguish the $S_4 \times U(1)$ SUSY GUT model from MFV. The most significant effects of the departure from MFV appear in the (12) down-type quark and charged lepton sectors, related to Kaon mixing observables and the branching ratio of $\mu \to e\gamma$. It was found that $(\delta^e_{LL})_{12}$ provides the dominant contribution to $\mathrm{BR}(\mu \to e\gamma)$ and that the model requires rather heavy sleptons, exceeding about 1 TeV, in order to satisfy the experimental bound. Another important area where the model gives observable deviations from MFV is CP violation, in particular the electron EDM, where again large (TeV scale) slepton masses are required for compatibility with current bounds to be achieved. Interestingly, it is therefore predicted that a signal should be observed in both $\mu \to e\gamma$ and the electron EDM within the expected sensitivity of future experiments.

It was also observed that with regard to CP violation in the Kaon system, the model contributes significantly to ϵ_K due to the phase of $(\delta^d_{RR})_{12}$. The SM prediction for this observable depends sensitively on $|V_{cb}|$, which differs when considering inclusive or exclusive decays, leading to

a lower central value in the latter case. However, even for inclusive values of $|V_{cb}|$, the SM expectation for ϵ_K is about 10% below the measurement. Thus, the model is capable of providing sufficient enhancement to explain the experimentally observed value of ϵ_K.

To summarise, in the first and main part of this thesis presented in Chapters 3 and 4, theories with discrete flavour symmetries such as the $S_4 \times U(1)$ SUSY GUT model, motivated by neutrino physics, seem to lead to MFV-like flavour changing expectations, but with some important exceptions. This study shows that, while observable deviations in B physics are generally not expected to show up, departures from MFV are expected in both $\mu \to e\gamma$ and the electron EDM within the foreseeable sensitivity of future experiments. CP violating effects may also be observed in ϵ_K, perhaps resolving some possible SM discrepancies.

The second part of this thesis was presented in Chapter 5 and described the computation of chromomagnetic matrix elements between heavy pseudoscalar B and D states and a light vector and pseudoscalar state plus an off-shell photon, by using the method of LCSRs, at leading twist-2 and leading α_s. The basic object was a correlation function with the B initial state interpolated by a current that has the same quantum numbers. As a result, not only the ground state was produced but also excited mesons and a continuum of states. The calculation starts with the four momentum invariants being far below any thresholds, such that perturbative QCD can be applied. Cauchy's formula was used in writing the dispersion representation of the correlation function in the variable of the B-current four momentum invariant, the aim being to extract the ground state. For the description of real particles, analytic continuation of the four momentum invariants to the physical domain is required. The discontinuities in the dispersion integrand (associated with non-zero imaginary parts of the correlation function) are usually interpreted as physically accessible states. Upon analytic continuation of a three-point function, the appearance of a complex anomalous threshold was observed, associated with the case where all the propagators are on the mass shell. This made the computation highly non-trivial, but, crucially, the anomalous threshold was well isolated from the m_B pole and it did not considerably affect the extraction of the matrix element.

An interesting feature of the computation was the appearance of a large CP-even (strong) phase, which was interpreted as a long distance effect. For that reason, the $G_\iota(q^2)$ scalar functions of the four momentum invariant, defined in Eqs. (5.2.1,5.2.2), were referred to as matrix elements, rather than form factors. Results for interesting flavour transitions were presented in Table 5.2 and in Figure 5.5. Contributions amongst spectator, non-spectator, and SD penguin photon emission were provided in Table 5.3. Finally, the results were compared with those obtained using the QCDF method. The comparison was not straightforward as the LCSRs contain long distance contributions, which are not present in leading order QCDF. The advantage is that the LCSRs computation does not suffer from endpoint divergences like the QCDF one. As a result of this work, the contribution of the chromomagnetic operator in these FCNC decays that had been unknown for a long time, can now be accounted for. As the $G_\iota(q^2)$-functions are small, they may not be relevant for the overall branching ratios but they can provide a significant contribution to isospin and CP asymmetries and their calculation allows for assessing whether any possible deviations from the SM expectations can be attributed to the associated C_8 Wilson coefficient.

Appendix A

S_4 and CP symmetry

The non-Abelian finite group S_4 can be defined in terms of the presentation

$$S^2 = \mathbb{1}\,, \quad T^3 = \mathbb{1}\,, \quad U^2 = \mathbb{1}\,,$$
$$(ST)^3 = \mathbb{1}\,, \quad (SU)^2 = \mathbb{1}\,, \quad (TU)^2 = \mathbb{1}\,, \quad (STU)^4 = \mathbb{1}\,,$$

where S, T and U denote the generators of the group. Explicit matrix representations are basis dependent. In this work we apply the basis where the T generator is diagonal and complex for the doublet and triplet representations. Defining $\omega = e^{2\pi i/3}$, we have

$$\begin{aligned}
\mathbf{1}: &\quad S = 1\,, && T = 1\,, && U = 1\,,\\
\mathbf{1}': &\quad S = 1\,, && T = 1\,, && U = -1\,,\\
\mathbf{2}: &\quad S = \begin{pmatrix} 1 & 0 \\ 0 & 1 \end{pmatrix}\,, && T = \begin{pmatrix} \omega & 0 \\ 0 & \omega^2 \end{pmatrix}\,, && U = \begin{pmatrix} 0 & 1 \\ 1 & 0 \end{pmatrix}\,,\\
\mathbf{3}: &\quad S = \frac{1}{3}\begin{pmatrix} -1 & 2 & 2 \\ 2 & -1 & 2 \\ 2 & 2 & -1 \end{pmatrix}\,, && T = \begin{pmatrix} 1 & 0 & 0 \\ 0 & \omega^2 & 0 \\ 0 & 0 & \omega \end{pmatrix}\,, && U = -\begin{pmatrix} 1 & 0 & 0 \\ 0 & 0 & 1 \\ 0 & 1 & 0 \end{pmatrix}\,,\\
\mathbf{3}': &\quad S = \frac{1}{3}\begin{pmatrix} -1 & 2 & 2 \\ 2 & -1 & 2 \\ 2 & 2 & -1 \end{pmatrix}\,, && T = \begin{pmatrix} 1 & 0 & 0 \\ 0 & \omega^2 & 0 \\ 0 & 0 & \omega \end{pmatrix}\,, && U = +\begin{pmatrix} 1 & 0 & 0 \\ 0 & 0 & 1 \\ 0 & 1 & 0 \end{pmatrix}\,.
\end{aligned}$$

The corresponding Clebsch-Gordan coefficients are all real and can be found e.g. in [10].

In addition to the flavour symmetry S_4, we impose the canonical CP symmetry in our theory. As has been discussed in the literature, see e.g. [171, 172], the consistent combination of a flavour and a CP symmetry requires certain conditions to be fulfilled; in particular that the subsequent application of a CP, a flavour and a further CP transformation leads to a transformation belonging to the flavour group. The possibility to combine the group S_4 with CP has been explored previously, see e.g. [58, 171]. Here we are interested in combining S_4 symmetry, defined in the above basis, with the canonical CP transformation, i.e. the CP transformation that acts trivially in flavour space with $X_{\mathbf{r}} = \mathbb{1}$ for all representations $\mathbf{r}$ of S_4. Note that this

particular CP transformation $X_{\mathbf{r}}$ fulfils the constraints of being a unitary and symmetric matrix. Moreover, it represents a consistent choice for a CP transformation (see e.g.[58]), which corresponds to the involutionary automorphism that maps the generators S, T and U in the following way

$$S \quad \to \quad S\,, \quad T \quad \to \quad T^2 = T^{-1} \quad \text{and} \quad U \quad \to \quad U\,, \tag{A.1}$$

since S and U are represented by real matrices in our chosen basis, while the generator T is given as a diagonal complex matrix in the two- and three-dimensional representations. As with all automorphisms of S_4, this is an inner one. In particular, one can check that the automorphism of Eq. (A.1) is "class-inverting" [82], i.e. it maps the group element g into the class which includes g^{-1}. This is true, since all automorphisms are inner ones and all classes of S_4 are ambivalent, i.e. the elements g and g^{-1} are in the same class.

With only real Clebsch-Gordan coefficients, a canonical CP symmetry imposed on the theory entails that all coefficients in the (super-)potential are real. Moreover, we observe that the residual symmetry in the neutrino sector at LO comprises the CP symmetry if all three neutrino flavons share the same phase factor. Following the comments of Footnote 2 of Appendix B, this is the case in our setup, cf. also Eqs. (B.1,B.2), so that the common phase can be factored out of the neutrino mass matrix, leading to an effective LO result which conserves CP. Furthermore, the canonical CP transformation $X_{\mathbf{r}} = \mathbb{1}$ commutes with the Klein group generated by S and U and thus at LO the residual symmetry is given by the direct product $Z_2 \times Z_2 \times \text{CP}$.

Appendix B

Vacuum alignment

The vacuum alignment of the flavon fields is achieved by coupling them to a set of so-called driving fields and requiring the F-terms of the latter to vanish. These driving fields, whose transformation properties under the family symmetry are shown in Table B.1, are SM gauge singlets and carry a charge of $+2$ under a continuous R-symmetry. The flavons and the GUT Higgs fields are uncharged under this $U(1)_R$, whereas the supermultiplets containing the SM fermions (or right-handed neutrinos) have charge $+1$. As the superpotential must have a $U(1)_R$ charge of $+2$, the driving fields can only appear linearly and cannot have any direct interactions with the SM fermions or the right-handed neutrinos.

Field	X_1^d	$\overline{X}_1^d$	$X_{1'}^{\nu d}$	X_1^u	Y_2^{du}	Y_2^d	Y_2^ν	$Z_{3'}^\nu$	V_0	V_1	V_η	X_1^{new}	$\tilde{X}_{1'}^{\text{new}}$
$SU(5)$	**1**	**1**	**1**	**1**	**1**	**1**	**1**	**1**	**1**	**1**	**1**	**1**	**1**
S_4	**1**	**1**	**1′**	**1**	**2**	**2**	**2**	**3′**	**1**	**1**	$\mathbf{1}^{(\prime)}$	**1**	**1′**
$U(1)$	-2	14	3	10	9	6	-16	-16	0	-8	-7	18	15

TABLE B.1: The transformation properties of the driving fields, as introduced in [11], which serve to align the flavon VEVs.

The LO alignment of the flavon fields, see Eq. (3.2.1), has been thoroughly discussed in [10, 11]. The particular setup also provides correlations amongst the VEVs. As described in Appendix D of [10] and in Section 4 of [11],[1] the vanishing of the F-terms of the driving fields X_1^{new}, $\tilde{X}_{1'}^{\text{new}}$, Y_2^ν, $Z_{3'}^\nu$, V_0, V_1 and V_η gives rise to the relations[2]

$$\begin{aligned} &\phi_2^u \sim \phi_2^d\,\tilde{\phi}_3^d\,, \qquad \phi_1^\nu \sim \phi_2^\nu \sim \phi_{3'}^\nu\,, \qquad (\phi_3^d)^2\phi_i^\nu \in \text{Re}\,, \\ &\tilde{\phi}_2^u \sim \frac{\phi_1^\nu}{\phi_2^\nu}\,, \qquad \tilde{\phi}_3^d \sim \phi_2^d\,(\phi_3^d)^3\,, \qquad \phi_{3'}^\nu \sim \frac{\eta}{(\phi_2^d)^3\phi_3^d}\,. \end{aligned} \tag{B.1}$$

[1] The introduction of the new flavon field η in [11] favours the exchange of the S_4 doublet driving field V_2, which was introduced in [10], by the S_4 singlet field V_1. Furthermore, the field V_η, transforming in the same representation of S_4 as η, is introduced in order to relate the new flavon field to an explicit mass scale.

[2] The proportionality constant between $\phi_{3'}^\nu$ and ϕ_2^ν is a square root of an order one real number, which we assume to be positive, such that $\phi_{3'}^\nu$ and ϕ_2^ν have the same phases.

Denoting the phase of each flavon VEV ϕ_ρ^f by θ_ρ^f, Eq. (B.1) correlates the LO phases as[3]

$$\begin{aligned} &\tilde{\theta}_2^u = 0 \ , \qquad \theta_2^u = 2\theta_2^d + 3\theta_3^d \ , \qquad \tilde{\theta}_3^d = \theta_2^d + 3\theta_3^d \ , \\ &\theta^\eta = 3\theta_2^d - \theta_3^d \ , \qquad \theta_{3'}^\nu = \theta_2^\nu = \theta_1^\nu = -2\theta_3^d \ , \end{aligned} \tag{B.2}$$

leaving as free variables only the two phases θ_2^d, θ_3^d, which correspond to the LO VEVs of the two flat superpotential directions: $\langle \Phi_{2,1}^d \rangle$ and $\langle \Phi_{3,2}^d \rangle$ respectively.

In order to find the higher order terms of the flavon VEVs, we start by writing each one of them as a series expansion in λ, up to and including order λ^{12}. For example, the leading operators of the superpotential fix $\langle \Phi_{2,1}^u \rangle / M$ to be zero up to λ^4, while $\langle \Phi_{2,2}^u \rangle / M$ has to be $\phi_2^u \, \lambda^4$ [10]. When considering the subleading operators, the VEVs of $\Phi_{2,1}^u$ and $\Phi_{2,2}^u$ receive corrections (shifts) which we parametrise as

$$\frac{\langle \Phi_2^u \rangle}{M} = \begin{pmatrix} 0 \\ \phi_2^u \, \lambda^4 \end{pmatrix} + \begin{pmatrix} \sum_{n=5}^{12} \delta_{2,1_{(n)}}^u \lambda^n \\ \sum_{n=5}^{12} \delta_{2,2_{(n)}}^u \lambda^n \end{pmatrix} . \tag{B.3}$$

All flavon VEVs are parametrised in a similar manner. The aim is to find the order of λ at which each shift δ has to be non-zero. The computation consists of taking into account all possible operators and solving the F-term conditions resulting from the set of driving field order by order in λ, up to λ^{12}. Each vanishing expression is solved for the lowest order shift involved. At the end, all shifts can be expressed in terms of the LO flavon VEVs. We find

$$\begin{aligned} &\frac{\langle \Phi_2^u \rangle}{M} = \begin{pmatrix} \delta_{2,1}^u \, \lambda^8 \\ \phi_2^u \, \lambda^4 + \delta_{2,2}^u \, \lambda^5 \end{pmatrix}, \quad \frac{\langle \tilde{\Phi}_2^u \rangle}{M} = \begin{pmatrix} \tilde{\delta}_{2,1}^u \, \lambda^6 \\ \tilde{\phi}_2^u \, \lambda^4 + \tilde{\delta}_{2,2}^u \, \lambda^5 \end{pmatrix}, \quad \frac{\langle \eta \rangle}{M} = \phi^\eta \lambda^4 + \delta^\eta \lambda^5, \\ &\frac{\langle \Phi_3^d \rangle}{M} = \begin{pmatrix} \delta_{3,1}^d \, \lambda^6 \\ \phi_3^d \, \lambda^2 \\ \delta_{3,3}^d \, \lambda^6 \end{pmatrix}, \quad \frac{\langle \tilde{\Phi}_3^d \rangle}{M} = \begin{pmatrix} \tilde{\delta}_{3,1}^d \, \lambda^7 \\ -\left(\tilde{\phi}_3^d \, \lambda^3 + \tilde{\delta}_{3,2_{(4)}}^d \, \lambda^4 + \tilde{\delta}_{3,2_{(5)}}^d \, \lambda^5 \right) \\ \tilde{\phi}_3^d \, \lambda^3 + \tilde{\delta}_{3,2_{(4)}}^d \, \lambda^4 + \tilde{\delta}_{3,3_{(5)}}^d \, \lambda^5 \end{pmatrix}, \quad \frac{\langle \Phi_2^d \rangle}{M} = \begin{pmatrix} \phi_2^d \, \lambda \\ \delta_{2,2}^d \, \lambda^7 \end{pmatrix}, \\ &\frac{\langle \Phi_{3'}^\nu \rangle}{M} = \begin{pmatrix} 1 \\ 1 \\ 1 \end{pmatrix} \left(\phi_{3'}^\nu \lambda^4 + \delta_{3'}^\nu \lambda^5 \right), \quad \frac{\langle \Phi_2^\nu \rangle}{M} = \begin{pmatrix} \phi_2^\nu \, \lambda^4 + \delta_{2,1}^\nu \, \lambda^5 \\ \phi_2^\nu \, \lambda^4 + \delta_{2,2}^\nu \, \lambda^5 \end{pmatrix}, \quad \frac{\langle \Phi_1^\nu \rangle}{M} = \phi_1^\nu \lambda^4 + \delta_1^\nu \lambda^5. \end{aligned} \tag{B.4}$$

Note that the shifts presented in Eq. (B.4) are the first non-trivial ones. However, in our calculations of the mass matrices we take into account all shifts up to $\mathcal{O}(\lambda^8)$. It should be pointed out that the alignment of $\Phi_{3'}^\nu$ is not perturbed up to order λ^8, so that it preserves the S symmetry to that level. On the other hand, the alignment of Φ_2^ν is already perturbed at order λ^5 which, however, does not break the S generator as it is nothing but the identity for the doublet representation. Taking into account also CN effects, one can show that m_ν^{eff} has the form of Eq. (3.4.22) up to $\mathcal{O}(\lambda^7)$.

Eq. (B.4) is in agreement with the discussion presented in Section 4 of [11], barring the absorptions of $\delta_{2,2}^u \, \lambda$, $\tilde{\delta}_{2,2}^u \, \lambda$, $\tilde{\delta}_{3,2_{(4)}}^d \, \lambda$, $\delta_{3'}^\nu \lambda$, $\delta_1^\nu \lambda$ and $\delta^\eta \, \lambda$ into the corresponding LO VEVs. Being interested in the CP transformation properties of the fields, such absorptions must not be made

[3] Here and in Eq. (B.6), a possible phase shift by π has been ignored as real coefficients can generally be positive or negative.

in the current work, as the phases of shifts and LO VEVs are generally different. In particular, we find the following relations between the shifts and the LO VEVs,

$$\begin{aligned}
&\delta^u_{2,1} \sim (\phi^d_2)^2(\phi^d_3)^3 \,, \qquad \delta^u_{2,2} \sim (\phi^d_2)^6(\phi^d_3)^4 \,, \qquad \tilde{\delta}^u_{2,1} \sim \tilde{\delta}^u_{2,2} \sim (\phi^d_2)^4\phi^d_3 \,, \qquad \delta^\eta \sim (\phi^d_2)^7, \\
&\delta^d_{3,1} \sim \delta^d_{3,3} \sim \phi^d_3 \,, \qquad \tilde{\delta}^d_{3,1} \sim \phi^d_2\,(\phi^d_3)^3 \,, \qquad \tilde{\delta}^d_{3,2_{(4)}} \sim (\phi^d_2)^5(\phi^d_3)^4 \,, \qquad \tilde{\delta}^d_{3,3_{(5)}} - \tilde{\delta}^d_{3,2_{(5)}} \sim (\phi^d_2)^5, \\
&\delta^d_{2,2} \sim (\phi^d_2)^5\phi^d_3 \,, \qquad \delta^\nu_{3'} \sim \delta^\nu_{2,1} \sim \delta^\nu_{2,2} \sim \delta^\nu_1 \sim \frac{(\phi^d_2)^4}{\phi^d_3} \,.
\end{aligned} \tag{B.5}$$

Similar relations also hold for higher order shifts. Although such shifts have to be taken into account when performing a systematical λ-expansion, their explicit expressions are irrelevant for our phenomenological study.

The phases of the LO shifts can be deduced straightforwardly from Eq. (B.5). Denoting the phase of $\delta^f_{\rho,i}$ by $\theta^f_{\rho,i}$ we obtain

$$\begin{aligned}
&\theta^u_{2,1} = 2\theta^d_2 + 3\theta^d_3 \,, \qquad \theta^u_{2,2} = 2(3\theta^d_2 + 2\theta^d_3) \,, \qquad \tilde{\theta}^u_{2,1} = \tilde{\theta}^u_{2,2} = 4\theta^d_2 + \theta^d_3 \,, \qquad \arg[\delta^\eta] = 7\theta^d_2 \,, \\
&\theta^d_{3,1} = \theta^d_{3,3} = \theta^d_3 \,, \qquad \tilde{\theta}^d_{3,1} = \theta^d_2 + 3\theta^d_3 \,, \qquad \tilde{\theta}^d_{3,2_{(4)}} = 5\theta^d_2 + 4\theta^d_3 \,, \qquad \arg[\tilde{\delta}^d_{3,3_{(5)}} - \tilde{\delta}^d_{3,2_{(5)}}] = 5\theta^d_2 \,, \\
&\theta^d_{2,2} = 5\theta^d_2 + \theta^d_3 \,, \qquad \arg[\delta^\nu_{3'}] = \theta^\nu_{2,1} = \theta^\nu_{2,2} = \arg[\delta^\nu_1] = 4\theta^d_2 - \theta^d_3 \,.
\end{aligned} \tag{B.6}$$

Appendix C

Basis transformations

C.1 Canonical normalisation

In order to find the transformations which map the Kähler potential into its canonical form, we express the hermitian matrix $\mathcal{K}_A$ as in Eq. (3.3.14), i.e. $P_A^\dagger P_A = \mathcal{K}_A$. Note that the matrix P_A is not unique since $P_A \to Q_A P_A$ with unitary Q_A will satisfy Eq. (3.3.14) just as well. Moreover, $\mathcal{K}_A$ can always be decomposed as

$$\mathcal{K}_A \;=\; (Q_A^\dagger \sqrt{D_A} Q_A)(Q_A^\dagger \sqrt{D_A} Q_A)\;, \tag{C.1.1}$$

where D_A is the diagonalised form of $\mathcal{K}_A$. Therefore it is sufficient to find a *hermitian* matrix P_A which satisfies Eq. (3.3.14), i.e. $P_A^\dagger P_A = P_A P_A = \mathcal{K}_A$. Expanding $\mathcal{K}_A$ and P_A in powers of λ,

$$\mathcal{K}_A = \sum_{n=0}^{\infty} k_n \lambda^n\,, \qquad P_A = \sum_{m=0}^{\infty} p_m \lambda^m\,, \tag{C.1.2}$$

with k_n, p_n being matrices, allows one to calculate P_A iteratively. With $k_0 = \mathbb{1}$, the result reads

$$p_0 = \mathbb{1}\,, \qquad p_1 = \frac{1}{2} k_1\,, \qquad p_n = \frac{1}{2}\left(k_n - \sum_{j=1}^{n-1} p_j p_{n-j}\right)\,. \tag{C.1.3}$$

C.2 SCKM transformations

The SCKM rotation matrices that diagonalise the Yukawas are found through the singular value decomposition. In particular, if $Y^f = U_L^f \tilde{Y}^f_{\text{diag}} (U_R^f)^\dagger$, then U_L^f and U_R^f consist of the eigenvectors of $Y^f (Y^f)^\dagger$ and $(Y^f)^\dagger Y^f$, respectively. These eigenvectors are only defined up to phase transformations

$$U_L^f \to U_L^f \Omega_L^f\,, \qquad \Omega_L^f = \text{diag}\left(e^{i\omega^f_{L_1}}, e^{i\omega^f_{L_2}}, e^{i\omega^f_{L_3}}\right)\,, \tag{C.2.1}$$

$$U_R^f \to U_R^f \Omega_L^f \Omega_R^f\,, \qquad \Omega_R^f = \text{diag}\left(e^{i\omega^f_{R_1}}, e^{i\omega^f_{R_2}}, e^{i\omega^f_{R_3}}\right)\,. \tag{C.2.2}$$

We fix the phases of the matrices Ω_L^f by requiring that the CKM and PMNS mixing matrices are given in the standard phase convention, while the phases of Ω_R^f are fixed by demanding real and positive charged fermion masses. To LO, we find the following structure of the SCKM transformation matrices in terms of their λ-suppression.

$$U_L^u \approx \begin{pmatrix} 1 & \lambda^4 & \lambda^6 \\ \lambda^4 & 1 & \lambda^5 \\ \lambda^6 & \lambda^5 & 1 \end{pmatrix}, \qquad U_R^u \approx \begin{pmatrix} 1 & \lambda^4 & \lambda^6 \\ \lambda^4 & 1 & \lambda^5 \\ \lambda^6 & \lambda^5 & 1 \end{pmatrix}, \tag{C.2.3}$$

$$U_L^d \approx \begin{pmatrix} 1 & \lambda & \lambda^3 \\ \lambda & 1 & \lambda^2 \\ \lambda^4 & \lambda^2 & 1 \end{pmatrix}, \qquad U_R^d \approx \begin{pmatrix} 1 & \lambda & \lambda^4 \\ \lambda & 1 & \lambda^4 \\ \lambda^4 & \lambda^4 & 1 \end{pmatrix}, \tag{C.2.4}$$

$$U_L^e \approx \begin{pmatrix} 1 & \lambda & \lambda^4 \\ \lambda & 1 & \lambda^4 \\ \lambda^4 & \lambda^4 & 1 \end{pmatrix}, \qquad U_R^e \approx \begin{pmatrix} 1 & \lambda & \lambda^3 \\ \lambda & 1 & \lambda^2 \\ \lambda^4 & \lambda^2 & 1 \end{pmatrix}. \tag{C.2.5}$$

With these SCKM transformations, it is straightforward to calculate the CKM mixing to leading order,

$$V_{\mathrm{CKM_{GUT}}} = (U_L^u)^T U_L^{d*} \approx \begin{pmatrix} 1 & \frac{\tilde{x}_2}{y_s}\lambda & \frac{\tilde{x}_2}{y_b}\lambda^3 \\ -\frac{\tilde{x}_2}{y_s}\lambda & 1 & \frac{y_s}{y_b}\lambda^2 \\ -e^{-i\theta_2^d}\frac{\tilde{x}_2^2}{y_s\, y_b}\lambda^4 & -\frac{y_s}{y_b}\lambda^2 & 1 \end{pmatrix}. \tag{C.2.6}$$

The associated measure of CP violation is given by the Jarlskog invariant $J^q_{\mathrm{CP_{GUT}}}$ and can be calculated from the imaginary part of $V_{\mathrm{CKM_{GUT_{21}}}} V_{\mathrm{CKM_{GUT_{32}}}} V^*_{\mathrm{CKM_{GUT_{22}}}} V^*_{\mathrm{CKM_{GUT_{31}}}}$. The explicit result can be found in Eq. (3.6.5).

Appendix D

Mass insertion parameters at the GUT scale

In the following we present the explicit expression for the various LO mass insertion parameters at the GUT scale whose λ-suppressions have been stated in Eqs. (3.7.4-3.7.6). Using the definitions of Eqs. (3.7.2,3.7.3), we obtain

$$\delta^u_{LL_{\rm GUT}} \approx \begin{pmatrix} 1 & \frac{e^{-i\theta^d_2}\tilde{b}_{12}}{b_{01}}\,\lambda^4 & \frac{e^{-i(4\theta^d_2+\theta^d_3)}\tilde{b}_{13}}{\sqrt{b_{01}\left(b_{02}+\upsilon_u^2\, y_t^2/m_0^2\right)}}\,\lambda^6 \\ \cdot & 1 & \frac{e^{-i(7\theta^d_2+2\theta^d_3)}\tilde{b}_{23}}{\sqrt{b_{01}\left(b_{02}+\upsilon_u^2\, y_t^2/m_0^2\right)}}\,\lambda^5 \\ \cdot & \cdot & 1 \end{pmatrix},$$

$$\delta^u_{RR_{\rm GUT}} \approx \begin{pmatrix} 1 & \frac{e^{-i\theta^d_2}\tilde{b}_{12}}{b_{01}}\,\lambda^4 & \frac{\tilde{b}_{13}}{\sqrt{b_{01}\left(b_{02}+\upsilon_u^2\, y_t^2/m_0^2\right)}}\,\lambda^6 \\ \cdot & 1 & \frac{e^{i(5\theta^d_2+\theta^d_3)}\tilde{b}_{23}}{\sqrt{b_{01}\left(b_{02}+\upsilon_u^2\, y_t^2/m_0^2\right)}}\,\lambda^5 \\ \cdot & \cdot & 1 \end{pmatrix}, \tag{D.1}$$

$$\delta^u_{LR_{\rm GUT}} \approx \frac{\upsilon_u\,\alpha_0}{m_0} \begin{pmatrix} \frac{\tilde{a}^u_{11}-y_u\frac{\mu}{t_\beta A_0}}{b_{01}}\lambda^8 & 0 & 0 \\ 0 & \frac{\tilde{a}^u_{22}-y_c\frac{\mu}{t_\beta A_0}}{b_{01}}\lambda^4 & \frac{e^{i\theta^d_2}\tilde{a}^u_{23}}{\sqrt{b_{01}\left(b_{02}+\upsilon_u^2\, y_t^2/m_0^2\right)}}\,\lambda^7 \\ 0 & \frac{e^{i(3\theta^d_2+\theta^d_3)}\tilde{a}^u_{23}}{\sqrt{b_{01}\left(b_{02}+\upsilon_u^2\, y_t^2/m_0^2\right)}}\,\lambda^7 & \frac{\tilde{a}^u_{33}-y_t\frac{\mu}{t_\beta A_0}}{b_{02}+\upsilon_u^2\, y_t^2/m_0^2} \end{pmatrix},$$

$$\delta^d_{LL_{\rm GUT}} \approx \begin{pmatrix} 1 & \frac{\tilde{B}_{12}}{b_{01}}\,\lambda^3 & \frac{e^{i\theta^d_2}\tilde{B}_{13}}{\sqrt{b_{01}\,b_{02}}}\,\lambda^4 \\ \cdot & 1 & \frac{\tilde{B}_{23}}{\sqrt{b_{01}\,b_{02}}}\,\lambda^2 \\ \cdot & \cdot & 1 \end{pmatrix}, \quad \delta^d_{RR_{\rm GUT}} \approx \begin{pmatrix} 1 & e^{i\theta^d_2}\tilde{R}_{12}\,\lambda^4 & -\,e^{i\theta^d_2}\tilde{R}_{12}\,\lambda^4 \\ \cdot & 1 & -\,\tilde{R}_{12}\,\lambda^4 \\ \cdot & \cdot & 1 \end{pmatrix}, \tag{D.2}$$

$$\delta^d_{LR_{\rm GUT}} \approx \frac{v_d\,\alpha_0}{m_0}\begin{pmatrix} \frac{1}{\sqrt{b_{01}}}\left(\tilde{a}^d_{11}-\frac{\mu\,t_\beta}{A_0}\frac{\tilde{x}_2^2}{y_s}\right)\lambda^6 & \frac{\tilde{a}^d_{12}}{\sqrt{b_{01}}}\,\lambda^5 & \frac{\tilde{a}^d_{12}}{\sqrt{b_{01}}}\lambda^5 \\ -\frac{\tilde{a}^d_{12}}{\sqrt{b_{01}}}\lambda^5 & \frac{1}{\sqrt{b_{01}}}\left(\tilde{a}^d_{22}-\frac{\mu\,t_\beta}{A_0}y_s\right)\lambda^4 & \frac{\tilde{a}^d_{23}}{\sqrt{b_{01}}}\,\lambda^4 \\ e^{-i\theta^d_2}\frac{\tilde{a}^d_{31}}{\sqrt{b_{02}}}\,\lambda^6 & \frac{\tilde{a}^d_{32}}{\sqrt{b_{02}}}\,\lambda^6 & \frac{1}{\sqrt{b_{02}}}\left(\tilde{a}^d_{33}-\frac{\mu\,t_\beta}{A_0}y_b\right)\lambda^2 \end{pmatrix},$$

$$\delta^e_{LL_{\rm GUT}} \approx \begin{pmatrix} 1 & \tilde{R}_{12}\,\lambda^4 & -\tilde{R}_{12}\,\lambda^4 \\ \cdot & 1 & -\tilde{R}_{12}\,\lambda^4 \\ \cdot & \cdot & 1 \end{pmatrix}, \quad \delta^e_{RR_{\rm GUT}} \approx \begin{pmatrix} 1 & -\frac{e^{i\theta^d_2}\tilde{B}_{12}}{3\,b_{01}}\,\lambda^3 & \frac{\tilde{B}_{13}}{3\sqrt{b_{01}b_{02}}}\,\lambda^4 \\ \cdot & 1 & \frac{3\tilde{B}_{23}}{\sqrt{b_{01}b_{02}}}\,\lambda^2 \\ \cdot & \cdot & 1 \end{pmatrix}, \tag{D.3}$$

$$\delta^e_{LR_{\rm GUT}} \approx \frac{v_d\,\alpha_0}{m_0}\begin{pmatrix} \frac{1}{3\sqrt{b_{01}}}\left(\tilde{a}^d_{11}-\frac{\mu\,t_\beta}{A_0}\frac{\tilde{x}_2^2}{y_s}\right)\lambda^6 & \frac{e^{i\theta^d_2}\tilde{a}^d_{12}}{\sqrt{b_{01}}}\,\lambda^5 & \frac{\tilde{a}^d_{31}}{\sqrt{b_{02}}}\lambda^6 \\ -\frac{e^{-i\theta^d_2}\tilde{a}^d_{12}}{\sqrt{b_{01}}}\lambda^5 & \frac{3}{\sqrt{b_{01}}}\left(\tilde{a}^d_{22}-\frac{\mu\,t_\beta}{A_0}y_s\right)\lambda^4 & \frac{\tilde{a}^e_{23}}{\sqrt{b_{02}}}\,\lambda^6 \\ -\frac{e^{-i\theta^d_2}\tilde{a}^d_{12}}{\sqrt{b_{01}}}\lambda^5 & \frac{3\tilde{a}^d_{23}}{\sqrt{b_{01}}}\,\lambda^4 & \frac{1}{\sqrt{b_{02}}}\left(\tilde{a}^d_{33}-\frac{\mu\,t_\beta}{A_0}y_b\right)\lambda^2 \end{pmatrix}.$$

These δ parameters are expressed in terms $\alpha_0 = A_0/m_0$ and the coefficients of the soft mass matrices in Eqs. (3.6.13-3.6.21), where we have defined:

$$\begin{aligned} &\tilde{b}_{12} = (b_2 - b_{01}k_2), \quad \tilde{b}_{13} = -(b_4 - b_{01}k_4), \quad \tilde{b}_{23} = -(b_3 - b_{01}k_3), \\ &\tilde{B}_{12} = 2\frac{\tilde{x}_2}{y_s}(b_1 - b_{01}k_1), \quad \tilde{B}_{13} = \frac{\tilde{x}_2^2}{y_b\,y_s}(b_{01} - b_{02}), \quad \tilde{B}_{23} = \frac{y_s}{y_b}(b_{01} - b_{02}), \quad \tilde{R}_{12} = B_3 - K_3, \end{aligned} \tag{D.4}$$

and

$$\begin{aligned} \tilde{a}^u_{11} &= a_u e^{i(\theta^a_u - \theta^y_u)}, \quad \tilde{a}^u_{22} = a_c e^{i(\theta^a_c - \theta^y_u)}, \quad \tilde{a}^u_{33} = a_t, \quad \tilde{a}^u_{23} = z^u_2\left(\frac{a_t}{y_t} - e^{i(\theta_2^{z_{u_a}} - \theta_2^{z_u})}\frac{z_2^{u_a}}{z_2^u}\right), \\ \tilde{a}^d_{11} &= \frac{\tilde{x}_2^2}{y_s}\left(2\frac{\tilde{x}^a_2}{\tilde{x}_2}e^{i(\theta^{\tilde{x}_a}_2 - \theta^{\tilde{x}}_2)} - \frac{a_s}{y_s}e^{i(\theta^a_s - \theta^y_s)}\right), \quad \tilde{a}^d_{22} = a_s e^{i(\theta^a_s - \theta^y_s)}, \quad \tilde{a}^d_{33} = a_b e^{i(\theta^a_b - \theta^y_b)}, \\ \tilde{a}^d_{12} &= \tilde{x}_2\left(\frac{\tilde{x}^a_2}{\tilde{x}_2}e^{i(\theta^{\tilde{x}_a}_2 - \theta^{\tilde{x}}_2)} - \frac{a_s}{y_s}e^{i(\theta^a_s - \theta^y_s)}\right), \quad \tilde{a}^d_{23} = y_s\left(\frac{a_s}{y_s}e^{i(\theta^a_s - \theta^y_s)} - \frac{a_b}{y_b}e^{i(\theta^a_b - \theta^y_b)}\right), \\ \tilde{a}^d_{31} &= z^d_3\left(\frac{a_b}{y_b}e^{i(\theta^a_b - \theta^y_b)} - \frac{z_3^{d_a}}{z_3^d}e^{i(\theta_3^{z_{d_a}} - \theta_3^{z_d})}\right), \\ \tilde{a}^d_{32} &= \frac{y_s^2}{y_b}\left(\frac{a_s}{y_s}e^{i(\theta^a_s - \theta^y_s)} - \frac{a_b}{y_b}e^{i(\theta^a_b - \theta^y_b)}\right) + z^d_2\left(\frac{a_b}{y_b}e^{i(\theta^a_b - \theta^y_b)} - \frac{z_2^{d_a}}{z_2^d}e^{i(\theta_2^{z_{d_a}} - \theta_2^{z_d})}\right), \\ \tilde{a}^e_{23} &= 9\frac{y_s^2}{y_b}\left(\frac{a_s}{y_s}e^{i(\theta^a_s - \theta^y_s)} - \frac{a_b}{y_b}e^{i(\theta^a_b - \theta^y_b)}\right) + z^d_2\left(\frac{a_b}{y_b}e^{i(\theta^a_b - \theta^y_b)} - \frac{z_2^{d_a}}{z_2^d}e^{i(\theta_2^{z_{d_a}} - \theta_2^{z_d})}\right). \end{aligned} \tag{D.5}$$

The phases $\theta^y_{u,c,s,b}, \theta^{z_{u,d}}_i, \theta^{\tilde{x}}_2$ can be expressed in terms of the flavon phases θ^d_2, θ^d_3 according to Eqs. (3.4.4,3.4.10). This has been done in Eq. (D.4), but we refrain from doing so in Eq. (D.5) in order to highlight the fact that all $\tilde{a}^f_{ij}$ become real in the limit where the contributions of the auxiliary components of the flavon superfields to the A-terms are neglected such that the relation $\theta^a_f = \theta^y_f$ holds.

Appendix E

Renormalisation group equations in SCKM basis

The renormalisation group equations for the parameters of the superpotential as well as the soft breaking terms are usually given in the gauge flavour basis, see e.g. [47], with the transformation to the SCKM basis being defined only at the electroweak scale. As already discussed in Section 3.6, we find it useful to diagonalise the Yukawa matrices already at the high scale. In such a high scale SCKM basis, the RGEs will explicitly depend on the CKM mixing matrix. Here we define for convenience

$$V = (U_L^d)^\dagger U_L^u = V_{\mathrm{CKM_{GUT}}}^T. \tag{E.1}$$

Introducing the parameter $t = \ln(\mu/M_x)$, with μ being the renormalisation scale and M_x the high energy scale, we have for the Yukawas and the trilinear A-parameters,

$$\begin{aligned}
16\pi^2 \frac{d\tilde{Y}^u}{dt} &= \left(3\tilde{Y}^u\tilde{Y}^{u\dagger} + V^\dagger\tilde{Y}^d\tilde{Y}^{d\dagger}V - \frac{16}{3}g_3^2 - 3g_2^2 - \frac{13}{15}g_1^2 + 3\mathrm{Tr}[\tilde{Y}^{u\dagger}\tilde{Y}^u] + \mathrm{Tr}[\tilde{Y}^{\nu\dagger}\tilde{Y}^\nu]\right)\tilde{Y}^u, \\
16\pi^2 \frac{d\tilde{Y}^d}{dt} &= \left(3\tilde{Y}^d\tilde{Y}^{d\dagger} + V\tilde{Y}^u\tilde{Y}^{u\dagger}V^\dagger - \frac{16}{3}g_3^2 - 3g_2^2 - \frac{7}{15}g_1^2 + 3\mathrm{Tr}[\tilde{Y}^{d\dagger}\tilde{Y}^d] + \mathrm{Tr}[\tilde{Y}^{e\dagger}\tilde{Y}^e]\right)\tilde{Y}^d, \\
16\pi^2 \frac{d\tilde{Y}^e}{dt} &= \left(3\tilde{Y}^e\tilde{Y}^{e\dagger} + U_L^{e\dagger}Y^\nu Y^{\nu\dagger}U_L^e - 3g_2^2 - \frac{9}{5}g_1^2 + 3\mathrm{Tr}[\tilde{Y}^{d\dagger}\tilde{Y}^d] + \mathrm{Tr}[\tilde{Y}^{e\dagger}\tilde{Y}^e]\right)\tilde{Y}^e,
\end{aligned} \tag{E.2}$$

$$\begin{aligned}
16\pi^2 \frac{d\tilde{A}^u}{dt} &= \left(5\tilde{Y}^u\tilde{Y}^{u\dagger} + V^\dagger\tilde{Y}^d\tilde{Y}^{d\dagger}V - \frac{16}{3}g_3^2 - 3g_2^2 - \frac{13}{15}g_1^2 + 3\mathrm{Tr}[\tilde{Y}^{u\dagger}\tilde{Y}^u] + \mathrm{Tr}[Y^{\nu\dagger}Y^\nu]\right)\tilde{A}^u + \\
&+ \left(4\tilde{A}^u\tilde{Y}^{u\dagger} + 2V^\dagger\tilde{A}^d\tilde{Y}^{d\dagger}V + \frac{32}{3}g_3^2M_3 + 6g_2^2M_2 + \frac{26}{15}g_1^2M_1 + 6\mathrm{Tr}[\tilde{Y}^{u\dagger}\tilde{A}^u] + 2\mathrm{Tr}[Y^{\nu\dagger}A^\nu]\right)\tilde{Y}^u, \\
16\pi^2 \frac{d\tilde{A}^d}{dt} &= \left(5\tilde{Y}^d\tilde{Y}^{d\dagger} + V\tilde{Y}^u\tilde{Y}^{u\dagger}V^\dagger - \frac{16}{3}g_3^2 - 3g_2^2 - \frac{7}{15}g_1^2 + 3\mathrm{Tr}[\tilde{Y}^{d\dagger}\tilde{Y}^d] + \mathrm{Tr}[\tilde{Y}^{e\dagger}\tilde{Y}^e]\right)\tilde{A}^d + \\
&+ \left(4\tilde{A}^d\tilde{Y}^{d\dagger} + 2V\tilde{A}^u\tilde{Y}^{u\dagger}V^\dagger + \frac{32}{3}g_3^2M_3 + 6g_2^2M_2 + \frac{14}{15}g_1^2M_1 + 6\mathrm{Tr}[\tilde{Y}^{d\dagger}\tilde{A}^d] + 2\mathrm{Tr}[\tilde{Y}^{e\dagger}\tilde{A}^e]\right)\tilde{Y}^d, \\
16\pi^2 \frac{d\tilde{A}^e}{dt} &= \left(5\tilde{Y}^e\tilde{Y}^{e\dagger} + U_L^{e\dagger}Y^\nu Y^{\nu\dagger}U_L^e - 3g_2^2 - \frac{9}{5}g_1^2 + 3\mathrm{Tr}[\tilde{Y}^{d\dagger}\tilde{Y}^d] + \mathrm{Tr}[\tilde{Y}^{e\dagger}\tilde{Y}^e]\right)\tilde{A}^e + \\
&+ \left(4\tilde{A}^e\tilde{Y}^{e\dagger} + 2U_L^{e\dagger}A^\nu Y^{\nu\dagger}U_L^e + 6g_2^2M_2 + \frac{18}{5}g_1^2M_1 + 6\mathrm{Tr}[\tilde{Y}^{d\dagger}\tilde{A}^d] + 2\mathrm{Tr}[\tilde{Y}^{e\dagger}\tilde{A}^e]\right)\tilde{Y}^e.
\end{aligned} \tag{E.3}$$

The running of the soft scalar masses in the SCKM basis is given by

$$\begin{aligned}
16\pi^2 \frac{d}{dt}(\tilde{m}_u^2)_{LL} &= G_Q \mathbb{1} + F_Q^u + V^\dagger F_Q^d V, \\
16\pi^2 \frac{d}{dt}(\tilde{m}_d^2)_{LL} &= G_Q \mathbb{1} + V F_Q^u V^\dagger + F_Q^d, \\
16\pi^2 \frac{d}{dt}(\tilde{m}_e^2)_{LL} &= G_L \mathbb{1} + F_L^e + F_L^\nu, \\
16\pi^2 \frac{d}{dt}(\tilde{m}_f^2)_{RR} &= G_f \mathbb{1} + F_f, \qquad f = u, d, e,
\end{aligned} \tag{E.4}$$

with:

$$\begin{aligned}
F_Q^u &= \tilde{Y}^u \tilde{Y}^{u\dagger} (\tilde{m}_u^2)_{LL} + (\tilde{m}_u^2)_{LL} \tilde{Y}^u \tilde{Y}^{u\dagger} + 2\tilde{Y}^u (\tilde{m}_u^2)_{RR} \tilde{Y}^{u\dagger} + 2(m_{H_u}^2) \tilde{Y}^u \tilde{Y}^{u\dagger} + 2\tilde{A}^u \tilde{A}^{u\dagger}, \\
F_Q^d &= \tilde{Y}^d \tilde{Y}^{d\dagger} (\tilde{m}_d^2)_{LL} + (\tilde{m}_d^2)_{LL} \tilde{Y}^d \tilde{Y}^{d\dagger} + 2\tilde{Y}^d (\tilde{m}_d^2)_{RR} \tilde{Y}^{d\dagger} + 2(m_{H_d}^2) \tilde{Y}^d \tilde{Y}^{d\dagger} + 2\tilde{A}^d \tilde{A}^{d\dagger}, \\
F_L^e &= \tilde{Y}^e \tilde{Y}^{e\dagger} (\tilde{m}_e^2)_{LL} + (\tilde{m}_e^2)_{LL} \tilde{Y}^e \tilde{Y}^{e\dagger} + 2\tilde{Y}^e (\tilde{m}_e^2)_{RR} \tilde{Y}^{e\dagger} + 2(m_{H_d}^2) \tilde{Y}^e \tilde{Y}^{e\dagger} + 2\tilde{A}^e \tilde{A}^{e\dagger}, \\
F_L^\nu &= U_L^{e\dagger} Y^\nu Y^{\nu\dagger} U_L^e (\tilde{m}_e^2)_{LL} + (\tilde{m}_e^2)_{LL} U_L^{e\dagger} Y^\nu Y^{\nu\dagger} U_L^e + 2U_L^{e\dagger} Y^\nu m_N^2 Y^{\nu\dagger} U_L^e + \\
&\quad + 2(m_{H_u}^2) U_L^{e\dagger} Y^\nu Y^{\nu\dagger} U_L^e + 2U_L^{e\dagger} A^\nu A^{\nu\dagger} U_L^e \,, \\
F_u &= 2\left(\tilde{Y}^{u\dagger} \tilde{Y}^u (\tilde{m}_u^2)_{RR} + (\tilde{m}_u^2)_{RR} \tilde{Y}^{u\dagger} \tilde{Y}^u + 2\tilde{Y}^{u\dagger} (\tilde{m}_u^2)_{LL} \tilde{Y}^u + 2(m_{H_u}^2) \tilde{Y}^{u\dagger} \tilde{Y}^u + 2\tilde{A}^{u\dagger} \tilde{A}^u \right), \\
F_d &= 2\left(\tilde{Y}^{d\dagger} \tilde{Y}^d (\tilde{m}_d^2)_{RR} + (\tilde{m}_d^2)_{RR} \tilde{Y}^{d\dagger} \tilde{Y}^d + 2\tilde{Y}^{d\dagger} (\tilde{m}_d^2)_{LL} \tilde{Y}^d + 2(m_{H_d}^2) \tilde{Y}^{d\dagger} \tilde{Y}^d + 2\tilde{A}^{d\dagger} \tilde{A}^d \right), \\
F_e &= 2\left(\tilde{Y}^{e\dagger} \tilde{Y}^e (\tilde{m}_e^2)_{RR} + (\tilde{m}_e^2)_{RR} \tilde{Y}^{e\dagger} \tilde{Y}^e + 2\tilde{Y}^{e\dagger} (\tilde{m}_e^2)_{LL} \tilde{Y}^e + 2(m_{H_d}^2) \tilde{Y}^{e\dagger} \tilde{Y}^e + 2\tilde{A}^{e\dagger} \tilde{A}^e \right), \\
G_Q &= -4\left(\frac{8}{3} g_3^2 |M_3|^2 + \frac{3}{2} g_2^2 |M_2|^2 + \frac{1}{30} g_1^2 |M_1|^2 - \frac{1}{10} g_1^2 (m_{H_u}^2 - m_{H_d}^2) \right), \\
G_L &= -4\left(\frac{3}{2} g_2^2 |M_2|^2 + \frac{3}{10} g_1^2 |M_1|^2 + \frac{3}{10} g_1^2 (m_{H_u}^2 - m_{H_d}^2) \right), \\
G_u &= -4\left(\frac{8}{3} g_3^2 |M_3|^2 + \frac{8}{15} g_1^2 |M_1|^2 + \frac{2}{5} g_1^2 (m_{H_u}^2 - m_{H_d}^2) \right), \\
G_d &= -4\left(\frac{8}{3} g_3^2 |M_3|^2 + \frac{2}{15} g_1^2 |M_1|^2 - \frac{1}{5} g_1^2 (m_{H_u}^2 - m_{H_d}^2) \right), \\
G_e &= -4\left(\frac{6}{5} g_1^2 |M_1|^2 - \frac{3}{5} g_1^2 (m_{H_u}^2 - m_{H_d}^2) \right).
\end{aligned}$$

For completeness, we also show the evolution of the μ parameter, i.e. the coupling of the bilinear superpotential term $H_u H_d$,

$$16\pi^2 \frac{d\mu}{dt} = \left(3\mathrm{Tr}[\tilde{Y}^{u\dagger} \tilde{Y}^u] + 3\mathrm{Tr}[\tilde{Y}^{d\dagger} \tilde{Y}^d] + \mathrm{Tr}[\tilde{Y}^{e\dagger} \tilde{Y}^e] + \mathrm{Tr}[Y^{\nu\dagger} Y^\nu] - 3g_2^2 - \frac{3}{5} g_1^2 \right) \mu \,, \tag{E.5}$$

where $g_i, M_i,\ i = 1, 2, 3$ are the gaugino couplings and masses respectively.

Appendix F

Renormalisation group running

In this appendix, we provide analytical expression for the RG evolved Yukawa couplings, soft terms and mass insertion parameters. We estimate the effects of RG running using the leading logarithmic approximation. In order to formulate the two-stage running (i) from $M_{\rm GUT}$ to M_R, where the right-handed neutrinos are integrated out, and (ii) from M_R to $M_{\rm SUSY} \sim M_{\rm W} \equiv M_{\rm low}$, we introduce the parameters

$$\eta = \frac{1}{16\pi^2} \ln\left(\frac{M_{\rm GUT}}{M_{\rm low}}\right), \quad \eta_N = \frac{1}{16\pi^2} \ln\left(\frac{M_{\rm GUT}}{M_{\rm R}}\right). \tag{F.1}$$

For $M_{\rm GUT} \approx 2 \times 10^{16}$ GeV, $M_{\rm R} \approx 10^{14}$ GeV and $M_{\rm low} \approx 10^3$ GeV, $\eta \approx 0.19$ is of the order of our expansion parameter $\lambda \approx 0.22$ and $\eta_N \approx 0.03$.

F.1 Low energy Yukawas

The SCKM transformations, discussed in Section 3.6, diagonalise the Yukawa matrices at high scales. RG running to low energies re-introduces off-diagonal elements in the low energy Yukawa matrices. These off-diagonal entries in $\tilde{Y}^u_{\rm low}$ and $\tilde{Y}^d_{\rm low}$ are proportional to the quark masses and the $V_{\rm CKM}$ elements. As the CKM matrix features only a mild running, the RG corrections can be treated as a perturbation. In $\tilde{Y}^e_{\rm low}$, the off-diagonal terms are proportional to the charged lepton masses and the elements of Y^ν. The corresponding RG equations are provided explicitly in Eq. (E.2) for convenience. To LO in λ, we find,

$$\tilde{Y}^u_{\rm low} \approx \begin{pmatrix} 1+R^y_u & 0 & 0 \\ 0 & 1+R^y_u & 0 \\ 0 & 0 & 1+R^y_t \end{pmatrix} \tilde{Y}^u_{\rm GUT} - \eta\, y_b\, y_t \begin{pmatrix} 0 & 0 & \tilde{x}_2\,\lambda^7 \\ 0 & 0 & y_s\,\lambda^6 \\ 0 & 0 & 0 \end{pmatrix}, , \tag{F.1.1}$$

$$\tilde{Y}^d_{\rm low} \approx \begin{pmatrix} 1+R^y_d & 0 & 0 \\ 0 & 1+R^y_d & 0 \\ 0 & 0 & 1+R^y_b \end{pmatrix} \tilde{Y}^d_{\rm GUT} + \eta\, y_t^2 \begin{pmatrix} 0 & 0 & e^{i\theta^d_2}\frac{\tilde{x}_2^2}{y_s}\lambda^6 \\ 0 & 0 & y_s\,\lambda^4 \\ 0 & \frac{y_s^2}{y_b}\lambda^6 & 0 \end{pmatrix}, \tag{F.1.2}$$

$$\tilde{Y}^e_{\rm low} \approx \begin{pmatrix} 1+R^y_e & 0 & 0 \\ 0 & 1+R^y_e & 0 \\ 0 & 0 & 1+R^y_e \end{pmatrix} \tilde{Y}^e_{\rm GUT} + \eta_N\, y_D\, R_\nu \begin{pmatrix} 0 & -3\,y_s\,\lambda^8 & y_b\,\lambda^6 \\ 0 & 0 & y_b\,\lambda^6 \\ 0 & 0 & 0 \end{pmatrix}, \tag{F.1.3}$$

with

$$R^y_u = \eta\left(\frac{46}{5}g_U^2 - 3y_t^2\right) - 3\eta_N\, y_D^2, \qquad R^y_t = R^y_u - 3\,\eta\, y_t^2, \tag{F.1.4}$$

$$R^y_d = \eta\frac{44}{5}g_U^2, \qquad R^y_b = R^y_d - \eta\, y_t^2, \tag{F.1.5}$$

$$R^y_e = \eta\frac{24}{5}g_U^2 - \eta_N\, y_D^2, \qquad R_\nu = z_1^D - y_D(K_3 + K_3^N). \tag{F.1.6}$$

where $g_U \approx \sqrt{0.52}$ is the universal gauge coupling constant at the GUT scale.

F.2 Low energy soft terms

Similar to the Yukawa matrices, the parameters of the soft terms have to be run down to low energies. Moreover, it is mandatory to perform further transformations to the "new" SCKM basis which render $\tilde{Y}^f_{\rm low}$ diagonal again. The running of the trilinear terms is similar to the one of the corresponding Yukawas. To LO in λ, η and η_N, we derive the following expressions in the "new" SCKM basis.

$$\begin{aligned} \frac{\tilde{A}^u_{\rm low}}{A_0} \approx{}& \begin{pmatrix} 1+R^y_u & 0 & 0 \\ 0 & 1+R^y_u & 0 \\ 0 & 0 & 1+R^y_t \end{pmatrix} \frac{\tilde{A}^u_{\rm GUT}}{A_0} - 2\begin{pmatrix} R^a_u & 0 & 0 \\ 0 & R^a_u & 0 \\ 0 & 0 & R^a_t \end{pmatrix} \tilde{Y}^u_{\rm GUT} \\ & - 2\eta\, y_t \begin{pmatrix} 0 & 0 & y_b\,\tilde{x}^a_2\, e^{i(\theta^{\tilde{x}^a}_2 - \theta^{\tilde{x}}_2)}\,\lambda^7 \\ 0 & 0 & y_b\, a_s\, e^{i(\theta^a_s - \theta^y_s)}\,\lambda^6 \\ 0 & y_t e^{i(3\theta^d_2 + \theta^d_3)}\tilde{a}^u_{23}\lambda^7 & 0 \end{pmatrix}, \end{aligned} \tag{F.2.1}$$

$$\begin{aligned} \frac{\tilde{A}^d_{\rm low}}{A_0} \approx{}& \begin{pmatrix} 1+R^y_d & 0 & 0 \\ 0 & 1+R^y_d & 0 \\ 0 & 0 & 1+R^y_b \end{pmatrix} \frac{\tilde{A}^d_{\rm GUT}}{A_0} - 2\begin{pmatrix} R^a_d & 0 & 0 \\ 0 & R^a_d & 0 \\ 0 & 0 & R^a_b \end{pmatrix} \tilde{Y}^d_{\rm GUT} \\ & + 2\eta\, y_s\, y_t \begin{pmatrix} 0 & 0 & 0 \\ 0 & 0 & a_t\,\lambda^4 \\ 0 & \frac{1}{y_b}\left(y_s\, a_t - y_t\,\tilde{a}^d_{23}\right)\lambda^6 & 0 \end{pmatrix}, \end{aligned} \tag{F.2.2}$$

$$\begin{aligned} \frac{\tilde{A}^e_{\rm low}}{A_0} \approx{}& \begin{pmatrix} 1+R^y_e & 0 & 0 \\ 0 & 1+R^y_e & 0 \\ 0 & 0 & 1+R^y_e \end{pmatrix} \frac{\tilde{A}^e_{\rm GUT}}{A_0} - 2R^a_e\,\tilde{Y}^e_{\rm GUT} \\ & + 2\eta_N\, y_D\, R_\nu\, y_b \begin{pmatrix} 0 & 0 & \frac{\alpha_D}{y_D}\,\lambda^6 \\ 0 & 0 & \frac{R^a_\nu}{R_\nu}\,\lambda^6 \\ 0 & 0 & 0 \end{pmatrix}, \end{aligned} \tag{F.2.3}$$

with

$$R_u^a = \eta\left(\frac{46}{5}g_U^2\frac{M_{1/2}}{A_0} + 3a_t\,y_t\right) + 3\eta_N\,y_D\,\alpha_D, \qquad R_t^a = R_u^a + 3\,\eta\,a_t\,y_t, \tag{F.2.4}$$

$$R_d^a = \eta\,\frac{44}{5}g_U^2\frac{M_{1/2}}{A_0}, \qquad R_b^a = R_d^a + \eta\,a_t\,y_t, \tag{F.2.5}$$

$$R_e^a = \eta\frac{24}{5}g_U^2\frac{M_{1/2}}{A_0} + \eta_N\,y_D\alpha_D, \tag{F.2.6}$$

$$R_\nu^a = z_1^{D_a}e^{i\theta_1^{z_{D_a}}} - \alpha_D(K_3 + K_3^N). \tag{F.2.7}$$

The first terms in Eqs. (F.2.1-F.2.3) are analogous to the first terms in Eqs. (F.1.1 - F.1.3); they are usually ignored. The second terms contain the universal gaugino mass $M_{1/2}$ contributions, which generate non-zero diagonal trilinear couplings through the running, even for $A_0 \to 0$. The sources of the off-diagonal entries in the Yukawa couplings are also present for the trilinear soft terms. We see that the (13) element in $\tilde{A}^u_{\rm low}$, which was zero in $\tilde{A}^u_{\rm GUT}$, is now filled in, and there is an $\mathcal{O}(\lambda^6)$ contribution (but additionally suppressed by a factor of η) to the (23) element, which was of order λ^7 in $\tilde{A}^u_{\rm GUT}$. The (32) element in $\tilde{A}^u_{\rm low}$, with $\tilde{a}^u_{23}$ given in Eq. (D.5), is of the same order in λ as the one that is already present in $\tilde{A}^u_{\rm GUT}$. All the off-diagonal elements generated by the running in $\tilde{A}^d_{\rm low}$ and in $\tilde{A}^e_{\rm low}$ are of the same order in λ as the ones that were already present at the high scale.

Analogously to the trilinear A-terms, we find for the soft scalar mass,

$$\frac{(\tilde{m}_u^2)_{LL_{\rm low}}}{m_0^2} \approx \frac{(\tilde{m}_u^2)_{LL_{\rm GUT}}}{m_0^2} + (6.5\,x + T_L^u)\,\mathbb{1} - \eta\begin{pmatrix} 0 & 0 & y_t^2\frac{(\tilde{m}_u^2)_{LL_{\rm GUT_{13}}}}{m_0^2} \\ . & 0 & y_t^2\frac{(\tilde{m}_u^2)_{LL_{\rm GUT_{23}}}}{m_0^2} \\ . & . & 2R_q \end{pmatrix}, \tag{F.2.8}$$

$$\frac{(\tilde{m}_u^2)_{RR_{\rm low}}}{m_0^2} \approx \frac{(\tilde{m}_u^2)_{RR_{\rm GUT}}}{m_0^2} + (6.15\,x + T_R^u)\,\mathbb{1} - 2\eta\begin{pmatrix} 0 & 0 & y_t^2\frac{(\tilde{m}_u^2)_{RR_{\rm GUT_{13}}}}{m_0^2} \\ . & 0 & y_t^2\frac{(\tilde{m}_u^2)_{RR_{\rm GUT_{23}}}}{m_0^2} \\ . & . & 2R_q \end{pmatrix}, \quad , \tag{F.2.9}$$

$$\frac{(\tilde{m}_d^2)_{LL_{\rm low}}}{m_0^2} \approx \frac{(\tilde{m}_u^2)_{LL_{\rm GUT}}}{m_0^2} + (6.5\,x + T_L^d)\,\mathbb{1} + \eta\begin{pmatrix} 0 & 0 & \left(\frac{2R_q}{b_{01}-b_{02}} + y_t^2\right)\frac{(\tilde{m}_d^2)_{LL_{\rm GUT_{13}}}}{m_0^2} \\ . & 0 & \left(\frac{2R_q}{b_{01}-b_{02}} + y_t^2\right)\frac{(\tilde{m}_d^2)_{LL_{\rm GUT_{23}}}}{m_0^2} \\ . & . & -2R_q \end{pmatrix}, \tag{F.2.10}$$

$$\frac{(\tilde{m}_d^2)_{RR_{\rm low}}}{m_0^2} \approx \frac{(\tilde{m}_d^2)_{RR_{\rm GUT}}}{m_0^2} + (6.1\,x + T_R^d)\,\mathbb{1}\,, \tag{F.2.11}$$

$$\frac{(\tilde{m}_e^2)_{LL_{\rm low}}}{m_0^2} \approx \frac{(\tilde{m}_e^2)_{LL_{\rm GUT}}}{m_0^2} + (0.5\,x + T_L^e - 2\eta_N\,R_l)\,\mathbb{1} - 2\eta_N\begin{pmatrix} 0 & \tilde{E}_{12} & -\tilde{E}_{12}^* \\ . & 0 & -\tilde{E}_{12} \\ . & . & 0 \end{pmatrix}\lambda^4, \tag{F.2.12}$$

$$\frac{(\tilde{m}_e^2)_{RR_{\rm low}}}{m_0^2} \approx \frac{(\tilde{m}_e^2)_{RR_{\rm GUT}}}{m_0^2} + (0.15\,x + T_R^e)\,\mathbb{1}, \tag{F.2.13}$$

where we have introduced the ratio $x = M_{1/2}^2/m_0^2$ and

$$R_q = (2b_{02} + c_{H_u})\, y_t^2 + \alpha_0^2\, a_t^2\,, \tag{F.2.14}$$

$$\tilde{E}_{12} = y_D^2 \left(\tilde{R}_{12} + B_3^N - K_3^N B_0^N\right) + R_l' - (K_3 + K_3^N) R_l\,, \tag{F.2.15}$$

$$R_l = (1 + B_0^N + c_{H_u}) y_D^2 + \alpha_0^2 \alpha_D^2\,, \tag{F.2.16}$$

$$R_l' = (1 + B_0^N + c_{H_u}) y_D\, z_1^D + \alpha_0^2 \alpha_D\, z_1^{D_a} e^{i\theta_1^{z_{Da}}}\,, \tag{F.2.17}$$

with $\alpha_0 = A_0/m_0$ and $c_{H_u} = m_{H_u\mathrm{GUT}}^2/m_0^2$. Furthermore, the small quantities $T_{L,R}^f$ are defined as

$$T_L^u = \frac{1}{m_0^2}\left(\frac{1}{20}T + \Delta_L^u\right), \qquad T_R^u = \frac{1}{m_0^2}\left(-\frac{1}{5}T + \Delta_R^u\right), \tag{F.2.18}$$

$$T_L^d = \frac{1}{m_0^2}\left(\frac{1}{20}T + \Delta_L^d\right), \qquad T_R^d = \frac{1}{m_0^2}\left(\frac{1}{5}T + \Delta_R^d\right), \tag{F.2.19}$$

$$T_L^e = \frac{1}{m_0^2}\left(-\frac{3}{20}T + \Delta_L^e\right), \qquad T_R^e = \frac{1}{m_0^2}\left(\frac{3}{10}T + \Delta_R^e\right), \tag{F.2.20}$$

with $T = \frac{1}{4\pi^2}\int_{\ln(M_{\mathrm{GUT}})}^{\ln(M_{\mathrm{low}})} g_U^2\,(m_{H_u}^2 - m_{H_d}^2)$, as well as

$$\Delta_L^u = \left(\frac{1}{2} - \frac{2}{3}\sin^2(\theta_W)\right)\cos(2\beta) M_Z^2\,, \qquad \Delta_R^u = \frac{2}{3}\sin^2(\theta_W)\cos(2\beta) M_Z^2\,, \tag{F.2.21}$$

$$\Delta_L^d = \left(-\frac{1}{2} + \frac{1}{3}\sin^2(\theta_W)\right)\cos(2\beta) M_Z^2\,, \qquad \Delta_R^d = -\frac{1}{3}\sin^2(\theta_W)\cos(2\beta) M_Z^2\,, \tag{F.2.22}$$

$$\Delta_L^e = \left(-\frac{1}{2} + \frac{1}{2}\sin^2(\theta_W)\right)\cos(2\beta) M_Z^2\,, \qquad \Delta_R^e = -\sin^2(\theta_W)\cos(2\beta) M_Z^2\,. \tag{F.2.23}$$

The contributions $T_{L,R}^f$ to the running soft masses are usually ignored, and it is common practice to set them to zero in a numerical scan. In our study, we will therefore not consider them any further.

The off-diagonal entries in the soft scalar masses which are induced by the running are of the same order in λ as the high scale ones, with an additional suppression by η. Only for the LL masses of the down-squarks and charged sleptons, the contributions due to R_q and $R_l^{(\prime)}$ can be relatively large as those factors take values up to ~ 35 in a numerical scan. Generally, however, the main effect of the RG evolution on the scalar masses is the change of the diagonal elements. The masses of the first two generations of $(\tilde{m}_u^2)_{LL_{\mathrm{low}}}$, $(\tilde{m}_u^2)_{RR_{\mathrm{low}}}$, $(\tilde{m}_d^2)_{LL_{\mathrm{low}}}$ and all three generations of $(\tilde{m}_d^2)_{RR_{\mathrm{low}}}$, $(\tilde{m}_e^2)_{RR_{\mathrm{low}}}$ are increased at low energy scales due to the second terms in Eqs. (F.2.8-F.2.13). The (33) elements of $(\tilde{m}_u^2)_{LL_{\mathrm{low}}}$, $(\tilde{m}_u^2)_{RR_{Low}}$ and $(\tilde{m}_d^2)_{LL_{\mathrm{low}}}$ can still remain relatively light, as they also feel the effect of R_q, defined in Eq. (F.2.14), entering with a negative sign. Similarly, the enhancement of all three diagonal entries of $(\tilde{m}_e^2)_{LL_{\mathrm{low}}}$ is reduced due to the term $-2\eta_N R_l$ which encodes seesaw effects.

F.3 Low energy mass insertion parameters

With these preparations, we can now formulate the mass insertion parameters at the low energy scale.

Up-type quark sector:

$$(\delta^u_{LL})_{12} = \frac{1}{(p^u_{L^{1G}})^2} e^{-i\theta^d_2}\, \tilde{b}_{12}\, \lambda^4, \tag{F.3.1}$$

$$(\delta^u_{LL})_{13} = \frac{1}{p^u_{L^{1G}} p^u_{L^{3G}}} e^{-i(4\theta^d_2+\theta^d_3)}(1-\eta\, y_t^2)\, \tilde{b}_{13}\, \lambda^6, \tag{F.3.2}$$

$$(\delta^u_{LL})_{23} = \frac{1}{p^u_{L^{1G}} p^u_{L^{3G}}} e^{-i(7\theta^d_2+2\theta^d_3)}(1-\eta\, y_t^2)\, \tilde{b}_{23}\, \lambda^5, \tag{F.3.3}$$

$$(\delta^u_{RR})_{12} = \frac{1}{(p^u_{R^{1G}})^2} e^{-i\theta^d_2}\, \tilde{b}_{12}\, \lambda^4, \tag{F.3.4}$$

$$(\delta^u_{RR})_{13} = \frac{1}{p^u_{R^{1G}} p^u_{R^{3G}}} (1-2\eta\, y_t^2)\, \tilde{b}_{13}\, \lambda^6, \tag{F.3.5}$$

$$(\delta^u_{RR})_{23} = \frac{1}{p^u_{R^{1G}} p^u_{R^{3G}}} e^{i(5\theta^d_2+\theta^d_3)}(1-2\eta\, y_t^2)\, \tilde{b}_{23}\, \lambda^5, \tag{F.3.6}$$

$$(\delta^u_{LR})_{11} = \frac{\alpha_0\, v_u}{m_0\, p^u_{L^{1G}}\, p^u_{R^{1G}}} y_u(1+R^y_u) \left(\frac{\tilde{a}^u_{11}}{y_u} - \frac{\mu(1+R_\mu)}{A_0\, t_\beta} - 2\frac{R^a_u}{1+R^y_u} \right) \lambda^8, \tag{F.3.7}$$

$$(\delta^u_{LR})_{22} = \frac{\alpha_0\, v_u}{m_0\, p^u_{L^{1G}}\, p^u_{R^{1G}}} y_c(1+R^y_u) \left(\frac{\tilde{a}^u_{22}}{y_c} - \frac{\mu(1+R_\mu)}{A_0\, t_\beta} - 2\frac{R^a_u}{1+R^y_u} \right) \lambda^4, \tag{F.3.8}$$

$$(\delta^u_{LR})_{33} = \frac{\alpha_0\, v_u}{m_0\, p^u_{L^{3G}}\, p^u_{R^{3G}}} y_t(1+R^y_t) \left(\frac{\tilde{a}^u_{33}}{y_t} - \frac{\mu(1+R_\mu)}{A_0\, t_\beta} - 2\frac{R^a_t}{1+R^y_t} \right), \tag{F.3.9}$$

$$(\delta^u_{LR})_{12} = (\delta^u_{LR})_{21} = (\delta^u_{LR})_{31} = 0, \tag{F.3.10}$$

$$(\delta^u_{LR})_{13} = -\frac{\alpha_0\, v_u}{m_0\, p^u_{L^{1G}}\, p^u_{R^{3G}}} \tilde{x}_2\, y_b\, y_t \left(\frac{\tilde{x}^a_2}{\tilde{x}_2} e^{i(\theta^{\tilde{x}_a}_2 - \theta^{\tilde{x}}_2)} + \frac{R^a_t}{1+R^y_t} \right) 2\eta\lambda^7, \tag{F.3.11}$$

$$(\delta^u_{LR})_{23} = \frac{\alpha_0\, v_u}{m_0\, p^u_{L^{1G}}\, p^u_{R^{3G}}} \Bigg\{ - y_s\, y_b\, y_t \left(\frac{a_s}{y_s} e^{i(\theta^a_s - \theta^y_s)} + \frac{R^a_t}{1+R^y_t} \right) 2\eta\lambda^6 + \tag{F.3.12}$$

$$+ \lambda^7 \Bigg[e^{i\theta^d_2} \tilde{a}^u_{23}(1 + R^y_t - \eta\, y_t^2) + 2\eta\, y_b\, y_t \Bigg(e^{i\theta^d_2} \tilde{a}^d_{12} + \left(\frac{a_s}{y_s} e^{i(\theta^a_s - \theta^y_s)} + \frac{R^a_t}{1+R^y_t} \right) \times$$

$$\times\, (\tilde{x}_2 \cos(\theta^d_2) - z^d_4 \cos(4\theta^d_2 + \theta^d_3)) + z^d_4 e^{i(4\theta^d_2 + \theta^d_3)} \left(e^{i(\theta^a_s - \theta^y_s)} - \frac{z^{d_a}_4}{z^d_4} e^{i(\theta^{z_{d_a}}_4 - \theta^{z_d}_4)} \right) \Bigg) \Bigg] \Bigg\},$$

$$(\delta^u_{LR})_{32} = \frac{\alpha_0\, v_u}{m_0\, p^u_{L^{3G}}\, p^u_{R^{1G}}} (1 + R^y_t - 2\eta\, y_t^2) e^{i(3\theta^d_2 + \theta^d_3)} \tilde{a}^u_{23}\, \lambda^7, \tag{F.3.13}$$

where, in Eq. (F.3.12), z^d_4 and $z^{d_a}_4$ parameterise the $\mathcal{O}(\lambda^5)$ NLO corrections of the (22) and (23) elements of the down-type Yukawa and soft trilinear structures, respectively. Originating from the second term of Eq. (3.4.7), $z^d_4 e^{i\theta^{z_d}_4} = y^d_2\, \tilde{\delta}^d_{3,2_{(4)}} \phi^d_2$, so that $\theta^{z_d}_4 = 6\theta^d_2 + 4\theta^d_3$. We see that the term proportional to $\eta\,\lambda^6$, which was generated in $\tilde{A}^u_{\text{low}_{23}}$ via th RG evolution, is the source of the associated term in $(\delta^u_{LR})_{23}$, which was of order λ^7 at the GUT scale. In Eqs. (F.3.1-F.3.13) we have defined the factors

$$p^u_{L^{1G}} = \sqrt{b_{01} + 6.5\, x}, \qquad p^u_{L^{3G}} = \sqrt{b_{02} + 6.5\, x - 2\eta R_q + \frac{v_u^2}{m_0^2} y_t^2 (1 + R^y_t)^2}\,,$$

$$p^u_{R^{1G}} = \sqrt{b_{01} + 6.15\, x}, \qquad p^u_{R^{3G}} = \sqrt{b_{02} + 6.15\, x - 4\eta R_q + \frac{v_u^2}{m_0^2} y_t^2 (1 + R^y_t)^2}\,, \tag{F.3.14}$$

which are related to the full sfermion mass matrices by

$$m_{\tilde{u}_{LL}} \approx m_{\tilde{c}_{LL}} \approx m_0\, p^u_{L^{1G}}\,, \qquad m_{\tilde{t}_{LL}} \approx m_0\, p^u_{L^{3G}}\,,$$

$$m_{\tilde{u}_{RR}} \approx m_{\tilde{c}_{RR}} \approx m_0\, p^u_{R^{1G}}\,, \qquad m_{\tilde{t}_{RR}} \approx m_0\, p^u_{R^{3G}}\,, \tag{F.3.15}$$

whose GUT scale definitions are given in Eq. (3.7.1). The μ parameter at the low energy scale can be estimated by

$$\mu_{\text{low}} \approx \mu\,(1 + R_\mu)\,, \qquad R_\mu = 4\eta \left(0.9\, g_U^2 - \frac{3}{4} y_t^2 \right) - 3\eta_N\, y_D^2\,. \tag{F.3.16}$$

Down-type quark sector:

$$(\delta^d_{LL})_{12} = \frac{1}{(p^d_{L^{1G}})^2} \tilde{B}_{12}\, \lambda^3, \tag{F.3.17}$$

$$(\delta^d_{LL})_{13} = \frac{1}{p^d_{L^{1G}} p^d_{L^{13}}} e^{i\theta^d_2} \frac{\tilde{x}_2^2}{y_b\, y_s} (b_{01} - b_{02} + 2\eta\, R_q) \left(1 + \frac{\eta\, y_t^2}{1 + R^y_b} \right) \lambda^4, \tag{F.3.18}$$

$$(\delta^d_{LL})_{23} = \frac{1}{p^d_{L^{1G}} p^d_{L^{13}}} \frac{y_s}{y_b} (b_{01} - b_{02} + 2\eta\, R_q) \left(1 + \frac{\eta\, y_t^2}{1 + R^y_b} \right) \lambda^2, \tag{F.3.19}$$

$$(\delta^d_{RR})_{12} = -(\delta^d_{RR})_{13} = \frac{1}{(p^d_R)^2} e^{i\theta^d_2}\, \tilde{R}_{12}\, \lambda^4, \tag{F.3.20}$$

$$(\delta^d_{RR})_{23} = -\frac{1}{(p^d_R)^2} \tilde{R}_{12}\, \lambda^4, \tag{F.3.21}$$

$$(\delta^d_{LR})_{11} = \frac{\alpha_0\, v_d}{m_0\, p^d_{L^{1G}}\, p^d_R} \frac{\tilde{x}_2^2}{y_s}(1+R^y_d)\left(\frac{\tilde{a}^d_{11}}{\tilde{x}_2^2/y_s} - \frac{\mu\, t_\beta(1+R_\mu)}{A_0} - 2\frac{R^a_d}{1+R^y_d}\right)\lambda^6, \tag{F.3.22}$$

$$(\delta^d_{LR})_{22} = \frac{\alpha_0\, v_d}{m_0\, p^d_{L^{1G}}\, p^d_R} y_s(1+R^y_d)\left(\frac{\tilde{a}^d_{22}}{y_s} - \frac{\mu\, t_\beta(1+R_\mu)}{A_0} - 2\frac{R^a_d}{1+R^y_d}\right)\lambda^4, \tag{F.3.23}$$

$$(\delta^d_{LR})_{33} = \frac{\alpha_0\, v_d}{m_0\, p^d_{L^{3G}}\, p^d_R} y_b(1+R^y_b)\left(\frac{\tilde{a}^d_{33}}{y_b} - \frac{\mu\, t_\beta(1+R_\mu)}{A_0} - 2\frac{R^a_b}{1+R^y_b}\right)\lambda^2, \tag{F.3.24}$$

$$(\delta^d_{LR})_{12} = -(\delta^d_{LR})_{21} = (\delta^d_{LR})_{13} = \frac{\alpha_0\, v_d}{m_0\, p^d_{L^{1G}}\, p^d_R}(1+R^y_d)\tilde{a}^d_{12}\, \lambda^5, \tag{F.3.25}$$

$$(\delta^d_{LR})_{23} = \frac{\alpha_0\, v_d}{m_0\, p^d_{L^{1G}}\, p^d_R} y_s(1+R^y_d)\left(\frac{\tilde{a}^d_{23}}{y_s} + 2\frac{\eta\, y_t^2}{1+R^y_b}\left(\frac{a_t}{y_t} + \frac{R^a_d}{1+R^y_d}\right)\right)\lambda^4, \tag{F.3.26}$$

$$(\delta^d_{LR})_{31} = \frac{\alpha_0\, v_d}{m_0\, p^d_{L^{3G}}\, p^d_R} e^{-i\theta^d_2}(1+R^y_b)\tilde{a}^d_{31}\, \lambda^6, \tag{F.3.27}$$

$$\begin{aligned}(\delta^d_{LR})_{32} = \frac{\alpha_0\, v_d}{m_0\, p^d_{L^{3G}}\, p^d_R}(1+R^y_b) y_b \Bigg(&\frac{\tilde{a}^d_{32}}{y_b} + 2\eta y_t^2 \frac{y_s^2}{y_b^2}\left[\frac{2(1+R^y_b)+\eta y_t^2}{2(1+R^y_b)^2}\frac{\tilde{a}^d_{23}}{y_s}\right.\\ &\left. + \left(\frac{a_t}{y_t} + \frac{R^a_d}{1+R^y_d}\right)\frac{(1+R^y_d)^2}{(1+R^y_b)^3}\right]\Bigg)\lambda^6,\end{aligned} \tag{F.3.28}$$

where

$$p^d_{L^{1G}} = \sqrt{b_{01} + 6.5\, x}, \qquad p^d_{L^{3G}} = \sqrt{b_{02} + 6.5\, x - 4\eta R_q}, \qquad p^d_R = \sqrt{1 + 6.1x}, \tag{F.3.29}$$

such that

$$\begin{aligned} m_{\tilde{d}_{LL}} &\approx m_{\tilde{s}_{LL}} \approx m_0\, p^d_{L^{1G}}\,, \qquad m_{\tilde{b}_{LL}} \approx m_0\, p^d_{L^{3G}}\,, \\ m_{\tilde{d}_{RR}} &\approx m_{\tilde{s}_{RR}} \approx m_{\tilde{b}_{RR}} \approx m_0\, p^d_R\,. \end{aligned} \tag{F.3.30}$$

Charged lepton sector:

$$(\delta^e_{LL})_{12} = -(\delta^e_{LL})_{23} = \frac{1}{(p^e_L)^2}\left(\tilde{R}_{12} - 2\eta_N \tilde{E}_{12}\right)\lambda^4, \tag{F.3.31}$$

$$(\delta^e_{LL})_{13} = -\frac{1}{(p^e_L)^2}\left(\tilde{R}_{12} - 2\eta_N \tilde{E}^*_{12}\right)\lambda^4, \tag{F.3.32}$$

$$(\delta^e_{RR})_{12} = -\frac{1}{(p^e_{R^{1G}})^2} e^{i\theta^d_2} \frac{\tilde{B}_{12}}{3} \lambda^3, \tag{F.3.33}$$

$$(\delta^e_{RR})_{13} = \frac{1}{p^e_{R^{1G}} p^e_{R^{3G}}} \frac{\tilde{B}_{13}}{3} \lambda^4, \tag{F.3.34}$$

$$(\delta^e_{RR})_{23} = \frac{1}{p^e_{R^{1G}} p^e_{R^{3G}}} 3\tilde{B}_{23} \lambda^2, \tag{F.3.35}$$

$$(\delta^e_{LR})_{11} = \frac{1}{p^e_L p^e_{R^{1G}}} \frac{v_d \alpha_0}{m_0} \frac{\tilde{x}_2^2}{3 y_s} (1 + R^y_e) \left(\frac{y_s}{\tilde{x}_2^2} \tilde{a}^d_{11} - \frac{\mu t_\beta}{A_0} (1 + R_\mu) - 2 \frac{R^a_e}{1 + R^y_e} \right) \lambda^6, \tag{F.3.36}$$

$$(\delta^e_{LR})_{22} = \frac{1}{p^e_L p^e_{R^{1G}}} \frac{v_d \alpha_0}{m_0} 3 y_s (1 + R^y_e) \left(\frac{\tilde{a}^d_{22}}{y_s} - \frac{\mu t_\beta}{A_0} (1 + R_\mu) - 2 \frac{R^a_e}{1 + R^y_e} \right) \lambda^4, \tag{F.3.37}$$

$$(\delta^e_{LR})_{33} = \frac{1}{p^e_L p^e_{R^{3G}}} \frac{v_d \alpha_0}{m_0} y_b (1 + R^y_e) \left(\frac{\tilde{a}^d_{33}}{y_b} - \frac{\mu t_\beta}{A_0} (1 + R_\mu) - 2 \frac{R^a_e}{1 + R^y_e} \right) \lambda^2, \tag{F.3.38}$$

$$(\delta^e_{LR})_{12} = \frac{1}{p^e_L p^e_{R^{1G}}} \frac{v_d \alpha_0}{m_0} (1 + R^y_e) e^{i\theta^d_2} \tilde{a}^d_{12} \lambda^5, \tag{F.3.39}$$

$$(\delta^e_{LR})_{13} = \frac{1}{p^e_L p^e_{R^{3G}}} \frac{v_d \alpha_0}{m_0} \left((1 + R^y_e) \tilde{a}^d_{31} + 2\eta_N y_D R_\nu y_b \left(\frac{\alpha_D}{y_D} + \frac{R^a_e}{1 + R^y_e} \right) \right) \lambda^6, \tag{F.3.40}$$

$$(\delta^e_{LR})_{21} = (\delta^e_{LR})_{31} = -\frac{1}{p^e_L p^e_{R^{1G}}} \frac{v_d \alpha_0}{m_0} (1 + R^y_e) e^{-i\theta^d_2} \tilde{a}^d_{12} \lambda^5, \tag{F.3.41}$$

$$(\delta^e_{LR})_{23} = \frac{1}{p^e_L p^e_{R^{3G}}} \frac{v_d \alpha_0}{m_0} \left((1 + R^y_e) \tilde{a}^e_{23} + 2\eta_N y_D R_\nu y_b \left(\frac{R^a_\nu}{R_\nu} + \frac{R^a_e}{1 + R^y_e} \right) \right) \lambda^6, \tag{F.3.42}$$

$$(\delta^e_{LR})_{32} = \frac{1}{p^e_L p^e_{R^{1G}}} \frac{v_d \alpha_0}{m_0} (1 + R^y_e) 3 \tilde{a}^d_{23} \lambda^4, \tag{F.3.43}$$

where

$$p^e_L = \sqrt{1 + 0.5\, x - 2\eta_N R_l}, \quad p^e_{R^{1G}} = \sqrt{b_{01} + 0.15\, x}, \quad p^e_{R^{3G}} = \sqrt{b_{02} + 0.15\, x}, \tag{F.3.44}$$

such that

$$\begin{aligned} m_{\tilde{e}_{LL}} &\approx m_{\tilde{\mu}_{LL}} \approx m_{\tilde{\tau}_{LL}} \approx m_0\, p^e_L\,, \\ m_{\tilde{e}_{RR}} &\approx m_{\tilde{\mu}_{RR}} \approx m_0\, p^e_{R^{1G}}\,, \qquad m_{\tilde{\tau}_{RR}} \approx m_0\, p^e_{R^{3G}}\,. \end{aligned} \tag{F.3.45}$$

Appendix G

Loop functions

The dimensionless functions C_B, C'_L, C'_R, C'_2, $C'_{B,R}$, $C'_{B,L}$ and C''_B which appear in the expressions for the EDM of the electron in Section 4.3.1 and the branching ratio of $\mu \to e\gamma$ in Section 4.3.2 are defined as [97]

$$C_i = \frac{m_0^4}{\mu^2} I_i \ , \tag{G.1}$$

where

$$I_B(M_1^2,\, m_L^2,\, m_R^2) = \frac{1}{m_R^2 - m_L^2} \left[y_L\, g_1\left(x_L\right) - y_R\, g_1\left(x_R\right) \right], \tag{G.2}$$

$$I'_L(m_L^2,\, M_1^2,\, \mu^2) = \frac{1}{m_L^2} \frac{y_L}{y_L - x_L} \left[h_1\left(x_L\right) - \, h_1\left(y_L\right) \right], \tag{G.3}$$

$$I'_R(m_R^2,\, M_1^2,\, \mu^2) = \frac{1}{m_R^2} \frac{y_R}{y_R - x_R} \left[h_1\left(x_R\right) - \, h_1\left(y_R\right) \right], \tag{G.4}$$

$$I'_2(m_L^2,\, M_2^2,\, \mu^2) = \frac{M_2 \cot^2\theta_W}{M_1 m_L^2} \frac{y_L}{y_L - x'_L} \left[h_2\left(x'_L\right) - \, h_2\left(y_L\right) \right], \tag{G.5}$$

$$I'_{B,R}(M_1^2,\, m_L^2,\, m_R^2) = -\frac{1}{m_R^2 - m_L^2} \left(y_R\, h_1\left(x_R\right) - m_R^2 I_B \right), \tag{G.6}$$

$$I'_{B,L}(M_1^2,\, m_L^2,\, m_R^2) = \frac{1}{m_R^2 - m_L^2} \left(y_L\, h_1\left(x_L\right) - m_L^2 I_B \right), \tag{G.7}$$

$$I''_B(M_1^2,\, m_L^2,\, m_R^2) = \frac{m_L^2\, m_R^2}{m_R^2 - m_L^2} \frac{1}{\mu^2} \left(y_R I'_{B,R} - y_L I'_{B,L} \right), \tag{G.8}$$

with

$$x_L = \frac{M_1^2}{m_L^2}, \qquad x_R = \frac{M_1^2}{m_R^2}, \qquad x'_L = \frac{M_2^2}{m_L^2}, \qquad y_L = \frac{\mu^2}{m_L^2}, \qquad y_R = \frac{\mu^2}{m_R^2}, \tag{G.9}$$

and

$$
\begin{aligned}
g_1(y) &= \frac{1-y^2+2y\ln(y)}{(1-y)^3}, \\
h_1(y) &= \frac{1+4y-5y^2+(2y^2+4y)\ln(y)}{(1-y)^4}, \\
h_2(y) &= \frac{7y^2+4y-11-2(y^2+6y+2)\ln(y)}{2(y-1)^4}.
\end{aligned} \tag{G.10}
$$

Note that we assume real and positive values for M_i and μ^2.

The loop functions appearing in the meson mixing amplitudes of Section 4.3.3 as well as the branching ratios of $B_{s,d} \to \mu^+\mu^-$ in Section 4.3.5 read [76]

$$f_6(y) = \frac{6(1+3y)\ln(y)+y^3-9y^2-9y+17}{6(y-1)^5}, \tag{G.11}$$

$$\tilde{f}_6(y) = \frac{6y(1+y)\ln(y)-y^3-9y^2+9y+1}{3(y-1)^5}, \tag{G.12}$$

$$f_1(y) = \frac{1}{1-y} + \frac{y}{(1-y)^2}\ln(y), \tag{G.13}$$

$$f_3(y) = -\frac{1+y}{2(1-y)^2} - \frac{y}{(1-y)^3}\ln(y), \tag{G.14}$$

$$f_4(x,y) = -\frac{x\ln(x)}{(1-x)^2(y-x)} - \frac{y\ln(y)}{(1-y)^2(x-y)} + \frac{1}{(1-x)(1-y)}, \tag{G.15}$$

$$f_5(y) = \frac{2+5y-y^2}{6(1-y)^3} + \frac{y}{(1-y)^4}\ln(y). \tag{G.16}$$

The relevant functions for the branching ratio of $b \to s\gamma$ in Section 4.3.4 are given by [13]

$$M_1(y) = \frac{1+4y-5y^2+4y\ln(y)+2y^2\ln(y)}{2(1-y)^4}, \tag{G.17}$$

$$M_3(y) = \frac{-1+9y+9y^2-17y^3+18y^2\ln(y)+6y^3\ln(y)}{12(y-1)^5}. \tag{G.18}$$

Finally, the loop functions entering the hadronic EDM expressions in Section 4.3.6 are [121]

$$N_1(y) = \frac{3+44y-36y^2-12y^3+y^4+12y(2+3y)\ln(y)}{6(y-1)^6}, \tag{G.19}$$

$$N_2(y) = -\frac{10+9y-18y^2-y^3+3(1+6y+3y^2)\ln(y)}{3(y-1)^6}. \tag{G.20}$$

Appendix H

LC-OPE results of the correlation function $\Pi^{V,P}$

Below are presented the results of the LC-OPE for the correlation functions for the vector and pseudoscalar case,s using the decompositions in Eq. (5.3.2). The same decomposition as in Eq. (5.4.2) is used for the various contributions on the DA (I.2.11) parts:

$$g_i^{(s)} = g_i^{(\perp)} + g_i^{(\parallel)} + .. \,, \qquad i = 0..3 \,. \quad g_T^{(s)} = g_T^{(P)}$$

The dots stand for higher twist contributions. In order for the results to be presented our in a compact way, the following abbreviations are introduced for the PV-functions:

$$\begin{aligned}
&B_a = B_0(u(p_B^2 - P^2), 0, m_b^2) \,, && B_b = B_0(p_B^2 - P^2, 0, m_b^2) \,, \\
&B_c = B_0(up_B^2 + \bar{u}q^2, 0, m_b^2) \,, && B_d = B_0(p_B^2, 0, m_b^2) \,, \\
&C_a = C_0(p_B^2, u(p_B^2 - P^2), \bar{u}P^2 + uq^2, 0, m_b^2, 0) \,, && C_b = C_0(p_B^2, p_B^2 - P^2, q^2, 0, m_b^2, 0) \,, \\
&C_c = C_0(up_B^2 + \bar{u}q^2, u(p_B^2 - P^2), q^2, m_b^2, 0, m_b^2) \,, && C_d = C_0(p_B^2, p_B^2 - P^2, q^2, m_b^2, 0, m_b^2)
\end{aligned} \tag{H.1}$$

Note only the PV-functions which depend on p_B^2 are listed, as the other ones do not enter the dispersion representation. Moreover, the functions on the right correspond to the functions on the left at $u = 1$.

$V_\perp$-transverse

It is found that for the transverse parts, the Lorentz-projections satisfy:

$$g_2^{(\perp)} = (1 - q^2/P^2) g_3^{(\perp)} \,, \quad g_2^{(\perp)} = (1 - q^2/P^2) g_1^{(\perp)} \,, \quad g_0^{(\perp)} = 0 \,. \tag{H.2}$$

The result $g_1^{(\perp)}(q^2)$ can be written as:

$$k_V^{-1} g_1^{(\perp)}(q^2) = \frac{\alpha_s}{4\pi} C_F (-\frac{1}{2}) f_V^\perp m_b^2 Q_b \int_0^1 du \, t_H^{(\perp)}(u) \, \phi_\perp(u) \tag{H.3}$$

where the $t_H^{(\perp)}(u)$ corresponds to the hard kernel and is given in terms of PV-functions:

$$t_H^{(\perp)}(u) = \sum_{i=a}^{d} (b_i^{\perp} B_i + c_i^{\perp} C_i), \tag{H.4}$$

where the sum extends alphabetically from a to d. The only non-zero coefficients are:

$$\begin{aligned} (b_a^{\perp}, b_c^{\perp}, b_d^{\perp}) &= \left(\frac{q_R}{uq^2 + \bar{u}P^2}, \frac{1}{\bar{u}q^2 + uP^2}, 2(b_a^{\perp} + b_c^{\perp})\right) , \\ (c_a^{\perp}, c_c^{\perp}) &= (-2q_R, -1) , \end{aligned} \tag{H.5}$$

with $q_R \equiv Q_q/Q_b$ being the charge ratio.

$V_{\parallel}$-longitudinal

The computation of $V_{\parallel}$ is in principle highly non-trivial due the extra coordinates x appearing in front of the integral in (I.2.11). The so-called ultra-relativistic limit can be employed,

$$\eta(p)_\alpha \to \frac{1}{m_V}\left(p_\alpha + \mathcal{O}\left(\frac{m_V^2}{E_V^2}\right)\zeta_\alpha\right) , \tag{H.6}$$

which is correct up to the relativistic correction, as indicated, and the vector ζ is a linear combination of p and η. In this limit, using the DA as given in appendix I.2, the $V_{\parallel}$ and P contributions are identical up to the replacements $f_V^{\parallel} \to -if_P$ and $\phi_{\parallel} \to \phi_P$. Noting that in the ultra-relativistic limit

$$P_1 \to 0 , \quad P_2 \to cP_3|_{\eta \to p/m_V} \tag{H.7}$$

with c a constant, it is clear that only g_3 receives a contribution. Taking further into account Eq.(I.1.2) one gets:

$$G_T^{(P)}(q^2) = \frac{p\cdot Q}{m_V}\frac{if_P}{f_V^{\parallel}}\frac{k_V}{k_P}G_3^{(\parallel)}(q^2)|_{\phi_{\parallel}\to\phi_P} = \frac{-(m_B^2 - q^2)}{2m_V(m_B - m_P)}\frac{f_P}{f_V^{\parallel}}G_3^{(\parallel)}(q^2)|_{\phi_{\parallel}\to\phi_P} . \tag{H.8}$$

Thus, the result for the longitudinal vector meson entirely follows from the pseudoscalar in the ultra-relativistic limit. Note that the sign of this relation changes when $(1+\gamma_5) \to (1-\gamma_5)$ in $\mathcal{O}_8$ (5.1.5).

P (pseudoscalar)

Analogously to (H.3), $g_T^{(P)}$ is parametrised as follows:

$$k_P^{-1} g_T^{(P)}(q^2) = \frac{\alpha_s}{4\pi} C_F(-\frac{1}{2}) f_P m_b^2 Q_b \int_0^1 du\, t_H^{(P)}(u)\, \phi_P(u) . \tag{H.9}$$

The entire expression of $t_H^{(P)}(u)$ is rather bulky, so only one coefficient for $t_H^{(P)}(u)$ is given,

$$c_b^P = \frac{4q_R P^2\left(m_b^4 + m_b^2(P^2 - 2p_B^2 + q^2) + p_B^2(p_B^2 - P^2)\right)}{m_b(m_B - m_P)\bar{u}\left(P^4 + 2P^2q^2 + q^2(q^2 - 4p_B^2)\right)} \,. \tag{H.10}$$

Q^2	$G_1^{(\perp)} \times 10^2$	$G_3^{(\parallel)} \times 10^2$	$G_1^{(\perp)} \times 10^2$	$G_3^{(\parallel)} \times 10^2$
	$B^- \to K^{*-}$	$B^- \to K^{*-}$	$\bar{B}^0 \to \bar{K}^{*0}$	$\bar{B}^0 \to \bar{K}^{*0}$
0.010	$0.2931 - 0.3960i$	$2.3443 + 0.8303i$	$0.2022 + 0.1980i$	$-1.1952 - 0.4151i$
0.261	$0.3204 - 0.3781i$	$1.0673 + 0.8213i$	$0.1661 + 0.1890i$	$-0.5574 - 0.4107i$
0.512	$0.3384 - 0.3604i$	$0.7999 + 0.8122i$	$0.1431 + 0.1802i$	$-0.4243 - 0.4061i$
0.764	$0.3526 - 0.3429i$	$0.6388 + 0.8029i$	$0.1251 + 0.1715i$	$-0.3443 - 0.4014i$
1.015	$0.3641 - 0.3257i$	$0.5217 + 0.7933i$	$0.1102 + 0.1629i$	$-0.2863 - 0.3966i$
1.266	$0.3736 - 0.3087i$	$0.4286 + 0.7834i$	$0.0975 + 0.1544i$	$-0.2403 - 0.3917i$
1.517	$0.3815 - 0.2920i$	$0.3508 + 0.7732i$	$0.0866 + 0.1460i$	$-0.2020 - 0.3866i$
1.768	$0.3878 - 0.2755i$	$0.2834 + 0.7628i$	$0.0771 + 0.1378i$	$-0.1688 - 0.3814i$
2.020	$0.3929 - 0.2593i$	$0.2235 + 0.7519i$	$0.0689 + 0.1297i$	$-0.1395 - 0.3760i$
2.271	$0.3969 - 0.2434i$	$0.1693 + 0.7407i$	$0.0617 + 0.1217i$	$-0.1129 - 0.3703i$
2.522	$0.3998 - 0.2277i$	$0.1196 + 0.7290i$	$0.0554 + 0.1139i$	$-0.0887 - 0.3645i$
2.773	$0.4018 - 0.2124i$	$0.0734 + 0.7168i$	$0.0499 + 0.1062i$	$-0.0662 - 0.3584i$
3.024	$0.4028 - 0.1974i$	$0.0300 + 0.7041i$	$0.0453 + 0.0987i$	$-0.0451 - 0.3521i$
3.275	$0.4030 - 0.1827i$	$-0.0110 + 0.6908i$	$0.0413 + 0.0913i$	$-0.0253 - 0.3454i$
3.527	$0.4024 - 0.1683i$	$-0.0500 + 0.6768i$	$0.0379 + 0.0842i$	$-0.0064 - 0.3384i$
4.786	$0.3883 - 0.1024i$	$-0.2248 + 0.5935i$	$0.0295 + 0.0512i$	$0.0775 - 0.2967i$
6.046	$0.3586 - 0.0489i$	$-0.3754 + 0.4758i$	$0.0323 + 0.0245i$	$0.1488 - 0.2379i$
7.305	$0.3177 - 0.0129i$	$-0.4908 + 0.2946i$	$0.0431 + 0.0065i$	$0.2019 - 0.1473i$
8.565	$0.2758 + 0.0000i$	$-0.4519 + 0.0224i$	$0.0562 - 0.0000i$	$0.1770 - 0.0112i$
9.824	$0.2492 + 0.0000i$	$-0.2972 + 0.0000i$	$0.0630 - 0.0000i$	$0.0933 - 0.0000i$
11.084	$0.2312 - 0.0000i$	$-0.2485 - 0.0000i$	$0.0669 + 0.0000i$	$0.0613 + 0.0000i$
12.343	$0.2176 - 0.0000i$	$-0.2243 - 0.0000i$	$0.0696 + 0.0000i$	$0.0400 + 0.0000i$
13.603	$0.2070 - 0.0000i$	$-0.2128 + 0.0000i$	$0.0718 + 0.0000i$	$0.0230 - 0.0000i$
14.862	$0.1986 + 0.0000i$	$-0.2101 + 0.0000i$	$0.0740 - 0.0000i$	$0.0076 - 0.0000i$
16.122	$0.1921 - 0.0000i$	$-0.2147 - 0.0000i$	$0.0763 + 0.0000i$	$-0.0080 + 0.0000i$
17.381	$0.1873 - 0.0000i$	$-0.2267 + 0.0000i$	$0.0790 + 0.0000i$	$-0.0252 - 0.0000i$
18.641	$0.1843 + 0.0000i$	$-0.2475 + 0.0000i$	$0.0824 - 0.0000i$	$-0.0459 - 0.0000i$
19.900	$0.1831 - 0.0000i$	$-0.2803 + 0.0000i$	$0.0869 + 0.0000i$	$-0.0725 - 0.0000i$
21.160	$0.1844 - 0.0000i$	$-0.3310 - 0.0000i$	$0.0932 + 0.0000i$	$-0.1097 + 0.0000i$
	$D^0 \to \rho^0$	$D^0 \to \rho^0$	$D^+ \to \rho^+$	$D^+ \to \rho^+$
0.010	$-7.0027 - 4.9787i$	$14.939 + 2.507i$	$-1.9295 + 2.4893i$	$19.589 - 1.254i$
0.048	$-6.5207 - 4.7048i$	$10.506 + 2.673i$	$-1.8309 + 2.3524i$	$0.5204 - 1.3366i$
0.087	$-6.2041 - 4.4945i$	$8.9314 + 2.7462i$	$-1.7662 + 2.2472i$	$-1.0918 - 1.3731i$
0.125	$-5.9599 - 4.3583i$	$7.9497 + 2.9176i$	$-1.7163 + 2.1792i$	$-1.4961 - 1.4588i$
0.163	$-5.7571 - 4.2099i$	$7.2213 + 3.1650i$	$-1.6766 + 2.1050i$	$-1.5870 - 1.5825i$
0.202	$-5.5875 - 4.1273i$	$6.6209 + 3.4331i$	$-1.6417 + 2.0637i$	$-1.5541 - 1.7166i$
0.240	$-5.4402 - 4.0195i$	$6.1014 + 3.5850i$	$-1.6115 + 2.0098i$	$-1.4644 - 1.7925i$
0.440	$-4.9159 - 3.4292i$	$3.7348 + 4.8267i$	$-1.4907 + 1.7146i$	$-0.5866 - 2.4133i$
0.640	$-4.6317 - 3.0393i$	$0.8816 + 6.7486i$	$-1.3979 + 1.5196i$	$0.8464 - 3.3743i$
0.840	$-4.4966 - 2.6815i$	$-3.643 + 11.193i$	$-1.3125 + 1.3407i$	$3.2215 - 5.5964i$
1.040	$-4.4921 - 2.1974i$	$-11.832 + 18.837i$	$-1.2174 + 1.0987i$	$7.4949 - 9.4187i$
1.240	$-4.6038 - 1.8406i$	$-27.338 + 33.651i$	$-1.1080 + 0.9203i$	$15.490 - 16.825i$
1.440	$-4.8063 - 1.2685i$	$-58.743 + 61.022i$	$-0.9925 + 0.6342i$	$31.511 - 30.511i$

TABLE H.1: q^2-dependance of the $G_1^{(\perp)}(q^2)$- and $G_3^{(\parallel)}(q^2)$-functions for the four characteristic cases, depending on whether the initial state is $B^-, \bar{B}^0, D^0$ or D^+-type.

Appendix I

Lorentz structures and distristribution amplitudes

The Lorentz structures of the vector meson are given by[1]:

$$\begin{aligned} P_1^\rho &= 2\epsilon^\rho{}_{\alpha\beta\gamma}\eta^{*\alpha}p^\beta q^\gamma \\ P_2^\rho &= i\{(m_B^2-m_V^2)\eta^{*\rho}-(\eta^*\cdot q)(p+p_B)^\rho\} \\ P_3^\rho &= i(\eta^*\cdot q)\{q^\rho-\frac{q^2}{m_B^2-m_V^2}(p+p_B)^\rho\}\ , \end{aligned} \tag{I.1}$$

and the one for the pseudoscalar meson is

$$P_T^\rho = \frac{1}{m_B+m_P}\{(m_B^2-m_P^2)q^\rho - q^2(p+p_B)^\rho\} \quad . \tag{I.2}$$

All projectors are transverse, i.e. $q\cdot P=0$ when on-shell momentum relations like $p_B^2=m_B^2$ etc are taken into account. The structure $P_3=P_3^\rho\epsilon(q)_\rho$ is absent for an on-shell photon since $\epsilon(q)\cdot P_3|_{q^2=0}=0$ and thus P_3 can be seen as a purely longitudinal part of the photon. Note: $P_3^\rho = i/(m_B-m_P)(\eta^*\cdot q)P_T^\rho|_{m_P\to m_V}$.

[1]The sign convention for the epsilon tensor is given by $\mathrm{tr}[\gamma_5\gamma_a\gamma_b\gamma_c\gamma_d]=4i\epsilon_{abcd}$ and are the ones used in the classic textbook of Bjorken & Drell.

I.1 Extension to include spurious momentum

The extension of the Lorentz structures to include the spurious momentum k in the vector case (I.1) is

$$\begin{aligned}
(p_1)_\rho &= 2\epsilon^\rho{}_{\alpha\beta\gamma}\eta^{*\alpha}p^\beta Q^\gamma \\
(p_2)_\rho &= i[((p_B+p)\cdot Q)\,\eta^*_\rho - (\eta^*\cdot Q)(p_B+p)_\rho] \\
(p_3)_\rho &= i[(\eta^*\cdot Q)Q_\rho - (\eta^*\cdot Q)(p_B+p)_\rho \frac{q^2}{Q\cdot(p_B+p)}] \\
(p_4)_\rho &= i[(\eta^*\cdot Q)k_\rho - (\eta^*\cdot Q)(p_B+p)_\rho \frac{k\cdot Q}{Q\cdot(p_B+p)}]
\end{aligned} \tag{I.1.1}$$

and in the pseudoscalar case (I.2) is:

$$\begin{aligned}
(p_T)_\rho &= (m_B - m_P)[(Q_\rho - \frac{q^2}{Q\cdot(p_B+p)}(p_B+p)_\rho] \\
(\bar{p}_{\bar{T}})_\rho &= (m_B - m_P)[(k_\rho - \frac{k\cdot Q}{Q\cdot(p_B+p)}(p_B+p)_\rho]
\end{aligned}$$

Essentially, we get one more structure due to a linearly independent vector k and the projectors are extended such that they remain transverse, i.e. $Q\cdot q = 0$. This is easy to verify using $q^2 = Q^2$. Since $p_3^\rho = (\eta\cdot Q)p_T^\rho$ we have got:

$$p_3^\rho \to \left(\frac{ip\cdot Q}{m_V(m_B - m_V)}\right) p_T^\rho = \left(\frac{i(P^2-q^2)}{2m_V(m_B-m_V)}\right) p_T^\rho\,, \tag{I.1.2}$$

in the ultra-relativistic limit $\eta \to p/m_V$. In the last equality we have used the approximation $p^2 = 0$.

I.2 Distribution amplitudes

The leading twist (twist 2) DAs for the pseudoscalar (e.g. [143]) and vector (e.g. [154]) mesons are defined as follows,

$$\begin{aligned}
\langle K(p)|[\bar{s}(x)]_\alpha..[q(z)]_\beta|0\rangle &= i\frac{f_K}{4}[\not{p}\gamma_5]_{\beta\alpha}\int_0^1 du\, e^{iux\cdot p + i\bar{u}z\cdot p}\,\phi_K(u) + ... \\
\langle K^*(p,\eta)|[\bar{s}(x)]_\alpha..[q(z)]_\beta|0\rangle &= \frac{f_{K^*}^\perp}{4}[\not{\eta}^*(p)\not{p}]_{\beta\alpha}\int_0^1 du e^{iux\cdot p + i\bar{u}z\cdot p}\phi_\perp(u) \\
&+ m_{K^*}\frac{f_{K^*}}{4}[\not{p}]_{\beta\alpha}\frac{\eta^*\cdot(x-z)}{p\cdot(x-z)}\int_0^1 du e^{iux\cdot p + i\bar{u}z\cdot p}\phi_\parallel(u) + ...\,,
\end{aligned} \tag{I.2.11}$$

which have been represented by the kaons for definiteness.

Appendix J

Analytic structure and dispersion representation

Let us parametrise a dispersion representation as follows:

$$f(p_B^2) = \int_0^\infty \frac{\rho_f}{s - p_B^2 - i0} + [f(p_B^2)]_{An} + \text{subtractions} \,. \tag{J.1}$$

The polynomial subtraction terms, as previously emphasised, are of no importance as they vanish under the Borel-transformation. The term $[f]_{An}$ corresponds to an anomalous threshold. Amongst the PV-functions (H.1) present in the results, given in appendix H, solely C_a[1] includes an anomalous threshold which extends into the lower complex half plane, c.f. Fig. J.1, at physical momenta $P^2, q^2 > 0$. This is discussed in section J.1 from various viewpoints. In addition, the density ρ_{C_a} necessitates many case distinctions, which is not uncommon for vertex function e.g. [166].

We have checked the dispersion relations by comparing them against LoopTools [169] which allow for numerical evaluation of the scalar PV-functions. Below, we shall quote the results, starting with the anomalous part of C_a:

$$[C_a(p_B^2)]_{An} = -2\pi i \int_{s_+}^{\text{Re}\, s_+} \frac{ds}{s - p_B^2} \frac{1}{\sqrt{\lambda}} \,. \tag{J.2}$$

s_+ is one of the two solutions of the leading Landau equations of the graph

$$s_\pm = \frac{(1+u)m_b^2 + uP^2 \pm \sqrt{(uP^2 - \bar{u}m_b^2)^2 - 4u^2 m_b^2 q^2 - i0}}{2u} \,. \tag{J.3}$$

[1] C_b corresponds to $C_a|_{u\to 1}$ and so we shall not discuss it separately as well as all other functions on the RHS of the list in Eq. (H.1)

where the $-i0$ implies that $\Im\, s_+ \leq 0$. The densities ρ_f of the representation (J.1) are:

$$\begin{aligned}
\rho_{B_a} &= \left(1 - \frac{m_b^2}{u(s-P^2)}\right)\Theta\left(s - \frac{m_b^2}{u} - P^2\right) \\
\rho_{B_c} &= \left(1 - \frac{m_b^2}{us + \bar{u}q^2}\right)\Theta\left(s - \frac{m_b^2 - \bar{u}q^2}{u}\right) \\
\rho_{C_a} &= \left(\frac{\mathrm{Im}[C_a]}{\pi} + \frac{1}{\sqrt{\lambda}}\left(\log_L\left(\frac{z_+ - z_L}{z_- - z_L}\right) - \log_-\left(\frac{z_+ - 1}{z_- - 1}\right)\right)\right)\Theta(s - m_b^2) \\
\rho_{C_c} &= \frac{\log\left(\frac{A-\sqrt{\lambda_1\lambda_3}}{A+\sqrt{\lambda_1\lambda_3}}\right)}{\sqrt{\lambda_3}}\left[\Theta\left(s - \frac{m_b^2 - \bar{u}q^2}{u}\right) - \Theta\left(s - \frac{m_b^2}{u} - P^2\right)\right] \\
&\quad + \frac{\log\left(\left(\frac{B-\sqrt{\lambda_2\lambda_3}}{B+\sqrt{\lambda_2\lambda_3}}\right)\left(\frac{A-\sqrt{\lambda_1\lambda_3}}{A+\sqrt{\lambda_1\lambda_3}}\right)\right)}{\sqrt{\lambda_3}}\Theta\left(s - \frac{m_b^2}{u} - P^2\right)\,,
\end{aligned} \tag{J.4}$$

where

$$\begin{aligned}
A &\equiv 2m_b^2 q^2 - u\left(q^2 - P^2\right)\left(m_b^2 + \bar{u}q^2 + us\right) \\
B &\equiv u\left(\left(q^2 - P^2\right)\left(m_b^2 + u\left(s - P^2\right)\right) - 2q^2\left(s - P^2\right)\right) \\
\lambda_1 &\equiv \lambda\left(us + \bar{u}q^2, m_b^2, 0\right)\,, \quad \lambda_2 \equiv \lambda\left(u(s-P^2), m_b^2, 0\right)\,, \\
\lambda_3 &\equiv \lambda\left(us + \bar{u}q^2, u(s-P^2), q^2\right)\,, \quad \lambda \equiv \lambda(p_B^2, \bar{u}P^2 + uq^2, u(p_B^2 - P^2))
\end{aligned} \tag{J.5}$$

and $\lambda(x,y,z) = (x - (y+z))^2 - 4yz$ is the Källén-function.

The notation $\log_-$ and $\log_L$ in the density ρ_{C_a} demands clarification:

$$\log_L\theta \to \begin{cases}
r_+ > 0 \wedge r_- > 0 & \log_+\theta \\
r_+ < 0 \wedge r_- > 0 & \begin{cases}
\lambda < 0 & \begin{cases} s < \mathrm{Re}s_+ & \log_+\theta \\ s > \mathrm{Re}s_+ & \log_-\theta \end{cases} \\
\lambda > 0 & \begin{cases}
\theta < 0 & \begin{cases} s < \lambda_- & \log_-\theta \\ s > \lambda_+ & \log_+\theta \end{cases} \\
\theta > 0 & \begin{cases} \mathrm{Re}s_+ < s < \lambda_- & \log\theta - 2\pi i \\ \lambda_+ < s < \mathrm{Re}s_+ & \log\theta + 2\pi i \\ \text{otherwise} & \log\theta \end{cases}
\end{cases}
\end{cases} \\
r_+ < 0 \wedge r_- < 0 & \log_-\theta
\end{cases} \tag{J.6}$$

The square root of λ, but not $\lambda_{1,2,3}$, in Eq. (J.4) is to be taken as:

$$\sqrt{\lambda} \to \begin{cases} \sqrt{\lambda} & s < \lambda_- \\ i\sqrt{-\lambda} & \lambda_- < s < \lambda_+ \\ -\sqrt{\lambda} & s > \lambda_+ \end{cases}\,. \tag{J.7}$$

Furthermore, $\log_\pm$ are defined as follows:

$$\log_+ x = \begin{cases} \log x & \mathrm{Im} x = 0 \\ \log(-x) + i\pi & \mathrm{Im} x \neq 0 \end{cases} \tag{J.8}$$

$$\log_- x = \log(-x) - i\pi \tag{J.9}$$

The remaining variables in ρ_{C_a} are given by:

$$\begin{aligned} \lambda_\pm &= \frac{\bar{u}P^2 + u(1+u)q^2 \pm 2u\sqrt{q^2(\bar{u}P^2 + uq^2)}}{\bar{u}^2} \,, \quad \lambda = \bar{u}^2(s-\lambda_+)(s-\lambda_-) \\ z_\pm &= \frac{(1+u)p_B^2 - P^2 - uq^2 \pm \sqrt{\lambda}}{2p_B^2} \,, \quad z_L = 1 + \frac{\bar{u}P^2 + uq^2}{m_b^2 - p_B^2} \\ r_\pm &= r(\lambda_\pm) \,, \quad r(p_B^2) = (1+u-2z_L)p_B^2 - P^2 - uq^2 \,. \end{aligned} \tag{J.10}$$

J.1 Analytic structure of $C_0(s, s-\beta, \alpha, 0, m_b^2, 0)$ in $\mathbb{C}_s$

In this section we shall discuss the analytic properties of the PV-function C_a through a function with simplified but equivalent variables, namely,

$$C_0(s, s-\beta, \alpha, 0, m_b^2, 0) \,, \tag{J.1.1}$$

with conventions as indicated in the caption of Fig. J.1. The function (J.1.1) corresponds to C_a in Eq. (H.1) with the following substitutions:

$$s = p_B^2 \,, \quad \alpha = uq^2 + \bar{u}P^2 \,, \quad \beta = uP^2 + \bar{u}s \,. \tag{J.1.2}$$

It is argued in a succession of rigour: first from the viewpoint of Landau equations J.1.1, then explicit one-loop solutions & uniqueness of analytic continuation J.1.2 and finally axiomatic results by Källén & Wightman J.1.2.1, that the correlation function has a complex anomalous threshold on the physical sheet for

$$\alpha > \alpha^* \equiv \frac{\beta^2}{4m_b^2} \,. \tag{J.1.3}$$

J.1.1 Singularities from the Landau equations

The Landau equations [137, 138] are a means to determine singularities of a perturbative diagram[2]. The crucial and limiting point is that, unless the singularities are real, there is no direct way to determine on which Riemann sheets they appear.

We shall be interested in determining the so-called leading Landau singularity of the triangle graph J.1, also known as an *anomalous threshold*. It corresponds to all three propagators being

[2]Singularities which arise due to infinite loop-momentum are possible to interpret through the Landau equations though not easily and have therefore been called singularities of the second-type or non-Landau singularities.

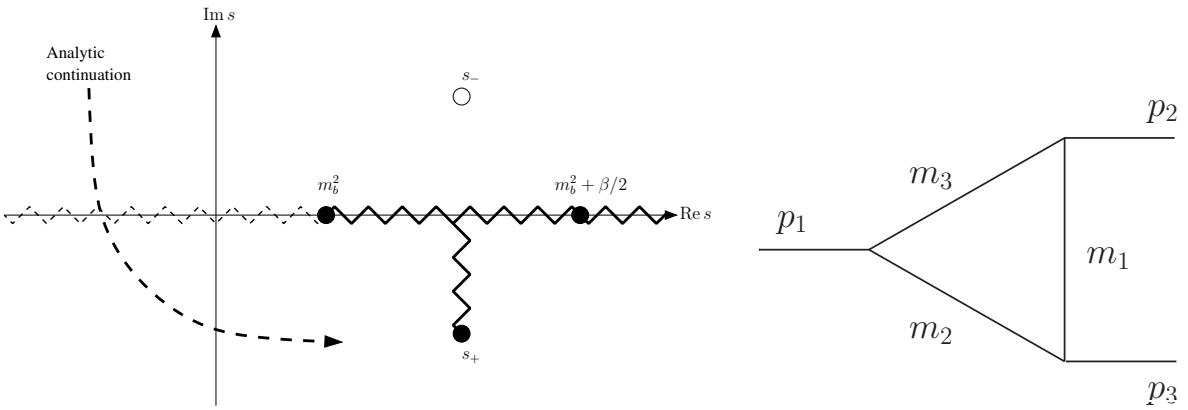

FIGURE J.1: Analytic structure of $C_0(s, s-\beta, \alpha, 0, m_b^2, 0)$. The path of the branch cut connected to the branch point s_+ can be inferred from a deformation analysis as in [170]. (left) Black spots correspond to branch points on the physical sheet. White spot branch point which is not on the physical sheet. Black zig-zag lines are branch cuts on the physical sheet. The dashed zig-zag line corresponds to a branch cut of C_a^F (J.1.2.1) but not of $C_a = C_0(s, s-\beta, \alpha, 0, m_b^2, 0)$ as explained in the text. The arrow indicates around which branch point C_a^F is analytically continued into the lower half plane. (right) Triangle graph corresponding to the $C_0(p_1^2, p_2^2, p_3^2, m_2^2, m_3^2, m_1^2)$ PV-function. The conventions are the same as in LoopTools [169] and Feyncalc [145].

on-shell. The condition can conveniently be written in terms of a determinant,

$$\det \begin{pmatrix} 1 & x_1 & x_2 \\ x_1 & 1 & x_3 \\ x_2 & x_3 & 1 \end{pmatrix} = 0 \,, \qquad x_i \equiv \frac{p_i^2 - m_j^2 - m_k^2}{2 m_j m_k} \,, \quad i \neq j \neq k \neq i \,, \tag{J.1.1.1}$$

where m_j and m_k are the masses of the propagators adjacent to the in-going momentum squares p_i^2. For the C_0 in question (J.1.1), this leads to the Landau surface

$$(s - m_b^2)(s - m_b^2 - \beta) + \alpha m_b^2 = 0 \tag{J.1.1.2}$$

whose solutions are given by

$$s_\pm = m_b^2 + \beta/2 \pm \sqrt{(\beta/2)^2 - \alpha m_b^2} \tag{J.1.1.3}$$

As long as $\alpha < \alpha^*$ (J.1.3) the solutions are real and we can decide of whether they are on the physical sheet or not by checking whether the Landau equations admit solutions where the Feynman parameter admit values between $[0, 1]$. As a matter of fact for any $q^2 > 0$, c.f. Eq. (J.1.2), there is exists some $u \in [0, 1]$ for which $\alpha > \alpha^*$. Thus we are lead to the question of whether or not the singularities $s_\pm$ are on the physical sheet. Some guidance can be gained following Mandelstam contour deformation prescription [170]. The idea is that one starts with values for P^2 and Q^2 such that $s_\pm$ are real. Then a dispersion representation can be constructed by checking which singularities are on the physical sheet. Upon deformation of the external momenta (P^2, Q^2) the contour is deformed such that no singularities are crossed. Applying this procedure we found that s_+ is on the physical sheet and s_- on an unphysical sheet. In the next section we shall show the same result to be true in a more explicit and possibly more transparent way from the known one loop result.

J.1.2 Complex branch points in the lower half-plane from analytic continuation of the Feynaman parameter representation

Here we discuss the function C_a (H.1) itself rather than C_0 (J.1.1) because reference is made to the variables used in ρ_{C_a} (J.4) and thereafter. Variables are restricted to the following values : $0 \leq u \leq 1$, $m_B^2 > m_b^2 > 0$, $P^2 = m_B^2 + i0$ and $q^2 - i0 = \mathrm{Re}[q^2] > 0$. Our two main ingredients are the uniqueness of analytic continuation from the real line and the fact that the lowest cut on the real line starts at m_b^2. The latter can be verified from the Landau equations.

The correlation function C_a, originally defined just above the real line of p_B^2 (at $\mathrm{Re}[p_B^2]+i0$), can be analytically continued into the entire upper half-plane by the Feynman-parameter integral representation,

$$C_a^F(p_B^2) = \int_0^1 dx \int_0^{1-x} dy \left[(1-x-y)(xp_B^2 + yu(p_B^2 - P^2) - m_b^2) + xy(\bar{u}P^2 + uq^2) + i0\right]^{-1}, \tag{J.1.2.1}$$

since it is free from singularities in this region. For $\Im[p_B^2] \neq 0$ (where the $i0$-prescription is irrelevant) $C_a^F(p_B^{2*}) = C_a^F(p_B^2)^*$ by inspection. This implies that C_a^F, but not necessarily C_a, has got a branch cut on the real axis whenever $\Im[C_a^F(p_B^2)] \neq 0$. Note these are the only possible singularities for the range of variables mentioned above.

Using the Feynman-parameter representation $C_a^F(p_B^2)$ as a starting point we construct an analytic continuation to the lower half-plane as follows:

$$C_a(p_B^2) = \begin{cases} C_a^F(p_B^2) & \Im[p_B^2] > 0 \\ C_a^F(p_B^{2*})^* + C_a^{\mathrm{rem}}(p_B^2) & \Im[p_B^2] < 0 \end{cases} . \tag{J.1.2.2}$$

With reminder-function $C_a^{\mathrm{rem}}(p_B^2)$ such that there is no branch cut below $p_B^2 < m_b^2$ for $C_a(p_B^2)$. To remove the branch cut near a given p_B^2 we require that $C_a(p_B^2)$ in (J.1.2.2) is equal immediately above and below the real line which enforces

$$C_a^{\mathrm{rem}}(p_B^2) = 2i\,\Im[C_a^F(p_B^2)] \,, \quad \Im[p_B^2] = 0 \,. \tag{J.1.2.3}$$

The resulting function eliminates the branch cut for $p_B^2 < m_b^2$. In this region a remainder function $C_a^{\mathrm{rem}}(p_B^2)$ may be derived from (J.1.2.3) and (J.1.2.1) using $1/(x+i0) = \mathrm{PP}[1/x] - i\pi\delta(x)$[3] to give

$$C_a^{\mathrm{rem}}(p_B^2) = -\frac{2\pi i}{\sqrt{\lambda}} \left(\log\left(\frac{z_+ - z_L}{z_+ - 1}\right) - \log\left(\frac{z_- - z_L}{z_- - 1}\right)\right) , \tag{J.1.2.4}$$

with $z_\pm$, z_L and λ as in (J.10)[4]. The branch points of the logarithms and square roots appear on all Riemann sheets unless there are cancellations between terms.

The branch cuts of the two logarithms start at $z_\pm = z_L$ (there are no solutions for $|p_B^2| < \infty$ to $z_\pm = 1$), which occurs at $p_B^2 = s_\pm$, and since the branch points $s_\pm$ are separate no cancellation

[3] PP stands for the principal part.

[4] Note whilst the directions of the cuts are ambiguous the branch points $s_\pm$ are unambiguous. Fortunately it is the latter we are interested in. In other words: The exact location of the cuts is somewhat analogous to the choice of a coordinate system whereas the branch points are not dependent on it.

occurs and there indeed must be a cut on all Riemann sheets of $C_a^{\rm rem}(p_B^2)$. $s_\pm$ is complex for physical momenta, and since we know that $C_a^{\rm rem}(p_B^2)$ is the only term with branch points away from the real line in (J.1.2.2) we conclude that analytically continuing (J.1.2.1) to $\Im[p_B^2] < 0$ across the real line, to the left of the branch point $p_B^2 = m_b^2$ c.f. Fig. J.1(left), necessarily results in a branch cut off the real line in the lower complex half plane. To this end we note that $C_a^{\rm rem}(p_B^2)$ corresponds to ρ_{C_a} (J.4) modulo the imaginary part. To this end we would like to add a clarifying remark. Whereas the Feynman parameter representation does satisfy the Schwarz reflection principle $(C_0^F(s^*))^* = C_0^F(s)$, as previously stated, the proper analytic continuation $(C_0(s^*))^* \neq C_0(s)$ does not. This is surely due to the complex singularity on the lower half-plane which is not balanced by a singularity on the upper half plane.

In the next section we are going to learn that the complex singularities are not an artefact of perturbation theory but are expected on most general grounds from axiomatic approaches.

J.1.2.1 The Källén-Wightman domain

Based on axioms such as Lorentz-covariance, assumption on the spectrum and microcausality Källén & Wightman [167] obtained results on the domain analyticity of the vacuum expectation value of three scalar fields. We note that the C_0 PV-function is simply a one-loop approximation in a specific theory with three point interactions. Denoting the three invariant momentum squares of the three vertices by $Z_i = p_i^2$, for $i = 1..3$, the domain can be separated into eight regions characterised by the signs of $\mathrm{Im}[Z_i]$; denoted by $[\pm\pm\pm]$. Those eight octants are partly separated by the normal cuts. In addition the domains with signatures $[++-]$ and $[--+]$ and permutations thereof have got the following boundaries [168]:

$$(Z_1 - r)(Z_2 - r) + rZ_3 = 0\,, \qquad r > 0\,; \tag{J.1.3.1}$$

with $\mathrm{Im}(Z_1)\mathrm{Im}(Z_2) > 0$. Thus for $(Z_1, Z_2, Z_3) = (s, s-\beta, \alpha + i0)$ with $\mathrm{Im}[s] < 0$ we find

$$(s - r)(s - \beta - r) + r\alpha = 0 \tag{J.1.3.2}$$

which corresponds to the Landau surface equation (J.1.1.2) upon identifying $r = m_b^2$.

Appendix K

Hadronic input values

The hadronic input for the vector DAs is summarised in Table K.1. For the pseudoscalar decay constants $f_\pi = 0.131\,\text{GeV}$ and $f_K = 0.160\,\text{GeV}$ are taken [158] the data for the pseudoscalar meson DAs is taken from Ref [159]:

$$a_2(\pi) = 0.29(3)(7)\,, \quad a_2(K) = 0.24(3)(7)\,, \quad a_1(K) = 0.074(2)(4) \tag{K.1}$$

The latter value is in good agreement with [160].

The sum rule specific input can be found in Table K.2. $s_0[f_H] = s_0[H] \equiv s_0$ is chosen throughout, with $s_0[B_q] = 35(1)\,\text{GeV}^2$ as a reference value. All others are determined to satisfy $(m_{H_q}+X)^2 = s_0[H_q]$ for "universal" X, where X is between the two pion mass and the rho-threshold. The Borel parameter $M^2[f_H]$ of (5.4.1) is chosen in the minimum of the Borel window and in addition it is verified that the dimension five operators are below 10% and that the continuum contribution, vulnerable to quark-hadron duality violation, does not exceed 30%. The Borel parameter $M^2[G]$ for the G_i is chosen such that the continuum is 30%; this choice suppresses higher twist-corrections, which have not been computed, maximally.

	$f^{\parallel}$[GeV]	$f^{\perp}$[GeV]	$a_2^{\parallel}$	$a_2^{\perp}$	$a_1^{\parallel}$	$a_1^{\perp}$
ρ	0.216(1)(6)	0.160(11)	0.17(7)	0.14(6)	–	–
ω	0.187(2)(10)	0.139(18)	0.15(12)	0.14(12)	–	–
K^*	0.211(7)	0.163(8)	0.16(9)	0.10(8)	0.06(4)	0.04(3)
ϕ	0.235(5)	0.191(6)	0.23(8)	0.14(7)	–	–

TABLE K.1: 1^{--}-mesons with odd G-parity have vanishing odd Gegenbauer moments. The scale dependent quantities $f^{\perp}$, $a_{1,2}^{\parallel,\perp}$ are evaluated at $\mu = 1\,\text{GeV}$. The value $\mathcal{B}(\tau \to K^*\nu_\tau) = 1.20(7)\cdot 10^{-2}$ is used [158] as compared to the PDG value used by the end of 2006 $\mathcal{B}(\tau \to K^*\nu_\tau) = 1.29(5)\cdot 10^{-2}$ in [141], which leads to a decay constant which changes $f_{K^*}^{\parallel}$ from 0.220 GeV to 0.211 GeV whereas all the others remain the same as in [141]; with a numerical error corrected for $f_\phi^{\parallel}$ as noted by the authors of [161]. The $f^{\perp}$ decay constants follow from the ratios $r[X] = f_X^{\perp}(2\,\text{GeV})/f_X^{\parallel}$ with $r[\rho] = 0.687(27)$, $r[K^*] = 0.712(12)$ and $r[\phi] = 0.750(8)$ in [162]. Further, $r[\omega] \simeq r[\rho]$ is used, in view of a lack of a lattice QCD determination of this quantity. For the DA parameters the values $a_1^{\parallel}$, $a_2^{\parallel}(\rho, K^*, \phi)$ from the lattice [159] are averaged with the sum rule determinations, keeping the relative sum rule uncertainty, which is larger, in order to account for neglecting higher Gegenbauer moments. The references for the sum rule values are [163] for the ρ, [164] for the ϕ and [160] and [165] for the K^*. In view of the lack of theoretical determinations of parameters for the ω, it is assumed that they have the same values as for the ρ enlarged uncertainty by a factor of 2.

H	s_0	$M^2[G]$	$M^2[f_H]$	m_H	f_H(5.4.1)	cond.	value	mass	value
B_s	36(1.5)	9(2)	5.0(5)	5.37	0.162	$\langle\bar{q}q\rangle$	$(-0.24(1))^3$	m_b	4.7(1)
B_q	35(1.5)	9(2)	5.0(5)	5.28	0.142	$\langle\bar{s}s\rangle$	$0.8(1)\langle\bar{q}q\rangle$	m_c	1.3(1)
D_s	6.7(7)	6(2)	1.5(2)	1.96	0.185	$\langle\bar{q}Gq\rangle$	$(0.8(1))^2\langle\bar{q}q\rangle$	$\bar{m}_s$	0.094(3)
D_q	6.2(7)	6(2)	1.5(2)	1.86	0.156	$\langle\bar{s}Gs\rangle$	$(0.8(1))^2\langle\bar{s}s\rangle$		

TABLE K.2: (left) H stands for heavy-light meson and q stands for either a u or d quark. Sum rule specific values in units of GeV to the appropriate power. f_H correspond to the decay constants obtained from a tree-level sum rule. They should not be compared with the true value of f_H as the latter have substantial radiative corrections in QCD sum rules. (middle) condensates relevant for the f_H sum rule (5.4.1). (right) Quark masses. The tree-level heavy quark masses are chosen to satisfy $m_H \simeq m_h + \bar{\Lambda}$ with $\bar{\Lambda} \simeq 0.6\,\text{GeV}$ approximately. The strange quark mass in the $\overline{\text{MS}}$ correspond to $\mu_{\overline{\text{MS}}} = 2$ GeV. In the the sum (5.4.1) $\bar{m}_s$ is scaled up to $\mu = \mu_F$.

Appendix L

Non-spectator corrections $G^{(ns)}$

The corrections which do not connect the gluon of the operator $\tilde{\mathcal{O}}_8$ with the spectator quark are depicted in Figure 5.2 (bottom). They have been computed for the inclusive $b \to sll$ [139] and their contribution is proportional to a function $F_8^{7(9)}(q^2/m_b^2)$ times the operator $\mathcal{O}_{7(9)}$. The latter reduces to the standard tensor and vector form factors $T_i(f_T)$ and $V, A_i(f_+)$ when taken between B and $V(P)$ states.

$$
\begin{aligned}
G_i^{(ns)}(q^2) &= \left(-\frac{\alpha_s(m_b)}{4\pi}\right)\left(\frac{Q_b}{-1/3}\right)\left(F_8^{(7)}\, T_i(q^2) - F_8^{(9)}\,\frac{q^2}{2m_b}\,\mathcal{V}_i(q^2)\right) \quad , i = 1..3\,, \\
G_T^{(ns)}(q^2) &= \left(-\frac{\alpha_s(m_b)}{4\pi}\right)\left(\frac{Q_b}{-1/3}\right)\Big(F_8^{(7)}\, f_T(q^2) - F_8^{(9)} \underbrace{\frac{q^2}{2m_b} v_T(q^2)}_{-\frac{m_B+m_P}{2m_b} f_+(q^2)}\Big)
\end{aligned}
\tag{L.1}
$$

where $F_8^{7(9)}$ are given in [139] in terms of an expansion in powers of q^2/m_c^2 and a logarithm. The functions $\mathcal{V}_i$ and v_T are defined as:

$$
\begin{aligned}
\langle V(p,\eta)|\bar{s}\gamma^\rho(1-\gamma_5)b|\bar{B}(p_B)\rangle &= P_1^\rho\,\mathcal{V}_1 + P_2^\rho\,\mathcal{V}_2 + P_3^\rho\,\mathcal{V}_3 + [i(\eta^*\cdot q)q^\rho]\mathcal{V}_P \\
\langle P(p)|\bar{s}\gamma^\rho b|\bar{B}(p_B)\rangle &= P_T^\rho\, v_T + q_\rho v_S
\end{aligned}
\tag{L.2}
$$

with

$$
\begin{aligned}
\mathcal{V}_P &= \frac{-2m_V}{q^2}A_0(q^2) & \mathcal{V}_1 &= \frac{-V(q^2)}{m_B+m_V} \\
\mathcal{V}_2 &= \frac{-A_1(q^2)}{m_B-m_V} & \mathcal{V}_3 &= \Big(\frac{m_B+m_V}{q^2}A_1(q^2) - \frac{m_B-m_V}{q^2}A_2(q^2)\Big) \\
v_s &= \frac{m_B^2-m_P^2}{q^2}f_0(q^2) & v_T &= \frac{-(m_B+m_P)}{q^2}\,f_+(q^2)\,,
\end{aligned}
\tag{L.3}
$$

where $V, A_i, f_+, f_0, f_T, T_i$ are all standard form factor notations in the literature. Note, as manifested by limiting the sum from $i = 1..3$, the $f_0(A_0)$ component does not contribute to $B \to Vll$ as the q^ρ vanishes upon contraction with $\bar{l}\gamma_\rho l$ or the photon polarization tensor $\epsilon(q)$.

List of Publications

Journal Publications

Published:

1. M. Dimou, J. Lyon and R. Zwicky, "Exclusive Chromomagnetism in heavy-to-light FCNCs", Phys. Rev. D **87** (2013) 074008 [arXiv:hep-ph/1212.2242].

2. M. Dimou, S. F. King and C. Luhn, "Approaching Minimal Flavour Violation from an $SU(5) \times S_4 \times U(1)$ SUSY GUT", JHEP **1602** (2016) 118 [arXiv:hep-ph/1511.07886].

Submitted:

1. M. Dimou, S. F. King and C. Luhn, "Phenomenological Implications of an $SU(5) \times S_4 \times U(1)$ SUSY GUT of Flavour", [arXiv:hep-ph/1512.09063].

Conference Publications

1. M. Dimou, J. Lyon and R. Zwicky, "Heavy-to-light chromomagentic matrix element", Nucl. Phys. Proc. Suppl. 241-242 (2013) 127-132 [arXiv:hep-ph/1305.5332].

Bibliography

[1] Paul Dirac, "The evolution of the Physicist's Picture", Nature Scientific American 208 (5) (1963).

[2] F. Englert and R. Brout, "Broken Symmetry and the Mass of Gauge Vector Mesons", Phys. Rev. Lett. **13** (1964) 321-323;
P. W. Higgs, "Broken symmetries, massless particles and gauge fields", Phys. Lett. **12** (1964) 132-133;
P. W. Higgs, "Broken Symmetries and the Masses of Gauge Bosons", Phys. Rev. Lett. **13** (1964) 508-509;
G. Guralnik, C. Hagen and T. Kibble, "Global Conservation Laws and Massless Particles", Phys. Rev. Lett. **13** (1964) 585-587;
P. W. Higgs, "Spontaneous Symmetry Breakdown without Massless Bosons", Phys. Rev. **145** (1966) 1156-1163;
T. Kibble, "Symmetry breaking in non-Abelian gauge theories", Phys. Rev. **155** (1967) 1554-1561.

[3] S. L. Glashow, "Partial Symmetries of Weak Interactions", Nucl. Phys. **22** (1961) 579S. Weinberg, "A Model of Leptons", Phys. Rev. Lett. **19** (1967) 1264-1266;
A. Salam, "Weak and Electromagnetic Interactions", Conf. Proc. **C680519** (1968) 367S. L. Glashow, J. Iliopoulos and L. Maiani, "Weak Interactions with Lepton-Hadron Symmetry, Phys. Rev. D **2** (1970) 1285.

[4] G. Aad et al., "Observation of a new particle in the search for the Standard Model Higgs boson with the ATLAS detector at the LHC", Phys. Lett. B **716** (2012), 1 [arXiv:hep-ex/1207.7214];
S. Chatrchyan et al., "Observation of a new boson at a mass of 125 GeV with the CMS experiment at the LHC", Phys. Lett. B **716** (2012), 30 [arXiv:hep-ex/1207.7235].

[5] C. D. Froggatt and H. B. Nielsen, "Hierarchy Of Quark Masses, Cabibbo Angles And CP Violation", Nucl. Phys. B **147** (1979), 277.

[6] S. F. King, "Neutrino mass models", Rept. Prog. Phys. **67** (2004) 107 [arXiv:hep-ph/0310204];
G. Altarelli and F. Feruglio, "Discrete Flavor Symmetries and Models of Neutrino Mixing", Rev. Mod. Phys. **82** (2010) 2701 [arXiv:hep-ph/1002.0211];
S. F. King and C. Luhn, "Neutrino Mass and Mixing with Discrete Symmetry", Rept. Prog. Phys. **76** (2013) 056201 [arXiv:hep-ph/1301.1340];
S. F. King, A. Merle, S. Morisi, Y. Shimizu and M. Tanimoto, "Neutrino Mass and Mixing:

from Theory to Experiment", New J. Phys. **16** (2014) 045018 [arXiv:hep-ph/1402.4271]; S. F. King, "Models of Neutrino Mass, Mixing and CP Violation", J. Phys. G: Nucl. Part. Phys. **42** (2015) 123001 [arXiv:hep-ph/1510.02091].

[7] P. Ballett, S. F. King, C. Luhn, S. Pascoli and M. A. Schmidt, "Testing atmospheric mixing sum rules at precision neutrino facilities", Phys. Rev. D **89** (2014) 1, 016016 [arXiv:hep-ph/1308.4314];
D. Meloni, "Checking Flavour Models at Neutrino Facilities", Phys. Lett. B **728** (2014) 118 [arXiv:hep-ph/1308.4578];
P. Ballett, S. F. King, C. Luhn, S. Pascoli and M. A. Schmidt, "Precision measurements of θ_{12} for testing models of discrete leptonic flavour symmetries", J. Phys. Conf. Ser. **598** (2015) 1, 012014 [arXiv:hep-ph/1406.0308];
P. Ballett, S. F. King, C. Luhn, S. Pascoli and M. A. Schmidt, "Testing solar lepton mixing sum rules in neutrino oscillation experiments", JHEP **1412** (2014) 122 [arXiv:hep-ph/1410.7573].

[8] P. Minkowski, "$\mu \to e\gamma$ at a Rate of One Out of 10^9 Muon Decays?", Phys. Lett. B **67** (1977) 421;
M. Gell-Mann, P. Ramond and R. Slansky, "Complex Spinors and Unified Theories", Conf. Proc. C **790927** (1979) 315 [arXiv:hep-th/1306.4669];
T. Yanagida, "Horizontal Symmetry And Masses Of Neutrinos", Conf. Proc. C **7902131** (1979) 95;
R. N. Mohapatra and G. Senjanovic, "Neutrino Mass and Spontaneous Parity Violation", Phys. Rev. Lett. **44** (1980) 912.

[9] S. Antusch, S. F. King and M. Malinsky, "Solving the SUSY Flavour and CP Problems with SU(3) Family Symmetry", JHEP **0806** (2008), 068 [arXiv:hep-ph/0708.1282];

[10] C. Hagedorn, S. F. King and C. Luhn,"A SUSY GUT of Flavour with $S_4 \times SU(5)$ to NLO", JHEP **1006** (2010), 048 [arXiv:hep-ph/1003.4249].

[11] C. Hagedorn, S. F. King and C. Luhn, "SUSY $S_4 \times SU(5)$ Revisited", Phys. Lett. B **717** (2012) 207 [arXiv:hep-ph/1205.3114].

[12] S. F. King and I. N. R. Peddie, "Canonical normalization and Yukawa matrices", Phys. Lett. B **586** (2004), 83 [arXiv:hep-ph/0312237];
S. F. King, I. N. R. Peddie, G. G. Ross, L. Velasco-Sevilla and O. Vives, "Kahler corrections and softly broken family symmetries", JHEP **0507** (2005) 049 [arXiv:hep-ph/0407012].

[13] F. Gabbiani, E. Gabrielli, A. Masiero and L. Silvestrini, 'A Complete analysis of FCNC and CP constraints in general SUSY extensions of the standard model", Nucl. Phys. B **477** (1996) 321 [arXiv:hep-ph/9604387];
M. Misiak, S. Pokorski and J. Rosiek, "Supersymmetry and FCNC effects", Adv. Ser. Direct. High Energy Phys. **15** (1998) 795 [arXiv:hep-ph/9703442].

[14] M. Dimou, S. F. King and C. Luhn, "Approaching Minimal Flavour Violation from an $SU(5) \times S_4 \times U(1)$ SUSY GUT", JHEP **1602** (2016) 118 [arXiv:hep-ph/1511.07886].

[15] M. Dimou, S. F. King and C. Luhn, "Phenomenological Implications of an $SU(5) \times S_4 \times U(1)$ SUSY GUT of Flavour", [arXiv:hep-ph/1512.09063].

[16] P. Colangelo and A. Khodjamirian, "QCD sum rules, a modern perspective," In *Shifman, M. (ed.): At the frontier of particle physics, vol. 3* 1495-1576 [arXiv:hep-ph/0010175].

[17] A. L. Kagan and M. Neubert, "Isospin breaking in $B \to K^*\gamma$ decays", Phys. Lett. B **539** (2002) 227 [arXiv:hep-ph/0110078].

[18] M. Dimou, J. Lyon and R. Zwicky, "Heavy-to-light chromomagentic matrix element", Nucl. Phys. Proc. Suppl. 241-242 (2013) 127-132 [arXiv:hep-ph/1305.5332].

[19] M. Dimou, J. Lyon and Roman Zwicky, "Exclusive Chromomagnetism in heavy-to-light FCNCs", Phys. Rev. D **87** (2013) 074008 [arXiv:hep-ph/1212.2242].

[20] G. t Hooft and M. Veltman, "Regularization and Renormalization of Gauge Fields", Nucl. Phys. B **44** (1972) 189-213.

[21] D. Gross and F. Wilczek, "Ultraviolet Behavior of Nonabelian Gauge Theories", Phys. Rev. Lett. **30** (1973) 1343-1346;
H. D. Politzer, "Reliable Perturbative Results for Strong Interactions?", Phys. Rev. Lett. **30** (1973) 1346-1349.

[22] T. Nakano and K. Nishijima, "Charge Independence for V-particles", Progress of Theoretical Physics **10** (5) (1953) 581-582;
K. Nishijima, "Charge Independence for V-particles", Progress of Theoretical Physics **13** (3) (1955) 285-304;
M. Gell-Mann,"The interpretation of the new particles as displaced charge multiplets", Il Nuovo Cimento **4** (2) (1956), 848-866.

[23] Particle Data Group Collaboration, K. A. Olive et al., Review of Particle Physics (RPP), Chin. Phys. C **38** (2014) 090001.

[24] N. Cabibbo, "Unitary Symmetry and Leptonic Decays", Phys. Rev. Lett. **10** (1963) 531-533;
M. Kobayashi and T. Maskawa, "CP Violation in the Renormalizable Theory of Weak Interaction", Progress of Theoretical Physics **49** (1973) 652

[25] L. L. Chau and W. Y. Keung, "Comments on the Parametrization of the Kobayashi-Maskawa Matrix, Phys. Rev. Lett. **53** (1984) 1802.

[26] J. Christenson, J. Cronin, V. Fitch and R. Turlay, "Evidence for the 2π Decay of the K_2 Meson", Phys. Rev. Lett. **13** (1964) 138

[27] L. Wolfenstein, "Parametrization of the Kobayashi-Maskawa Matrix, Phys. Rev. Lett. **51** (1983) 1945.

[28] C. Jarlskog, "Commutator Of The Quark Mass Matrices In The Standard Electroweak Model And A Measure Of Maximal CP Violation", Phys. Rev. Lett. **55** (1985) 1039.

[29] Bruce T. Cleveland et al., "Measurement of the Solar Electron Neutrino Flux with the Homestake Chlorine Detector", Astrophys. J. **496** (1998) 505;
SAGE Collaboration, J. N. Abdurashitov et al., "Measurement of the solar neutrino capture rate with gallium metal. III: Results for the 2002-2007 data-taking period", Phys. Rev. C **80** (2009), 015807, 0901.2200;
GNO Collaboration, M. Altmann et al., "Complete results for five years of GNO solar neutrino observations", Phys. Lett. B **616** (2005), 174;
Super-Kamiokande Collaboration, K. Abe et al., "Solar neutrino results in Super-Kamiokande-III", Phys. Rev. D **83** (2011), 052010, 1010.0118;
SNO Collaboration, B. Aharmim et al., "Low Energy Threshold Analysis of the Phase I and Phase II Data Sets of the Sudbury Neutrino Observatory", Phys. Rev. C **81** (2010), 055504, 0910.2984;
Borexino Collaboration, S. Davini, "Precision measurement of the Be-7 solar neutrino rate and absence of day-night asymmetry in Borexino", Nuovo Cim. C **034N06** (2011), 156.

[30] Super-Kamiokande Collaboration, G. Mitsuka et al., "Study of Non-Standard Neutrino Interactions with Atmospheric Neutrino Data in Super-Kamiokande I and II", Phys. Rev. D **84** (2011), 113008, 1109.1889;
KamLAND Collaboration, S. Abe et al., "Precision Measurement of Neutrino Oscillation Parameters with KamLAND", Phys. Rev. Lett. **100** (2008), 221803 , 0801.4589.

[31] DAYA-BAY Collaboration, F. P. An et al., "Observation of Electron-Antineutrino Disappearance at Daya Bay", Phys. Rev. Lett. **108** (2012), 171803 , 1203.1669.

[32] S. Weinberg, "Baryon And Lepton Nonconserving Processes", Phys. Rev. Lett. **43** (1979) 1566.

[33] B. Pontecorvo, "Neutrino experiments and the question of leptonic-charge conservation", Sov. Phys. JETP **26** (1968) 984 [Zh. Eksp. Teor. Fiz. 53 (1967) 1717];
Z. Maki, M. Nakagawa and S. Sakata, "Remarks On The Unified Model Of Elementary Particles", Prog. Theor. Phys. **28** (1962) 870.

[34] M. C. Gonzalez-Garcia, M. Maltoni and T. Schwetz, "Updated fit to three neutrino mixing: status ofleptonic CP violation", JHEP **1411** (2014), 052 [arXiv:hep-ph/1409.5439].

[35] S. Weinberg, "Implications of Dynamical Symmetry Breaking", Phys. Rev. D **13**(1976) 974;
L. Susskind, "Dynamics of Spontaneous Symmetry Breaking in the Weinberg-Salam Theory", Phys. Rev. D **20** (1979) 2619;
E. Gildener, "Gauge Symmetry Hierarchies", Phys. Rev. D **14** (1976) 1667;
G. 't Hooft, "Recent Developments in Gauge Theories", Proceedings, Nato Advanced Study Institute, Cargese, France, 1979, (Plenum, 1980).

[36] F. Zwicky, "Spectral displacement of extra galactic nebulae", Helv. Phys. Acta. **6** (1933), 110.

[37] J. R. Bond et al., "Massive neutrinos and the large-scale structure of the universe", Phys. Rev. Lett. **45** (1980), 1980-1984.

[38] A. Merle, "keV Neutrino Model Building", Int. J. Mod. Phys. D **22** (2013), 1330020 [arXiv:hep-ph/1302.2625].

[39] M. Fukugita and T. Yanagida, "Barygenesis without grand unification", Phys. Lett. B **174** (1986), 45;
P. Di Bari, "An introduction to leptogenesis and neutrino properties", Contemp. Phys. **53** (2012) 4, 315 [arXiv:hep-ph/1206.3168];
S. Blanchet and P. Di Bari, "The minimal scenario of leptogenesis", New J. Phys. **14** (2012), 125012 [arXiv:hep-ph/1211.0512].

[40] M. Grll-Man, "The Eightfold Way: A Theory of Strong Interaction Symmetry", CTSL-20, TID-12608 (1961).

[41] S. Coleman and J. Mandula, "All Possible Symmetries of the S Matrix", Phys. Rev. **159** (1967), 1251.

[42] R. Haag, Jan T. opuszaski and M. Sohnius, "All possible generators of supersymmetries of the S-matrix", Nucl. Phys. B **88** (1975), 257.

[43] Yu. A. Golfand and E. P. Likhtman, "Extension of the Algebra of Poincare Group Generators and Violation of p Invariance", JETP Lett. **13** (1971) 323;
A. Neveu and J. H. Schwarz, "Factorizable Dual Model of Pions", Nucl. Phys. B **31** (1971) 86;
J. L. Gervais and B. Sakita, "Field theory interpretation of supergauges in dual models", Nucl. Phys. B **34** (1971) 632;
D. V. Volkov and V. P. Akulov, "Is the neutrino a Goldstone particle?", Phys. Lett. B **46** (1973) 109.

[44] J. Wess and B. Zumino, "Supergauge transformations in four dimensions", Nucl. Phys. B **70** (1974), 39.

[45] S. P. Martin,",," Adv. Ser. Direct. High Energy Phys. **21** (2010) 1 [Adv. Ser. Direct. High Energy Phys. **18** (1998) 1] [arXiv:hep-ph/9709356].

[46] Y. Shirman, "Introduction to Supersymmetry and Supersymmetry Breaking", Proceedings of Theoretical Advanced Study Institute in Elementary Particle Physics on The dawn of the LHC era (TASI 2008) 359 [arXiv:hep-ph/0907.0039].

[47] D. J. H. Chung, L. L. Everett, G. L. Kane, S. F. King, J. D. Lykken and L. T. Wang, "The Soft supersymmetry breaking Lagrangian: Theory and applications", Phys. Rept. **407** (2005) 1 [arXiv:hep-ph/0312378].

[48] S. Dimopoulos and D. W. Sutter, "The Supersymmetric Flavour Problem", Nucl. Phys. B **452** (1995) 496 [arXiv:hep-ph/9504415];
H. E. Haber, "The Status of the Minimal Supersymmetric Standard Model and Beyond", Nucl. Phys. Proc. Suppl. **62** (1998) 469 [arXiv:hep-ph/9709450].

[49] A. H. Chamseddine, R. L. Arnowitt and P. Nath, "Locally Supersymmetric Grand Unification", Phys. Rev. Lett. **49** (1982) 970;
L. J. Hall, J. Lykken and S. Weinberg, "Supergravity as the Messenger of Supersymmetry

Breaking", Phys. Rev. D **27** (1983) 2359 ;
L. Alvarez-Gaume, J. Polchinski, and M. B. Wise, "Minimal Low-Energy Supergravity", Nucl. Phys. B **221** (1983) 495;

[50] A. Pomarol and D. Tommasini, "Horizontal symmetries for the supersymmetric flavor problem", Nucl. Phys. B **466** (1996) 3 [arXiv:hep-ph/9507462];
R. Barbieri, G. R. Dvali and L. J. Hall, "Predictions From A $U(2)$ Flavour Symmetry In Supersymmetric Theories", Phys. Lett. B **377** (1996) 76 [arXiv:hep-ph/9512388];
R. Barbieri, L. J. Hall, S. Raby and A. Romanino, "Unified Theories With $U(2)$ Flavor Symmetry", Nucl. Phys. B **493** (1997) 3 [arXiv:hep-ph/9610449];
R. Barbieri, L. J. Hall and A. Romanino, "Consequences Of A $U(2)$ Flavour Symmetry", Phys. Lett. B **401** (1997) 47 [arXiv:hep-ph/9702315].

[51] S. Antusch and S. F. King, "From hierarchical to partially degenerate neutrinos via type II upgrade of type I see-saw models", Nucl. Phys. B **705** (2005) 239 [arXiv:hep-ph/0402121];
S. F. King and M. Malinsky, "Towards a complete theory of fermion masses and mixings with $SO(3)$ family symmetry and 5d $SO(10)$ unification", JHEP **0611** (2006) 071 [arXiv:hep-ph/0608021];
S. F. King, "Predicting neutrino parameters from $SO(3)$ family symmetry and quark-lepton unification, JHEP **0508** (2005) 105 [arXiv:hep-ph/0506297].

[52] S. Antusch, S. F. King, M. Malinsky and G. G. Ross, "Solving the SUSY Flavour and CP Problems with Non-Abelian Family Symmetry and Supergravity", Phys. Lett. B **670** (2009) 383 [arXiv:hep-ph/0807.5047].

[53] G. G. Ross, L. Velasco-Sevilla and O. Vives, "Spontaneous CP violation and non Abelian family symmetry in SUSY", Nucl. Phys. B **692** (2004) 50 [arXiv:hep-ph/0401064].

[54] S. F. King and G. G. Ross, "Fermion masses and mixing angles from $SU(3)$ family symmetry", Phys. Lett. B **520** (2001) 243 [arXiv:hep-ph/0108112];
J. L. Chkareuli, C. D. Froggatt and H. B. Nielsen, "Minimal mixing of quarks and leptons in the $SU(3)$ theory of flavour", Nucl. Phys. B **626** (2002) 307 [arXiv:hep-ph/0109156];
G. G. Ross and L. Velasco-Sevilla, "Symmetries and fermion masses", Nucl. Phys. B **653** (2003), 3 [arXiv:hep-ph/0208218];
S. F. King and G. G. Ross, "Fermion masses and mixing angles from $SU(3)$ family symmetry and unification", Phys. Lett. B **574** (2003) 239 [arXiv:hep-ph/0307190];
I. de Medeiros Varzielas and G. G. Ross, "$SU(3)$ family symmetry and neutrino bi-trimaximal mixing", Nucl. Phys. B **733** (2006) 31 [arXiv:hep-ph/0507176];
L. Calibbi, J. Jones-Perez, A. Masiero, J. h. Park, W. Porod and O. Vives, "FCNC and CP Violation Observables in a $SU(3)$-flavoured MSSM", Nucl. Phys. B **831** (2010) 26 [arXiv:hep-ph/0907.4069].

[55] G. Altarelli and F. Feruglio, "Tri-bimaximal neutrino mixing from discrete symmetry in extra dimensions", Nucl. Phys. B **720** (2005) 64 [arXiv:hep-ph/054165]; G. Altarelli and F. Feruglio, "Tri-bimaximal neutrino mixing, A_4 and the modular symmetry", Nucl. Phys. B **741** (2006) 215 [arXiv:hep-ph/0512103].

[56] X. G. He, Y. Y. Keum and R. R. Volkas, "A_4 flavour symmetry breaking scheme for understanding quark and neutrino mixing angles", JHEP **0604** (2006), 039 [arXiv:hep-ph/0601001];
G. Altarelli, F. Feruglio and Y. Lin, "Tri-bimaximal neutrino mixing from orbifolding", Nucl. Phys. B **775** (2007) 31 [arXiv:hep-ph/0610165];
G. Altarelli and D. Meloni, "A Simplest A_4 Model for Tri-Bimaximal Neutrino Mixing", J. Phys. G **36** (2009), 085005 [arXiv:hep-ph/0905.0620];
D. Aristizabal Sierra, F. Bazzocchi, I. de Medeiros Varzielas, L. Merlo and S. Morisi, "Tri-Bimaximal Lepton Mixing and Leptogenesis", Nucl. Phys. B **827** (2010) 34 [arXiv:hep-ph/0908.0907];
Y. Lin, "Tri-bimaximal Neutrino Mixing from A_4 and $\theta_{13} \sim \theta_C$", Nucl. Phys. B **824** (2010) 95 [arXiv:hep-ph/0905.3534];
Y. Lin, "A predictive A_4 model, Charged Lepton Hierarchy and Tri-bimaximal Sum Rule", Nucl. Phys. B **813** (2009) 91 [arXiv:hep-ph/0804.2867];
F. Bazzocchi, S. Kaneko and S. Morisi, "A SUSY A_4 model for fermion masses and mixings", JHEP **0803** (2008), 063 [arXiv:hep-ph/0707.3032];
F. Bazzocchi, M. Frigerio and S. Morisi, "Fermion masses and mixing in models with $SO(10) \times A_4$ symmetry", Phys. Rev. D **78** (2008) 116018 [arXiv:hep-ph/0809.3573].

[57] F. Bazzocchi, L. Merlo and S. Morisi, "Fermion Masses and Mixings in a S_4-based Model", Nucl. Phys. B **816** (2009) 204 [arXiv:hep-ph/0901.2086];
F. Bazzocchi and S. Morisi, "S_4 as a natural flavor symmetry for lepton mixing", Phys. Rev. D **80** (2009) 096005 [arXiv:hep-ph/0811.0345].

[58] G. J. Ding, S. F. King, C. Luhn and A. J. Stuart, "Spontaneous CP violation from vacuum alignment in S_4 models of leptons", JHEP **1305** (2013) 084 [arXiv:hep-ph/1303.6180];
F. Feruglio, C. Hagedorn and R. Ziegler, "A realistic pattern of lepton mixing and masses from S_4 and CP", Eur. Phys. J. C **74** (2014) 2753 [arXiv:hep-ph/1303.7178].

[59] C. Luhn, "Trimaximal TM_1 neutrino mixing in S_4 with spontaneous CP violation", Nucl. Phys. B **875** (2013) 80 [arXiv:hep-ph/1306.2358].

[60] P. F. Harrison, D. H. Perkins and W. G. Scott,"Tri-Bimaximal Mixing and the Neutrino Oscillation Data", Phys. Lett. B **530** (2002) 167 [arXiv:hep-ph/0202074];
P. F. Harrison and W. G. Scott, 11", Phys. Lett. B **535** (2002) 163 [arXiv:hep-ph/0203209];
P. F. Harrison and W. G. Scott, "", Phys. Lett. B **557** (2003) 76 [arXiv:hep-ph/0302025].

[61] C. I. Low and R. R. Volkas, "Tri-bimaximal mixing, discrete family symmetries and a conjecture connecting the quark and lepton mixing matrices", Phys. Rev. D **68** (2003) 033007 [arXiv:hep-ph/0305243].

[62] C. S. Lam, "The Horizontal Symmetry for Neutrino Mixing", Phys. Rev. Lett. **101** (2008) 121602 [arXiv:hep-ph/0804.2622];
C. S. Lam, "The Unique Horizontal Symmetry of Leptons", Phys. Rev. D **78** (2008) 073015 [arXiv:hep-ph/0809.1185].

[63] J. K. Ahn et al. (RENO collaboration), "Observation of Reactor Electron Antineutrino Disappearance in the RENO Experiment", Phys. Rev. Lett. **108** (2012) 191802, [arXiv:hep-ex/1204.0626].

[64] P. Adamson et al. (MINOS Collaboration), "", Phys. Rev. Lett. **110** (2013) 251801, [arXiv:hep-ex/1304.6335].

[65] F. P. An et al. (Daya Bay Collaboration), "Spectral measurement of electron antineutrino oscillation amplitude and frequency at Daya Bay" Phys. Rev. Lett. **112** (2014) 061801 [arXiv:hep-ex/1310.6732].

[66] K. Abe et al. (T2K collaboration), "Observation of Electron Neutrino Appearance in a Muon Neutrino Beam", Phys. Rev. Lett. **112** (2014) 061802 [arXiv:hep-ex/1311.4750].

[67] M. Malinsky, "Tackling the SUSY flavour and CP problem: SUGRA versus $SU(3)$", SUSY 2007 proceedings, 15th International Conference on Supersymmetry and Unification of Fundamental Interactions, July 26 - August 1, 2007, Karlsruhe, Germany, [arXiv:hep-ph/0710.2430]

[68] G. G. Ross and O. Vives, "Yukawa structure, flavor and CP violation in supergravity", Phys. Rev. **B67** (2003) 095013 [arXiv:hep-ph/0211279].

[69] F. Feruglio, C. Hagedorn and L. Merlo, "Vacuum Alignment in SUSY A_4 Models", JHEP **1003** (2010) 084 [arXiv:hep-ph/0910.4058].

[70] H. Georgi and S. Glashow (1974). "Unity of All Elementary-Particle Forces", Phys. Rev. Lett. **32** (8), 438.

[71] H. Georgi and C. Jarlskog, "A new lepton-quark mass relation in a unified theory", Phys. Lett. B **86** (1979) 297.

[72] B. Grinstein, M. Redi and G. Villadoro, "Low Scale Flavor Gauge Symmetries", JHEP **1011** (2010), 067 [arXiv:hep-ph/1009.2049];

[73] R. S. Chivukula and H. Georgi, "Composite Technicolor Standard Model", Phys. Lett. B **188** (1987) 99;
L. J. Hall and L. Randall, "Weak scale effective supersymmetry", Phys. Rev. Lett. **65** (1990) 2939;
A. J. Buras, P. Gambino, M. Gorbahn, S. Jäger and L. Silvestrini, "Universal unitarity triangle and physics beyond the standard model", Phys. Lett. B **500** (2001) 161 [arXiv:hep-ph/0007085].

[74] G. D'Ambrosio, G. F. Giudice, G. Isidori and A. Strumia, "Minimal flavor violation: An Effective field theory approach," Nucl. Phys. **B645** (2002), 155 [arXiv:hep-ph/0207036];
V. Cirigliano, B. Grinstein, G. Isidori and M. B. Wise,"Minimal flavor violation in the lepton sector," Nucl. Phys. **728** (2005), 121 [arXiv:hep-ph/0507001].

[75] C. Bobeth, T. Ewerth, F. Kruger and J. Urban, "Enhancement of B(anti-B(d) $\to \mu^+\mu^-$) / B(anti-B(s) $\to \mu^+\mu^-$) in the MSSM with minimal flavor violation and large tan beta", Phys. Rev. D **66** (2002) 074021 [arXiv:hep-ph/0204225].

[76] W. Altmannshofer, A. J. Buras, S. Gori, P. Paradisi and D. M. Straub, "Anatomy and Phenomenology of FCNC and CPV Effects in SUSY Theories," Nucl. Phys. B **830** (2010) 17 [arXiv:hep-ph/0909.1333].

[77] A. J. Buras and J. Girrbach, "BSM models facing the recent LHCb data: A First look", Acta Phys. Polon. B **43** (2012) 1427 [arXiv:hep-ph/1204.5064];
D. M. Straub, "Overview of Constraints on New Physics in Rare B Decays", arXiv:1205.6094.

[78] S. Antusch and M. Spinrath, "Quark and lepton masses at the GUT scale including SUSY threshold corrections", Phys. Rev. D **78** (2008) 075020 [arXiv:0804.0717].

[79] Y. Yamada, "SUSY and GUT threshold effects in SUSY SU(5) models", Z. Phys. C **60** (1993) 83.

[80] R. Gatto, G. Sartori and M. Tonin, "Weak Selfmasses, Cabibbo Angle, and Broken SU(2) x SU(2)", Phys. Lett. B **28** (1968) 128.

[81] X. G. He and A. Zee, "Minimal modification to the tri-bimaximal neutrino mixing", Phys. Lett. B **645** (2007) 427 [arXiv:hep-ph/0607163];
W. Grimus and L. Lavoura, "A Model for trimaximal lepton mixing", JHEP **0809** (2008) 106 [arXiv:hep-ph/0809.0226]; C. H. Albright, A. Dueck and W. Rodejohann, "Possible Alternatives to Tri-bimaximal Mixing", Eur. Phys. J. C **70** (2010) 1099 [arXiv:hep-ph/1004.2798]; H. Ishimori, Y. Shimizu, M. Tanimoto and A. Watanabe, "Neutrino masses and mixing from S_4 flavor twisting", Phys. Rev. D **83** (2011) 033004 [arXiv:hep-ph/1010.3805]; Y. Shimizu, M. Tanimoto and A. Watanabe, "Breaking Tri-bimaximal Mixing and Large θ_{13}", Prog. Theor. Phys. **126** (2011) 81 [arXiv:hep-ph/1105.2929]; E. Ma and D. Wegman, "Nonzero theta(13) for neutrino mixing in the context of A(4) symmetry", Phys. Rev. Lett. **107** (2011) 061803 [arXiv:hep-ph/1106.4269]; X. G. He and A. Zee, "Minimal Modification to Tri-bimaximal Mixing", Phys. Rev. D **84** (2011) 053004 [arXiv:hep-ph/1106.4359]; S. F. King and C. Luhn, "Trimaximal neutrino mixing from vacuum alignment in A4 and S4 models", JHEP **1109** (2011) 042 [arXiv:hep-ph/1107.5332]; I. K. Cooper, S. F. King and C. Luhn, "A4xSU(5) SUSY GUT of Flavour with Trimaximal Neutrino Mixing", JHEP **1206** (2012) 130 [arXiv:hep-ph/1203.1324].

[82] M. C. Chen, M. Fallbacher, K. T. Mahanthappa, M. Ratz and A. Trautner, "CP Violation from Finite Groups", Nucl. Phys. B **883** (2014) 267 [arXiv:hep-ph/1402.0507].

[83] S. Antusch and V. Maurer, "Running quark and lepton parameters at various scales", JHEP **1311** (2013) 115 [arXiv:hep-ph/1306.6879].

[84] S. Antusch and M. Spinrath, "Quark and lepton masses at the GUT scale including SUSY threshold corrections", Phys. Rev. D **78** (2008) 075020 [arXiv:hep-ph/0804.0717].

[85] J. A. Casas and S. Dimopoulos, "Stability bounds on flavor violating trilinear soft terms in the MSSM", Phys. Lett. B **387** (1996) 107 [arXiv:hep-ph/9606237].

[86] H. Baer, V. Barger, P. Huang, D. Mickelson, A. Mustafayev and X. Tata, "Radiative natural supersymmetry: Reconciling electroweak fine-tuning and the Higgs boson mass", Phys. Rev. D **87** (2013) 11, 115028 [arXiv:hep-ph/1212.2655].

[87] S. Heinemeyer, "MSSM Higgs physics at higher orders", Int. J. Mod. Phys. A **21** (2006) 2659 [arXiv:hep-ph/0407244].

[88] T. Hahn, S. Heinemeyer, W. Hollik, H. Rzehak and G. Weiglein, "Prediction of the light CP-even Higgs-Boson Mass of the MSSM: Towards the ILC Precision", International Workshop on Future Linear Colliders (LCWS13) Tokyo, Japan, November 11-15, 2013 [arXiv:hep-ph/1404.0186].

[89] N. Carrasco *et al.*, "$D^0 - \bar{D}^0$ mixing in the standard model and beyond from $N_f = 2$ twisted mass QCD", Phys. Rev. D **90** (2014) 1, 014502 [arXiv:hep-ph/1403.7302].

[90] E. Gabrielli and S. Khalil, "Constraining supersymmetric models from B(d) - anti-B(d) mixing and the B(d) $\to J/\psi$ K(S) asymmetry", Phys. Rev. D **67** (2003) 015008 [arXiv:hep-ph/0207288].

[91] A. Behring, C. Gross, G. Hiller and S. Schacht, "Squark Flavor Implications from B $\to$ K* l+ l-", JHEP **1208** (2012) 152 [arXiv:hep-ph/1205.1500].

[92] A. Crivellin and U. Nierste, "Supersymmetric renormalisation of the CKM matrix and new constraints on the squark mass matrices", Phys. Rev. D **79** (2009) 035018 [arXiv:hep-ph/0810.1613].

[93] A. Masiero, S. K. Vempati and O. Vives, "Flavour physics and grand unification", Particle physics beyond the standard model. Proceedings, Summer School on Theoretical Physics, 84th Session, Les Houches, France, August 1-26, 2005 [arXiv:hep-ph/0711.2903].

[94] M. Arana-Catania, S. Heinemeyer and M. J. Herrero, "Updated Constraints on General Squark Flavor Mixing", Phys. Rev. D **90** (2014) 7, 075003 [arXiv:hep-ph/1405.6960].

[95] M. Arana-Catania, S. Heinemeyer and M. J. Herrero, "New Constraints on General Slepton Flavor Mixing", Phys. Rev. D **88** (2013) 1, 015026 [arXiv:hep-ph/1304.2783].

[96] J. Baron *et al.* [ACME Collaboration], "Order of Magnitude Smaller Limit on the Electric Dipole Moment of the Electron," Science **343** (2014) 269 [arXiv:1310.753].

[97] I. Masina and C. A. Savoy, "Sleptonarium: Constraints on the CP and flavor pattern of scalar lepton masses", Nucl. Phys. B **661** (2003) 365 [arXiv:hep-ph/0211283].

[98] J. Hisano, D. Kobayashi, W. Kuramoto and T. Kuwahara, "Nucleon Electric Dipole Moments in High-Scale Supersymmetric Models", JHEP **1511** (2015) 085 [arXiv:hep-ph/1507.05836].

[99] J. Adam *et al.* [MEG Collaboration], "New constraint on the existence of the $\mu^+ \to e^+\gamma$ decay", Phys. Rev. Lett. **110** (2013) 201801 [arXiv:hep-ex/1303.0754].

[100] A. M. Baldini *et al.*, "MEG Upgrade Proposal" (2013) [arXiv:1301.7225].

[101] Z. Ligeti, M. Papucci and G. Perez, "Implications of the measurement of the $B_s^0 - \bar{B}_s^0$ mass difference", Phys. Rev. Lett. **97** (2006) 101801 [arXiv:hep-ph/0604112].

[102] A. J. Buras and J. Girrbach, "Towards the Identification of New Physics through Quark Flavour Violating Processes", Rept. Prog. Phys. **77** (2014) 086201 [arXiv:hep-ph,1306.3775].

[103] T. Inami and C. S. Lim, "Effects of Superheavy Quarks and Leptons in Low-Energy Weak Processes k(L) —¿ mu anti-mu, K+ —¿ pi+ Neutrino anti-neutrino and K0 ¡—¿ anti-K0," Prog. Theor. Phys. **65** (1981) 297 [Prog. Theor. Phys. **65** (1981) 1772];
G. Buchalla, A. J. Buras and M. E. Lautenbacher, "Weak decays beyond leading logarithms", Rev. Mod. Phys. **68** (1996) 1125 [hep-ph/9512380].

[104] E. Golowich, J. Hewett, S. Pakvasa, A. A. Petrov and G. K. Yeghiyan, "Relating B_s Mixing and $B_s \to \mu^+\mu^-$ with New Physics", Phys. Rev. D **83** (2011) 114017 [arXiv:hep-ph/1102.0009].

[105] J. Laiho, E. Lunghi and R. S. Van de Water, "Lattice QCD inputs to the CKM unitarity triangle analysis", Phys. Rev. D **81** (2010) 034503 [arXiv:hep-ph/0910.2928].

[106] S. Aoki *et al.*, "Review of lattice results concerning low-energy particle physics", Eur. Phys. J. C **74** (2014) 2890 [arXiv:hep-lat/1310.8555].

[107] Y. Amhis *et al.* [Heavy Flavor Averaging Group (HFAG) Collaboration], "Averages of b-hadron, c-hadron, and τ-lepton properties as of summer 2014," [arXiv:hep-ex/1412.7515].

[108] M. Artuso, G. Borissov and A. Lenz, "CP Violation in the B_s^0 system", [arXiv:hep-ph/1511.09466].

[109] T. Aushev *et al.*, "Physics at Super B Factory", [arXiv:hep-ex/1002.5012].

[110] R. Aaij *et al.* [LHCb Collaboration], "Measurement of CP violation in $B^0 \to J/\psi K_S^0$ decays", Phys. Rev. Lett. **115** (2015) 3, 031601 [arXiv:hep-ex/1503.07089].

[111] J. Charles *et al.*, "Current status of the Standard Model CKM fit and constraints on $\Delta F = 2$ New Physics", Phys. Rev. D **91** (2015) 7, 073007 [arXiv:hep-ph/1501.05013].

[112] J. Yu, "K_L-K_S mass difference from Lattice QCD", PoS LATTICE **2013** (2014) 398 [arXiv:hep-lat/1312.0306].

[113] K. A. Olive *et al.* [Particle Data Group Collaboration], "Review of Particle Physics", Chin. Phys. C **38** (2014) 090001.

[114] A. J. Buras and D. Guadagnoli, "Correlations among new CP violating effects in Δ F = 2 observables", Phys. Rev. D **78** (2008) 033005 [arXiv:hep-ph/0805.3887].

[115] J. J. A. Bailey *et al.* [SWME Collaboration], "Standard Model evaluation of ε_K using lattice QCD inputs for $\hat{B}_K$ and V_{cb}", Phys. Rev. D **92** (2015) 3, 034510 [arXiv:hep-lat/1503.05388].

[116] A. Bevan *et al.*, "Standard Model updates and new physics analysis with the Unitarity Triangle fit", Nucl. Phys. Proc. Suppl. **241-242** (2013) 89.

[117] M. Misiak *et al.*, "Updated NNLO QCD predictions for the weak radiative B-meson decays," Phys. Rev. Lett. **114** (2015) 221801 [arXiv:hep-ph/1503.01789].

[118] C. Bobeth, M. Gorbahn, T. Hermann, M. Misiak, E. Stamou and M. Steinhauser, "$B_{s,d} \to l^+l^-$ in the Standard Model with Reduced Theoretical Uncertainty", Phys. Rev. Lett. **112** (2014) 101801 [arXiv:hep-ph/1311.0903].

[119] V. Khachatryan *et al.* [CMS and LHCb Collaborations], "Observation of the rare $B_s^0 \to \mu^+\mu^-$ decay from the combined analysis of CMS and LHCb data", Nature **522** (2015) 68 [arXiv:hep-ex/1411.4413].

[120] A. Buras, "Flavour Expedition to the Zeptouniverse", PoS FWNP (2015) 003 [arXiv:hep-ph/1505.00618].

[121] J. Hisano and Y. Shimizu, "Hadronic EDMs induced by the strangeness and constraints on supersymmetric CP phases", Phys. Rev. D **70** (2004) 093001 [arXiv:hep-ph/0406091].

[122] J. Hisano, M. Nagai and P. Paradisi, "Flavor effects on the electric dipole moments in supersymmetric theories: A beyond leading order analysis", Phys. Rev. D **80** (2009) 095014 [arXiv:0812.4283].

[123] G. Degrassi, E. Franco, S. Marchetti and L. Silvestrini, "QCD corrections to the electric dipole moment of the neutron in the MSSM", JHEP **0511** (2005) 044 [arXiv:hep-ph/0510137].

[124] W. Dekens and J. de Vries, "Renormalization Group Running of Dimension-Six Sources of Parity and Time-Reversal Violation2, JHEP **1305** (2013) 149 [arXiv:hep-ph/1303.3156];
V. Khachatryan *et al.* [CMS Collaboration], "Measurement of the inclusive 3-jet production differential cross section in protonproton collisions at 7 TeV and determination of the strong coupling constant in the TeV range", Eur. Phys. J. C **75** (2015) 5, 186 [arXiv:hep-ex/1412.1633];
G. Dissertori, "The Determination of the Strong Coupling Constant", [arXiv:hep-ex/1506.05407].

[125] C. A. Baker *et al.*, "An Improved experimental limit on the electric dipole moment of the neutron", Phys. Rev. Lett. **97** (2006) 131801 [arXiv:hep-ex/0602020].

[126] W. C. Griffith, M. D. Swallows, T. H. Loftus, M. V. Romalis, B. R. Heckel and E. N. Fortson, "Improved Limit on the Permanent Electric Dipole Moment of Hg-199", Phys. Rev. Lett. **102** (2009) 101601.

[127] Y. Singh and B. K. Sahoo, "Rigorous limits for hadronic and semi-leptonic CP-violating coupling constants from the electric dipole moment of ^{199}Hg", Phys. Rev. A **91** (2015) 3, 030501 [arXiv:1408.4337].

[128] J. Engel, M. J. Ramsey-Musolf and U. van Kolck, "Electric Dipole Moments of Nucleons, Nuclei, and Atoms: The Standard Model and Beyond", Prog. Part. Nucl. Phys. **71** (2013) 21 [arXiv:nucl-th/1303.2371].

[129] M. Pospelov, "Best values for the CP odd meson nucleon couplings from supersymmetry", Phys. Lett. B **530** (2002) 123 [arXiv:hep-ph/0109044].

[130] S. W. Bosch and G. Buchalla, "The Radiative decays $B \to V\gamma$ at next-to-leading order in QCD," Nucl. Phys. B **621** (2002) 459 [arXiv:hep-ph/0106081].

[131] J. Lyon and R. Zwicky, "Anomalously large $\mathcal{O}_8$ and long-distance chirality from $A_{\rm CP}[D^0 \to (\rho^0, \omega)\gamma](t)$", [arXiv:hep-ph/1210.6546].

[132] A. J. Buras, "Weak Hamiltonian, CP violation and rare decays", Proceedings, Summer School in Theoretical Physics, NATO Advanced Study Institute, 68th session, Les Houches, France, July 28-September 5, 1997. Pt. 1, 2 [arXiv:hep-ph/9806471].

[133] P. Ball and R. Zwicky, "$B(D,S) \to \rho, \omega, K^*, \phi$ decay form-factors from light-cone sum rules revisited", Phys. Rev. D **71** (2005) 014029 [arXiv:hep-ph/0412079].

[134] M. A. Shifman, A. I. Vainshtein and V. I. Zakharov, "QCD And Resonance Physics. Sum Rules," Nucl. Phys. B **147** (1979) 385.

[135] S. Weinberg, "The Quantum theory of fields. Vol. 1: Foundations," Cambridge, UK: Univ. Pr. (1995) 609 p

[136] G. Källén, "On the definition of the Renormalization Constants in Quantum Electrodynamics," Helv. Phys. Acta **25** (1952) 417.
H. Lehmann, "On the Properties of propagation functions and renormalization contants of quantized fields," Nuovo Cim. **11** (1954) 342.

[137] R. J. Eden P. V. Landshoff D. I. Olive and J. C. Polkinghorne "The Analytic S-Matrix," Cambridge: Cambridge University Press, 1966.

[138] I. T. Todorov "Analytic Properties of Feynman Diagrams in Quantum Field Theory," Pergamon (1971)

[139] H. H. Asatrian, H. M. Asatrian, C. Greub and M. Walker, "Two loop virtual corrections to B $\to$ X(s) lepton+ lepton- in the standard model," Phys. Lett. B **507** (2001) 162 [hep-ph/0103087].

[140] P. Ball and R. Zwicky, "Time-dependent CP Asymmetry in B $\to$ K* gamma as a (Quasi) Null Test of the Standard Model," Phys. Lett. B **642** (2006) 478 [hep-ph/0609037].

[141] P. Ball, G. W. Jones and R. Zwicky, "B $\to$ V gamma beyond QCD factorisation," Phys. Rev. D **75** (2007) 054004 [hep-ph/0612081].

[142] L. Maiani and M. Testa, "Final state interactions from Euclidean correlation functions," Phys. Lett. B **245** (1990) 585.

[143] A. Khodjamirian, "B $\to$ pi pi decay in QCD," Nucl. Phys. B **605** (2001) 558 [arXiv:hep-ph/0012271].

[144] A. V. Smilga and M. A. Shifman, "Procedure Of Unitary Borelization In Three Point Sum Rules Of Qcd. (in Russian)," Sov. J. Nucl. Phys. **37** (1983) 958 [Yad. Fiz. **37** (1983) 1613].
B. L. Ioffe and A. V. Smilga, "Meson Widths and Form-Factors at Intermediate Momentum Transfer in Nonperturbative QCD," Nucl. Phys. B **216** (1983) 373.

[145] R. Mertig, M. Bohm, A. Denner, "FEYNCALC: Computer algebraic calculation of Feynman amplitudes," Comput. Phys. Commun. **64** (1991) 345-359.

[146] G. Passarino, M. J. G. Veltman, "One Loop Corrections for e+ e- Annihilation Into mu+ mu- in the Weinberg Model," Nucl. Phys. **B160** (1979) 151.

[147] E. Bagan, P. Ball and V. M. Braun, "Radiative corrections to the decay $B \to \pi e \nu$ and the heavy quark limit," Phys. Lett. B **417** (1998) 154 [hep-ph/9709243].

[148] T. M. Aliev and V. L. Eletsky, "On Leptonic Decay Constants of Pseudoscalar D and B Mesons," Sov. J. Nucl. Phys. **38** (1983) 936 [Yad. Fiz. **38** (1983) 1537].

[149] S. J. Lee, M. Neubert and G. Paz, "Enhanced Non-local Power Corrections to the anti-B $\to$ X(s) gamma Decay Rate," Phys. Rev. D **75** (2007) 114005 [hep-ph/0609224].

[150] Y. Amhis *et al.* [Heavy Flavor Averaging Group Collaboration], "Averages of B-Hadron, C-Hadron, and tau-lepton properties as of early 2012," arXiv:1207.1158 [hep-ex].

[151] J. Lyon and R. Zwicky, "Isospin asymmetries in $B \to (K^*, \rho)\gamma/l^+l^-$ and $B \to Kl^+l^-$ in and beyond the Standard Model," arXiv:1305.4797 [hep-ph].

[152] J. Charles, A. Le Yaouanc, L. Oliver, O. Pene and J. C. Raynal, "Heavy to light form-factors in the heavy mass to large energy limit of QCD," Phys. Rev. D **60** (1999) 014001 [hep-ph/9812358].

[153] V. M. Braun, A. Khodjamirian and M. Maul, "Pion form-factor in QCD at intermediate momentum transfers," Phys. Rev. D **61** (2000) 073004 [hep-ph/9907495].

[154] P. Ball and R. Zwicky, "B/(d,s) –¿ rho, omega, K*, Phi decay form factors from light-cone sum rules revisited," Phys. Rev. D **71** (2005) 014029 [arXiv:hep-ph/0412079].

[155] Y. -L. Wu, M. Zhong and Y. -B. Zuo, "B(s), D(s) $\to$ pi, K, eta, rho, K*, omega, phi Transition Form Factors and Decay Rates with Extraction of the CKM parameters $|V(ub)|$, $|V(cs)|$, $|V(cd)|$," Int. J. Mod. Phys. A **21** (2006) 6125 [arXiv:hep-ph/0604007].

[156] M. Beneke, G. Buchalla, M. Neubert and C. T. Sachrajda, "QCD factorisation for exclusive, nonleptonic B meson decays: General arguments and the case of heavy light final states," Nucl. Phys. B **591** (2000) 313 [arXiv:hep-ph/0006124].

[157] T. Muta, "Foundations of quantum chromodynamics. Second edition," World Sci. Lect. Notes Phys. **57** (1998) 1.

[158] J. Beringer *et al.* [Particle Data Group Collaboration], Phys. Rev. D **86** (2012) 010001.

[159] R. Arthur, P. A. Boyle, D. Brommel, M. A. Donnellan, J. M. Flynn, A. Juttner, T. D. Rae and C. T. C. Sachrajda, "Lattice Results for Low Moments of Light Meson Distribution Amplitudes," Phys. Rev. D **83** (2011) 074505 [arXiv:hep-lat/1011.5906].

[160] P. Ball and R. Zwicky, "SU(3) breaking of leading-twist K and K* distribution amplitudes: A Reprise," Phys. Lett. B **633** (2006) 289 [arXiv:hep-ph/0510338].

[161] M. Jung, X. -Q. Li and A. Pich, "Exclusive radiative B-meson decays within the aligned two-Higgs-doublet model," [arXiv:hep-ph/1208.1251].

[162] C. Allton *et al.* [RBC-UKQCD Collaboration], "Physical Results from 2+1 Flavor Domain Wall QCD and SU(2) Chiral Perturbation Theory," Phys. Rev. D **78** (2008) 114509 [arXiv:hep-lat/0804.0473].

[163] P. Ball and V. M. Braun, "The Rho meson light cone distribution amplitudes of leading twist revisited," Phys. Rev. D **54** (1996) 2182 [arXiv:hep-ph/9602323].

[164] P. Ball and G. W. Jones, "Twist-3 distribution amplitudes of K* and phi mesons," JHEP **0703** (2007) 069 [hep-ph/0702100 [HEP-PH]].

[165] P. Ball and R. Zwicky, "$|V_{td}/V_{ts}|$ from $B \to V\gamma$," JHEP **0604** (2006) 046 [hep-ph/0603232].

[166] C. Fronsdal, K. Mahanthappa and R. E. Norton, "Integral Representations For Vertex Functions," Physical Review Vol 127 No 5 (1962) p1847-1850

[167] G. Källén and A. S. Wightman: "The Analytic Properties of the Vacuum Expectation Value of a Product of Three Scalar Local Fields." Mat. Fys. Skr. Dan. Vid. Selsk. 1, No. 6 (1958).

[168] B.Anderson "Dispersion Relations for the Vertex Function from Local Commutativity." Commun. math. Phys. 25, 283–307 (1972).

[169] T. Hahn, M. Perez-Victoria, "Automatized one loop calculations in four-dimensions and D-dimensions," Comput. Phys. Commun. **118** (1999) 153-165. [hep-ph/9807565].

[170] S. Mandelstam, "Unitarity Condition Below Physical Thresholds in the Normal and Anomalous Cases," Phys. Rev. Lett. **4** (1960) 84.

[171] F. Feruglio, C. Hagedorn and R. Ziegler, "Lepton Mixing Parameters from Discrete and CP Symmetries," JHEP **1307** (2013) 027 [arXiv:hep-ph/1211.5560]; M. Holthausen, M. Lindner and M. A. Schmidt, "CP and Discrete Flavour Symmetries," JHEP **1304** (2013) 122 [arXiv:hep-ph/1211.6953].

[172] W. Grimus and M. N. Rebelo, "Automorphisms in gauge theories and the definition of CP and P," Phys. Rept. **281** (1997) 239 [arXiv:hep-ph/9506272].